The mobility of uranium and thorium series radionuclides in groundwaters

Trivedi, D. P.

Award date:
1989

Awarding institution:
University of Bath

THE MOBILITY OF URANIUM AND THORIUM SERIES RADIONUCLIDES IN GROUNDWATERS

submitted by

D.P. TRIVEDI

For the degree of Ph.D. of the
University of Bath

1989

ProQuest LLC
789 East Eisenhower Parkway
P.O. Box 1346
Ann Arbor, MI 48106-1346

DEDICATION

Dedicated to the memory of my grandfather,

MANSHANKER TRIVEDI (1890-1968)

A man whose equal I have never, and will

probably never, meet.

ACKNOWLEDGEMENTS

I would like to thank my supervisor, Dr J N Andrews, for his help and guidance during my studentship. Also I wish to acknowledge the considerable help given to me by my fellow colleagues at the University of Bath, Derrick Ford, Barry Smith, Trevor Elliot and especially Najid Hussain for many helpful discussions and Mike Youngman for his considerable number of radium determinations.

My special thanks go to my parents, especially my father who spent many days (and nights!) producing most of the diagrams. Mrs Jenny Emery typed my thesis and must be thanked for her sterling effort over what must have seemed a never-ending task.

Finally, I acknowledge N.E.R.C. for providing me with a research grant which enabled me to carry out this research.

TABLE OF CONTENTS

LIST OF TABLES PAGE

LIST OF FIGURES

ABSTRACT

The effects of groundwater residence time, aquifer lithology and groundwater chemistry upon the mobility of the naturally occurring radionuclides in the uranium and thorium decay series have been investigated in this study.

For the radium nuclides ^{226}Ra and ^{228}Ra this study showed that waters with a high residence time tend to have high ^{226}Ra activities and low $^{228}Ra/^{226}Ra$ activity ratios compared with that for the aquifer $^{232}Th/^{238}U$ ratio. This is shown to result from redistribution of U and Th series radionuclides in the groundwater flow system due to alpha recoil injection of nuclides from aquifer rock into water, or the preferential leaching of some nuclides from recoil damaged minerals.

Radium nuclide activities correlate with the dissolved calcium content of waters. This, coupled with the fact that many investigated waters were saturated with calcium minerals, suggests that radium contents are to some extent controlled by exchange equilibrium reactions with secondary calcium minerals as well as by adsorption on aquifer minerals. Radium speciation was calculated in many waters based upon recently available thermodynamic data. The data for the species $RaHCO_3^+(aq)$ was also extrapolated from the properties of other group II elements in this study. The predominant species in solution were found to be $Ra^{2+}(aq)$, $RaSO_4^o(aq)$

and $RaHCO_3^+(aq)$. However speciation based upon this data could not adequately explain the variation of radium activities with groundwater chemistry.

The full range of lead and radium radionuclides were measured in the King's Spring geothermal waters of Bath. Based upon first order adsorption/desorption kinetics, the results for the ^{228}Ra-^{228}Th-^{224}Ra triad gave a ^{228}Th residence time of 10.5 days. A minimum residence time of 18 days was calculated for radium based upon the observed $^{224}Ra/^{228}Ra$ ratio.

The observed $^{214}Pb/^{222}Rn$ and $^{212}Pb/^{214}Ra$ ratios result in a lead residence time of between 134 minutes and 53 hours. Measurement of the $^{210}Pb/^{222}Rn$ ratio further constrains the lead residence time to the limits 560-850 minutes.

A thorough investigation of uranium and thorium series radionuclides can be used to determine the residence times of these nuclides in groundwaters. This provides estimates of the residence times of chemically similar groundwater contaminants, such as heavy metals and artificial radionuclides, which may be released into the aquifers.

OBJECTIVES OF THIS WORK

The major objectives of this study were:

1. To develop preconcentration techniques and analytical methods for the measurement of radium radionuclides in groundwaters.
2. To develop methods for the measurement of the naturally occurring lead radionuclides: ^{214}Pb, ^{212}Pb and ^{210}Pb, in groundwaters.
3. To investigate Ra and Ra-isotope groundwater geochemistry in a variety of geological settings.
4. To establish the geochemical constraints governing the mobility of Ra in groundwater.
5. To determine the residence times of Ra and Pb isotopes in groundwaters.
6. To study the hydrochemistry of the lead radionuclides in the naturally occurring uranium and thorium radioactive decay series.

CHAPTER ONE: INTRODUCTION

1.1.1 Radioactive Decay

Radioactive decay is the process whereby the unstable atomic nucleus of one element spontaneously disintegrates to form the nucleus of another element. The rate of decay of a radioactive substance is proportional to the number of atoms present. This can be expressed by the relationship:

$$-\frac{dN}{dt} \propto N \qquad (1.1)$$

where N is the number of atoms present at time, t.
Upon the introduction of a proportionality constant, λ, this relationship becomes:

$$-\frac{dN}{dt} = \lambda N \qquad (1.2)$$

The constant λ is called the decay constant and is characteristic of the radionuclide under consideration. It represents the fraction of the total number of atoms decaying within a stated unit time interval, chosen such that N does not significantly change within that time interval.
Equation (1.2) can be re-arranged and integrated:

$$-\int \frac{dN}{N} = \lambda \int dt \qquad (1.3)$$

This gives

$$\ln N = \lambda t + C \qquad (1.4)$$

The constant of integration can be determined by noting that at time t=0, $N=N_0$, the initial number of parent atoms.
Therefore c = -ln No

$$N = No\ e^{-\lambda t} \qquad (1.5)$$

This is the basic radioactive decay equation, and gives the number of parent atoms (N) remaining at a time t from an original number of parent atoms (No) at time t=0.

The rate of decay of a radioactive nuclide is normally given in terms of the half-life ($t_{\frac{1}{2}}$) of that nuclide. This is the time required for the initial number of atoms to decay to half of the original number. Thus at time $t = t_{\frac{1}{2}}$, $N = No/2$ and from (1.5):

$$\ln\left(\tfrac{1}{2}\right) = -\lambda t_{\frac{1}{2}}$$

$$\text{therefore} \quad t_{\frac{1}{2}} = \frac{\ln 2}{\lambda} = \frac{0.693}{\lambda} \qquad (1.6)$$

The radioactivity of a sample is not normally given in terms of the number of atoms (N) present. Instead it is given in terms of the rate of decay of the sample, its activity (A) defined by equation (1.2) with

$$A = \frac{dN}{dt}$$

The commonly quoted unit of activity is the curie (Ci) which is historically defined as the rate of disintegration of one gram of pure radium. It is now defined as the quantity of any radioactive nuclide in which the disintegration rate is $3.7 \times 10^{10} s^{-1}$. The activities found in the environment are very much smaller than the curie. Instead commonly quoted radioactivity units are

microcuries, nanocuries and picocuries, 10^{-6}, 10^{-9} and 10^{-12} respectively.

The S.I. unit of radioactivity is the Becquerel (Bq) defined by:

1 Becquerel (Bq) = 1 disintegration per second

Activity is also commonly quoted in disintegration per minute (dpm), thus

1 curie = 2.22×10^{10} dpm.

1.1.2 Radioactive Equilibria

The daughter resulting from a radioactive decay may itself be radioactive and decay with its own characteristic half-life. The rate of decay of the parent nuclide (N_1) is given by:

$$\left(\frac{dN_1}{dt}\right) = -\lambda_1 N_1 \quad \text{and} \quad N_1 = N_1^0\, e^{-\lambda_1 t} \qquad (1.7)$$

but the radioactive daughter N_2, is formed at the same rate as the parent, and is removed by its own decay:

$$\left(\frac{dN_2}{dt}\right) = \lambda_1 N_1 - \lambda_2 N_2 \qquad (1.8)$$

substituting (1.7) into 1.8) gives:

$$\frac{dN_2}{dt} = \lambda_1 N_1^0\, e^{-\lambda_1 t} - \lambda_2 N_2 \qquad (1.9)$$

re-arranging gives:

$$\frac{dN_2}{dt} + \lambda_2 N_2 = \lambda_1 N_1^0\, e^{-\lambda_1 t} \qquad (1.10)$$

This is a first order differential equation, the solution of which when N_2 is the value of N_1 at $t = 0$, is:

$$N_2 = \frac{\lambda_1}{\lambda_2 - \lambda_1}\, N_1^0\, (e^{-\lambda_1 t} - e^{-\lambda_2 t}) + N_2^0 e^{-\lambda_2 t} \qquad (1.11)$$

There are two limiting cases for this equation when a state of radioactive equilibrium is reached. When $\lambda_1 < \lambda_2$, for large values of t, $e^{-\lambda_2 t}$ will be negligible compared to $e^{-\lambda_1 t}$ and equation (1.11) becomes:

$$N_2 = \frac{\lambda_1}{\lambda_2 - \lambda_1}\, N_1^0 e^{-\lambda_1 t}$$

which since $N_1 = N_1^0 e^{-\lambda_1 t}$ becomes

$$N_2 = \left(\frac{\lambda_1}{\lambda_2 - \lambda_1}\right) N_1$$

which re-arranged gives:

$$\frac{N_1}{N_2} = \left(\frac{\lambda_2-\lambda_1}{\lambda_1}\right) = \text{constant} \qquad (1.12)$$

Therefore the measured activities of N_1 and N_2 will reach a constant value where after 5 half lives of the daughter nuclide N_2. This is called Transient Equilibrium and is illustrated by the ingrowth of ^{212}Bi from ^{212}Pb (Fig. 1.1)

The second case of equation (1.11) is that observed in the naturally occurring radioactive decay series of ^{238}U, ^{235}U and $^{232}_{90}Th$ where the parent is very much longer-lived than its daughters. Then $\lambda_1 << \lambda_2$ and $(\lambda_2-\lambda_1) \simeq \lambda_2$. Then:

$$\frac{N_1}{N_2} = \frac{\lambda_2}{\lambda_1} \qquad (1.13)$$

Re-arranging, $\lambda_1 N_1 = \lambda_2 N_2$ or $A_1 = A_2$.

In other words, the activity of the daughters will equal those of their parents. This is called Secular Equilibrium and is illustrated by the ingrowth of ^{226}Ra in ^{230}Th (Fig. 1.2)

This treatment can extend to cases with many successive decays but the mathematics become more and more complicated. Fortunately, H. Bateman (1910) provided the general solution for "n" successive decays, assuming that initially only the parent nuclide is present, that is:
$N_1 = N_1^0 = N_2^0 = N_3^0 = N_4^0 \ldots N_n^0$ at time $t = 0$. The number of atoms in the N^{th} member of the chain at time t is given by:

$$N_n = C_1 e^{-\lambda_1 t} + C_2 e^{-\lambda_2 t} + C_3 e^{-\lambda_3 t} \ldots + C_n e^{-\lambda_n t}$$

where

$$C_1 = \frac{\lambda_1 \lambda_2 \ldots \lambda_{n-1}}{(\lambda_2-\lambda_1)(\lambda_3-\lambda_1) \ldots (\lambda_n-\lambda_1)} N_1^0$$

$$C_n = \frac{\lambda_1 \lambda_2 \ldots \lambda_{n-1}}{(\lambda_1-\lambda_n)(\lambda_2-\lambda_n) \ldots (\lambda_{n-1}-\lambda_n)} N_1^0$$

Solutions for the general cases when N_2^0, N_3^0 ...$N_n^0 \neq 0$ can be obtained by adding to the Bateman equation for N_n members a second solution for the N_{n-1} membered chain with N_2 as the parent. This process is continued until the required solution is reached.

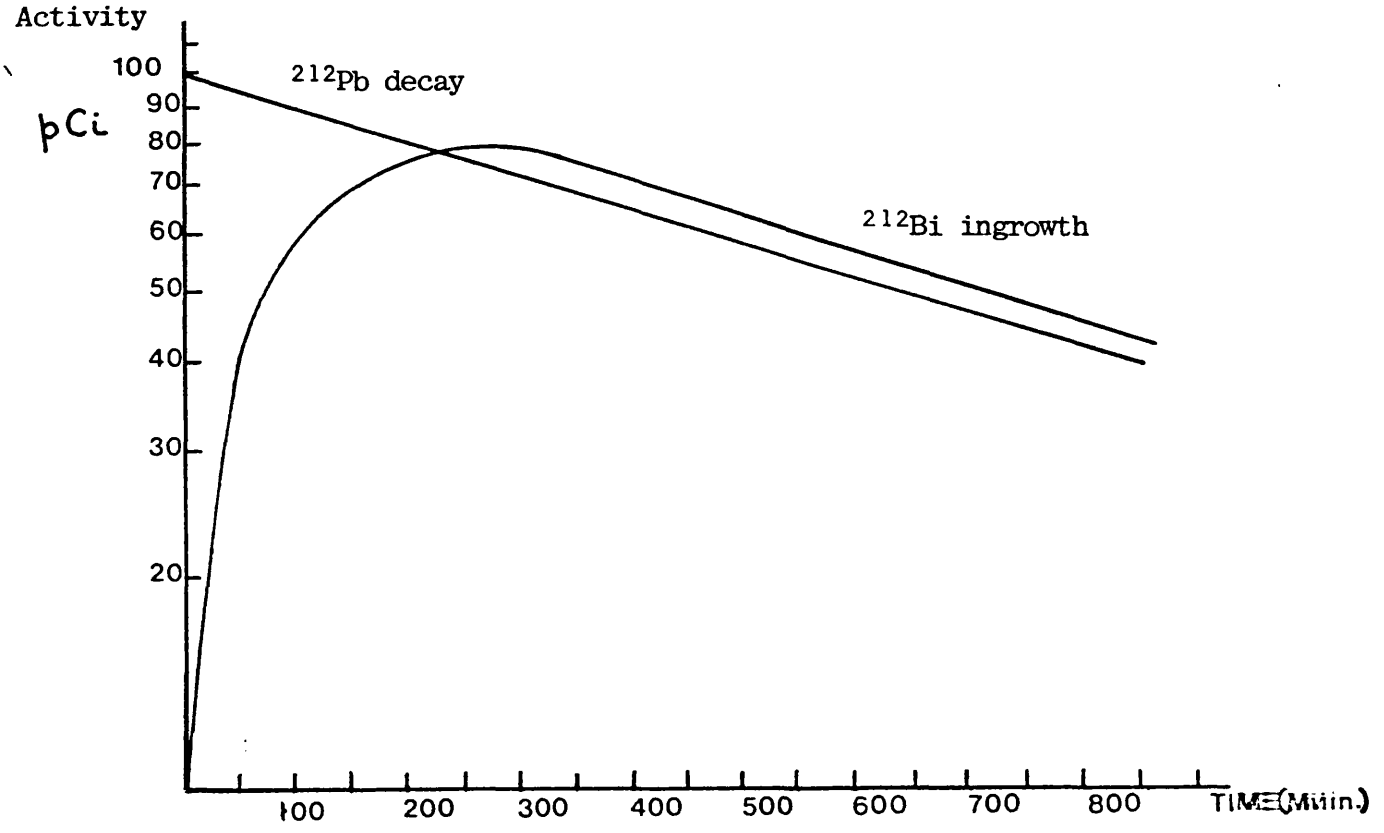

Fig. 1.1 Transient equilibrium illustrated by ^{212}Bi ingrowth from [illegible]

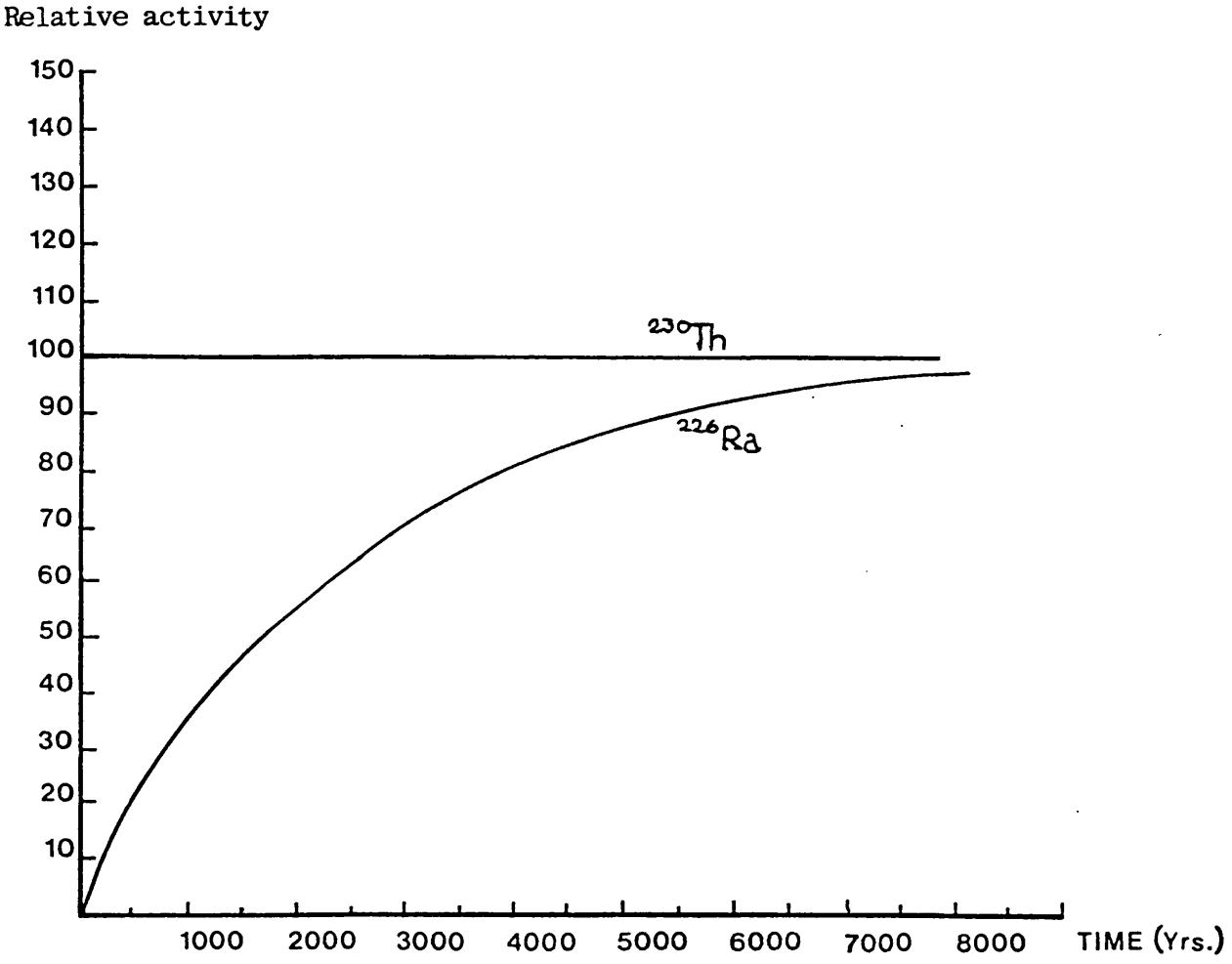

Fig. 1.2 Secular equilibrium illustrated by the ingrowth of ^{226}Ra into equilibrium with its parent ^{230}Th.

1.2 Radioactive Decay Processes

1.2.1 Alpha Decay

Nuclear decay producing a daughter nuclide and an alpha particle is termed α-decay, and is represented by the equation:

$$ {}^{A}_{Z}P \rightarrow {}^{4}_{2}He^{2+} + {}^{A-4}_{Z-2}D \qquad (1.14) $$

where P is the parent nucleus, D is the daughter nucleus and ${}^{4}_{2}He^{2+}$ is the α-particle. As shown by this equation, the α-particle is simply a helium nucleus without any orbiting electrons. The α-particles are ejected from the parent nucleus upon decay. Their kinetic energy is rapidly lost by collision with atoms in matter. This results in production of electron-positive ion pairs until the α-particle energy is exhausted and the α-particle picks up 2 electrons to become a helium atom. The range the α-particle travels depends upon the energy imparted to the particle and the density of matter through which it passes. Thus α-particle ranges in air are several centimetres, while in solids they are generally stopped within a few microns.

Alpha decay results in discrete energies imparted to the emitted α-particle. This energy is characteristic for the particular decay producing the α-particle. This means that determining the α-spectrum of an α-emitting substance allows the identification of the decaying parent nucleus.

However, the energy produced during decay is shared between the α-particle and the daughter nucleus as kinetic energy to the α-particle and recoil energy to the daughter nucleus. The energy imparted to the daughter nucleus can be calculated using the laws of conservation of momentum and energy:

by conservation of momentum:

$$M_D V_D = M_\alpha V_\alpha \qquad (1.15)$$

where M_D, M_α, V_D and V_α are the masses and velocities of the daughter nucleus and α-particle respectively.

also $E_D = \frac{1}{2} M_D V_D^2 \qquad (1.16)$

where E_D is the energy of recoiling daughter,

and $E_\alpha = \frac{1}{2} M_\alpha V_\alpha^2 \qquad (1.17)$

where E_α is the kinetic energy of the α-particle.

Combining equations:

$$E_D = \frac{M_\alpha}{M_D} E_\alpha \qquad (1.18)$$

But the total energy of the disintegration is given by E

Therefore $E = E_D + E_\alpha \qquad (1.19)$

This gives:

$$E = E\alpha \left[1 + \frac{M_\alpha}{M_D} \right] \qquad (1.20)$$

$$E_\alpha = \left(\frac{M_D}{M_D + M_\alpha} \right) \cdot E \simeq \frac{M_D}{Mp} E$$

similarly:

$$E_D \simeq \frac{M_\alpha}{M_p} E \qquad (1.21)$$

The α-recoil energy of the daughter nucleus is much smaller than the kinetic energy of the α-particle, but is sufficient to break several hundred chemical bonds. In the natural environment the α-recoil phenomenon has important hydrochemical consequences.

Many of the uranium and thorium series radionuclides are produced by α-decay processes. If there are decaying parent nuclides on a rock surface at the water–rock interface, then

a fraction of the daughter nuclides may α-recoil directly into solution, or will be present in α-recoil damaged lattice sites which are readily leachable by groundwater. This process has important consequences for ^{238}U-^{234}U disequilibria in groundwaters and ^{226}Ra and ^{222}Rn production.

1.2.2 Beta Decay

Beta decay processes cause production or removal of negatrons (β^-) or positrons (β^+) from the atomic nucleus (negatrons and positrons are effectively electrons with negative and positive charges, respectively). Beta decay can take place via the following processes; negatron or positron emission or internal conversion of an electron. However, in the naturally occurring radioactive decay series, β-decay predominantly involves β^- emissions:

$$ {}^{A}_{Z}P \rightarrow {}^{A}_{Z+1}D + \beta^- + \bar{\nu} \qquad (1.22) $$

The change in the atomic number is due to the conversion of a neutron to a proton. In positron emission, it is the other way around. There is an additional particle, the neutrino (ν) emitted in addition to a β-particle and the daughter nucleus. This is chargeless and has no rest mass, but serves to conserve angular momentum and energy during decay. Neutrinos are emitted during positron emission and anti-neutrinos during negatron emission.

Because the decay energy can be shared between β-particles, the emitted β-particle no longer has a discrete energy. The resultant β-particle energy spectrum is basically a broad continuum with a cut-off point corresponding to the decay where nearly all of the decay energy is transferred to the β-particle.

Unlike α-decay, there is only a minor daughter nucleus recoil effect. A similar equation to (1.21) can be derived, replacing E_α with E_β and M_α with M_β:

$$E_D \simeq \frac{M_\beta}{M_p} E \qquad (1.23)$$

It shows that the recoil energy imparted to the daughter nucleus will be negligible due to the small mass of the β-particle.

It therefore seems likely that β-decay recoil cannot eject nuclides into solution resulting in diseqilibrium between radioelements, although Laul et al (1985) have proposed that β-recoil could facilitate desorption of ^{234}U from ^{234}Th adsorbed onto rock surfaces.

1.2.3 Gamma Radiation

Decay of atoms by α or β decay frequently leaves the resulting daughter nuclei in an excited energy state. Nuclei will de-excite to a more stable nuclear ground state by emission of a γ-ray photon. There are two possible ways in which nuclei can de-excite by emission of γ-ray photons.

In the first, the nucleus de-excites directly to the ground state. The emitted γ-ray photon will therefore have an energy equal to the energy difference between the ground state and the excited state. Secondly, the nucleus can "cascade" through a series of excited states of progressively lower energy, until the ground state is reached. This will result in the emission of several γ-ray photons, each with an energy characteristic of the energy difference between successive energy levels. Both of these processes are illustrated in Figure 1.3.

Often, excited nuclei can de-excite by several different transition schemes. This will result in a complex γ-ray emission spectrum. However, the probability that any particular γ-ray will be emitted per decay can be calculated. This is expressed as the "photon abundance" or the number of photons emitted per decay of the parent nucleus, for that particular γ-ray. These are expressions of the relative intensities of the γ-rays produced by the decay of a particular nuclide.

Because nuclear energy levels are all well defined, the energies of the emitted γ-rays are mono energetic for specific

energy level transitions (therefore γ-ray spectroscopy can be used to identify γ-ray emitting nuclei). In the natural radioactive decay series γ-ray energies range between 40 kev and 2600 keV.

Fig. 1.3 Decay of ^{214}Pb as an example of different γ-ray production processes

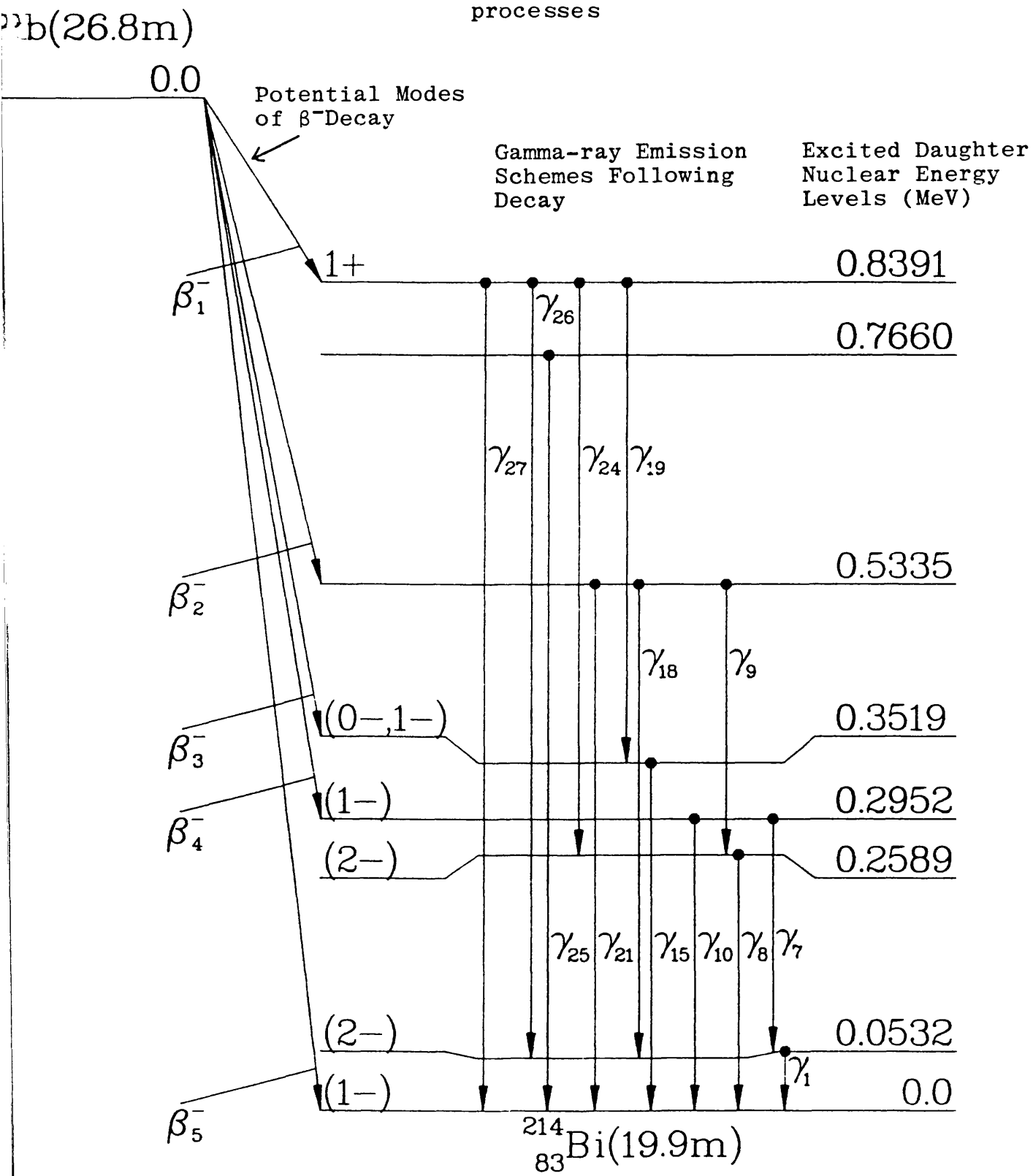

1.3 The Natural Radioactive Decay Series

It is found that most of the naturally occurring radioactive elements are members of three long chains of decay or radioactive decay series. These are named the Uranium, Actinium and Thorium series after the longest-lived nuclides in each series found in nature, $^{238}_{92}U$, $^{235}_{92}U$ and $^{232}_{90}Th$ respectively. As alpha decay results in the loss of 4 mass units from the parent nucleus, while β decay only results in a change in the atomic number, the mass difference between members of a decay chain differ by multiples of 4. For this reason, the mass numbers of all members of the uranium series are multiples of (4n+2) where n is an integer. Therefore the uranium series is sometimes called the (4n+2) series. Similarly, the actinium and thorium series are called the (4n+3) and 4n series respectively because they obey the appropriate mass nuclear relationships. The decay schemes of ^{238}U and ^{232}Th are given in table 1.

It is noticeable that several isotopes can decay in more than one way. For instance, ^{212}Bi can decay either by alpha decay to form ^{208}Tl or beta decay to form ^{212}Po. This is called branched decay. Both branches of the decay will themselves produce the same nuclide, in this case ^{206}Pb.

The half-lives of $^{238}_{92}U$, $^{235}_{92}U$ and $^{232}_{90}Th$ are much larger than those of all their radioactive daughters. This means that secular equilibrium can be established within a uranium or thorium containing mineral provided that the mineral is a

closed system, i.e. there is no gain or loss of parent or daughter nuclides from outside the mineral. When secular equilibrium is reached, the activities of the daughters will equal that of the parent:

$$\lambda_{^{238}U} N_{^{238}U} = \lambda_{^{234}Th} N_{^{234}Th} = \ldots\ldots = \lambda_{^{210}Po} N_{^{210}Po}$$

The time taken to reach secular equilibrium within a rock mineral will be five half lives of the longest lived daughter in each decay series. Therefore equilibrium should be established within uranium and thorium bearing minerals in approximately 1.2 million years (5 x $t_{\frac{1}{2}}$ of ^{234}U).

It is a common assumption that in rocks older than this time, uranium and thorium bearing minerals are in secular equilibrium with their daughters.

The uranium (4n+2) and thorium (4n) decay series are given in Tables (1.1) and (1.2).

Uranium/Radium (4n+2) series

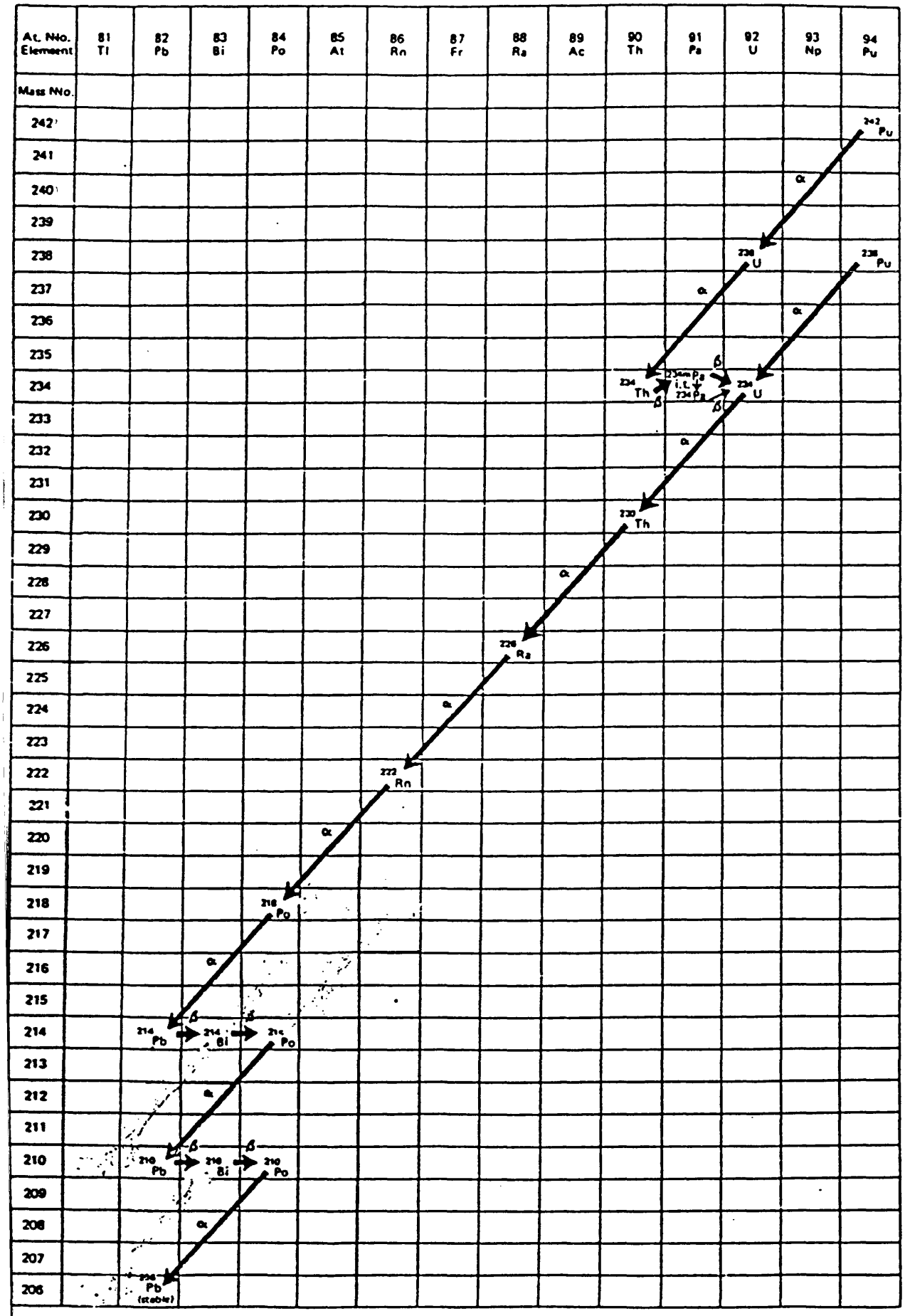

Table I (continued) : Natural Thoruim Decay Series

Uranium/Thorium (4n) series

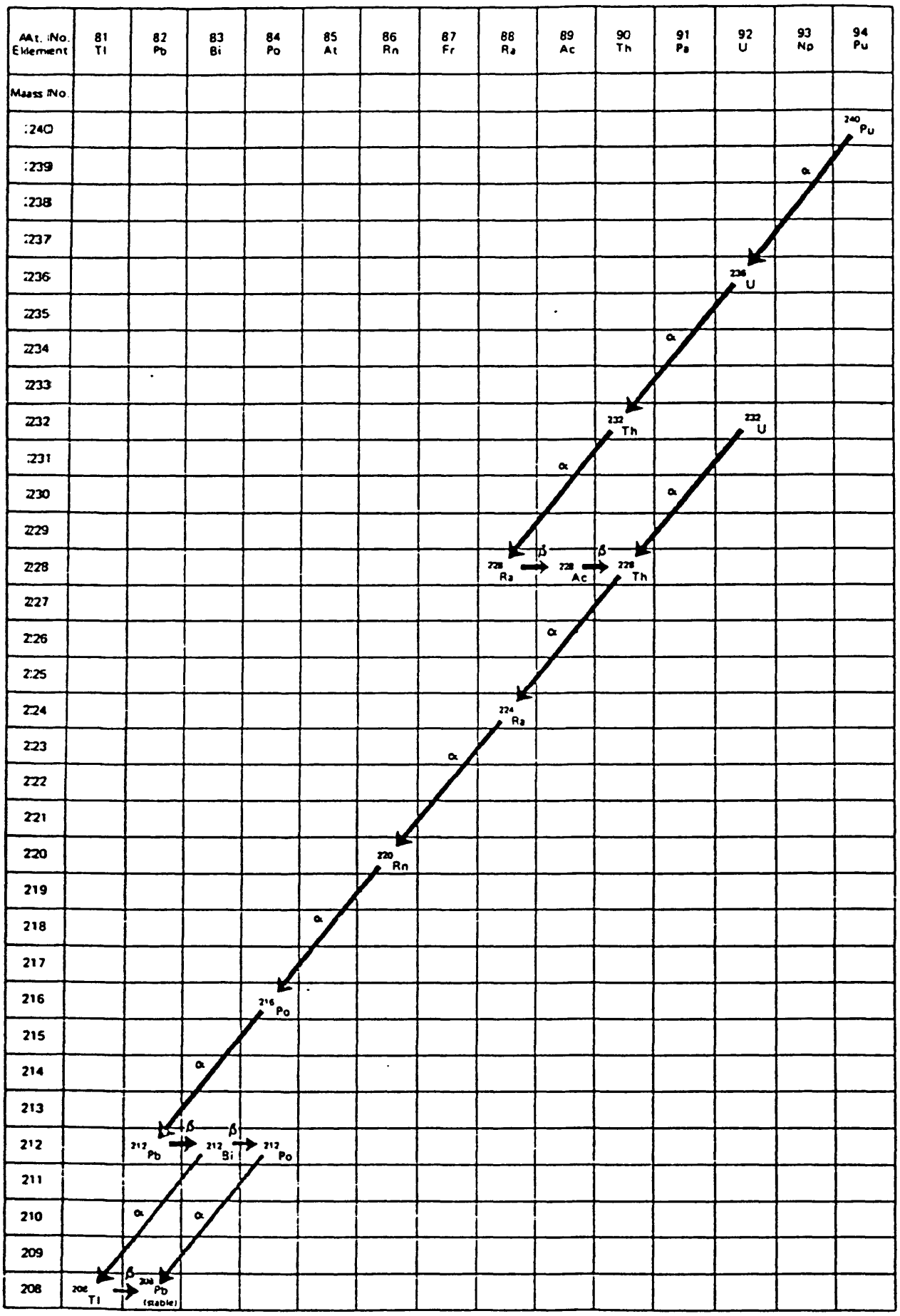

Both tables taken from "The Radiochemical Manual" published by The Radiochemical Centre, Amersham, Buckinghamshire.

1.4 The Geochemistry of Uranium and Thorium

Geologically both uranium and thorium are strongly lithophilic elements, and are closely associated with each other as illustrated by the lack of variation in the crustal rock ratios of 3.5 (Rogers and Adams, 1969).

Their distribution in rocks is dominated by their charge/radius ratios. They readily form solid solutions with each other and with similar elements of a similar ionic size, such as Ce, Zr, Ta, etc., in minerals such as uranothorite, cerianite, zircon and tantalates. Table 1.3 illustrates that they both have similar ionic sizes which explains why they form solid solutions with each other.

Because of their large ionic size, both are precluded from the early crystallising rock forming minerals during magmatic processes, and are instead incorporated into residual fluids resulting in their incorporation into pegmatites and substitute into minerals of rare earths with similar ionic size.

Both occur in the +4 oxidation states however uranium can also be oxidised to the +6 oxidation state as UO_2^{2+}:

$$U^{4+} + 2H_2O \rightleftharpoons UO_2^{6+} + 4H^+ + 2e \quad E^0 = {}^+0.33\ V$$

This is well within the redox potential range in geological environments (Krauskopt, 1967).

The U^{6+} ion is much more soluble than the U^{4+} ion. The U^{4+} species tends to precipitate as coffinite or uraninite $UO_2(S)$. Langmuir (1978) showed that at the pH range of natural waters the predominant U^{4+} dissolved species were

hydroxyl complexes, but that their concentrations tended to be below 0.05 ppb, the detection limit . Uraninite is slightly more soluble in the presence of fluoride ions, but only at pH<4.

Uranium is transported by groundwaters as the uranyl ion, complexed with phosphate, carbonate or fluoride anions, also as the UO_2^{2+} species. The conversion between uranyl and uraneous ions is highly dependant upon Eh and pH conditions. Stability diagrams showing the most stable uranyl and uraneous ions at differing Eh and pH conditions were first constructed by Hostetler and Garrels (1962), and subsequently updated by Langmuir (1978), Fig. 1.4. Such diagrams are constructed from thermodynamic data and can be used to determine the ability of a groundwater to dissolve or precipitate uranium.

Thorium can exist only as Th^{4+} in the natural environment. The mobility of thorium as a dissolved species is limited due to the insolubility of thorium minerals, for instance, thoraninite has a solubility of 0.00001 ppb in pure water. Complexing of $Th^{4+}(aq)$ with ions such as hydroxides and sulphates increases the solubility of thoraninite. This explains why ^{232}Th concentrations of up to 0.00064 ppb have been measured in surface ocean waters (Langmuir and Herman, 1980).

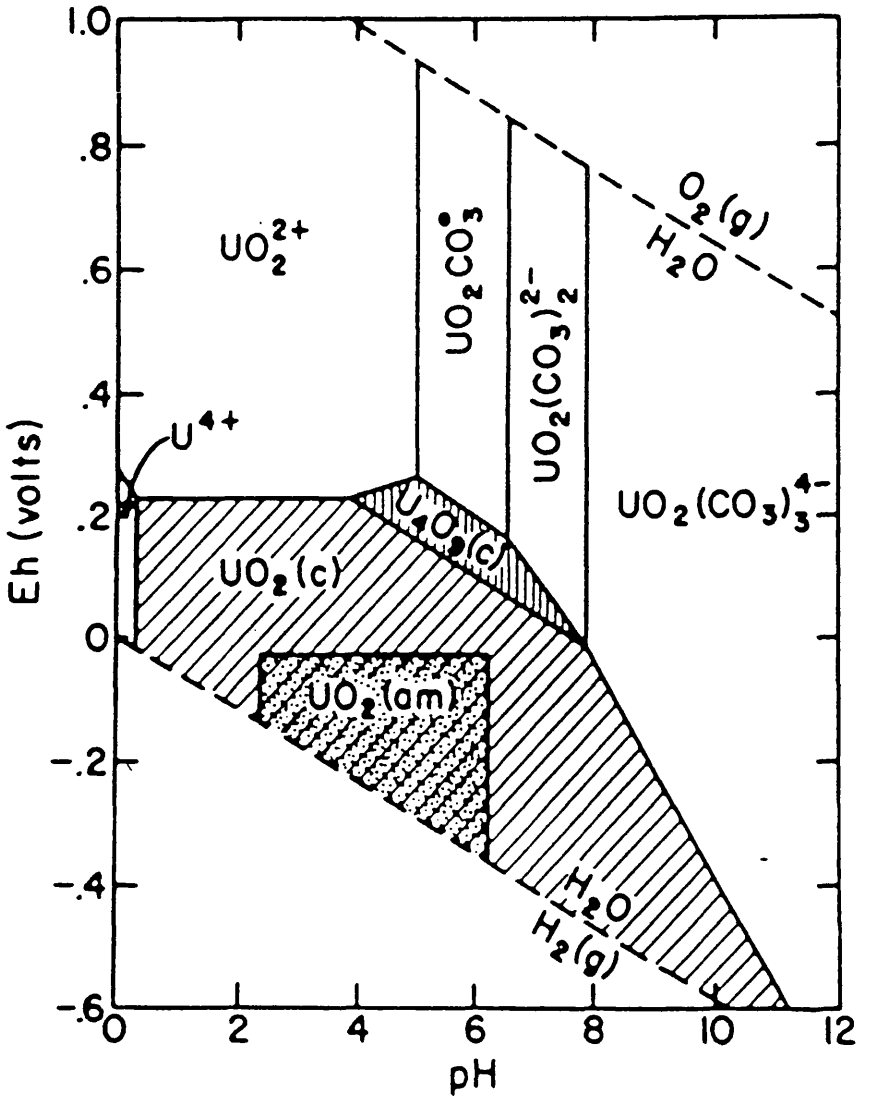

Fig. 1.4 Eh–pH diagram in the $U–O_2–CO_2–H_2O$ system at 25°C for $P_{CO_2} = 10^{-2}$ atm, showing the stability fields of amorphous UO_2[UO_2 (am)], ideal uraninite [UO_2 (c)] and U_4O_9 (c). Solid–solution boundaries are drawn at 10^{-6} M (0.24 ppm) dissolved uranium species.

1.4.1 Uranium and Thorium in Igneous Rocks

Because of their large ionic size, uranium and thorium are incorporated into the late crystallising magmatic fluids which give rise to granites and pegmatites. Senftle and Keevil (1974) showed that the average Th/U ratio in acid igneous rocks was 3.4, whereas in intermediate igneous rocks it was 4.0. This suggests that some differentiation of U and Th can occur in magmatic processes.

Their ionic size also prevents their incorporation into the granitic rock forming minerals such as feldspars and quartz. Instead they are incorporated into the late crystallising minerals of elements with similar ionic size. Substitution into the lattices of minerals such as zircon and cerianite incorporates them into minerals resistant to weathering which are often found in stream beds and alluvial deposits (Plant, 1983).

The geochemistry of thorium is characterised by its similar ionic size to uranium, zircon and the rare earth elements. Thorium is found in 2 independent minerals, thoraninite $(Th,U)O_2$ and thorite ($ThSiO_4$), both of which occur in pegmatites. Thorite is isomorphous with zircon, $ZrSiO_4$, and both uranium and thorium are found incorporated into the minerals isomorphous with zircon.

Thorium is strongly associated with uranium in many uraniferous accessory minerals. Thorianite forms part of a solid solution series with uraninite, UO_2, with thorianite as one end member (Rankama and Sahama, 1950). The close chemical similarity of thorium and the rare-earth elements is reflected in its geochemical association with many rare-

earth minerals, for instance, monazite and allanite contain considerable quantities of thorium.

Uranium is found predominantly as the oxide UO_2. In an amorphous state this oxide forms pitchblende, found in hydrothermal sulphide and arsenide veins. In the crystalline state UO_2 occurs as uraninite, found in granites and pegmatites.

In hydrothermal magmatic stages uranium occurs in high temperature tin veins associated with sulphide and sulphurosalts of nickel, bismuth and arsenic. It also occurs in low temperature sulphide-arsenide veins of cobalt nickel and bismuth.

Secondary uranium compounds are readily produced by oxidation of primary uranium minerals such as uraninite or coffinite, to form secondary phases such as autunite $Ca(UO_2)_2(PO_4)_2$, torfenite $Cu(UO_2)(PO_4)_2.12H_2O$ and carnotite $K_2(UO_2)_2(VO_4)$. nH_2O. Secondary thorium minerals are rare, but in thorium minerals $(OH)_4$ can substitute for (SiO_4); for instance, thorite, $ThSiO_4$ becomes thorogummite, $Th(SiO_4)_{1-x}(OH)_{4x}$, which is isostructural with the uranium mineral coffinite.

1.4.2 Uranium and Thorium in Sedimentary Rocks

The uranium and thorium content of sedimentary rocks depends upon the mode of formation of the rocks. However, table 1.4 illustrates that uranium and thorium are depleted in sedimentary rocks compared to the igneous rocks from which they are generally derived.

Primary uranium and thorium bearing minerals resistant to chemical weathering, such as monazite and euxenite, may be reduced by attrition in clastic sediments. However zircons may be highly resistant to mechanical attrition and may accumulate in placer deposits and in clastic sediments.

Pitchblende and uraninite in igneous rocks may be readily converted to soluble uranyl salts. These secondary minerals are highly soluble, especially in the presence of carbonate ions. The uranyl ion may be precipitated by a number of anions such as phosphate and vanadate, particularly when waters contain low HCO_3^- and CO_3^{2-} ions (Dall'Aglio et al., 1974).

Reduction of uranyl ions to uranate may be accomplished by the presence of organic matter, H_2S or pyrite in sediments. Sufficient quantities of uranium may be present to form economic ore deposits. Because of its oxidative-reductive behaviour, fluctuating redox conditions cause uranium deposits to "roll" away from the zone of most intense oxidation to form "roll front" uranium deposits (Adler, 1974).

In seawater, phosphate ions will complex with uranium to form ions such as $(UO_2HPO_4)_2^{2-}$. The precipitation of such complexes has led to substantial quantities of uranium incorporated into phosphate deposits.

Both uranium and thorium are readily adsorbed onto clay minerals and ferric oxyhydroxides and onto silica gels. Uranium is also adsorbed onto organic material, which accounts for its high content in organic rich shales and some peat and lignite deposits.

Thorium is unable to form soluble complexes and is therefore transported mainly in clastic and resistite minerals. However Langmuir and Hem (1980) showed that thorium can be complexed by organic compounds such as E.D.T.A. However, its strong adsorption in the geological environment is illustrated by its high content in bauxite, pelagic clays and shales (Rogers and Dan, 1969).

Table 1.3 Physical properties of U and Th and some of their daughters

Element	Z	Oxidation state	Ionic radii (A)	q/r*
U	92	4+ 6+	0.93	4.30
Th	90	4+	0.90	4.44
Ac	89	3+	1.11	2.70
Ra	88	2+	1.52	1.32
Pb	82	2+	1.32	1.52

*Charge/radius ratio
from Ivanovich and Harmon (1982)

Table 1.4 The normal range of U and Th and the Th/U ratio in different rock types.

Rock Type	Name	U (ppm)	Th (ppm)	Th/U
Igneous	granite granodionite rhyolite	2.2-6.1	8-33	3.5-6.3
	gabbro	0.8	3.8	4.3
	basalts	0.1-1.0	0.2-0.5	2-4.3
	ultramafics	<0.015	<0.05	variable
Metamorphic	eclogite granulite	0.3-3.0	0.2-0.5	2-4.3
	gneiss	2.0	5-27	1-30
	schist	2.5	7.5-19	>3
	slate	2.7	7.5	2.8
Sedimentary	orthoquartzite	0.45-3.2	1.5-9	1.6-3.8
	greywackes	0.5-2.0	1-7	∿2
	shales: grey-green	2-4	10-13	2.7-7
	black	3-1250		low
	bauxite	11.4	49	∿5
	limestones	∿2	0-2.4	<1
	phosphates	50-300	1-5	<0.1
	ocean sediments	0.7-4	1-30	0.4-10
	peat	1-12	1-5	<1
	lignite	<50-80	-	-
	coal	<10- 6000	-	-

from Ivanovich and Harmon (1982)

1.5 Uranium and Thorium Decay Series Disequilibrium in Groundwaters

The previous section showed that uranium and thorium are widely distributed within lithospheric rocks, and that in most rock matrices they should be in secular equilbrium with their decay daughters.

Within aquifer systems, aquifer rocks are in intimate contact with circulating groundwaters. A variety of physical and chemical processes occur at the water-rock interface. Under these conditions U and Th series decay daughters at the water-rock interface can be removed into solution at different rates depending upon their physical and geochemical characteristics, and also upon their half-lives.

Once in solution, several processes such as cation exchange, co-precipitation, surface adsorption and decay in solution affect the dissolved species of radionuclides. Thus the solution of decay daughters from rock matrices is strongly influenced by their physico-chemical properties. Unlike like the rock matrices, groundwaters will be in radioactive disequilibrium with respect to decay series nuclides.

There are two important applications of the study of radioactive disequilibrium in groundwaters:

1. Hydrologically important information, such as the rate of mixing between different groundwaters, the presence of reducing barriers, the presence of uranium ore deposits and perhaps the groundwater age, may be determined.

2. Study of the mobility of the nuclides themselves is important due to the concern over the health hazards they pose. They may also provide information concerning the behaviour of similar elements which may be released into aquifers as a result of industrial pollution or accidental release of nuclear waste products into aquifers.

The type of information that can be obtained by studying a particular nuclide is dependant upon the nuclide's geochemical characteristics. The following discussion is a short review showing how the geochemical properties of uranium and radon have been used to provide hydrological information.

1.5.1 Application of Uranium nuclides in hydrology

Uranium is readily leached from aquifer rock matrices in oxidising groundwaters, such as those commonly observed in shallow groundwater aquifers. Under these conditions uranium may be conservative in nature. The $^{234}U/^{238}U$ activity ratio under these conditions is commonly greater than 1 due to leaching of ^{234}U from radiation damaged sites (Rosholt et al., 1961) or by direct α-recoil of ^{234}Th, the precursor of ^{234}U, into solution.

The combined effect of recoil and leaching has been investigated by Andrews and Kay (1978). The leaching was assumed to be a first order surface etch with different rate constants for ^{234}U and ^{234}Th. The α-recoil model was a modified version of that given by Kigoshi (1971):

$$^{234}U/^{238}U = \frac{0.235R\rho\ ^{238}U\,^{238}\lambda(1-e^{-^{234}\lambda t}) + {}^{234}k\,^{234}\lambda\,^{234}U \cdot t}{^{238}k\,^{238}\lambda\,^{238}U\ t} \qquad (1.24)$$

where:

t = reaction time

$^{238}\lambda, ^{234}\lambda$ = decay constants of ^{238}U and ^{234}U

^{238}U = number of atoms ^{238}U/g rock

R = recoil range of ^{234}Th

ρ = rock density

$^{238}k, ^{234}k$ = effective rock surface etch rates (for ^{238}U and ^{234}U).

This simplifies to:

$$^{234}U/^{238}U = \frac{0.235R\rho(1-e^{-^{234}\lambda t})}{^{238}kt} + \frac{^{234}k}{^{238}k} \qquad (1.25)$$

For $^{238}k = {}^{234}k$ this study showed that alpha-recoil can only be significant at very low etch rates ($<10^{-10}$cm y^{-1}), but at these etch rates the dissolved ^{238}U content of waters would be very low. Instead a preferential etch of ^{234}U, i.e. $^{234}k > {}^{238}k$, accounts for uranium activity ratios in oxidising groundwaters (Fig. 1.5). This effect has been illustrated by investigations of the oxidised groundwaters in the East Midlands Triassic Sandstone (Andrews and Kay, 1983).

As groundwaters with an enhanced uranium activity ratio move away from the oxidising recharge zone, chemical etching may decrease leading to decay of the 'excess' unsupported ^{234}U. This has been shown for the Tertiary Triassic sediments in Nebraska (Spalding et al., 1984). It was shown in this study that the uranium content and the uranium activity ratio decreased with increasing total dissolved solids. (Figure 1.6).

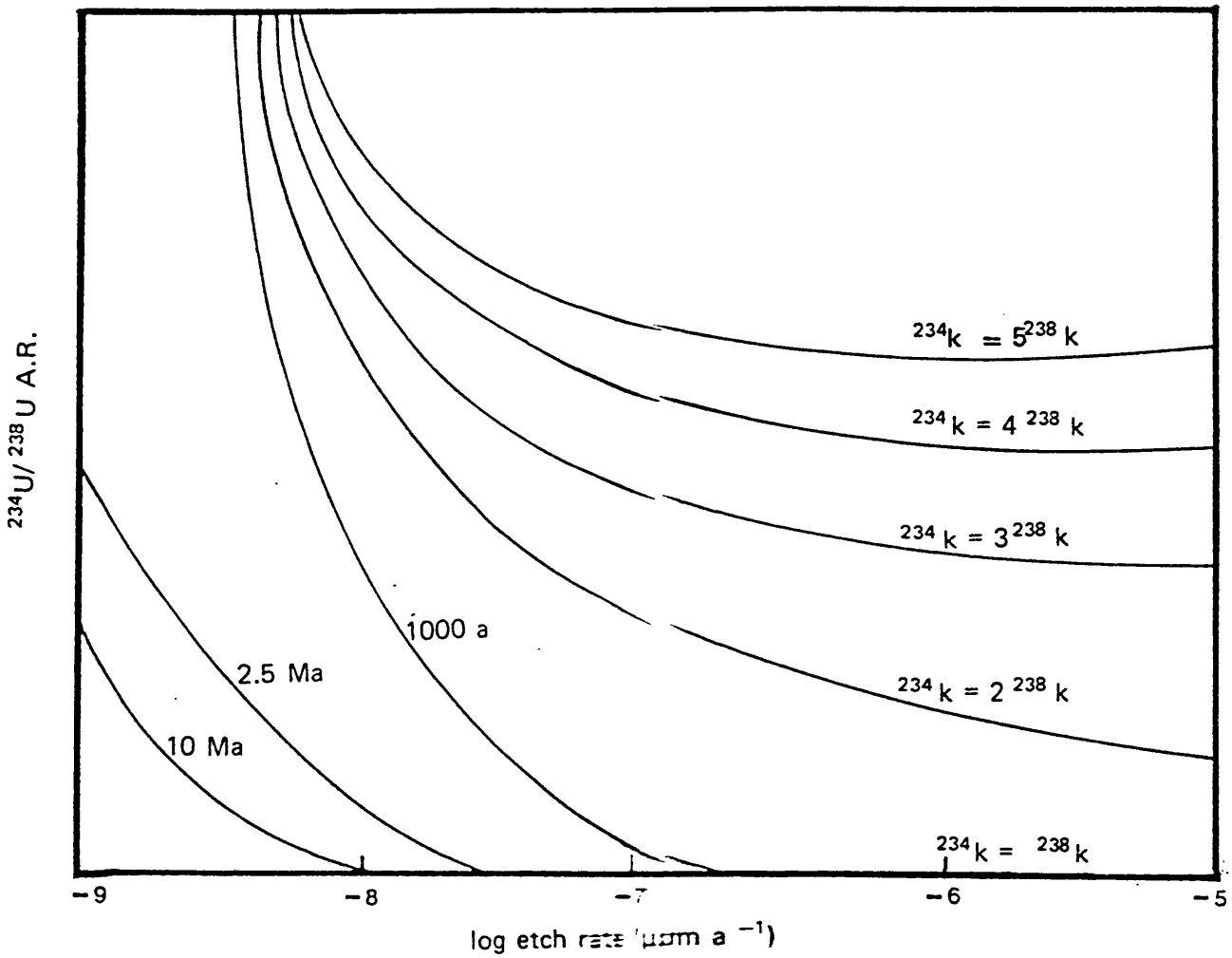

Fig 1.5 Evolution of Groundwater $^{234}U/^{238}U$ recoil and etch using Equation 1.25

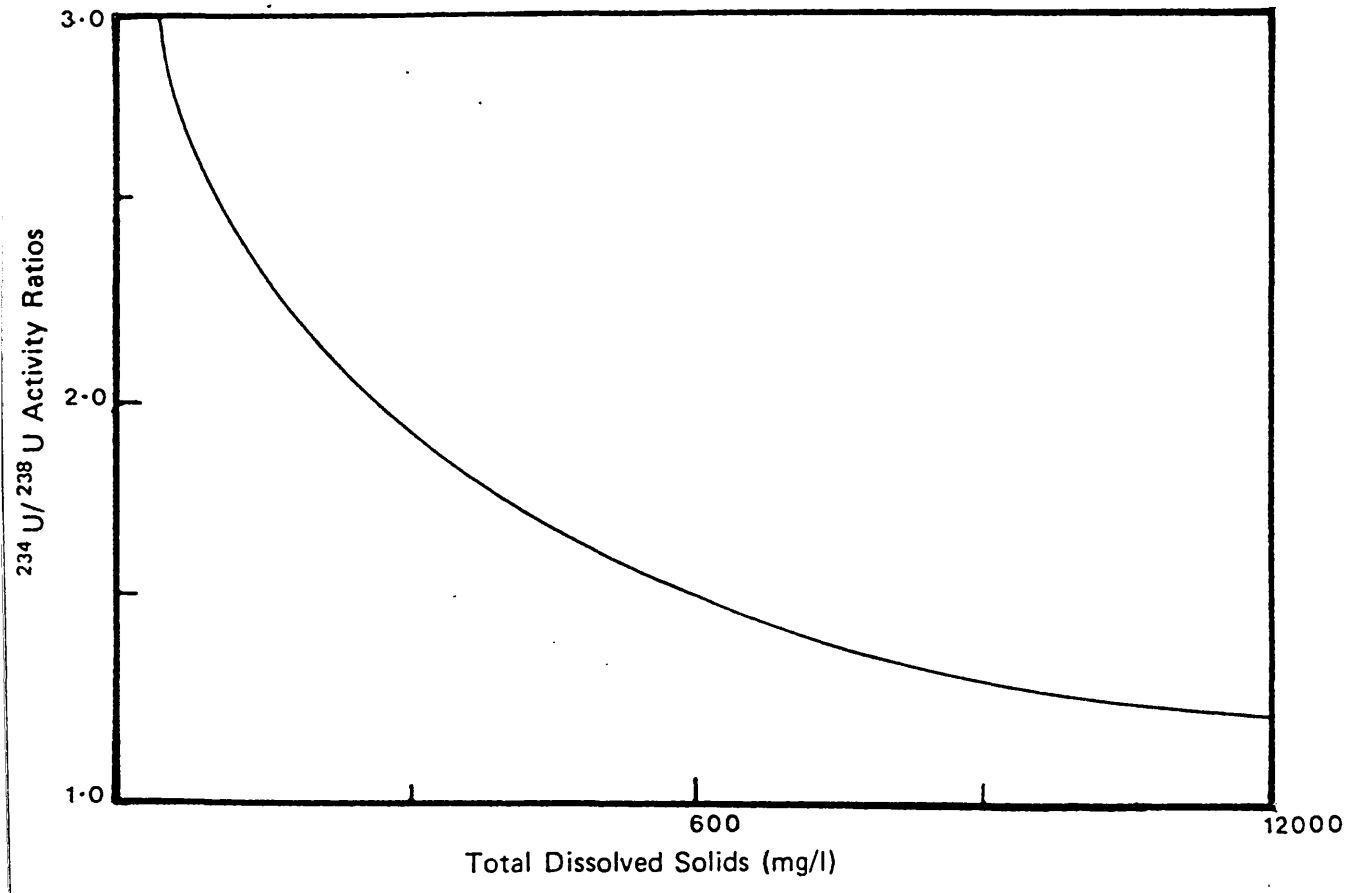

Fig 1.6 Decreasing Uranium A.R.'s with Increasing T.D.S. in the Tertiary Sediments of Nebraska

Assuming that there was no leaching or recoil of additional uranium isotopes, groundwater ages of ~167,000 years were calculated using the equation:

$$AR_t = 1 + (AR_i - 1)\, e^{-\lambda t} \qquad (1.26)$$

where AR_i = initial $^{234}U/^{238}U$ activity ratio

AR_t = activity ratio at time t

t = reaction time

However leaching/recoil can continue away from the recharge zone. Thus the activity ratio may be enhanced along the direction of flow. Evolution of AR's due to recoil supply can be modelled by the equation (Andrews et al., 1982):

$$AR_t = 1+(AR_i-1)e^{-\lambda t} + 0.235\rho [U]_R SR(1-e^{-\lambda t})/[U]s \qquad (1.27)$$

where ρ = rock density

S = surface area/unit volume water

R = recoil range of ^{234}Th

$[U]_R$ = activity of uranium per gram rock

$[U]_s$ = activity of uranium in the water

High activity ratios can only be generated when there is a low initial uranium content and a long groundwater residence time, and when chemical etching has ceased (the groundwater moves to reducing conditions and precipitates U).

However attempts to apply these equations to determine groundwater residence times are limited due to continued uranium etching, especially in waters where uranyl carbonate is stable, and also due to groundwater mixing, as between fracture and interstitial water as demonstrated for Lincolnshire Limestone groundwaters (Andrews and Kay, 1982).

Apart from groundwater dating, other potential uses of uranium isotopes in hydrology are the determination of groundwater mixing volumes and locating certain types of uranium ore bodies. The last application was proposed by Osmond and Cowart (1974) for Sandstone Uranium ore deposits. These deposits are formed when oxidising groundwaters become reducing at depth and precipitate uranium. The groundwaters in such reducing conditions will have high uranium activity ratios and low dissolved uranium content ratios.

Osmond and Cowart (1974) showed that the Eocene Carrizo sandstone aquifer of Texas displayed high uranium contents (>1 µg/ℓ) and low uranium ARs (∿1) in oxidising waters close to recharge, and high uranium ARs (∿9) and low U concentrations (<0.01 µg/ℓ) at a reducing 'barrier' (Fig. 1.7) which they said resulted from recoil supply of ^{234}U from uranium coated onto the surface of mineral grains.

1.5.2 Applications of ^{222}Rn to hydrology

Radon is potentially useful as a geochemical tracer due to its chemical inertness. Its activity in waters is controlled only by the rate of supply by recoil decay of ^{226}Ra on aquifer rock surfaces and by its decay in solution. However its short half-life, 3.8 days, means that its usefulness as a hydrological tracer is limited.

The fact that ^{222}Rn is produced only by α-recoil has been used by Krishnaswami et al. (1982), as an indication of the

Fig. 1.7 Uranium Concentration and Activity Ratio Variations along the Eocene Carrizo Sandstone Aquifer, Texas.

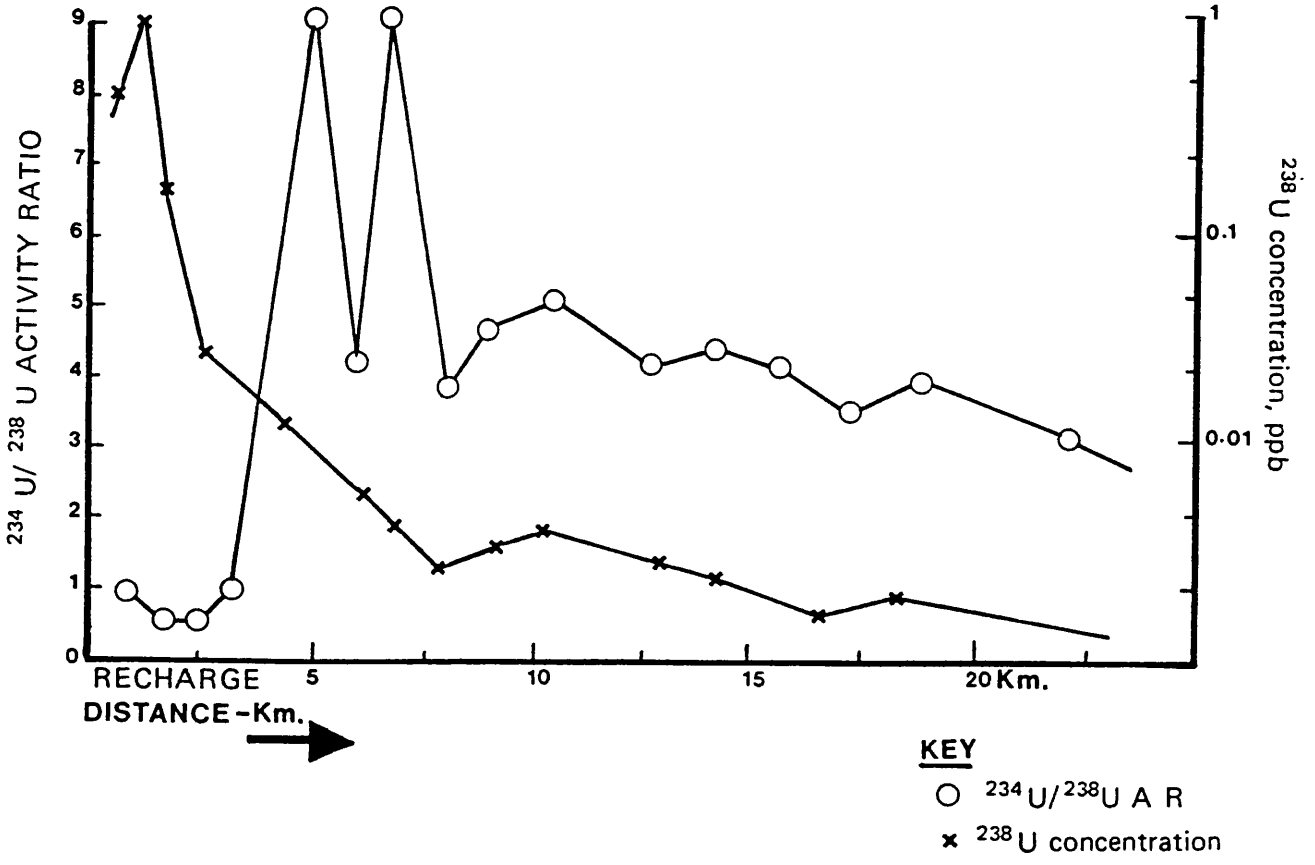

α-recoil supply rates of other elements in the uranium decay series. The reasoning is that the ^{222}Rn activity is a maximum after 21 days according to the equation:

$$A_t = Ae(1-e^{-e\lambda t}) \qquad (1.28)$$

where λ = decay constant for ^{222}Rn

t = reaction time

Ae = equilibrium activity

A_t = activity at time t

Therefore for a groundwater residence time greater than 21 days ^{222}Rn will have reached its equilibrium value. The radon activity may then be used to determine the recoil rate of other nuclides using the equation:

$$Fi = \left(\frac{FrQi}{Qr}\right)\varepsilon \qquad (1.29)$$

where Fi = recoil supply rate of nuclide i to groundwater

Fr = recoil supply rate of ^{222}Rn to groundwater

Qi, Qr = production rate of nuclide i and ^{222}Rn in the aquifer solids

ε = recoil rate of i divided by the ^{222}Rn

However these assumptions neglect the findings of Andrews and Wood (1972) who showed that radon diffuses along mineral fracture planes. Rama and Moore (1984) showed that abundant 'nucleopores' exist even in sand grains which would absorb nuclides other than radon. Both these observations show that mechanisms exist whereby radon can escape into bulk groundwater and other nuclides become adsorbed on aquifer rock surfaces.

However, ^{222}Rn transport in groundwaters can be adequately modelled. Andrews and Wood (1972) showed that the ^{222}Rn activity in the loosely packed Midford Sand aquifer could be modelled using the equation:

$$^{222}Rn = a \frac{\rho [Ra]}{f} (1-e^{-\lambda x/N})(e^{-\lambda x^1/v^1}) \qquad (1.30)$$

where

^{222}Rn = radon concentration

ρ = aquifer solids density

$[Ra]$ = ^{226}Ra content of the aquifer solids

f = fractional pore space in the sands

λ = decay constant for ^{222}Rn

x, x^1 = distance of water travel through the sands

v, v^1 = transport velocity of water within the sand beds

a = ratio of equilibrium content of ^{222}Rn in the water to ^{226}Ra activity in the sands

Predicted ^{222}Rn activities ranged from 300 - 600 pCi/ℓ compared to the ∿480-560 pCi/ℓ actually found.

Models such as this for radon transport in groundwaters are rare; investigations are usually qualitative not quantitative. However, an interesting application for radon measurements is the fact that radon increases in groundwaters during an earthquake. Figure 1.8 shows that the ^{222}Rn activities increased during an earthquake in the Tashkent Basin (Ulomov and Mavashev, 1967). This phenomenon may be related to the fact that increased fracturing produces high surface area/water volume ratios during an earthquake; this favours increased recoil production into solution.

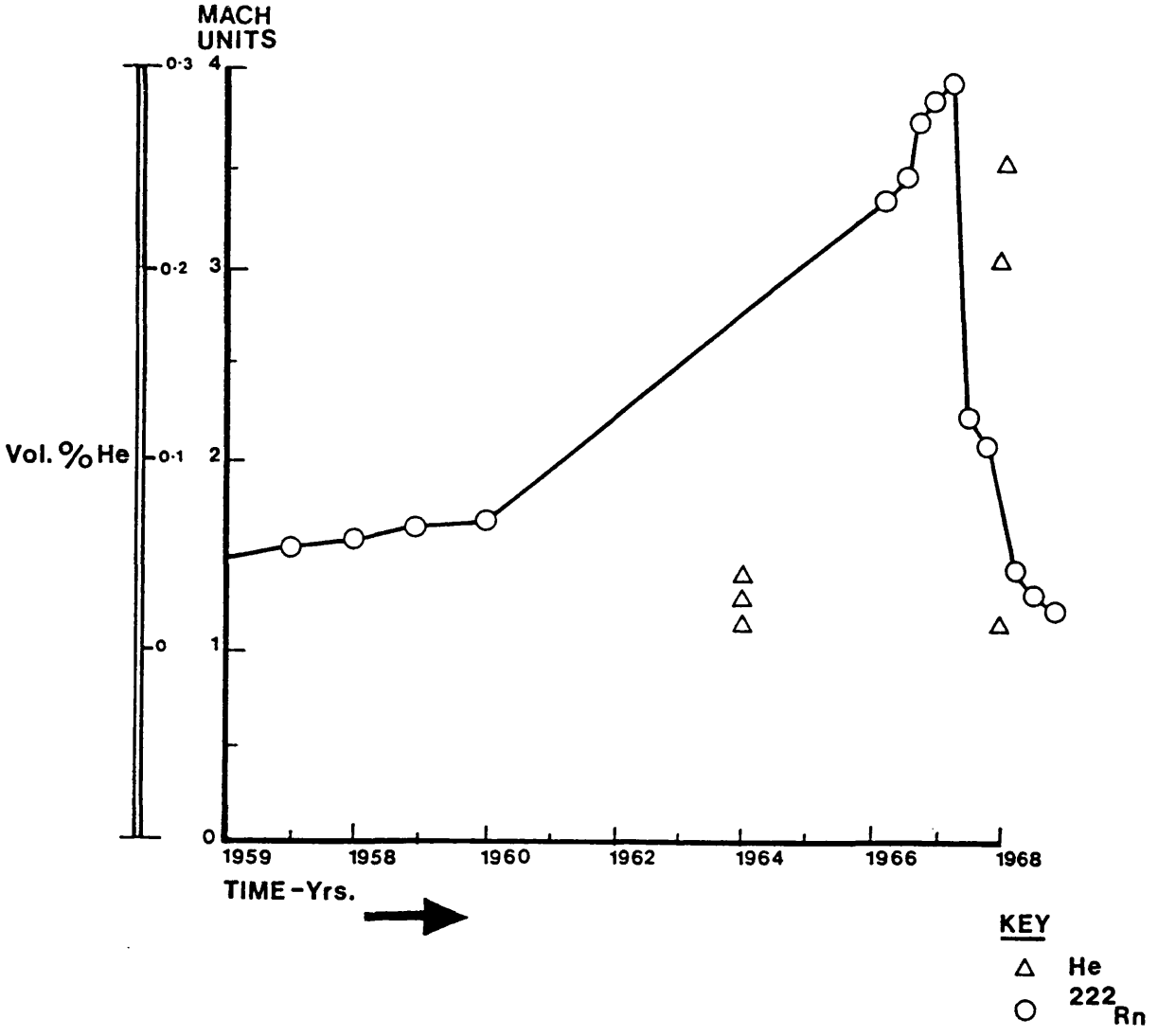

Fig. 1.8 Radionuclide variation during a Tashkent Basin earthquake (from Ulomov and Mavashev, 1967).

Note: The translation from Russian quotes ^{222}Rn in "MACH" units which do not appear to relate to pCi or Bq. Also, no ^{222}Rn measurements were performed between 1960 and 19-5, which makes the extrapolation between these dates tenuous.

1.6 Geochemistry of Radium

1.6.1 General Chemistry

Radium is a member of the group II or alkali earths in the Periodic Table of elements. These elements are highly electropositive and are therefore strongly ionic in character. The general chemistry of radium is consistent with its position as the last member of the group and hence the most electropositive. This is seen in Table 1.5 which shows that the high electropositivity of radium is caused by the low charge/radius ratio which makes it very difficult to polarise. The group trends are that the sulphates, nitrates and chlorides decrease in solubility down the group while the solubilities of the carbonates increase.

The element with the most similar chemistry to radium is barium. This explains why radium and barium show similar behaviour in the environment; for instance, the ratio between ^{226}Ra and Ba in the Galapagos Drift hydrothermal waters was shown to be the same as the ^{226}Ra/Ba ratio in the host basalts (Krishnaswami and Turekian, 1982). Similarly, desorption of barium from river borne sediments in the Amazon estuary have been shown to correlate to desorption of radium isotopes from those sediments.

Table 1.5 Ionic radii of group II cations in Octahedral coordination

Cation	"Effective" ionic radii (A)*
Ca^{2+}	1.12
Sr^{2+}	1.26
Ba^{2+}	1.42
Ra^{2+}	1.48

* Obtained from Shannon (1976). The value is different for radium from Table 1.3 as these values represent the radii within a crystal lattice rather than the bare ion.

1.6.2 Radium hydrochemistry

The natural decay series produce four radium isotopes: ^{224}Ra ($t_{\frac{1}{2}}$ = 3.64 days) and ^{228}Ra ($t_{\frac{1}{2}}$ = 5.74 years) in the thorium (4n) series, ^{226}Ra ($t_{\frac{1}{2}}$ = 1600 years) in the uranium (4n + 2) series and ^{223}Ra ($t_{\frac{1}{2}}$ = 11.4 days) in the actinium (4n + 3) series. The levels of each isotope present in crustal rocks is dependent upon the amounts of uranium and thorium present within the rock, due to the establishment of radioactive secular equilibrium within the rock.

However, the groundwater activities are unlikely to be the same as those of their uranium and thorium parents due to their differing chemical properties to other elements within the decay series. The activities of the radium nuclides measured in groundwaters will depend upon the extent of processes which supply and remove radium from groundwaters.

1.6.2.1 Processes supplying radium to groundwaters

The supply rate of radium isotopes into groundwaters may be controlled by 3 processes (Krishnaswami et al., 1982):

(i) In situ decay of the dissolved parent nuclide.

(ii) Chemical solution by leaching or dissolution of the aquifer rock.

(iii) Direct recoil across the solid/liquid boundary as a result of radioactive decay of the parent on the rock surface.

In situ decay of the dissolved parent nuclide can be estimated by determining the activities of the dissolved radium parents. However, the immediate parents are ^{230}Th (parent of ^{226}Ra), ^{232}Th (parent of ^{228}Ra) and ^{228}Th (parent of ^{224}Ra). Thorium activities in groundwaters are generally very low due to the insolubility of its hydroxide and high rate of adsorption on aquifer solids. Therefore in situ production is considered a negligible source of radium activities in groundwaters.

Chemical solution (also termed weathering or leaching) is highly dependent upon the salinity of the groundwater. This is illustrated by high ^{228}Ra, ^{226}Ra and ^{224}Ra activities in saline seepages in Western Australia (Dickson et al., 1985) and numerous observations of high radium activities in oil field brines and formation waters (Bloch and Key, 1981). The saline seepages study showed that laboratory leaching of uranium ore with NaCl solution resulted in ^{224}Ra, ^{228}Ra, ^{226}Ra and ^{223}Ra entering solution in the same ratios as the $^{223}Ra/^{226}Ra$, $^{224}Ra/^{228}Ra$ and $^{228}Ra/^{226}Ra$ ratios of the uranium ore. This was consistant with the radium activity ratios in the groundwaters of a similar salinity, which also reflected the radium activity ratios of the aquifer rock. The absolute rates of chemical solution are difficult to quantify. They will depend upon the resistance of minerals containing uranium and thorium to chemical leaching, and the ability of the groundwater to leach or dissolve these minerals.

Recoil ejection of radionuclides from minerals into solution was first observed by Kigoshi (1971). The recoil process occurs because the momentum imparted to the alpha particle ejected during decay must be balanced by an equal and opposite momentum imparted to the daughter nuclide. Enough energy is generated in decay to allow the recoiling daughter to travel distances of a few angstrom units. If decays in rock matrices occur close to the water/rock interface, then this can result in the ejection of the daughter nucleus into water.

For a plane surface the rate of alpha recoil into water at the water/rock interface is given by:

$$\frac{dN}{dt} = \tfrac{1}{4}LS\rho\left[^{238}U\right] \qquad (1.31)$$

Where L is the recoil range of the daughter nucleus, N is the number of atoms at time t, S is the surface area of rock in contact with unit volume of water, ρ is the rock density. The activity/gram rock of the parent nuclide is given as $\left[^{238}U\right]$. In general the activity of the parent nuclide/gram rock is given as the activity of uranium or thorium because radionuclides are assumed to be in secular equilibrium within the rock.

Although it is theoretically possible to calculate recoil supply rates, in practice the aquifer porosity, surface area of aquifer solids, recoil ranges and rock radio-element contents are rarely available. Attempts have been made to calculate radium nuclide residence times in

groundwaters assuming that the activity of ^{222}Rn represents the alpha recoil production rate of uranium series radioelements (Krishnaswami, et al., 1982). Radon is an inert gas not subject to chemical processes such as adsorption. Its groundwater activities are too large to be supplied by rock dissolution, therefore it should be supplied by alpha recoil. Provided that groundwater residence times are greater than ~21 days so that an equilibrium state is reached where the rate of recoil supply equals the rate of radon removal by decay, then groundwater radon activities will equal the recoil supply rate of radon. Radium nuclide residence times were calculated by Krishnaswami et al., (1982) using radon as a measure of recoil production in the uranium series, and assuming that the recoil flux in the thorium series is given by

$$^{232}\text{Th series alpha-recoil flux} = A_{^{222}Rn} \times \left(\frac{Th}{U}\right)$$

where Th is the activity/gram of ^{232}Th and U is the activity of ^{238}U/g rock.

However, because of radon diffusion along grain boundaries and adsorption of nuclides in nanopores, the residence times that they obtained must be regarded as a minimum estimate of true residence times.

Cherdyntsev (1971) has shown that laboratory tests with radioactive minerals resulted in accumulation of ^{223}Ra and ^{224}Ra in solution obeying the relationship:

$$At = Ae\ (1-e^{-\lambda t}) \qquad (1.32)$$

where At is the activity at time t, Ae is the equilibrium activity and λ is the decay constant for that radionuclide.

This equation implies α-recoil production of radium nuclides into solution. Assuming that radioactive decay is the only process removing radium from solution, then the following mass balance equation can be established: for ^{226}Ra

$$\frac{dN_{226}}{dt} = \tfrac{1}{4}LS\rho\,[U] - \lambda N_{226} \qquad (1.33)$$

where N_{226} is the concentration of ^{226}Ra in solution. Integrating with respect to time:

$$\lambda_{226}N_{226} = A_{226} = \tfrac{1}{4}LS\rho[U]\ (1-e^{-\lambda_{226}t}) \qquad (1.34)$$

where A_{226} = activity of ^{226}Ra in solution.
Comparing Equation 1.34 with (1.32) gives the relationship:

$$Ae = \tfrac{1}{4}LS\rho\,[U]$$

The equilibrium radium activity is therefore equal to the α-recoil production rate. If radium nuclides are produced by α-recoil in groundwaters then the $^{223}Ra/^{226}Ra$ and $^{224}Ra/^{228}Ra$ activity ratios in very 'young' groundwaters would be very high due to the slow rate of accumulation of long-lived radium nuclides.

1.6.2.2 Speciation of Radium in Groundwaters

When radium has reached solution by processes such as rock dissolution, selective leaching or α-recoil, it can be removed by processes such as adsorption on clay minerals and ferro-manganese oxyhydroxide minerals or co-precipitation with rare-earth minerals. However, radium may also complex with groundwater ligands to produce soluble aqueous complexes which will increase radium solubility and mobility.

Modelling of radium speciation requires accurate thermodynamic data of aqueous radium complexes and ion-pairs in solution. Such data has been limited until Langmuir and Riese (1985) empirically calculated the enthalpy, Gibbs free energy and entropy of formation of aqueous radium species.

The thermodynamic properties of $RaOH^+$, $RaCl^+$, $RaCO_3^o$ and $RaSO_4^o$ were derived by plotting alkali earth thermodynamic properties against effective ionic radii (Shannon, 1976) and extrapolating to determine radium species data. The results are given in Table 1.6.

Surprisingly, the thermodynamic properties of $RaHCO_3^+$ were not determined even thought the bicarbonate complex is important in the chemistry of other alkali-earth elements. Therefore the thermodynamic properties of $RaHCO_3^+(aq)$ were determined in this study by using the methods proposed by Langmuir and Riese (1985). The association constants for $MgHCO_3^+(aq)$, $CaHCO_3^+(aq)$,

Table 1.6 Formation constants and solubility products of radium complexes and solids, and enthalpies of reaction at 25°C.*

	Reaction	log Kassoc or logKsp	ΔH^o (Kcal/mole)
1.	$Ra^{2+} + OH^- = RaOH^+$	0.5	1.1
2.	$Ra^{2+} + Cl^- = RaCl^+$	-0.1	0.5
3.	$Ra^{2+} + CO_3^{2-} = RaCO_3^0$	2.5	1.07
4.	$Ra^{2+} + SO_4^{2-} = RaSO_4^0$	2.75	1.3
5.	$RaCO_3(S) = Ra^{2+} + CO_4^{2-}$	-8.3	-2.8
6.	$RaSO_4(S) = Ra^{2+} + SO_4^{2-}$	-10.26	-9.4
7.	$Ra^{2+} + HCO_3^- = Ra\ HCO_3^+$	1.67	6.05

*From Langmuir and Riese (1985), except for $RaHCO_3^+(aq)$, see text.

$SrHCO_3^+(aq)$ and $BaHCO_3^+(aq)$ have been listed by Busenberg et al (1984). These were plotted against effective ionic radii and the resulting curve extrapolated to give the association constant for $RaHCO_3^+(aq)$ (Fig. 1.9). The results are given in Table 1.6.

However the enthalpys of many alkali-earth bicarbonates are unknown, so the enthalpy of $RaHCO_3^+(aq)$ could not be calculated. The only recourse was to assume that the enthalpy of $RaHCO_3^+(aq)$ was the same as $SrHCO_3^+(aq)$, for which data was available.

Given the thermodynamic data base for radium complexes and the groundwater concentrations of complexing ligands the speciation of radium within a groundwater can be calculated. The approach taken in this study is essentially that of Hem (1981) utilising both mass balance and chemical equilibria calculations.

The concentrations of ligands within groundwaters cannot be directly used in speciation calculation with radium, because they themselves are involved in speciation with other cations. The activity of 'free' ligands were therefore determined by inputing groundwater chemical analysis into the WATEQF computer program (Plummer et al., 1976). This program calculates the distribution of anions and cations within aqueous complexes in the groundwater, and calculates the activity of free ions remaining. Activity and concentrations are related by the expression:

$$a = \gamma m \qquad (1.35)$$

Fig 1.9 Determination of the Association Constant for $RaHCO_3^+$

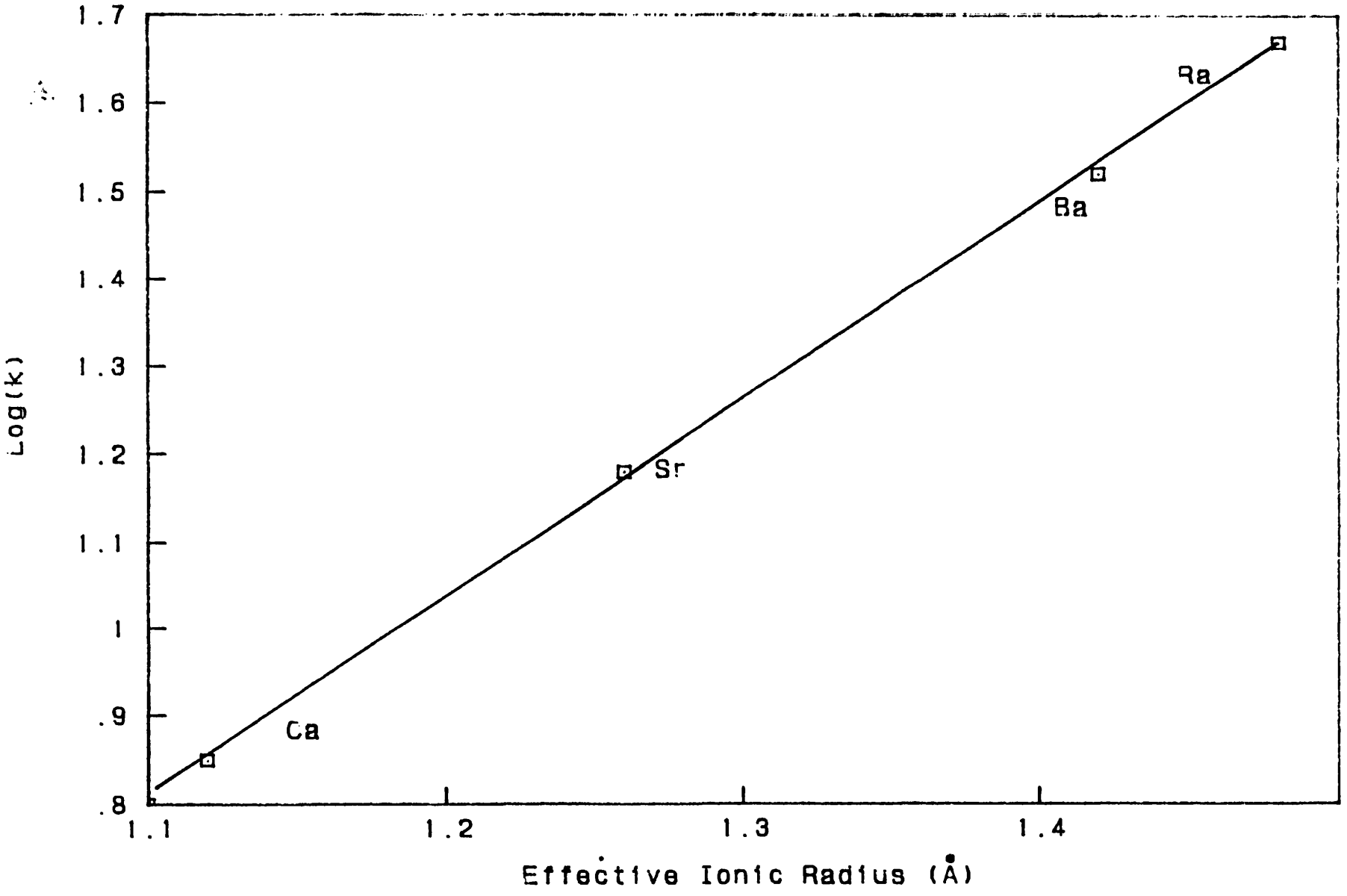

where a is the ion activity

γ is the activity coefficient

m is the ion concentration

The total concentration of radium in solution is the sum of all its dissolved aqueous species. This mass balance is represented by the equation:

$$[Ra]_t = [Ra^{2+}] + [Ra\ OH^+] + [Ra\ Cl^+] + [Ra\ HCO_3^+] + [RaCO_3^0] + [Ra\ SO_4^0] \quad (1.36)$$

where $[Ra]_t$ is the total radium concentration.

It is commonly assumed that groundwaters are in equilibrium with respect to their dissolved constituents. Thus each complexed species is constrained by equilibrium relationships such as:

$$Ra^{2+}(aq) + Cl^-(aq) \rightleftharpoons RaCl^+(aq)$$

This relationship is characterised by an equilibrium association constant:

$$K_{RaCl^+} = \frac{[RaCl^+]}{[Ra^{2+}][Cl^-]} \cdot \frac{\gamma_{RaCl^+}}{\gamma_{Ra^{2+}}\ \gamma_{Cl^-}} \quad (1.37)$$

where K_{RaCl^+} is the equilibrium constant

γ_{RaCl^+}, γ_{Ra^+}, γ_{Cl^-} are the activity coefficients for $RaCl^+$, Ra^{2+} and Cl^- respectively.

Similar expressions can be derived for the complexed species $RaOH^+$, $RaHCO_3^+$, $RaSO_4^0$ and $RaCO_3^0$. The relative importance of each complex in contributing to the total radium concentration is given by its distribution coefficient in solution.

This is expressed by the relationship:

$$\alpha_{Ra^X} = \frac{[RaX]}{[Ra]_T} \qquad (1.38)$$

Where $\alpha_{Ra}X$ is the distribution coefficient for the dissolved species RaX

$[RaX]$ is the concentration of the aqueous species

$[Ra]_T$ is the total dissolved concentration of radium.

The concentrations of aqueous complexes and ion pairs cannot be determined by direct measurement. Instead equilibrium is assumed between dissolved aqueous species, and expressions similar to equation (1.37) substituted into the mass balance equation (1.36):

$$[Ra]_T = [Ra^{2+}]\left\{1 + \gamma_{Ra}\left(\frac{K_{RaCl^+}(Cl^-)}{\gamma_{RaCl^+}} + \frac{K_{OH}(OH^-)}{\gamma_{RaOH^+}}\right.\right.$$

$$+ \frac{K_{RaHCO_3^+}(HCO_3^-)}{\gamma_{RaHCO_3^+}} + \frac{K_{RaCO^\circ}(CO_3^{2-})}{\gamma_{RaCO^\circ}}$$

$$\left.\left. + \frac{K_{RaSO_4^0}(SO_4^{2-})}{\gamma_{RaSO_4^0}}\right)\right\} \qquad (1.39)$$

Combining this expression with (1.38) gives:

$$\alpha_{Ra^{2+}} = \frac{[Ra^{2+}]}{[Ra]_T}$$

$$= \frac{1}{1 + \gamma_{Ra^{2+}}\left(\frac{K_{RaCl^+}(Cl^-)}{\gamma_{RaCl^+}} + \ldots + \frac{K_{RaSO_4^0}(SO_4^{2-})}{\gamma_{RaSO_4^\circ}}\right)} \qquad (1.40)$$

This last equation means that given the activities of Cl^-, OH^-, HCO_3^-, CO_3^{2-} and SO_4^{2-} and the association constants of the aqueous species, it is possible to calculate radium species distribution coefficients. Having obtained $\alpha_{Ra^{2+}}$, the other distribution coefficients can be calculated using relationships such as:

$$\alpha_{RaX} = \frac{[RaX]}{[Ra]_T} = \frac{[RaX][Ra^{2+}]}{[Ra^{2+}][Ra]_T} = \frac{\alpha_{Ra^{2+}} \cdot K_{RaX} (X) \gamma_{Ra^{2+}}}{\gamma_{RaX}}$$

where (X) is the activity of the dissolved anion. (1.41)

The activity coefficients of the groundwater ligands are calculated by the WATEQF program. However the activity coefficients for radium species must be calculated separately. Activity coefficients are normally estimated by using the Debye-Huckel approximations:

$$\log \gamma = \frac{- A Z_i^2 \sqrt{I}}{1+Ba_o \sqrt{I}} \qquad (1.42)$$

where I is the solution ionic strength

A,B are the temperature dependent constants

a_o is the effective ionic radius of the species

Z_i is the charge on the i^{th} species

This approximation is only valid for charged species in solution. Reardon and Langmuir (1976) gave a relationship for uncharged species which was derived experimentally:

$$\log \gamma = -0.5\sqrt{I} \qquad (1.43)$$

The values for the effective ionic radius for radium complexes were obtained from Langmuir and Melchior (1985).

Examples of speciation calculations

Both Langmuir (1978) and Langmuir and Herman (1980) illustrated the importance of uranium and thorium aqueous complexes respectively, by calculating speciation in various "typical" groundwaters. The results were plotted as diagrams representing complex distribution against pH. This approach is taken here. The distributions of aqueous radium species for different water compositions were calculated to establish the relative importance of radium complexes in "typical" natural waters.

Example 1

The distributions of radium complexes in a carbonate system containing a total of 10^{-2} moles total carbonate are shown over the pH range 1-14 in Fig. 1.10.

Below pH5, radium is present as the free Ra^{2+} ion. Between pH5-9, Ra^{2+} still predominates although $RaHCO_3^+(aq)$ is the main complexed species. Above pH 9, the $RaCO_3^0(aq)$ species predominates, although $RaOH^+(aq)$ increases in importance above pH 12.

This shows that the amount of $Ra^{2+}(aq)$ available for adsorption and co-precipitation decreases with increasing pH. Therefore below pH 5, all Ra^{2+} should be readily adsorbed by ion exchange minerals. However, Langmuir and Melchior (1985) stated that competition between Ra^{2+} and H^+ for exchange sites prevented radium adsorption, an observation also made for competitive adsorption between Th^{4+} and H^+ on clay minerals at low pH's (Langmuir and Herman, 1980).

Fig 1.10 Radium Speciation in a Carbonate Groundwater

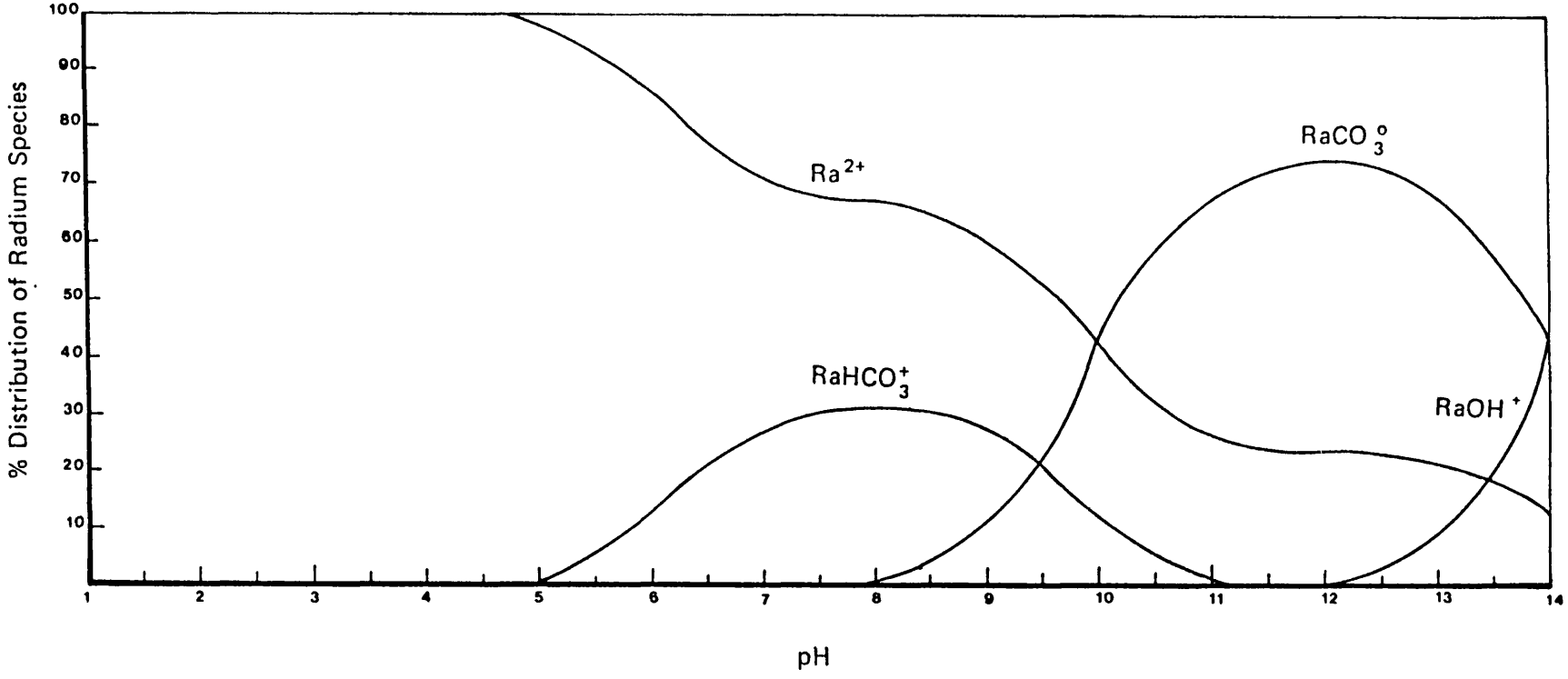

$^{226}Ra = 1$ dpm/l $CO_3^{2-} = 10^{-2}$ moles/l

Ames et al. (1983) showed that radium adsorption increases with increasing pH. This may be explained by the increasing significance of $RaOH^+(aq)$. Stumm and Morgan (1970) commented that $CaOH^+(aq)$ is readily adsorbed due to its decreased hydrated sphere compared to the $Ca^{2+}(aq)$ ion. Lamgmuir and Herman (1980) showed that thorium hydroxide complexes are readily adsorbed. A similar behaviour may also be exhibited by $RaOH^+(aq)$.

Example 2

Tripathi (1974), Langmuir (1978) and Langmuir and Herman (1980) give examples of uranium and thorium speciation in a "typical" groundwater composed of 100 mg/ℓ sulphate, 10 mg/ℓ chloride and 10^{-2} molar total carbonate. The radium speciation for such a groundwater is illustrated over the range pH 1-14 (Fig. 1.11). Chloride and sulphate anions were assumed to be non-ideal and activity coefficients were calculated using the Debye-Huckel relationship.

The results show that although $Ra^{2+}(aq)$ again predominates, a substantial amount of radium is complexed as $RaSO_4^0(aq)$ at all pH values. Therefore the solubility of radium should be increased over Fig. 1.10, where no sulphate ions were present. This contradicts the results of Dickson (1985) who stated that increasing quantities of Na_2SO_4 added to a leaching experiment on uranium ore formed radium sulphate complexes which inhibited radium leaching until "the effects of increasing the cation (Na^+) overcame the sulphate anion".

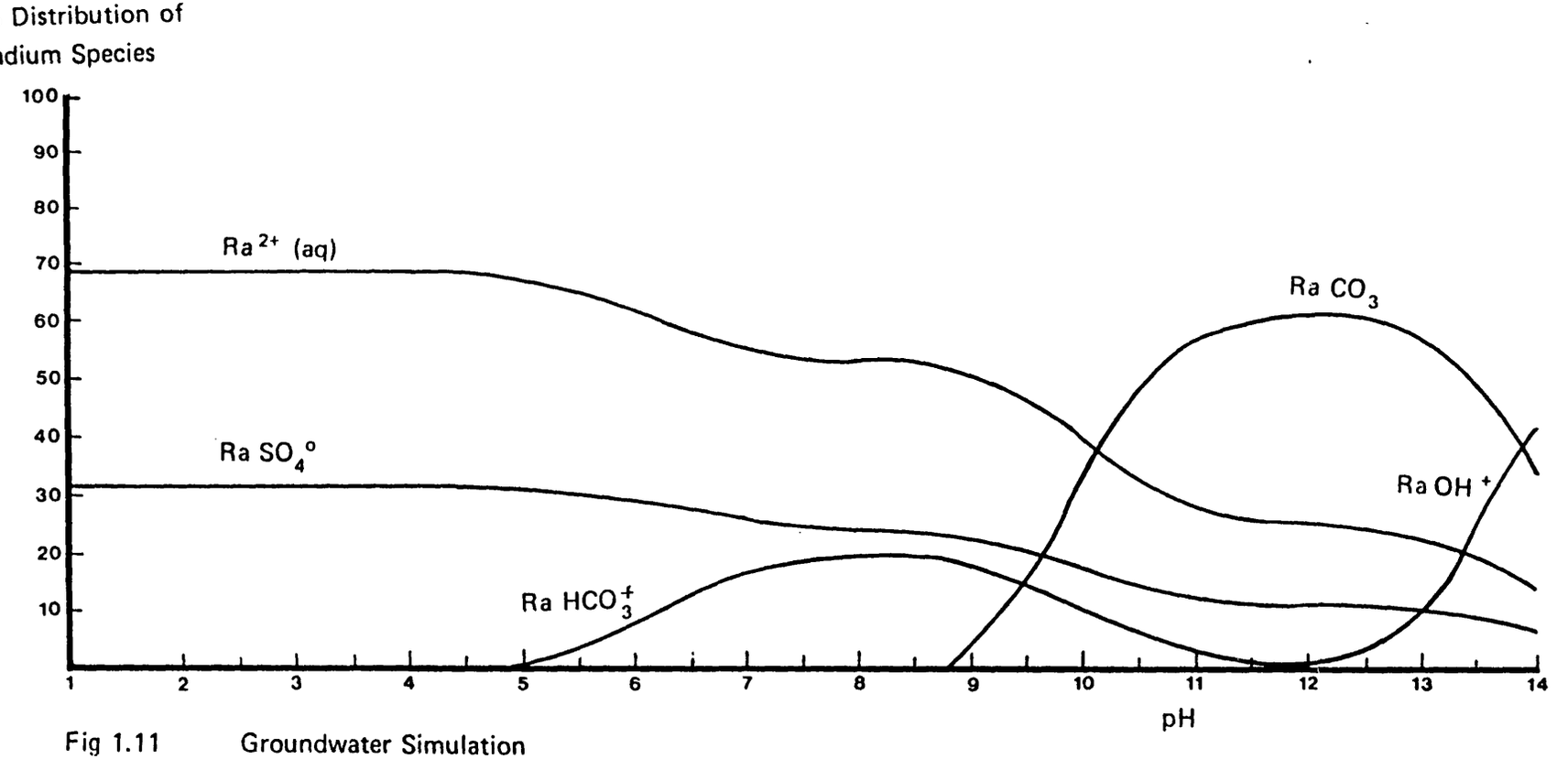

Fig 1.11 Groundwater Simulation

Cl = 10ppm SO_4 = 100ppm, $CO_3 = 10^{-2}$m/l ^{226}Ra = 1 dpm/l

The alternative explanation is possible by observing that in many rock leaching experiments calcium increases in solution until calcite or gypsum precipitates. Addition of Na_2SO_4 in a leach solution may cause calcite or gypsum supersaturation which may remove radium from solution due to co-precipitation.

Despite high (10 mg/ℓ) chloride ion concentration, there is no occurrence of $RaCl^+(aq)$. Bloch and Key (1981) argued that high radium concentrations in oil field brines were due to the formation of soluble radium chloride complexes. This study shows that the association constant for $RaCl^+(aq)$ is so small (Table 1.6) that $RaCl^+(aq)$ can only become important in groundwaters with chloride contents greater than 1000 mg/ℓ.

These calculations depend upon the achievement of thermodynamic equilibrium between radium and dissolved ligands in a groundwater. However they do not take into consideration the kinetic rate at which equilibrium is reached. However the decay of radium isotopes imposes kinetic limits upon the time for equilibrium to be reached.

Using equation (1.32), within 5 half-lives, 99% of a radionuclide dissolved in solution will have decayed. Thus for equilibrium between radium nuclides and solution to be achieved, the rate of complexing must be equal to or greater than the decay rate of the radium nuclide.

Langmuir and Melchior (1985) stated that complexation and adsorption/desorption reactions go to completion within seconds to a few hours. The shortest lived radium nuclide has a half-life of 3.6 days, therefore all naturally occurring radium nuclides must participate in speciation reactions in groundwaters.

1.6.2.3 Processes removing radium from groundwaters

1. Decay of dissolved radionuclides.

Radioactive decay will limit the activity of dissolved radium nuclides when the decay rate is greater than the rate of adsorption onto mineral surfaces or co-precipitation. For instance, the activity of ^{226}Ra in a solution in which decay is the only removal process, is given by equation (1.32)

with:

λ_{226} = decay constant for ^{226}Ra

A_t = activity of ^{226}Ra in solution at time t

Ae = equilibrium activity of ^{226}Ra

The groundwater activity will therefore reach a state of equilibrium after 8000 years (5 x $t_{\frac{1}{2}}$, ^{226}Ra). For shorter lived radium nuclides, equilibrium will be reached correspondingly faster.

2. Adsorption on aquifer rock minerals.

King et al., (1982) found that ^{228}Ra and ^{226}Ra activities varied widely in the Fall Line aquifer near Leesville, a series of aquifers in sedimentary rocks. This was despite sampling in boreholes situated closely together. These results were interpreted as showing that radium nuclides have very low mobilities in groundwaters due to adsorption and cannot migrate far from their point of origin.

Laboratory studies of radium adsorption on secondary minerals (Ames et al., 1982) showed that ^{226}Ra was most efficiently adsorbed on clay minerals which have high cation

exchange capacities, and poorly adsorbed on opal and silica gel which are analogues of quartz. The adsorbance behaviour of radium was found to fit a Freundlich sorption isotherm of the form:

$$\left(\frac{X}{m}\right) = KC^n \qquad (1.44)$$

where (X/m) is the equilibrium concentration of sorbed components in the solid (moles/g); C is the equilibrium solution concentration (moles/ml); K,n are constants.

The values of (X/m) were used to determine distribution coefficients (D) specific to each investigated mineral:

$$D = \frac{\text{equilibrium adsorbed concentration}}{\text{equilibrium solution concentration}} = \frac{(X/m)}{C}, \text{ ml/g}$$

The variation of D values with radium concentration and solution temperature for adsorption on the minerals biotite, kaolinite and silica are shown in Figure 1.12. Although adsorption was investigated at 5, 25 and 65°C, no relationship could be derived relating adsorption to solution temperature. However, for cation exchanging minerals, increasing temperature resulted in decreasing adsorption.

The distribution coefficient D, and the dimensionless distribution coefficient (K) relating to adsorbed nuclide concentration to solution concentration in groundwaters, are related by the expression:

$$K = D\rho\left(\frac{1 - \phi}{\phi}\right) \qquad (1.44)$$

where ρ = rock density, g/cm^3

ϕ = aquifer porosity

Fig 1.12 Sorption Isotherm of Radium on Biotite, Kaolinite and Silica gel in Laboratory Experiments.

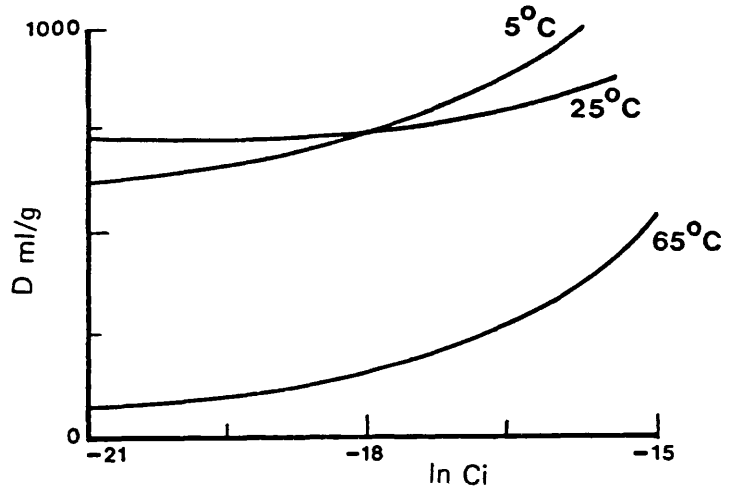

1.12(a) Equilibrium Sorption on biotite in 0.01m NaCl

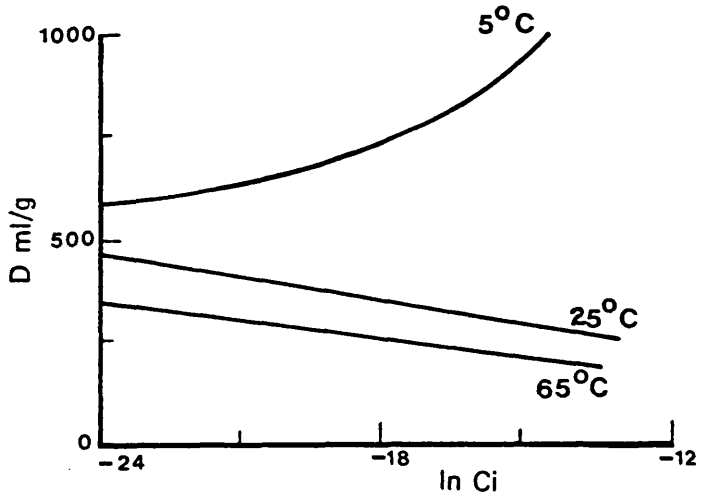

(b) Equilibrium Sorption of radium on Kaolinite in 0.01m NaCl

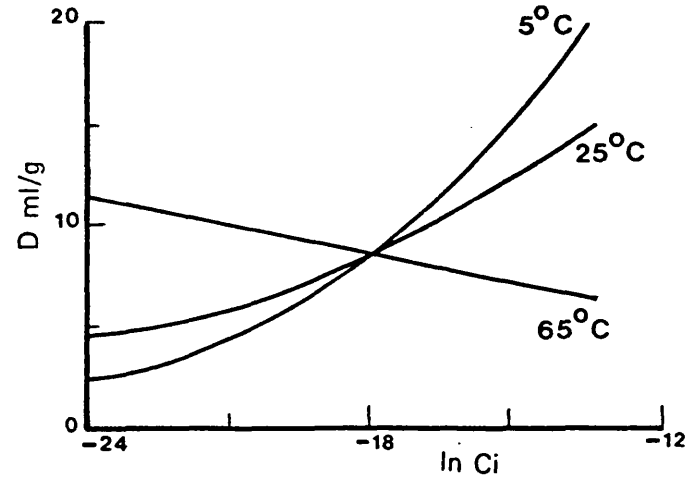

(c) Equilibrium Sorption of radium on Silica gel in 0.01m NaCl

Ci = Initial Radium Concentration (M)

D = Equilibrium adsorbed concentration (ml/g)

However the application of laboratory determined adsorption constants to model groundwater nuclide behaviour is of limited value because laboratory measurements are made in simple systems and not the complex chemical solutions that are groundwaters. Therefore effects such as the competition for adsorption sites between radium and dissolved alkaline earth elements (Nathwani and Phillips, 1979) are not taken into consideration.

3. Co-precipitation.

Radium can be removed from solution by co-precipitation with calcium and barium minerals such as barite, calcite, aragonite and anhydrite. During co-precipitation, radium is substituted into the lattice sites occupied by calcium and barium due to its similar ionic radius and the same ionic charge (Table 1.5).

Radium has been removed from uranium mine waters and mill tailings by co-precipitation with barium sulphate (e.g. Sebasta et al., 1981). Co-precipitation with $BaSO_4$ has also been hypothesised as a process removing radium from oil field brines (Kramer and Ried, 1984). However the process has been modelled only by Langmuir and Reise (1985), as an equilibrium exchange process between radium in solution and the co-precipitated mineral.

Their model proposes that the exchange reaction can be formulated as:

$$Ra^{2+}(aq) + MX = M^{2+}(aq) + RaX$$

where M is the major divalent cation in the mineral

X is the anion or counter-ion to the cation

This relationship has an equilibrium constant defined by:

$$K_{ex} = \frac{\gamma_{m^{2+}} M_{m^{2+}}}{\gamma_{Ra^{2+}} M_{Ra^{2+}}} \quad \frac{\lambda_{Rax} N_{Rax}}{\lambda_{mx} N_{mx}} \qquad (1.45)$$

where γ, M = ion activity coefficient and molality in solution

λ, N = activity coefficient and mole fraction in the solid

But, the ratio ($M_{Ra^{2+}}/M_{m^{2+}}$) can be measured in groundwaters to yield a distribution coefficient, D:

$$\frac{M_{Ra^{2+}}}{M_{m^{2+}}} \quad D = \frac{N_{Rax}}{N_{mx}} \qquad (1.46)$$

In dilute solutions such as groundwaters, $\gamma_{m^{2+}} = \gamma_{Ra^{2+}}$. Also, because RaX is a trace component it has a negligible concentration in the solid, so $\lambda_{mx} \approx 1$. Equation (1.46) becomes:

$$N_{Rx} = D\left(\frac{M_{Ra^{2+}}}{M_{m^{2+}}}\right) \qquad (1.47)$$

Temperature corrections for D can be calculated from the relationship

$$K_{ex} = D.\lambda_{Rax} \qquad (1.48)$$

Noting that the Gibbs free energy for the exchange reaction is:

$$\Delta G^{o}_{ex} = -RT \ln K_{ex} \qquad (1.49)$$

then the Vant Hoff isotherm can be applied to calculate the temperature correction:

$$\Delta H^{o}_{ex}(D) = 4.576\left[\log\left(\frac{D_2}{D_1}\right)\right]\left(\frac{T_2 T_1}{T_2 - T_1}\right) \qquad (1.50)$$

Values of $\Delta H^{o}_{ex}(D)$ for many minerals have been tabulated by Langmuir and Kiere (1985).

For radium to be removed by co-precipitation, the host mineral must be precipitating from solution. This is difficult to establish with certainty in a groundwater, but by putting the groundwater chemical data into an equilibrium speciation program such as WATEQF (Plummer et al., 1976) the state of saturation of the host mineral with respect to the groundwater can be determined. The results are expressed as the Saturation Indices (S.I.) of the mineral, defined by:

$$S.I. = \log \frac{IAP}{Ksp} \qquad (1.51)$$

where IAP = ionic activity product of the mineral in the water

Ksp = theoretical solubility product of the mineral at the same pressure and temperature

When a mineral is super saturated in a groundwater then equation (1.47) can be used to determine N_{Rx} for that mineral in the groundwater, which can then be used to determine the concentration of radium precipitated with the host mineral. This approach has been applied to the groundwaters of the granite wash facies and woolfcamp brines of the Paulo Dura Basin in North Texas, USA (Langmuir and Melchior, 1985) where it was shown that dissolved radium may be controlled by equilibration with barite within the aquifer rock matrix.

1.6.3 Geochemistry of radiogenic lead isotopes

There are three naturally occurring radioactive lead isotopes, ^{214}Pb ($t_{\frac{1}{2}}$ = 26.8 mins), ^{210}Pb ($t_{\frac{1}{2}}$ = 22.3 years) in the uranium (4n + 2) series and ^{212}Pb ($t_{\frac{1}{2}}$ = 10.6 hours) in the thorium 4n series. Because of the short half-lives of these nuclides, secular equilibrium should be rapidly established within rock minerals, and their activities should reflect the activities of ^{238}U and ^{232}Th within rock minerals.

However, lead nuclides in groundwaters are generally in disequilibrium with ^{238}U and ^{232}Th and other members of the decay series because of their differing chemical properties. Disequilibrium between lead nuclides and their predecessors in the decay series has been used to derive residence times for lead nuclides in groundwaters (e.g. Krishnaswami et al., 1982 and Hussain and Krishnaswami, 1982). In the study by Krishnaswami et al, 1982, production of ^{210}Pb was assumed to be by alpha recoil from the rock surface into solution. Assuming that ^{222}Rn was produced solely by alpha recoil, then providing that the groundwater residence times were greater than 21 days, the ^{222}Rn activity gave a direct measurement of recoil supply of nuclides in the uranium decay series. Residence times were calculated after setting up mass balance equation for ^{210}Pb:

In the aqueous phase:

$$P + k_2\bar{c} = \lambda c + k_1 c \qquad (1.52)$$

in the adsorbed state

$$k_1 c = \lambda\bar{c} + k_2\bar{c} \qquad (1.53)$$

where

P = supply rate by recoil into solution

λ = decay constant for ^{210}Pb

k_1 = adsorption rate constant

k_2 = desorption rate constant

c = concentration of nuclide in solution

$\bar{c}$ = concentration of nuclide adsorbed onto rock surfaces

Assuming that the recoil supply can be given by the ^{222}Rn activity (the groundwater residence time is greater than 21 days), and λc is the ^{210}Pb activity in solution, then the residence time of ^{210}Pb is given by $1/k_1$. The groundwaters sampled were from a wide variety of aquifer lithologies, ranging from crystaline bedrock to triassic-jurassic arkose and glacial drifts. The resulting calculation for a well from an arkose lithology was a residence time of 385 minutes and a retardation factor (defined by $Rf = 1 + k$, where k is the distribution coefficient between dissolved and adsorbed states) of 43,000.

The study of Hussain and Krishnaswami (1982) concentrated on ^{210}Pb activities in Na-HCO_3-Cl dominated groundwaters from Gujarat, India, although the lithologies were not given.

In these groundwaters the ^{214}Pb residence times were calculated using the equation:

$$P + \lambda_p N_p = (\lambda d + \psi)Nd \qquad (1.54)$$

where $\lambda_p N_p$ is the production rate of ^{214}Pb by decay of ^{222}Rn in solution, P is the production rate of ^{210}Pb by α-recoil ejection of ^{214}Pb into solution from the rock surface, λd

and ψ are the decay constant and first order removal constand for ^{214}Pb.

The production of ^{214}Pb due to the decay of ^{222}Rn was estimated as the ^{222}Rn activity in solution. Two cases were considered in calculating the residence times:

1) No recoil production of ^{214}Pb into solution, i.e. $P = 0$.
2) Recoil production the same as the groundwater ^{222}Rn activity, i.e. $P = \lambda_p N_p$.

The estimated ^{214}Pb residence times ranged between 7 and 16 minutes for case 1 and 3 and 7 minutes for case 2 . The ^{210}Pb residence times for the same wells ranged between 0 and 800 minutes for case 1 and 0 and 905 minutes for case 2 . The discrepancy between these two results was attributed to the desorption of lead nuclides from rock surfaces. However the results were not accurate enough to calculate desorption rate constants.

CHAPTER TWO: EXPERIMENTAL METHODS

Introduction

The radioactive nature of isotopes investigated in this study allowed the radiometric measurement of these isotopes after preconcentration from groundwaters and processing into sources suitable for counting.

For each analytical method developed, the method of sampling and preconcentration is described, followed by any chemical separations and the preparation of a source for counting.

The detector calibration and counting procedure are then described. Finally, the analytical errors and detection limits are discussed.

The radiometric detection systems employed in this study are described in Appendix.1

2.1 Analysis of ^{228}Ra and ^{226}Ra in groundwaters

Analysis of ^{226}Ra in natural waters can be performed using a number of techniques such as alpha counting after $BaSO_4$ co-precipitation (Michel et al., 1981); cation exchange extraction followed by scintillation counting (Higuchi et al., 1984) or adsorption on manganese dioxide impregnated fibres followed by ^{222}Rn emanation (Reid et al., 1979). Analysis of ^{226}Ra in this study was performed by emanation of ^{222}Rn from 5-litre samples stored in glass containers.

Measurement of ^{228}Ra has been performed by following the ingrowth of its daughter ^{228}Th (half-life 1.9 years) by alpha counting (Moore, 1969) and also by chemical separation followed by liquid scintillation counting (Asikainen, 1981). However both of these methods are time consuming and can only be applied to small volume samples. An alternative method is to preconcentrate radium isotopes and measure ^{228}Ra via the γ-rays produced by its daughter ^{228}Ac. To obtain the high energy resolution required to separate peaks belonging to ^{226}Ra and its daughters from peaks belonging to ^{228}Ac, a high resolution intrinsic germanium γ-ray spectrometer was used in this study. Such detectors have low detection efficiencies. For instance, the largest germanium detectors with effective volumes of about 30 cm^3 having approximately 4% efficiency for a 1 Mev γ-ray, whereas a 3" by 3" NaI detector will have a 20% efficiency at the same energy (Dearnally and Northrop, 1966). For this reason it was necessary to preconcentrate

radium from large sample volumes to obtain sufficient activities to measure by γ-ray spectrometry. Various preconcentration techniques were investigated using ^{226}Ra tracer solutions, such as $BaSO_4$ and $CaSO_4$ co-precipitation and extraction by cation exchange resins. However these proved unsatisfactory due either to poor yields or limited applicability.

Instead the technique chosen to preconcentrate radium isotopes was adsorption onto MnO_2 , either by adsorption onto the commercially available powder or onto MnO_2 loaded acrylic fibre. Both of these methods are discussed below.

Because ^{226}Ra was measured with high accuracy by ^{222}Rn emanation, ^{228}Ra activities could be determined simply by preconcentrating radium from large sample volumes and accurately determining the $^{228}Ra/^{226}Ra$ activity ratio. The ^{228}Rn activity is then simply calculated by combining the independent ^{226}Ra activity measurement with the $^{228}Ra/^{226}Ra$ activity ratio.

Using this method, the preconcentration of radium isotopes for the determination of $^{228}Ra/^{226}Ra$ activity ratios do not have to be quantitative provided that ^{226}Ra activities are determined with low error. However sufficient ^{228}Ra and ^{226}Ra activities have to be preconcentrated to allow the accurate measurement of the $^{228}Ra/^{226}Ra$ activity ratio within a feasible count time (a maximum of 3 days).

2.1.1 ^{226}Ra analysis by ^{222}Rn emanation

2.1.1.1 Sample collection

Samples were collected in 5-litre polythene bottles. The water was initially filtered through a 5 micron millipore filter, to ensure that any sediments carried in the sample did not adsorb or contribute ^{226}Ra to the sample. The bottles were immediately acidified to pH <2 using 30-50 mls 6M HCl to ensure that ^{226}Ra did not get adsorbed onto the surface of the containers.

In the laboratory, samples were transferred into 5-litre glass bottles, accurately weighing the water as well, to allow calculation of the ^{226}Ra activity/kg sample. The transfer was necessary because ^{222}Rn is known to diffuse through polythene (M. Youngman, pers. comm.).

Activities of ^{226}Ra were determined by measuring the activity in solution of ^{222}Rn, after allowing ^{222}Rn to grow into equilibrium with its parent. Samples were therefore stored for at least 21 days, by which time ^{222}Rn had grown into 96% equilibrium with its parent. However, the ^{222}Rn activity in waters may be in great excess over that of ^{226}Ra ($^{222}Rn/^{226}Ra$ activity ratios can reach >1000). The 0.7% unsupported ^{222}Rn still remaining in solution after 21 days of ingrowth may cause erroneously high ^{226}Ra activities to be determined. For this reason samples were outgassed before storing for ingrowth to remove the ^{222}Rn in the water at the time of sampling. Also, some samples with low ^{226}Ra activities

were stored for another 21 days after the first determination and re-determined, by which time any excess ^{222}Rn should have decayed.

2.1.1.2 Analytical procedures

After storing, ^{222}Rn should have reached 96% equilibrium with its parent ^{226}Ra. The ^{222}Rn was removed from solution by outgassing with 10 times the solution volume using ^{222}Rn-free nitrogen gas. This was bubbled through a scintered glass disc at a flow rate of $1\ell min^{-1}$. This should result in 99% removal of the radon from solution (Andrews and Wood, 1973).

The gas was dried by passing it through a drying 'U' tube packed with $CaCl_2$ and by bubbling through conc. H_2SO_4. ^{222}Rn was trapped in a charcoal trap at -80°C using a CO_2/ethanol coolant (Fig. 2.1).

The charcoal trap was connected to a vacuum line onto which was attached an evacuated 50 cm^3 flask, coated with ZnS(aq) scintillator. The charcoal trap was evacuated and heated to 200°C to desorb ^{222}Rn. This was flushed into the scintillation flask by slowly admitting dry air into the system until atmospheric pressure had been reached. The flask was then removed from the vacuum line and stored for $\geq 2\frac{1}{2}$ hours to allow equilibrium to be established between ^{222}Rn and its short-lived daughters ^{214}Pb and ^{214}Bi (half-lives of 26.8 mins and 18 mins respectively).

Fig 2.1 ^{222} Rn Outgassing and Recovery on Activated Charcoal

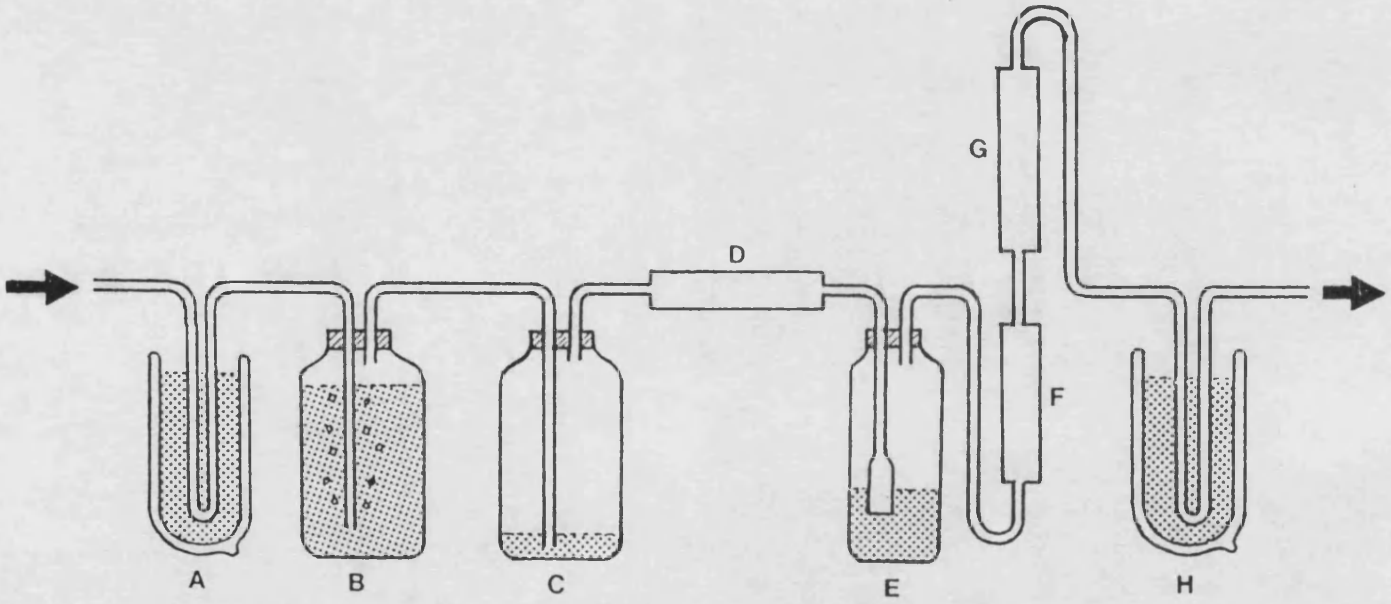

A. Charcoal trap at $^{-}80\,^{\circ}c$ to remove radon from air stream if air is used for outgassing.
B. 0.25 – 20 litres water sample.
C. Overflow bottle
D. $Ca\,Cl_2$ drying tube.
E. Concentrated $H_2\,SO_4$ drying bottle.
F. Glass bead vapour trap.
G. Flowmeter 0.5 – 2.0 litres min^{-1}
H. Charcoal trap at $^{-}80^{\circ}c$ (solid CO_2 /ethanol) for ^{222}Rn adsorption.

The scintillation rate of the flasks were determined by counting them on a 3" diameter photomultiplier tube (EM1 type 9708 kA). The count rates were corrected for decay of ^{222}Rn due to the time elapsed between outgassing and counting. Corrections were also made for the flask background count rates, which arise due to the build up of ^{210}Pb in the flasks.

Activities were determined by comparing the sample count rate with those obtained by outgassing ^{222}Rn from ^{226}Ra standard solutions in equilibrium with ^{222}Rn.

2.1.2 Preconcentration of radium radionuclides

2.1.2.1 Principles of adsorption on MnO_2

The ability of hydrated manganese oxides to limit trace metal mobility in groundwaters is well documented. Suarez and Langmuir (1976) showed that various trace metals such as Co, Ni, Pb and Cd in Pennsylanvian soils were present largely in hydrated manganese oxides and ferric oxy-hydroxides. Manganese oxides are used in analytical chemistry for the removal of radioelements from solution (Hasany and Chaudhary, 1981) and for the separation of alkali earth cations (Grey and Malati, 1979) and trace elements (Gadde and Laitinen, 1974) from solution.

The adsorption properties of δMnO_2 (similar to natural birnissite) for heavy metals was summarised by Murray (1975). In many studies it had been noticed that 1 mole of H^+ was released for every mole of adsorbed cation. Murray suggested that this could be explained by the adsorption mechanism:

$$Mn—X\text{-}OH + M^{2+} \rightleftharpoons Mn—XOM^{+} + H^{+}$$

Selectivity of manganese oxides for different cations appears to relate to the size of the hydrated cations. Grey and Malati (1979) showed that the adsorption of the aklali-earth cations proceeded in the order

$$Ba^{2+} > Sr^{2+} \geq Ca^{2+} > Mg^{2+}$$

This was the reverse order of the hydrated cation size and suggested that small cation sizes result in a greater

electrostatic attraction between the cation and the surface charges on the MnO_2. The hydrated cation sizes of the alkali-earth cations are in the order $Mg^{2+} > Ca^{2+} > Ba^{2+} > Ra^{2+}$, (Cotton and Wilkinson, 1972).
On the basis of the explanation given above the small size of Ra^{2+} should mean that it is highly adsorbed by MnO_2.

Radium isotopes have been preconcentrated by passing water samples through MnO_2 loaded onto acrylic fibres. These were first developed by Moore and Reid (1973) and improved by Michel et al. (1981). It was shown that radium isotopes were almost (99%) quantatively extracted from groundwaters using these fibres, and that extraction efficiency was the same for both seawater and a variety of groundwaters.

2.1.2.2 Tracer experiments to determine the optimum recovery of radium on powdered MnO_2

To enable the use of adsorption on powdered MnO_2 as a method for the preconcentration of radium from groundwater samples the optimum conditions for radium recovery must first be established. The effect of salinity, sample volume, equilibration time and amount of MnO_2 on adsorption were investigated.

Adsorbance was investigated by equilibrating a solution containing a known amount of ^{226}Ra tracer with a known weight of added MnO_2. The solutions were initially acidified to a pH ≤ 2 before the addition of ^{226}Ra tracer to prevent adsorption of the radium onto the plastic container walls. A weighed amount of ^{226}Ra from a standard solution was added and the solution was thoroughly mixed to ensure a homogeneous distribution of radium. A known weight of MnO_2 was added and the solution immediately raised to pH $\simeq 7$ using ammonium hydroxide (adsorption is negligible at pH <3, Gray and Malati, 1979). The solution was then stirred by aeration for a predetermined time to allow equilibration to be attained between the MnO_2 and the solution.

After aeration the solid was allowed to settle and isolated by syphoning off the supernatant water. Excess water was removed by centrifugation followed by drying in an oven at approximately 60°C until a constant weight of solid remained. Activities of the adsorbed ^{226}Ra

were determined by measuring its γ-ray activity by high resolution intrinsic germanium γ-ray spectrometry. The results of these experiments are given in Table 2.1.

Variation of radium adsorbance with weight of MnO_2 and sample volume.

Initial experiments on radium adsorbance were performed to determine the amount of MnO_2 required to remove radium quantitatively from solution. Between 0.5 and 25 g of MnO_2 was used on volumes ranging from 1 litre to 60 litres. It was found that MnO_2 was highly efficient in adsorbing radium from small volume samples, for instance the radium recovery yields using 0.5 g of MnO_2 were between 96 and 100% from 1 litre and 5 litres of solution.

The effect of varying the weight of MnO_2 was investigated by using 2 g and 10 g of MnO_2 on 20 and 25 litres of solution. Recovery yields were 89 and 84% radium extracted respectively. This indicated that for the 3 hour equilibration period, 2 g of MnO_2 was sufficient to extract a substantial proportion of radium in solution.

Increasing the weight of MnO_2 to 25 g and the sample volume to 50 litres resulted in a quantitative extraction within 1 standard deviation error of the result. However a similar experiment using 25 g MnO_2 and 60 litres of solution resulted in only 71% recovery. The reason for this discrepancy is not known. Loss of MnO_2 during its isolation from solution could be a problem is small amounts

Table 2.1 Tracer experiments to determine the recovery of ^{226}Ra under varying conditions.

Sample volume (ℓ)	MnO_2 weight (g)	Aeration time (hours)	NaCl concentration (g/ℓ)	Activity of ^{226}Ra added (pCi/ℓ)	Activity of ^{226}Ra recovered (pCi/ℓ)	^{226}Ra recovered (%)
1	0.5	9 mins	-	250	240 ± 11	96
5	0.5	5 mins	-	250	261 8	104
20	2	3	-	250	217 9	84
25	10	3	-	495	431 14	87
60	25	3	-	490	348 10	71
25	10	3	-	1000	894 55	89
50	25	3	-	495	491 11	99
50	25	7	-	495	368 9	74
50	25	18	-	495	367 12	74
50	25	24	-	495	348 11	70
50	25	3	-	0(blank)	3 5	-
50	25	0	-	495	404 13	82
60	25	3	30	495	442 9	84
60	25	3	60	495	415 12	89

of MnO_2 were used to extract radium from large volumes of water. For this reason, it was decided that 25 g of MnO_2 would be used to preconcentrate radium from 60 litres of sample.

Variation of radium adsorption with equilibration time

Radium recovery yields as a function of the equilibration time between MnO_2 and the solution was investigated over the range 3-24 hours. Solutions were mixed using an aerator to which was attached a CO_2 trap. Sample volumes were kept at 60 litres throughout and 495 pCi ^{226}Ra was added as a tracer to the solutions. Figure 2.2 shows how the radium recovery varies with equilibration time.

Instead of the expected increase in radium adsorption with equilibration time it was found that the radium recoveries decreased. A study of the adsorbance properties of MnO_2 for alkali-earth cations (Gray and Malati, 1979) also found that a limited amount of desorption occurred with these cations, but gave no explanation of their results. The MnO_2 used in these experiments was obtained in the dehydrated form. It is possible that slow surface hydrolysis processes occur when it is placed in water, and this may cause some desorption of the radium. It is noticable that Hasany and Chaudhary (1981) hydrolysed the MnO_2 used in their experiments with water for 24 hours before use.

The maximum radium recovered in these experiments occured after 3 hours aeration. It should be noted that all of

Fig. 2.2 Variation of 226Ra Recovery with Stirring Time

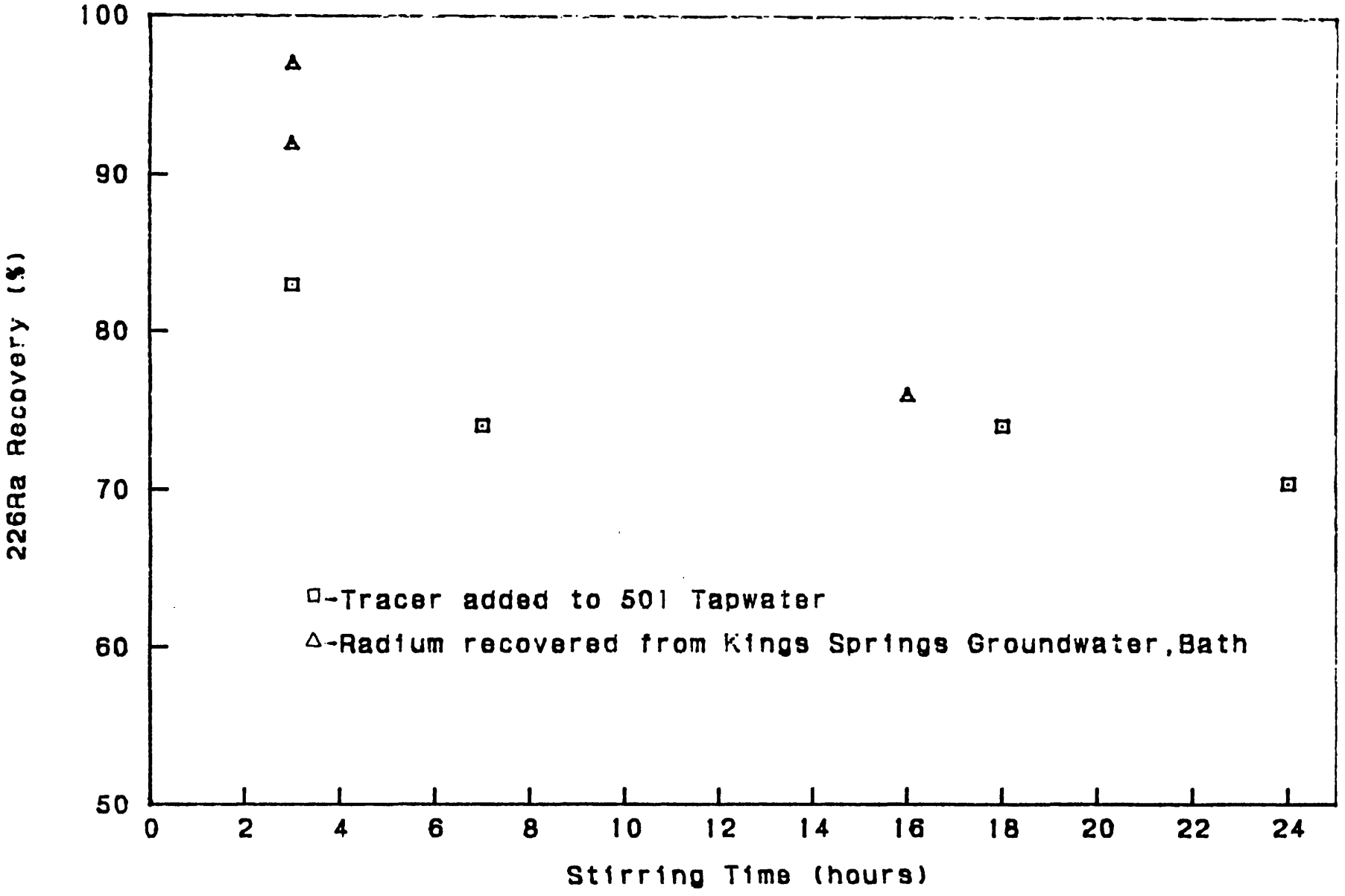

the studies on radium recovery with equilibration time resulted in radium recoveries above 70%.

Variation of radium adsorbance with salinity

Experiments to investigate the effect of salinity upon adsorbance were performed using 60 litres of water containing 30 and 60 g/litre NaCl and 495 pCi of ^{226}Ra. The maximum salt concentration is equivalent to twice the seawater NaCl content (30.1 g NaCl/kg seawater; Riley and Skidrow, 1975). The adsorbance of radium from both solutions was essentially the same. This was a surprise because radium is desorbed from sediments carried by freshwater when it mixes with ocean water in estuaries (Elsinger and Moore, 1983). Adsorbed radium in sediments is thought to be held by ferric and manganese oxyhydroxides (Dyck, 1978). The adsorption of radium at the high salinities shown by these experiments must indicate that radium adsorption by MnO_2 is highly selective and unaffected by the salinities used in these experiments. These results are similar to those obtained by Matthews (1983) and Hasany and Chaudhary (1981).

2.1.2.3 Adsorption of radium on MnO_2 impregnated fibres

Although the preconcentration of radium from large sample volumes is possible by adsorption on powdered MnO_2, the largest sample volume was only 60ℓ. For very low activity samples (^{226}Ra activity <1 pCi ℓ^{-1}), good counting statistics are only obtained after very long count times even with 60ℓ samples.

However radium can be adsorbed on MnO_2 impregnated fibres following Moore and Ried (1971). This allows near-quantitative adsorption of radium from large volumes of water. The detection limit for radium will then depend only upon the volume of water passing through the fibre.

Preparation of fibres

The acrylic base material was 100 g of commonly available spun acrylic synthetic 'wool'. There was no difference in the properties of the prepared fibres using acrylic material from different manufacturers. Fibres were immersed in 2ℓ of 0.125M (20 g $KMnO_4$/litre) of $KMnO_4$ solution at 80°C in 5-litre glass containers. This results in thermal degradation of $KMnO_4$ to produce MnO_2 which forms an even deposit upon the fibre. The fibres were removed after 30 minutes by which time they were jet-black in colour.

The fibres were washed twice with 1 litre distilled water to remove any loosely attached MnO_2 particles. They were then stored in plastic bags or containers before use in order to retain moisture.

Various molarities and temperatures of $KMnO_4$ solution were tried but it was found that the treatment above gave the greatest loading of MnO_2 upon the fibres (12g/100g fibre, determined by atomic absorption spectroscopy).

Extraction of radium from water

Water was passed through the fibres in the manner appropriate at different sampling sites. At pumped boreholes, water was passed through PVC columns packed with 100g Mn-fibre. These had flow rates of 1 litre per minute which was as fast as water could be passed through them. However these columns were inappropriate for boreholes which released a lot of gas as well as water. For these sites water was flowed through a 5-litre plastic bottle containing 100g Mn-fibre (see Fig. 2.3).

For sample sites which were springs emanating from bedrock, Mn-fibres were enveloped in plastic netting and suspended in the spring as close as possible to the sampling site.

Removal of radium from the fibres

The fibres were washed twice with 1 litre distilled water to remove any sediments which may have adhered to their surfaces. They were then leached by placing in 5-litre glass containers containing sufficient 3m HCl to cover the fibres, generally 1 litre of solution. The mixture was heated for 30 minutes by which time the

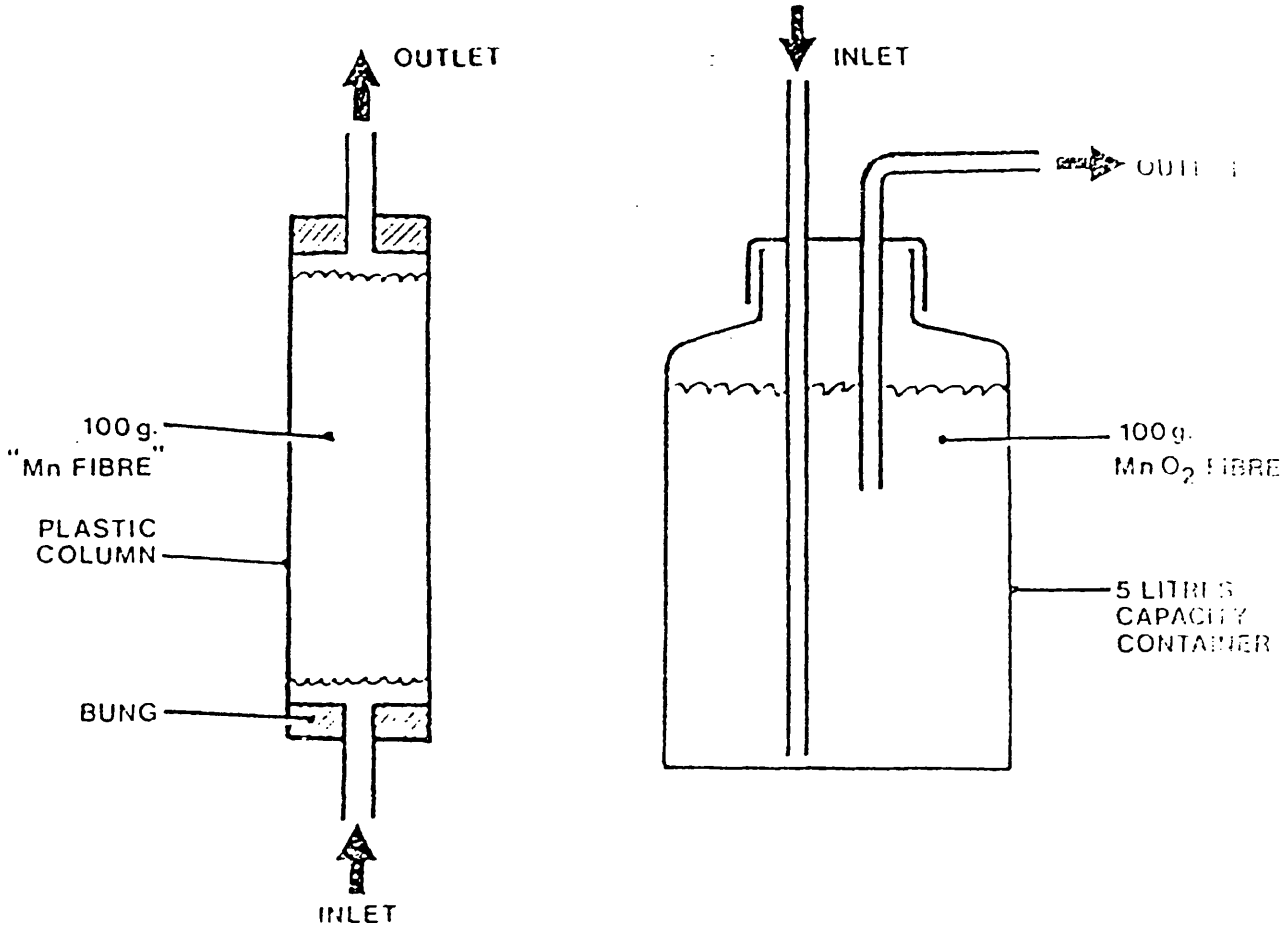

Fig 2.3 Apparatus Used to Preconcentate Radium Nuclides

MnO_2 was reduced by the HCl to soluble $MnCl_2$. Any radium adsorbed on the MnO_2 was therefore released into the solution. At this stage, the fibres had changed colour from black to pale yellow.

The leachate containing the radium was separated by filtration. The fibres were washed several times with distilled water and the washings added to the leachate, giving approximately 3 litres of solution. The radium was removed from this solution by co-precipitating with $BaSO_4$. Sufficient $BaCl_2$ to precipitate 5 g $BaSO_4$ was dissolved in the minimum of distilled water and added to the leachate. The solution was stirred for 10 minutes to homogeneously distribute the barium. Radium was then co-precipitated by dropwise addition of 15 mls 2m H_2SO_4 over 30 minutes while stirring the solution.

The precipitate was allowed to settle and excess water removed by syphoning. It was then isolated into plastic counting vials, centrifuged to remove any remaining water and dried under an infra-red lamp. After ageing for 2 days to allow ^{228}Ac to reach secular equilibrium with its parent ^{228}Ra, the vials were counted by placing them on top of the intrinsic Ge γ-ray spectrometer.

Radium recovery yields

The extraction efficiencies were determined by passing water of known activity through columns filled with 100 g Mn-fibre. The flow rates were between 0.4 and 1 litre/min. Recovery yields varied between 92% and 99%

with an average of 96%. This agrees with the results of Michel et al. (1981) who found radium extraction efficiencies of >90% in similar Mn-fibre packed columns. It was notable that these authors also achieved quantitative radium recovery by passing water dropwise through the fibres.

Recovery yields using 5-litre plastic bottles were also determined (Table 2.2). Radium recoveries averaged 40%. However, it was not necessary to achieve quantitative recovery on the fibres as long as sufficient ^{228}Ra and ^{226}Ra activities were accumulated to determine accurately the $^{228}Ra/^{226}Ra$ activity ratios. This is necessary because the combined errors on the $^{228}Ra/^{226}Ra$ activity ratio and the separate ^{226}Ra activity determination will dictate the size of the error upon the measured ^{228}Ra activity.

Table 2.2 Extraction efficiency of ^{226}Ra from groundwater samples using MnO_2 impregnated fibres

Sample Name	Preconcentration technique	Sample volume (ℓ)	Flow rate (ℓ/min)	Total ^{226}Ra activity in sample (pCi)	Activity of extracted ^{226}Ra (pCi)	Recovery yield (%)
Kings Spring 1	column packed with fibre	162	0.6	2106	1948	92
Kings Spring 2	"	2049	0.4	20900	20039	96
Kings Spring 3	"	135	1.2	1512	1490	98.5
Stripa V1	5ℓ plastic bottle with fibre	14000	0.46	1848000	940800	51
Stripa V2/2	"	14450	-	1109760	561000	50.6
Stripa V2/3	"	14500	-	1083150	662000	61.1
Stripa V2/4	"		-	1798000	223000	12.4
Stripa V2/5	"	19550	-	347990	23700	7.0
Stripa E1	"	1700	1.4	7650	4403	58

2.1.3 Measurement of $^{228}Ra/^{226}Ra$ ratios and ^{228}Ra activities after preconcentration

2.1.3.1 Calibration of the intrinsic germanium γ-spectrometer

After preconcentration using either the MnO_2 adsorption or Mn-fibre methods, $^{228}Ra/^{226}Ra$ activity ratios were determined by measuring the activities of scavenged ^{228}Ra and ^{226}Ra (hereafter called "bulk" ^{228}Ra and ^{226}Ra activities) by γ-ray spectrometry. The spectrometer used in this study was an intrinsic germanium (Canberra) Model γ-ray spectrometer, characterised by a relative efficiency of 20%, a full width half maxima resolution of 2.02 KeV at 1332 KeV and a peak to Compton ratio of 40.5:1.

Count rates were measured as peak areas above the Compton scattering background, divided by the detector count time in minutes. All peaks were corrected for backgrounds, which again were measured as the count rate of peaks above the Compton scattering background, this time in "blank" samples using the same reagents as those used in the samples.

Activities of ^{226}Ra were measured via its direct disintegration γ-ray produced at 186 KeV. For ^{228}Ra there are no measurable γ-rays produced by direct decay, but several are produced by its daughter ^{228}Ac. Samples were therefore stored for at least 30 hours so that ^{228}Ac grew into at least 97% equilibrium with its parent ^{228}Ra. Therefore ^{228}Ra was measured via the γ-ray peaks produced by its ^{228}Ac daughter. Michel et al. (1981) stored their samples

for a minimum of 21 days to allow equilibrium to be attained between ^{214}Pb and ^{214}Bi and their parent ^{226}Ra. Activities of ^{226}Ra were then measured via the γ-rays produced by its daughters. In this study, utilizing the direct ^{226}Ra decay peak at 186 KeV avoided the 21 day delay in counting to allow equilibrium to be attained between ^{226}Ra and its daughters. A potential problem exists in that ^{235}U produces a direct decay γ-ray peak at 185.7 KeV which cannot be resolved from the ^{226}Ra peak. However, the natural abundance of ^{235}U is 0.72% that of ^{238}U, furthermore, in groundwaters ^{226}Ra is greatly in excess of ^{238}U. Therefore any ^{235}U which is picked up by the detector will have a negligible effect on the count rate of the 186 KeV peak.

The counting system was calibrated by preparing radium standards in the same form and counting geometry as the samples. This meant that standards for the MnO_2 adsorption method were prepared by adsorption of radium standards on 25 g MnO_2, and Mn-fibre standards were prepared by co-precipitation of radium standard solution with 5 g $BaSO_4$. These were prepared in the same way as the samples except that co-precipitation and adsorption were performed within the final counting vials. All supernatant liquids were evaporated to dryness within the vials to ensure that all of the radium standard remained within the vials.

For ^{226}Ra, standards were prepared from a ^{226}Ra stock solution obtained from the Radiochemical Centre, Amersham, Bucks.

Aged ^{232}Th nitrate was to be used to prepare ^{228}Ra standards. However, preliminary calibration of this source by α-spectrometry showed that the $^{228}Th/^{232}Th$ ratio was 0.6, i.e. that there was disequilibrium between ^{232}Th-^{228}Ra-^{228}Th. The thorium nitrate could not therefore be used to prepare ^{228}Ra standards for the calibration of the detector.

An alternative method was used to determine the ^{228}Ra calibration. The photon abundances of ^{226}Ra and its ^{214}Pb and ^{214}Bi daughters are well known. Standards prepared with ^{226}Ra were sealed with epoxy resin to ensure that there was no escape of ^{222}Rn. These were stored for 21 days to ensure that equilibrium was achieved between ^{226}Ra and its daughters.

The γ-ray spectra of these standards were measured over the full 40-2300 KeV energy range of the detector. Peak count, rates, photon abundances and activities were used to determine the efficiency of detection for each peak, using the relationship:

$$\varepsilon = \frac{C}{2.22A.fa} \times 100 \qquad (2.1)$$

ε = detector efficiency (%)
C = count rate (cpm)
A = source activity)pCi)
fa = photon abundance of the γ-ray producing the peak

Using the γ-ray peaks produced by ^{214}Bi and ^{214}Pb, this relationship was used to determine energy-detector efficiency curve for all the sample counting geometries.

The spectra of a ^{226}Ra source is illustrated in Fig. 2.4. Figure 2.5 illustrates the energy-efficiency curve for a 5 g $BaSo_4$ source.

An unbiased fit to the calculated efficiencies was obtained by non-linear regression analysis. The equation produced by regression was used to determine the detector efficiencies at 129, 209, 270, 338 and 912 KeV, the energies of the highest intensity γ-ray peaks produced by ^{228}Ac. Rearrangement of equation (2.1) yields:

$$\frac{2.22\varepsilon f_a}{100} = \frac{C}{A} \qquad (2.2)$$

where C/A = count rate/unit activity (cpm/pCi)

Substitution of the efficiencies for the ^{228}Ac peaks into equation (2.2) and using the photon abundances given by Schotzig and Debertin (1983) gives the calibration for ^{228}Ac peaks.

These peaks were used to obtain the ^{228}Ra activities of samples in the same form and geometry as the ^{226}Ra standards used to prepare the energy-efficiency curve. Table 2.3 gives the ^{226}Ra and ^{228}Ra calibrations for samples counted as co-precipitates with 5 g $BaSO_4$, and adsorbed on 25 g MnO_2.

Fig. 2.4 : Gamma-Ray Spectra of a 1000 pCi, ^{226}Ra, Source Produced by Co-precipitation of Radium with 2g $BaSO_4$. Area under each peak is used to calibrate that peak for measuring unknown activities.

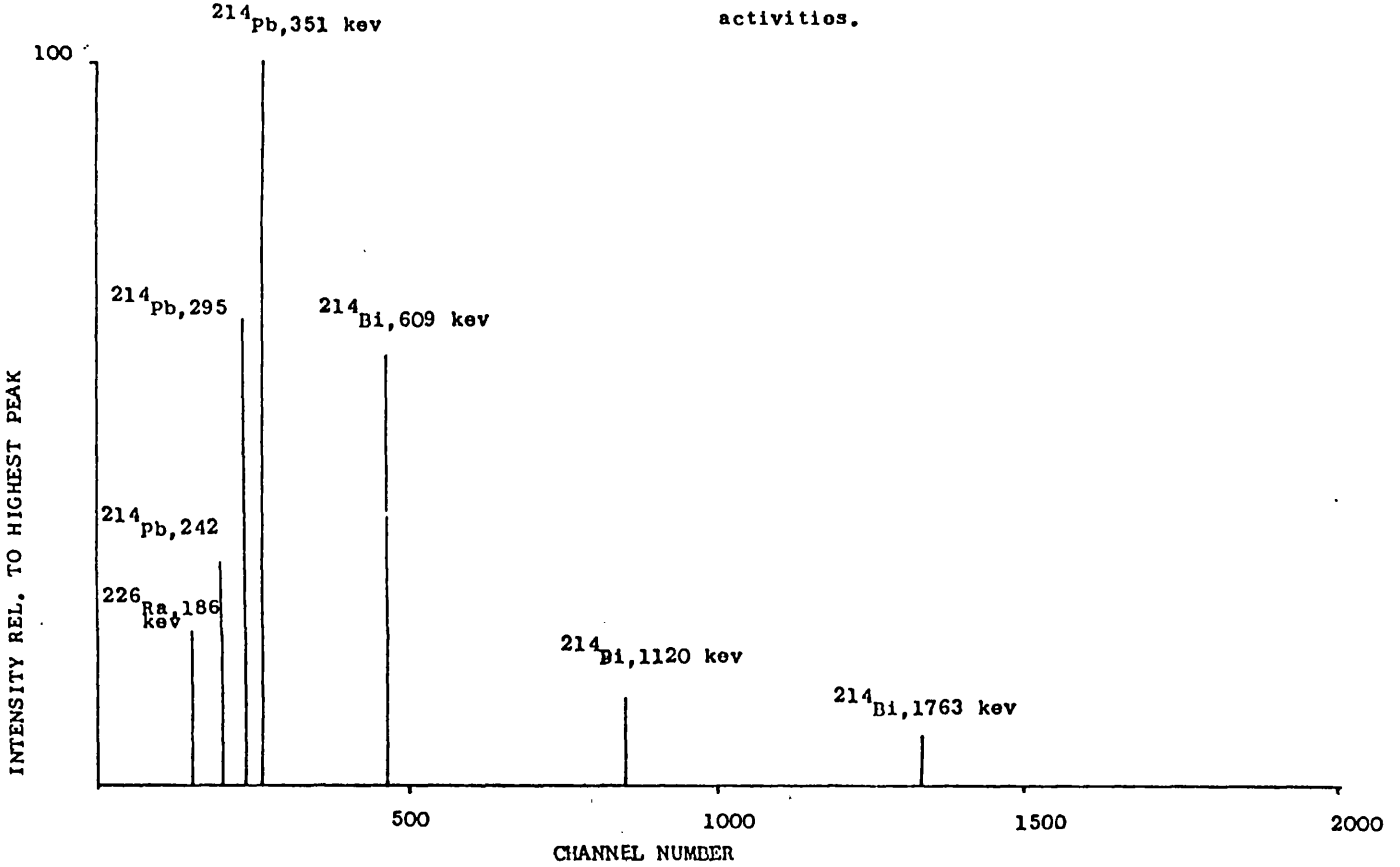

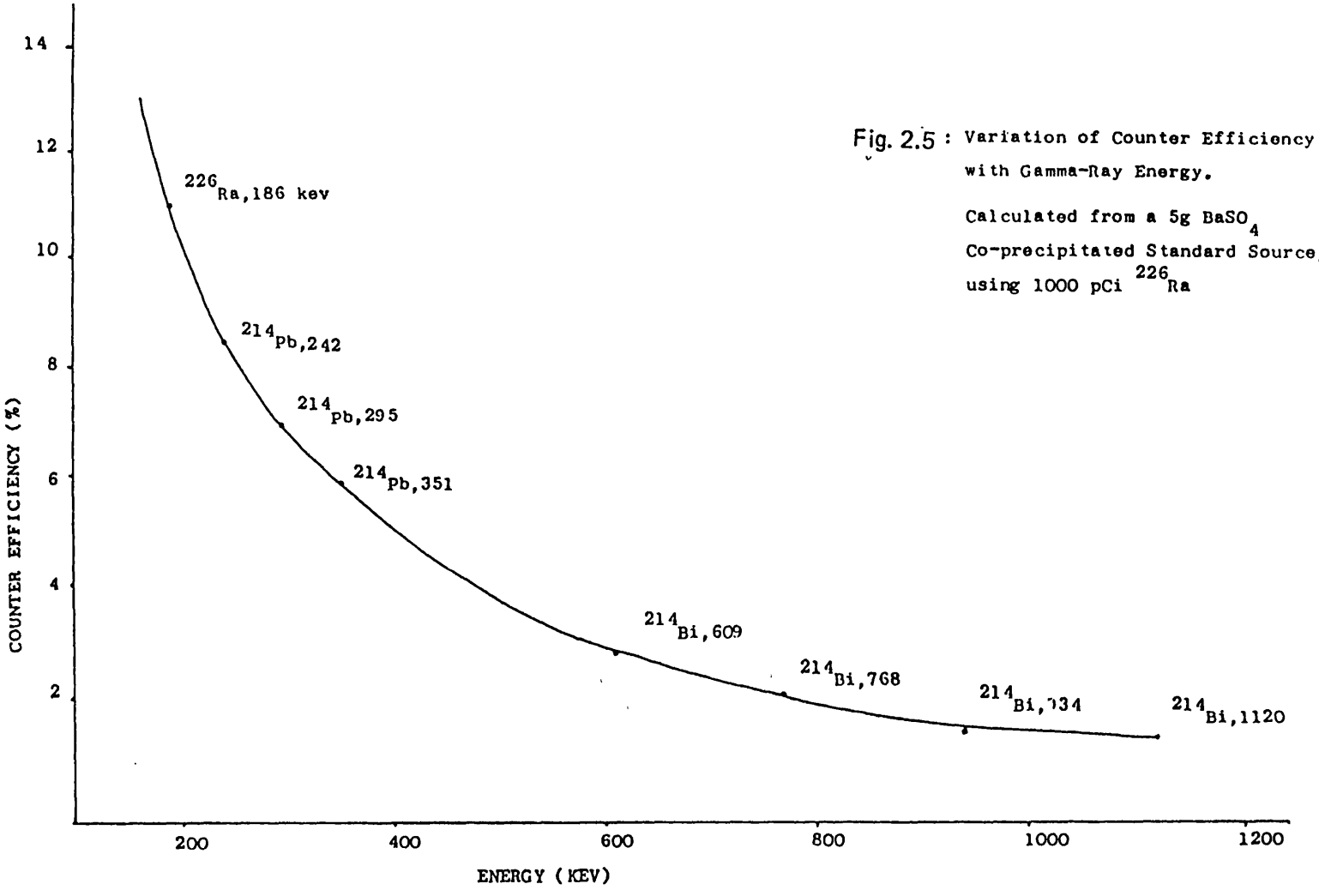

Fig. 2.5 : Variation of Counter Efficiency with Gamma-Ray Energy.

Calculated from a 5g $BaSO_4$ Co-precipitated Standard Source, using 1000 pCi ^{226}Ra

Table 2.3 ^{226}Ra and ^{228}Ra calibrations of sources produced by preconcentration on Mn-fibres followed by $BaSO_4$ co-precipitation

^{226}Ra and its daughters:

Nuclide	Energy (KeV)	Calibration (C/A) (cpm/pCi)	Background (cpm)
^{226}Ra	186	0.00753	0.33
^{214}Pb	241	0.01078	0.25
^{214}Pb	295	0.02348	0.47
^{214}Pb	351	0.03737	0.73
^{214}Bi	609	0.038	0.015

^{228}Ra and its daughters:

Nuclide	Energy (KeV)	Calibration (cpm/pCi)	Background (cpm)
^{228}Ac	129	0.0041	0.0202
^{228}Ac	209	0.00685	0.0
^{228}Ac	270	0.00471	0.0
^{228}Ac	338	0.01247	0.0
^{228}Ac	912	0.01019	0.0

2.1.3.2 Corrections applied for sample loss during preconcentration onto powdered MnO_2.

Bulk ^{226}Ra and ^{228}Ra activities were determined using the calibrations described above, and the relationship:

$$Ai = \frac{(Ci - bi)}{Pci} \qquad (2.3)$$

where Ai = activity of the i^{th} measured γ-ray peak
Ci = count rate " " " " " (cpm)
bi = background count rate " " " (cpm)
Pci = calibration " " " " " cpm/pCi

Recovery of MnO_2 from the initial 25 g MnO_2 added to 25-60ℓ samples was found to be as low as 60% (15g MnO_2 recovered). The geometry of samples with low yield of MnO_2 will be different from the calibration geometry. Although bulk $^{228}Ra/^{226}Ra$ activity ratios will be independant of geometry (as geometry changes have an equal effect on all γ-rays of any energy reaching the detector), bulk activities of ^{226}Ra and ^{228}Ra will not be correct.

The variation of detector efficiency with sample geometry was investigated by preparing 5, 10, 15 and 25 g MnO_2 sources of equal ^{226}Ra activity (Fig. 2.6). The slope of the resulting log-normal graph was used to determine the geometry correction for samples as follows:

Let Wx = weight of MnO_2 in the sample
W_{25} = weight of MnO_2 in the calibrated standard (25g)
Fy = efficiency of the 186 KeV γ-ray at the sample weight, x.

Fig. 2.6 Variation of γ-ray detection with weight of MnO_2

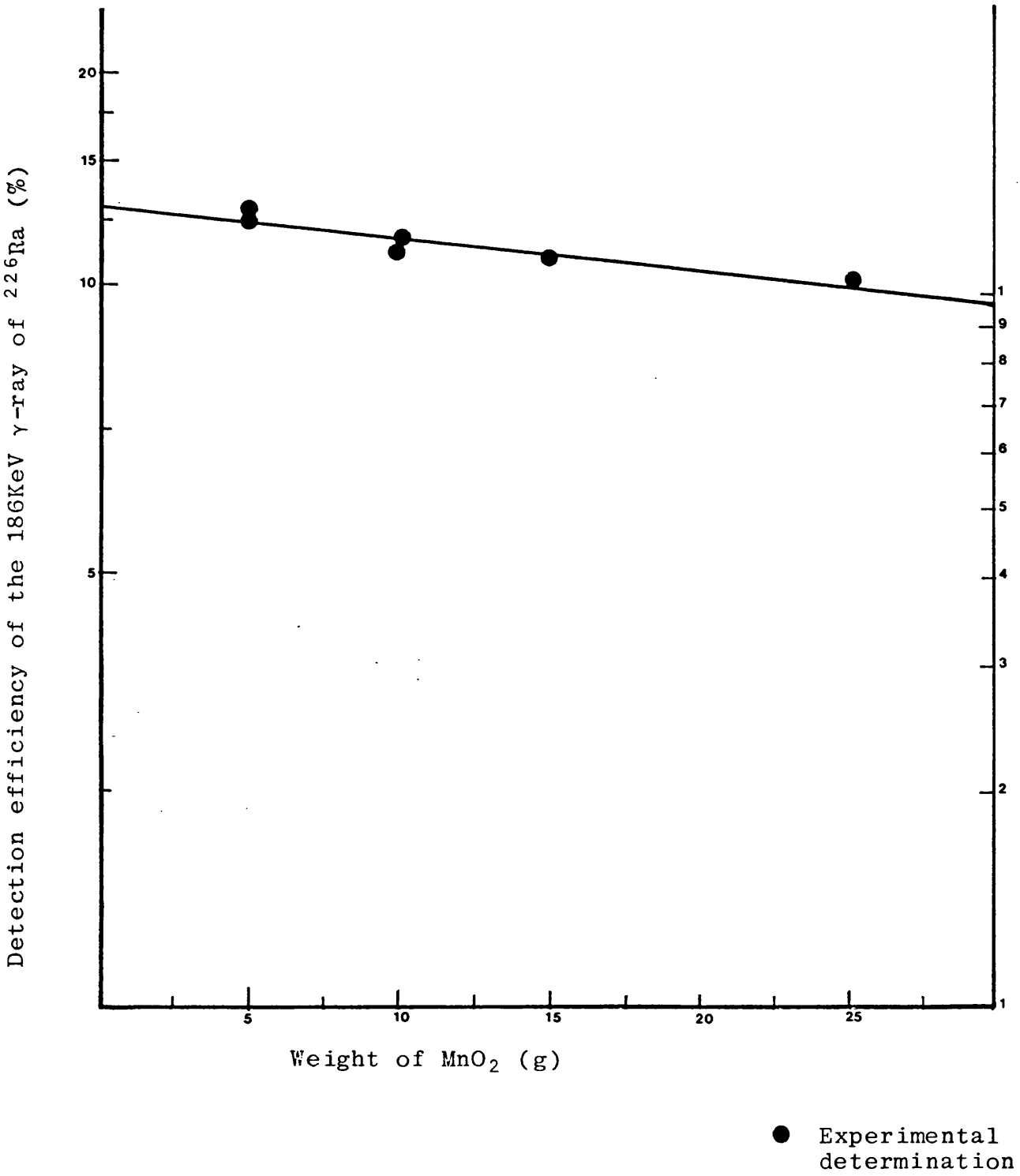

F_{25} = efficiency of the 186 KeV γ-ray of the 25 g standard

then the slope of the graph, m, is given by:

$$m = \frac{\log F_{25} - \log Fy}{Wx_{25} - Wxi}$$

$$\text{therefore } Fy = F_{25}\, 10^{-m(W_{25}-Wx)} \qquad (2.4)$$

But, the efficiency is directly proportional to the calibration (Equation 2.2), and as stated earlier, the geometry correction will be independent of γ-ray energy. Therefore the following relationship holds:

$$\frac{Pcx}{Pc_{25}} = \frac{Fy}{F_{25}} \quad \text{or} \quad Pcx = Pc_{25}\frac{Fy}{F_{25}} \qquad (2.5)$$

where Pcx = peak calibration at weight x
Pc_{25} = peak calibration of the 25g standard

Using this result and equation (2.4) and substituting into equation (2.3) yields:

$$A = \frac{(C-b)}{Pc\ 10^{-m(25-x)}} \qquad (2.6)$$

To determine the total radium isotopes picked up by the added 25g MnO_2 it is necessary to first correct the recovery yield of MnO_2. Therefore the individual bulk activities of nuclides preconcentrated by adsorption on MnO_2 were calculated using:

$$A = \frac{c-b}{Pc\ 10^{-m(25-x)}.Fc} \qquad (2.7)$$

where Fc was the fractional MnO_2 recovery yield.

2.1.3.3 Calculation of bulk $^{228}Ra/^{226}Ra$ activity ratios and ^{228}Ra activities

Defining "bulk" activities as those measured by γ-ray spectrometry on preconcentrated sample sources, then the "bulk" activity of ^{228}Ra on the sources was determined as the average of the activities of the individual ^{228}Ac γ-ray peaks. The bulk ^{226}Ra activity, measured by the ^{226}Ra γ-ray peak at 186 KeV, was then used to obtain the $^{228}Ra/^{226}Ra$ activity ratio of the preconcentrated source.

Having obtained the $^{228}Ra/^{226}Ra$ activity ratio the activity of ^{228}Ra was determined as the activity ratio times the ^{226}Ra activity determined by ^{222}Rn emanation from a separate 5-litre sample.

Table 2.4 illustrates these calculations for a range of sample activities and count times.

Table 2.4 Examples illustrating the calculations of bulk ^{226}Ra and ^{228}Ra activities

Sample	Count Time (mins)	Bulk ^{226}Ra ^{226}Ra, 186 KeV	±	Bulk ^{228}Ra activities (pCi) (nuclide, energy) ^{228}Ac, (129)	±	^{228}Ac, (209)	±	^{228}Ac, (338)	±	^{228}Ac, (912)	±	Average bulk ^{228}Ra	±	$^{228}Ra/^{226}Ra$	±
Stripa V2/1	1147	12470	66	2122	94	1750	50	1978	23	2032	21	1971	28	0.158	0.002
L3153	3224	848	11	212	17	206	12	190	4	196	4	201	5	0.237	0.007
1925-13	1344	24465	77	2366	105	1930	5	219	26	2170	21	2164	123	0.088	0.005
ALØ1	4405	42	3	27	6	27	4	26	2	27	1	27	2	0.64	0.07

Errors are quoted as 1σ from the mean.

2.1.3.4 Errors in the determination of ^{226}Ra, $^{228}Ra/^{226}Ra$ and ^{228}Ra.

There are two classifications of errors, random errors and systematic errors. Random errors are associated with the reproducibility of a result, that is, its precision. Systematic errors are a measure of the uncertainties in the accuracy of an analysis; the difference between the determined and actual sample value. Both of these are discussed below with respect to measurement of radium nuclide activities.

Random errors

1) Counting statistics

Due to the inherent random nature of radioactive decay there is always a random error associated with the measurement of nuclear count rates. Fortunately this error can be calculated because of the statistical nature of decay. If a sample count rate was measured many times, the measurements would form a Gaussian Distribution. For such a distribution, the error on a single measurement is given by:

$$\sigma = \sqrt{x} \qquad (2.18)$$

where σ = standard deviation from the mean

x = n^{o} of counts in a single measurement

This error is obviously reduced by collecting as many counts on the detector as possible. Therefore wherever possible, at least 10,000 counts were accumulated on the γ-ray peaks used for radium nuclide analysis. This reduces the counting errors to 1% fractional error.

2) Experimental errors

The analytical precision for $^{228}Ra/^{226}Ra$ determinations can be seen by the result of 4 replicate analyses performed on samples collected within a 2 week period from the King's Spring, Bath (Table 2.5). On the assumption that absolute radium activities will have negligible variation within this period, the results show that each measurement was within 1σ counting error of the mean value for the $^{228}Ra/^{226}Ra$ activity ratio. Therefore experimental errors cannot be of greater significance than counting errors on these samples. Assuming that the same is true for other measurements of the $^{228}Ra/^{226}Ra$ activity ratio, counting errors have been taken as the error in precision of analysis.

Systematic errors

Lee (1980) and M. Youngman (pers. comm.) have both performed repeated measurements of ^{226}Ra from standard solutions. On the basis of these experiments there is a 5% variation in ^{226}Ra determinations in the system used. This is greater than the counting error of most determinations, and is therefore used as the systematic error in all ^{226}Ra analysis.

Errors in ^{228}Ra activities were determined by combining errors in ^{226}Ra and $^{228}Ra/^{226}Ra$ analysis by standard error propagation formulae as outlined in Appendix I. All errors in ^{226}Ra, ^{228}Ra and $^{228}Ra/^{226}Ra$ are quoted

as 1 standard deviation (1σ) from the mean. Table 2.6 describes the detection limits for ^{226}Ra and ^{228}Ra analysis, as defined in the Table.

Table 2.5 Errors in precision on $^{228}Ra/^{226}Ra$ measurement based upon repeated analysis of King's Spring, Bath.

Sample name	Collection date	$^{226}Ra/^{228}Ra$	±	Preconcentration method
1925-10a)	17-2-85	0.079	0.005	MnO_2 powder
1925-10b)	19-2-85	0.086	0.005	Mn-fibre
1925-10c)	19-2-85	0.080	0.004	Mn-fibre
1925-10d)	24-2-85	0.079	0.005	Mn-fibre
		$\bar{X}$ = 0.081	0.003*	

* 0.003 represents the average standard deviation of each value. The actual error of the mean value is $\sigma/\sqrt{N}$ = 0.002.

Table 2.6 Detection limits for bulk ^{226}Ra and ^{228}Ra determined by intrinsic (Ge) γ-spectrometry

Count time (d)	Detection limit* (pCi) Statistical error (1σ)					
	1%		3.1%		5%	
	^{226}Ra	^{228}Ra	^{226}Ra	^{228}Ra	^{226}Ra	^{228}Ra
1	922	557	92	56	37	22
2	461	278	42	28	18	11
3	307	186	31	19	12	7

*Defined as the activity (in pCi) required to obtain the fractional error quoted for one standard deviation counting statistics, given the count time quoted.

Note: The values above were calculated from a 5g $BaSO_4$ co-precipitated radium standard. There is little difference between the limits quoted above and those for a 5g MnO_2 radium standard.

2.2 Analysis of ^{214}Pb, ^{212}Pb and ^{210}Pb in groundwaters

2.2.1 Sample collection

Both ^{214}Pb and ^{212}Pb have short half-lives. ^{214}Pb is present in the ^{238}U series with $t_{\frac{1}{2}}$=26.8 mins, ^{212}Pb is in the ^{232}Th series with $t_{\frac{1}{2}}$=10.6 hours. Due to their short half-lives samples could only be analysed from the closest available groundwater, the King's Spring borehole, Bath.

Before sample collection the borehole was flushed by running the borehole for at least 20 minutes. This removes stagnant water in which the nuclides are not present due to decay or adsorption onto the borehole walls. For the determination of ^{214}Pb and ^{212}Pb, 5-10 litres of water was collected. Sufficient 7m HNO_3 was added to acidify the water to pH <2, 300 mg Fe^{3+} and 50 mg Pb^{2+} had initially been placed within the sample containers. Therefore when water was added the stirring action of the inflowing water ensured a homogeneous distribution of Pb^{2+} and Fe^{3+} carriers.

Immediately, conc NH_4OH was added to the sample to cause co-precipitation of Pb^{2+} with $Fe(OH)_3$. The times of sample collection and ferric hydroxide precipitation were noted.

The samples were brought back to the laboratories for further analysis.

The longer half-life of ^{210}Pb ($t_{\frac{1}{2}}$=22.3 years) means that there is no problem of its decay before analysis. In addition to the 5-10 litre samples collected above,

^{210}Pb was also measured in 20 and 100 litre samples. These samples were brought to the laboratories and out-gassed with air to remove any dissolved ^{222}Rn that could decay to eventually produce ^{210}Pb.

2.2.2 Sample processing

As soon as the $Fe(OH)_3$ precipitates were brought back to the laboratories they were separated from the water by syphoning and centrifugation and dissolved in glacial acetic acid. Approximately 5 mls saturated K_2CrO_4 was added to precipitate $PbCrO_4$. This was isolated by centri-fugation, and dissolved in a few drops of 7M HNO_3. Ensuring that the pH was ≈4 by addition of ammonium acetate a few drops of conc H_2SO_4 were added to the solution to precipitate lead sulphate. The sulphate was isolated by centrifugation, washed with 50% water/EtOH, then EtOH. The precipitate was then made into a slurry by the addition of a few drops of EtOH and transferred onto a weighed planchette using a pipette. The preci-pitate was then dried under an infra-red lamp, weighed and immediately counted on an intrinsic Ge γ-ray spectro-meter to measure ^{214}Pb and ^{212}Pb via their γ-ray peaks. The planchettes were then stored for 25 days, then ^{210}Pb measured via its ^{210}Bi daughter using a beta counter.

2.2.3 Detector Calibrations

2.2.3.1 Gamma-ray spectrometer

The activities of ^{214}Pb were sufficient for it to be measured using a high resolution intrinsic Ge γ-ray spectrometer, which allows resolution of peaks produced by ^{214}Pb from those produced by other decaying nuclides.

To prepare a standard source for detector calibration, excess conc H_2SO_4 was added to 50 mg Pb^{2+}. The resulting $PbSO_4$ was isolated onto a weighed planchett and dried. The chemical recovery yield of $PbSO_4$ was then determined.

A weighed amount of ^{226}Ra standard solution was added to the planchett and evaporated to dryness. The surface of the $PbSO_4$ was then sealed with a layer of cellulose acetate to prevent escape of ^{222}Rn. The planchett was further sealed by covering with a perspex disc held in place with epoxy resin (Fig. 2.7).

The planchett was stored for 21 days to allow equilibrium to be established between ^{226}Ra and its daughters. The source was then counted by γ-ray spectrometry and the resulting peak count rates used to establish a full energy - efficiency curve as described in section 2.1.3.1 Then, ^{214}Pb was determined via the count rates on the γ-rays produced on decay of ^{214}Pb at 241, 295 and 351 KeV. The calibrations for these peaks given as count rate/pCi of ^{214}Pb are given in Table 2.7.

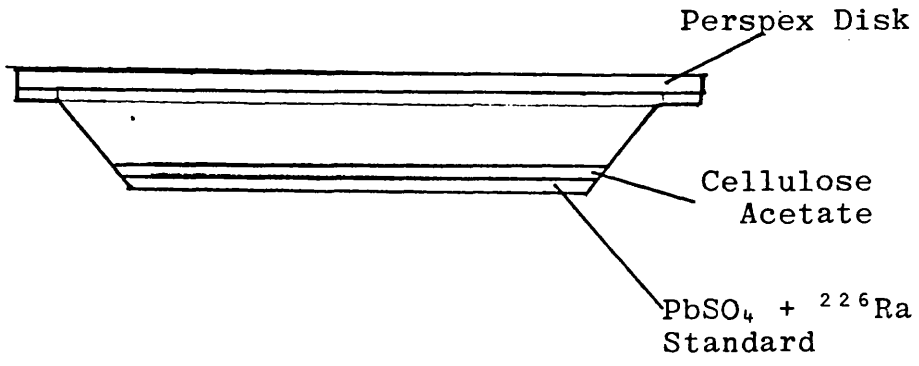

Figure 2.7 Sealed Planchett prepared for the calibration of gamma-rays used to determine ^{214}Pb and ^{212}Pb.

Table 2.7 γ-spectrometer calibration for ^{214}Pb and ^{212}Pb in a sealed planchett*.

Nuclide	Energy (KeV)	Photon abundance (%)	Count rate (cpm)	Detector efficiency (%)	Calibration cpm/pCi
^{226}Ra	186	3.51	3.24	16.2	0.0054
^{214}Pb	242	7.12	3.76	8.8	0.0063
^{214}Pb	295	18.2	8.03	7.35	0.0134
^{214}Pb	352	85.1	13.16	6.25	0.0219
^{214}Bi	609	44.6	7.68	2.9	0.0128
^{214}Bi	1120	14.2	1.42	1.7	0.0024
^{212}Pb**	239	43.5	-	10.0	0.0448
^{212}Pb**	300	3.27	-	7.18	0.0024

* See Fig. 2.8

** ^{212}Pb efficiencies and calibrations determined from Fig. 2.8

There were no standard ^{212}Pb sources available. However, its calibration was performed by fitting a regression equation to the energy-efficiency curve of the ^{226}Ra source at equilibrium with its daughters (see 2.1.3.1). This equation was then used to determine the efficiency of the γ-ray detector at 239 KeV, the energy of the most intense ^{212}Pb γ-ray. Using the photon abundance of this peak given by Schotzig and Debertin (1983), the calibration was determined as the count rate of the ^{212}Pb γ-ray peak at 239 KeV per pCi of ^{212}Pb.

2.2.3.2 Beta counter calibration

A series of ^{210}Pb standards for ^{210}Pb beta counting were prepared by precipitating between 100 - 400 pCi of ^{210}Pb (from a standard solution obtained from the Radiochemical Centre, Amersham) with between 40 - 200 mg Pb^{2+}. These standards were prepared by the addition of conc H_2SO_4 to a solution containing Pb^{2+} and ^{210}Pb. The precipitate was washed and dried as previously described and the chemical recovery of $PbSO_4$ determined. These standards were stored for 25 days then counted by beta counting after covering with a 16 mg/cm^2 aluminium foil to absorb any α-particles, and beta particles with energies of 15 and 61 KeV produced by ^{210}Pb. This enabled the measurement of beta particles with a maximum energy of 1161 KeV produced by ^{210}Bi.

Figure 2.8 shows the linear relationship between count rate and weight of $PbSO_4$ for the prepared sources. showing that there is no self absorption of beta particles up to the maximum of 200 mg $PbSO_4$ source.

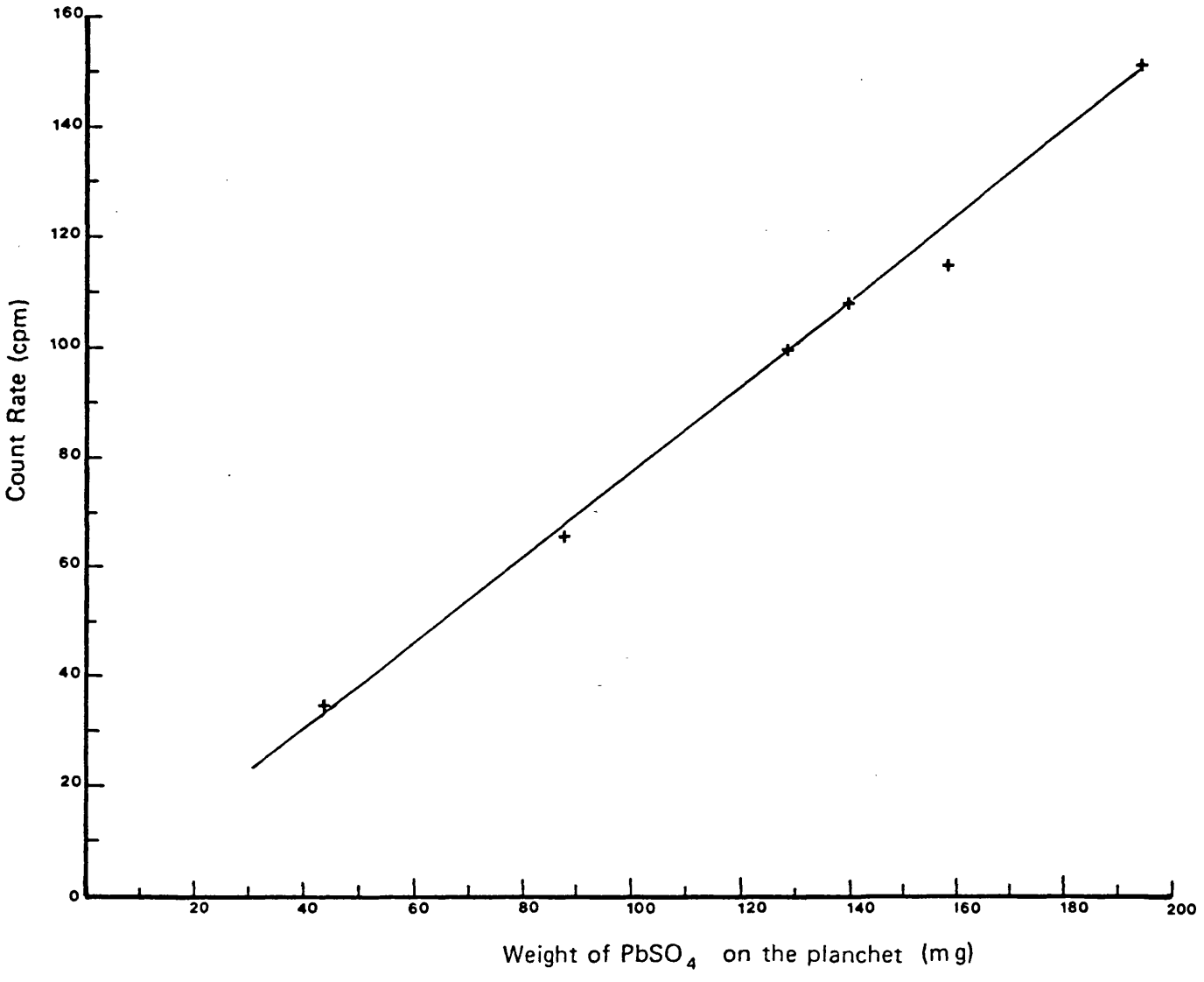

Fig 2.8 Count Rate of ^{210}Bi against Weight of $PbSO_4$ carrier on Planchets

Detector efficiencies were calibrated using the expression

$$\varepsilon = \frac{(Std - b)}{2.22.fc\ A} \times 100$$

Where ε = detector efficiency (%)

fc = fractional chemical yield of $PbSO_4$

A = standard activity (pCi)

Std = count rate of standard (cpm)

b = background count rate (cpm)

Generally 50 mg $PbSO_4$ was isolated. The beta counter efficiency calculated for a source of this weight was 26%, and was the efficiency used in ^{210}Pb activity determination.

2.2.4 Calculation of sample activities

2.2.4.1 ^{212}Pb and ^{214}Pb

The activity of ^{214}Pb was measured by counting samples every 3 minutes for 1 hour or until its decay was no longer observed. For each counting period the activity of ^{214}Pb present at that time was calculated using the relationship:

$$A_t = \frac{(C_t - b)}{fc\ fd\ V} \qquad (2.9)$$

where C_t = count rate of sample at time t, from collection

A_t = sample activity at time t, (pCi/l)

V = sample volume (l)

b = background count rate (cpm)

fc = fractional chemical yield of $PbSO_4$

fd = detector calibration (cpm/pCi)

The ^{214}Pb activities were all calculated using its γ-ray peak at 351 keV. This peak had the highest γ-ray photon abundance of all the ^{214}Pb γ-rays, and therefore the highest count rates. This minimised the error due to counting statistics.

For each counting period, the ^{214}Pb activity at time, t, was used to calculate the activity at t=0, the time of sample collection, using the relationship:

$$A_t = A_o\ e^{-\lambda t} \qquad (2.10)$$

where λ = decay constant of ^{214}Pb.

Therefore a series of values of A_o were obtained which could be averaged to give the value of ^{214}Pb activity in the sample.

A similar process was performed for ^{212}Pb. After all the ^{214}Pb had decayed, ^{212}Pb was measured via the γ-rays produced by its decay of energy 239KeV. This is a very intense γ-ray peak (photon abundance of ≈44%) but may suffer interference from the ^{214}Pb peak at 241 KeV. Hence the measurement after ^{214}Pb decay.

Samples were counted every 2 hours for 10 hours. Counting normally started 2 hours after sample collection, by which time only 12% of the initial ^{212}Pb had decayed. Activities were calculated in the same way as described for ^{214}Pb.

2.2.4.2 ^{210}Pb

After ^{212}Pb measurement, samples were stored for 25 days to allow equilibrium to be established between ^{210}Pb and ^{210}Bi. The beta activity of the sample was then measured and the ^{210}Pb activity determined by using Equation 2.9 with:

C_S = sample count rate (cpm)

b = background count rate (cpm)

fc = fractional chemical yield of $PbSO_4$

fe = fractional counter efficiency

V = sample volume (l)

2.2.5 Errors in the determination of ^{214}Pb, ^{212}Pb and ^{210}Pb

2.2.5.1 Counting statistical errors

Because ^{214}Pb samples were measured repeatedly every 3 minutes, statistical errors were high, between 10-20% fractional error. Decay of ^{214}Pb meant that the initial count rates were much higher, with lower statistical error, than the final measurements. A simple geometrical average result does not take into account the better precision of measurements with lowest errors.

Therefore the mean result and its standard deviation were calculated as "weighted" means and errors. The "weights", indicating the importance of particular measurements, were given the value $1/\sigma^2$ where σ is the standard deviation of any measurement. The mean is given by:

$$\langle A \rangle = \frac{\sum_{c}^{n} Wi\ Ai}{\sum_{i}^{n} Wi} \qquad (2.11)$$

where Wi = weight of i^{th} measurement

Ai = activity of i^{th} measurement

$\langle A \rangle$ = weighted average activity

The standard deviation of the weighted mean is given by:

$$\frac{1}{\sigma^2} = \sum_{c}^{n} \frac{1}{\sigma i^2} \qquad (2.12)$$

where σ = standard deviation of the mean

σ_i = standard deviation of the i^{th} measurement

The deviation and uses of these formulae are described in standard texts on statistics.

The mean and standard deviation for ^{212}Pb measurements were determined as described above. The activity of ^{210}Pb was measured using only one period of counting, so the statistical error in that case was only due to the total number of background corrected counts picked up in the single measurement.

2.2.5.2 Experimental errors

The total random experimental error, due to uncertainties in measuring sample volumes, counting statistics, chemical yield determinations, etc., can simply be determined by standard combinations of errors, as outlined in Appendix 2. For instance, the uncertainty of ^{210}Pb activities are given by the uncertainties of each value in equation (2.9), giving:

$$\sigma_A^2 = A^2 \left[\frac{(\sigma_{cs}^2 + \sigma_b^2)}{(cs-b)^2} + \frac{\sigma_c^2}{fc^2} + \frac{\sigma_e^2}{fe^2} + \frac{\sigma_v^2}{v^2} \right] \qquad (2.13)$$

where σ_A = standard deviation on the ^{210}Pb activity

σ_{cs} = standard deviation of the sample count rate

σ_b = standard deviation of the background count rate

σ_c = standard deviation of the chemical yield

σ_e = standard deviation of the detector efficiency

σ_v = standard deviation of the sample volume

The uncertainty in ^{214}Pb and ^{212}Pb measurements were obtained using similar expressions derived from equation (2.9). The greatest error in all of these determinations was found to be that of counting statistics. For instance, ^{214}Pb counting statistical errors averaged 5% fractional error, whereas the total errors were ~6%.

If experimental errors are representative of all errors on ^{214}Pb, ^{212}Pb and ^{210}Pb determinations, then measurements of these nuclides should be repeatable within experimental uncertainties. Analysis was performed on several solutions containing known activities of ^{210}Pb and ^{214}Pb (Table 2.8). The results show that there is a difference of approximately 10% between the known and measured nuclide activities. The experimental uncertainties are only ~4%. This discrepancy may be attributable to lack of equilibrium between added Pb^{2+} carrier and the lead nuclides in solution. However, it is impossible to determine the extent of equilibrium attained between lead carriers and dissolved radionuclides. The only recourse was to ensure that solutions were thoroughly mixed to ensure that equilibrium was attained and to use experimental errors as the uncertainties.

Table 2.8 Experiments testing the recovery of ^{210}Pb and ^{214}Pb from solutions of known activity

Nuclide	Description of the solution	Solution volume (l)	Pb^{2+} carrier weight (mg)	Pb^{2+} recovery yield, %	Solution activity (pCi)	Recovered activity (pCi)	+/-[B]
^{210}Pb	acidified distilled water	5	25	94	513	469	19
^{210}Pb	acidified tapwater	5	50	41	513	480	10
^{210}Pb	acidified tapwater	5	100	63	513	433	16
^{214}Pb	^{226}Ra 'spiked' tapwater	5	50	68	1000[A]	966	54
^{214}Pb	Stripa V1	5	50	36	620±38[A]	531	43

[A]The solutions were stored for >21 days to establish equilibrium between ^{226}Ra and ^{214}Pb.

[B]Errors are quoted as 1σ from the mean, from counting statistics and experimental uncertainties.

2.3 The analysis of ^{232}Th and ^{238}U in aquifer rock samples.

2.3.1 Introduction

An investigation of the radioelement content of groundwaters must by necessity include measurement of the bulk aquifer U and Th activities from which the radionuclides originate. In this study U and Th contents were measured by γ-ray spectrometry using two detectors:

a) NaI (Thallium activated) crystal γ-spectrometer with a crystal size of 4" x 6" in diameter.

b) High purity intrinsic germanium γ-ray spectrometer.

The accuracy of these methods was checked by α-spectrometry measurement after rock dissolution and chemical separation.

2.3.2 Sample preparation

Unweathered freshly cut rock samples were collected from outcrops, quarries or boreholes close to the sampling locations for water samples. The rocks were crushed into fragments using a jaw crusher then pulverised into a fine powder using a Tema machine. These procedures were carried out at the rock crushing facility at the Department of Geology, University of Bristol.

About 200 g of the crushed powder was placed into a tin (10 cm diameter x 4 cm) for γ-counting. To establish secular equilibrium between ^{222}Rn and its ^{214}Pb and ^{214}Bi daughters the sample was sealed and stored for 21 days.

2.3.3 Measurement of U and Th by γ-spectrometry

2.3.3.1 Introduction

In this study all γ-rays emitted by nuclides in the U and Th series were investigated to assess their suitability for measuring the activity of the parent nuclides. It was assumed that since the rocks analysed were generally older than 1.25 m years that secular equilibrium had been established throughout the U and Th series.

For measurement of uranium the 1001 keV γ-ray from ^{234}Pa, the 63 kev peak from ^{234}Th and 186 keV peak of ^{226}Ra would be ideal for measurement (e.g. Kehinde et al., 1983; Kim and Burnett, 1983; see also table 2.9). However for the γ-ray spectrometer used in this study the 1001 keV peak was at a region of low detector efficiency and gave very poor counting statistics. The 186 kev peak measured in rocks is actually a combination of the 185.7 keV γ-ray of ^{235}U and 186.2 keV γ-ray of ^{226}Ra. (Piatt, et al, 1982). In order to use this peak it must be assumed that:

a) equilibrium has been established between ^{226}Ra and ^{238}U.

b) there is a constant ratio between ^{238}U and ^{235}U in all measured rocks.

The γ-rays due to ^{214}Pb and ^{214}Bi were also measured to assess their suitability for rock U measurement.

For ^{232}Th there are no direct decay γ-photons. However ^{228}Ac produces numerous γ-ray photons which are ideal

Uranium/Radium (4n+2) series

nuclide	half life	type of decay	particle energies and transition probabilities: energy MeV	transition probability	electromagnetic transitions: photon energy MeV	photons emitted	transitions internally converted	photon energy MeV	photons emitted	transitions internally converted
Plutonium-242	$3{\cdot}87 \times 10^5$y	α	4·856	21·1%	0·045	0%	21·1%			
			4·900	78·9%						
Uranium-238	$4{\cdot}49 \times 10^9$y	α	4·145	23%	0·048	0%	23%			
			4·195	77%						
Thorium-234	24·1d	β⁻	0·100	12%	0·030	0%	8·2%	0·093	3·6%	
			0·101	21%	0·063	5·7%	2·3%			
			0·193	67%	0·092	3·2%	16·5%			
Protactinium-234m	1·17m	β⁻	2·29	98%	0·043	0%	1%	0·810	0·5%	
			others	low	0·767	0·2%		1·001	0·6%	
		i.t.		0·13%						
Protactinium-234	6·70h	β⁻	present in the series only in very low abundance							
Plutonium-238	87·75y	α	5·445	28·7%	0·043	~0%	~28·5%	0·011–0·022	~13% (U L X-rays)	
			5·499	71·1%	0·094–0·115	~2·1 x 10^{-4}% (U K X-rays)				
			others	0·2%						
Uranium-234	$2{\cdot}48 \times 10^5$y	α	4·723	27·5%	0·053	0·1%	27·4%			
			4·773	72·5%						
Thorium-230	$7{\cdot}7 \times 10^4$y	α	4·618	23·4%	0·068	0·4%	22·6%			
			4·684	76·3%						
			others	0·3%						
Radium-226	1600y	α	4·598	5·5%	0·186	3·4%	2·1%			
			4·781	94·5%						
Radon-222	3·824d	α	5·486	100%						
Polonium-218	3·05m	α	6·000	~100%						
		β⁻	0·277	~0·02%						
Astatine-218	~2s	α, β⁻	present in the series only in very low abundance							
Radon-218	$3{\cdot}0 \times 10^{-2}$s	α	present in the series only in very low abundance							
Lead-214	26·8m	β⁻	0·21	0·5%	0·053	~0%	~11%			
			0·51	15·5%	0·242	6·7%	5·3%			
			0·69	42%	0·295	16·9%	8·1%			
			0·74	36%	0·352	32·0%	10·0%			
			1·03	6%						
Bismuth-214	19·8m	α	4·9–5·5	0·02%	0·273	5·3%	0·3%			
		β⁻	0·42	11%	0·609	41·7%				
			1·02	23%	0·769	5·3%				
			1·51	18%	1·120	14·3%				
			1·55	15%	1·238	5·0%				
			1·88	9%	1·378	4·8%				
			2·6	4%	1·764	15·9%				
			3·27	20%	2·204	5·3%				
Polonium-214	$1{\cdot}62 \times 10^{-4}$s	α	7·688	100%						
Thallium-210	1·30m	β⁻	present in the series only in very low abundance							
Lead-210	22·3y	β⁻	0·015	~80%	0·046	~4%	~76%	0·009–0·017	~21% (Bi L X-rays)	
			0·061	~20%						
Bismuth-210	5·01d	α	~4·67	~$1{\cdot}3 \times 10^{-4}$%						
		β⁻	1·161	~100%						
Polonium-210	138·38d	α	5·305	100%						
Thallium-206	4·20m	β⁻	present in the series only in very low abundance							
Lead-206	stable									

Percentages relate to disintegrations of the individual nuclides.

Table 2.9 α, β and γ-ray data for the ^{238}U series

for measurement (Table 2.10).

2.3.3.2 Preparation of ^{238}U, ^{232}Th and ^{40}K standards

The U, Th and ^{40}K standards used for γ-spectrometry calibration in this study had previously been prepared by A. Zereski (1981).

The uranium standard had been prepared by mixing gummite (28.1% U_3O_8) with 200 g sand to give a 100μg U/g sand standard.

The thorium standard was prepared by heating $Th(NO_3)_2 . nH_2O$ to 300°C then 1000°C to convert it into the stoichiometric oxide ThO_2. The standard was prepared by mixing the oxide with acid washed sand to give a 1294.8 μg Th/g sand standard.

The ^{40}K standard was prepared by dissolving the appropriate amount of KCl in distilled water, adding this to 200 g sand and evaporating to dryness while stirring. This assured a homogenous distribution of KCl within the sand.
All standards were prepared in sealed 10 cm diameter x 4" tins.

2.3.3.3 Gamma-ray calibration

Standards were counted on the γ-ray spectrometer by placing them directly on top of the detector crystals or end cap. The NaI(Th) detector measurements were made by counting for 80,000 seconds. The Int. germanium spectrometer measurements were counted for longer (3 days)

Uranium/Thorium (4n) series

nuclide	half life	type of decay	particle energies and transition probabilities: energy MeV	transition probability	electromagnetic transitions: photon energy MeV	photons emitted	transitions internally converted	photon energy MeV	photons emitted	transitions internally converted
Plutonium-240	6537y	α	5·014	~0·09%	0·045	0%	24%			
			5·123	~24%						
			5·168	~76%						
Uranium-236	$2{\cdot}40 \times 10^7$y	α	4·331	~0·3%	0·050	0%	26%			
			4·443	~26%	0·113	0%	0·3%			
			4·493	~74%						
Thorium-232	$1{\cdot}405 \times 10^{10}$y	α	3·830	~0·2%	0·059	0%	22%			
			3·963	~23%	0·124	0%	0·2%			
			4·012	~77%						
Radium-228	5·75y	β^-	0·048	100%	0·007	0%	100%			
Actinium-228	6·13h	β^-	0·45	4·9%	0·058	0·6%	79·4%	0·783	1·4%	
			0·49	5·6%	0·099	0%	5%	0·796	4%	
			0·62	5·7%	0·129	2·8%	7·2%	0·836	2·5%	
			0·99	7·3%	0·184	1·7%	5·6%	0·912	23%	
			1·02	4·0%	0·209	4·3%	0·2%	0·966	7%	
			1·12	6·5%	0·270	4·1%	0·2%	0·970	13%	
			1·17	33%	0·328	5·3%	0·2%	1·464	1·1%	
			1·76	20%	0·338	15%	1%	1·503	2·5%	
			2·10	13%	0·410	2·5%	0·5%	1·593	4·5%	
					0·463	3·6%	0·6%	1·642	2·4%	
Uranium-232	72y	α	5·137	0·3%	0·058	0·2%	31·8%			
			5·263	31·7%	0·129	0·08%	0·22%			
			5·320	68%						
Thorium-228	1·913y	α	5·140	0·03%	0·085	1·6%	27·4%			
			5·176	0·2%	0·132	0·19%	0·01%			
			5·211	0·4%	0·167	0·12%	0·18%			
			5·341	28%	0·216	0·29%	0·01%			
			5·424	71%						
			others	low						
Radium-224	3·64d	α	5·447	5·2%	0·241	4·2%	1·0%			
			5·684	94·8%						
Radon-220	55·3s	α	5·747	0·07%	0·542	0·07%				
			6·288	99·93%						
Polonium-216	0·15s	α	5 984	~0·002%	0·808	0·002%				
			6·777	~100%						
Lead-212	10·6h	β^-	0·155	5%	0·115	0·6%	4·1%			
			0·332	82%	0·239	44·8%	37·5%			
			0·571	13%	0·300	3·4%	1·5%			
Bismuth-212	60·6m	α	5·607	0·4%	0·040	1%	28%			
			5·768	0·6%	0·288	0·3%	0·1%			
			6·051	25·2%	0·326	0·1%				
			6·090	9·6%	0·453	0·4%				
			others	low	0·727	6·6%	0·1%			
					0·785	1·1%	0·1%			
		β^-	0·445	0·7%	0·893	0·4%				
			0·572	0·3%	0·952	0·2%				
			0·630	1·9%	1·079	0·5%				
			0·738	1·5%	1·513	0·3%				
			1·524	4·5%	1·621	1·5%				
			2·251	55·2%	1·680	0·1%				
			others	low	1·806	0·1%				
Polonium-212	$3{\cdot}05 \times 10^{-7}$s	α	8·785	100%						
Thallium-208	3·07m	β^-	1·032	3·4%	0·253	0·8%	0·6%	0·860	12·3%	0·3%
			1·073	0·6%	0·277	6·9%	3·7%	1·093	0·4%	
			1·285	24%	0·511	23·0%	2·0%	2·615	99·8%	0·2%
			1·518	22%	0·583	85·8%	2·2%			
			1·795	50%	0·763	1·8%	0·1%			
Lead-208	stable									

Percentages relate to the disintegrations of the individual nuclides.

Table 2.10 α, β and γ-ray data for the ^{232}Th series

due to its poorer detection efficiency.

All measured peaks were measured above the Compton Scattering continuum. Backgrounds were measured from 200 g acid washed sand as the count rate of the peak (if present) above the Compton continuum. All samples and standards were of the same weight and counting geometry to avoid correcting for variations. It was assumed that self absorption is negligible within the samples. This assumption may introduce small errors in the results as varying rock densities have produced absorption effects as shown by other studies (Chouk et al, 1978; Sato et al, 1980; Kehinde et al, 1983).

Intrinsic Ge γ-ray detector results were calibrated according to the following expression:

$$C_i = \frac{(P_i - b)}{A} \qquad (2.14)$$

where C_i = cpm/unit nuclide i activity (in 200 g of standard)

P_i = peak count rate (cpm)

A = activity of the parent nuclide

b = background count rate (cpm)

The results for the U and Th series radionuclides are given in table 2.14. Some peaks produced by ^{232}Th series nuclides were found to give widely varying results compared to other ^{232}Th series peaks in different samples. It was found that γ-rays from nuclides in the ^{235}U series may be the cause. Despite the low abundance

(^{235}U : ^{238}U ratio is 1:21.7) some γ-rays produced by ^{235}U series nuclides are produced with high γ-ray photon abundances (n^{o} photons produced/disintegration) which may result in their detection. Several of these photons are produced sufficiently close to ^{232}Th series γ-rays as to be indistinguishable in the current detector. The ^{235}U series γ-ray photons which cause interferences and the interfered peaks are given in table 2.11.

2.3.4 Calculation of sample activities

To achieve good counting statistics samples were counted for up to 3 days. The results were calculated simply by re-arranging equation (2.14) to determine sample activity (A) given the calibration (C_i). The results for the U and Th series γ-rays were simply averaged to produce the average U and Th content.

2.3.5 Precision and accuracy of U and Th measurements

2.3.5.1 Determination of analytical precision

a) Counting statistical errors The error in precision due to counting statistics is easily calculated from the number of counts accumulated. For low activity samples good counting statistics were achieved with long count times, up to a maximum of 3 days.

b) Sampling errors Precision errors also occur due to the incomplete mixing of the powdered rock sample. To estimate the importance of sampling error, 7 separate γ-ray measurements were performed upon a 2 kg sample of Stripa "3DP1" granite. The results are given in table 2.12. The mean uranium value is 51.5 +/- 3.4 (2 sigma)

Table 2.11 ^{235}U series gamma rays interfering with ^{232}Th series gamma ray measurement

γ-ray peak				Interfering peak			
Energy (kev)	Nuclide	Series	Photon abundance (%)	Energy (kev)	Nuclide	Series	Photon abundance (%)
239	^{212}Pb	^{232}Th	44.8	236	^{227}Th	^{235}U	13.
270	^{228}Ac	^{232}Th	4.1	269.4	^{223}Ra	^{235}U	13.6
338	^{228}Ac	^{232}Th	15.	338.	^{223}Ra	^{235}U	2.78

Table 2.12 Precision of ^{238}U and ^{232}Th analysis of rock samples by intrinsic germanium γ-ray spectrometry

Sample No.	Uranium Content µg/g (±2σ)		Thorium Content µg/g (±2σ)		Th/U activity ratio (±2σ)	
1	52.6	1.8	33.6	2.7	0.21	0.02
2	49.4	1.5	35.9	2.6	0.24	0.02
3	51.2	0.7	34.7	1.3	0.23	0.01
4	51.2	1.8	35.8	2.9	0.23	0.02
5	53.6	0.7	34.0	1.2	0.21	0.01
6	50.8	1.0	33.4	1.7	0.22	0.01
7	49.0	0.7	31.6	1.0	0.22	0.01
Averages (% error)	51.1	3.3(2σ) (6.4%)	34.1	3.0(2σ) (8.8%)	0.22	0.02(2σ) (9.1%)

The errors quoted are the errors on the average (or mean) value, not taking into account the error on the analysis. The error is an upper limit as the true error can be obtained by a weighted error calculation.

The two sigma errors are calculated from the standard deviation of the mean of 7 results. However this error is greater than the statistical error for any of the individual determinations, despite attempts to reduce sampling error by shaking the container before collecting the 200 g samples. Sampling error is therefore likely to be greater than counting statistical errors using the Int. Germanium gamma-detector.

2.3.5.2 Accuracy of rock analysis

The accuracy or systematic error was determined by 2 methods:

(i) comparing the Int. Ge γ-detector results with those from the previously calibrated NaI(Tl) γ-detector.

(ii) performing α-spectroscopy measurements of ^{238}U and ^{232}Th on samples.

Figure 2.9 shows the comparison between the 2 detectors for a variety of samples. As no certified rock standards were available at the time, a more accurate determination of the U and Th content of some of the samples was made by α-spectrometry. A brief description of the analytical method used during the α-spectrometry measurement of rocks is given in Appendix 3. The results are given in Table 2.13.

From Fig. 2.9 it is immediately obvious that there are differences between the results analysed by the intrinsic germanium and NaI(Tl) crystal α-detectors. For uranium analysis the high purity intrinsic germanium

Table 2.13 Comparison between NaI and Int(Ge) γ-spectrometry and α-spectrometric determination of ^{232}Th and ^{238}U in rocks.

Sample description	Int. Germanium γ-ray spectroscopy				NaI Gamma ray* spectroscopy				Rock analysis by α-ray spectroscopy			
	U, ppm	+/-	Th, ppm	+/-	U, ppm	+/-	Th, ppm	+/-	U, ppm	+/-	Th, ppm	+/-
Stripa granite V1 (25)	47.	3.7	41.2	5.9	37.4	6.2	29.2	3.8	39.6	0.3	29.9	0.3
Stripa leptite (finely powdered)	5.7 5.5	0.5 0.5	17.4 17.4	2.1 1.7	5.4	3.1	17.9	1.4	5.5	0.1	13.3	0.2
Rosemanowes granite (finely powdered)	19.9	3.0	24.9	4.3					16.6	0.3	15.9	0.4
Stripa granite 3 DP1	51.1		34.1		44.47 40.6	0.24 0.35	43.13 50.96	0.95 0.72	56.7 51.4 40.7	0.7 0.5 0.5	26.6 29.9 28.5	0.3[2] 0.6 1.8
Burrington Adit ORS (1)	2.3	0.4	13.1	0.2	2.25	0.13*	9.76	0.69*				
Burrington Adit ORS (2)	2.5	0.04	11.6	0.2	2.12	0.23	11.7	0.7*				
Pennant sandstone (finely powdered)	1.2	0.1	7.6	0.14	2.61	0.15	12.77	0.87				

* Errors are indicated as +/- 2σ by counting statistics.

[2] Stripa 3 DP1 average U = 49.6 ppm by α-spec.
average Th = 28.3 ppm

Fig 2.9 Comparison of Uranium and Thorium Rock Analysis by NaI Gamma-Ray Spectrometry and Intrinsic Germanium Gamma-Ray Spectrometry.

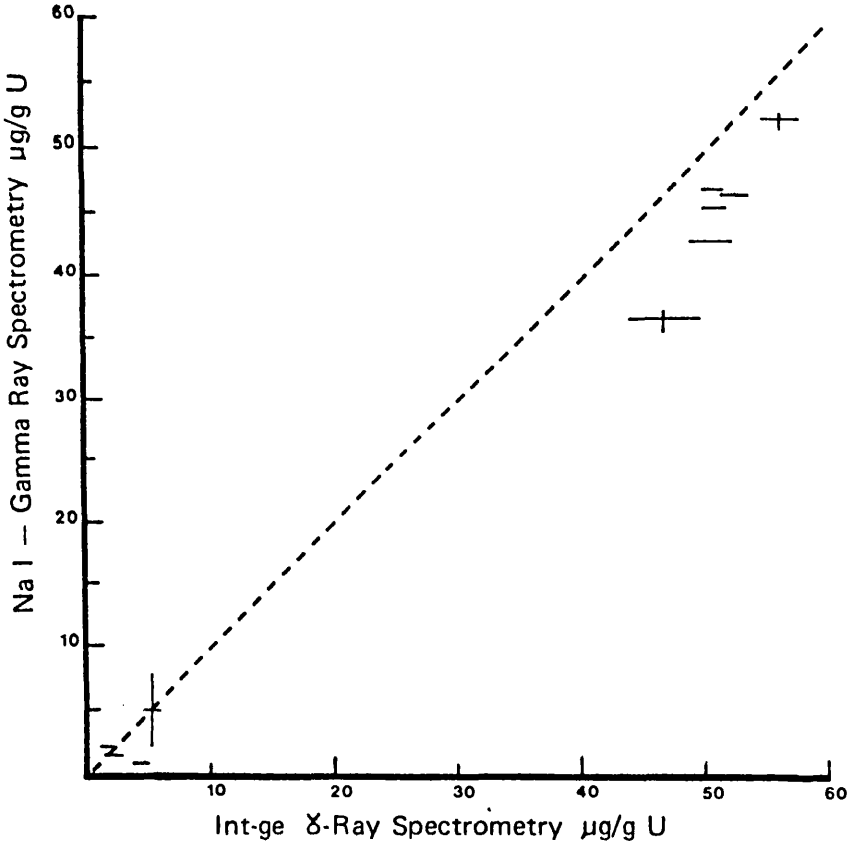

(A)

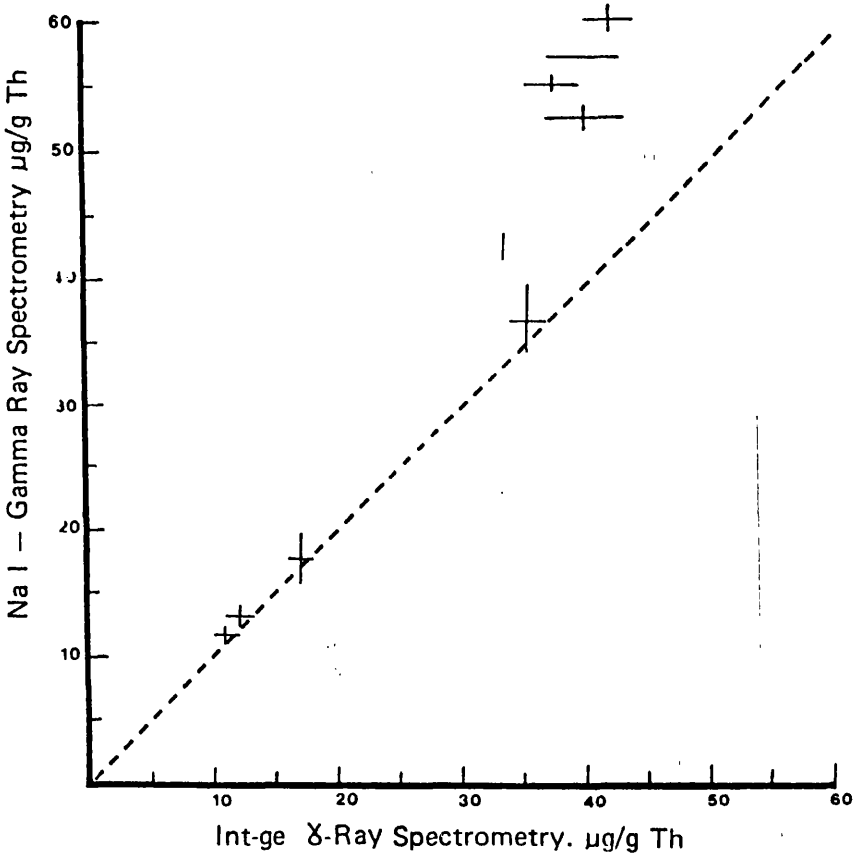

(B)

spectrometer results are higher than the NaI(Tl) detector. For thorium analysis the NaI(Tl) detector produces higher results.

There are several effects which could alter α-spectroscopy calibrations between different samples:

(i) geometry effects

(ii) self absorption between samples

(iii) disequilibrium within the standards

(i) and (ii) could produce variances between samples simply because of varying densities: high density samples will result in smaller samples with greater self adsorption. However both effects should have an equal effect upon both detectors.

Radioactive disequilibrium within the thorium standard (iii), appears to be the most reasonable explanation. Figure 2.10 shows the γ-spectra of a rock sample measured by the NaI(Tl) detector. Thorium is measured via the γ-ray emitted by ^{208}Tl at 2614 kev. However this result is then used to calculate a correction for the Th series γ-rays co-incident in the uranium regions of interest in the spectra. If ^{208}Tl is lower than equilibrium in the Th standard then this will result in high thorium measurements of rock samples and low uranium results (as a result from over-correction of thorium γ-rays in uranium regions of interest in the rock sample). This of course assumes that the thorium nuclides are at equilibrium in the rock samples themselves.

Fig. 2.10 Uranium, thorium and potassium analysis by γ-spectrometry Sample ..BBS....BARRINGTON A01T (1)..... Date..21-1-86

Results: U (region 2) U (region 4) Th (region 1) K (region 3)

Scale factor X ....O.K.. ..... ppm ..... ppm ..... ppm ..... %

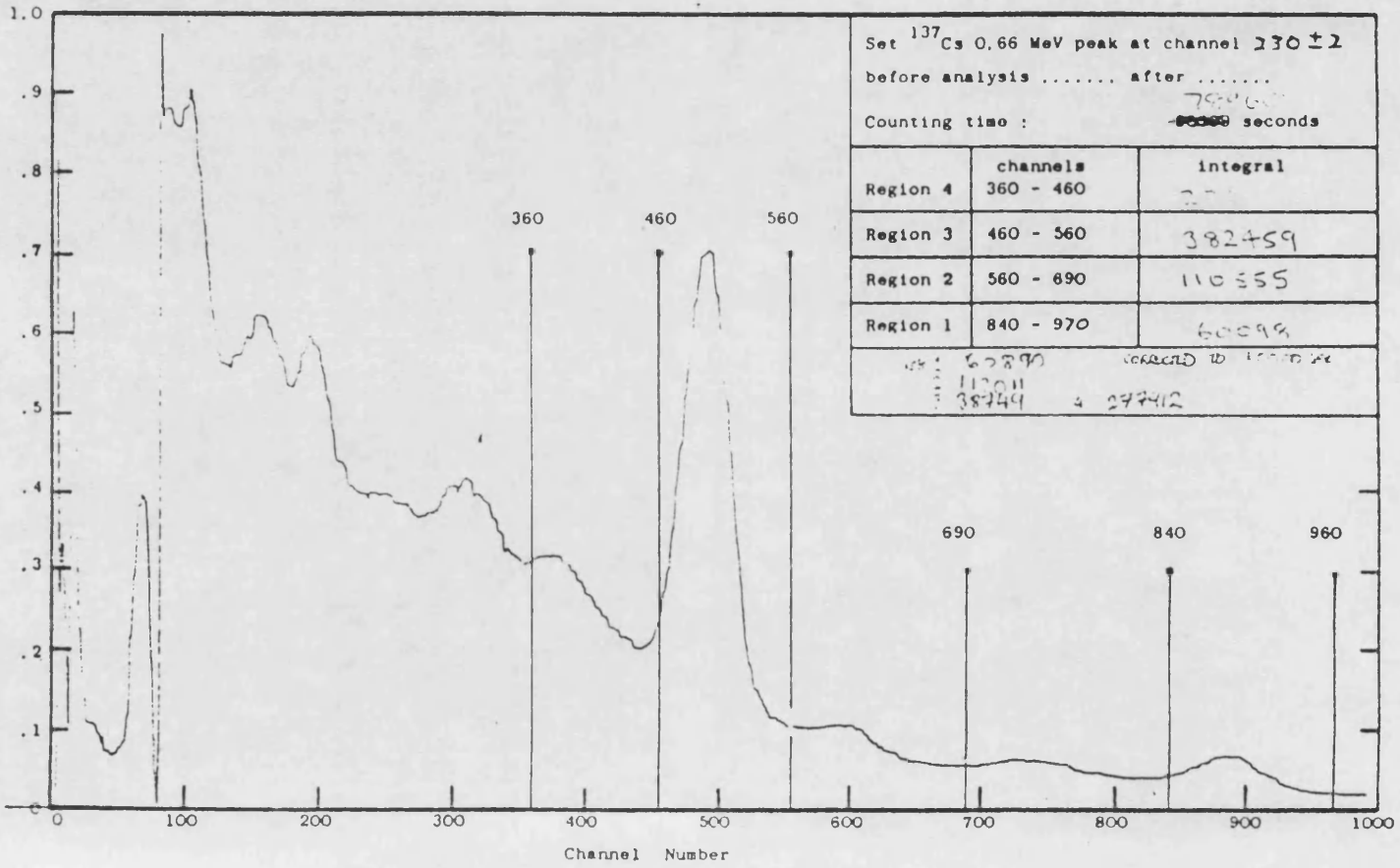

Set ^{137}Cs 0,66 MeV peak at channel 230 ± 2

before analysis ..... after .....

Counting time : 7500 seconds

	channels	integral
Region 4	360 - 460	
Region 3	460 - 560	382459
Region 2	560 - 690	110555
Region 1	840 - 970	60093

62390 corrected to
110211
38744 + 27741

The above sequence does not occur for intrinsic germanium γ-ray spectra because Th was measured via its daughter ^{228}Ac and not ^{208}Tl. Also the thorium results were not needed to add a correction onto the uranium result, due to the superior energy resolution of the semiconductor detector.

To show that this equilibrium between ^{232}Th and ^{208}Tl may be occurring, the $^{228}Th/^{232}Th$ activity ratio in the two available thorium nitrate containers in the sample were measured. Both showed $^{228}Th/^{232}Th$ <1.0 results which indicate that there was radioactive disequilibrium within the nitrates which may have been the source of thorium for the rock standard. However this still does not prove that the standard itself is at disequilibrium because the standard itself was not analysed.

Comaprison between α-spectrometry and Int. Ge γ-ray spectrometry analysis of rock samples.

Several rock samples were analysed by α-spectrometry (Table 2.13). The results seem to be more closely associated with the Int. Germanium γ-spectrometry results than for the NaI(Tl) detector. However there is a considerable amount of scatter compared to results by either γ-ray methods. This may be due to sampling errors due to non-homogenous samples. This is expected to be even more accute for α-spectroscopy samples than γ-ray samples due to the small size (1 g) as opposed to 200 g for γ-spectrometry measurements.

Detection limits by Intrinsic Germanium γ-ray spectrometry

Detection limits were calculated assuming that a one standard deviation counting statistical error of 10% (in terms of fractional error) was the maximum acceptable for a 3-day count. The detection limits were then calculated by the expression:

$$\text{detection limit} = \frac{100}{4320} \times \frac{1}{C} \qquad (2.15)$$

where 100 = n° counts required to give 10% fractional error

4320 = n° minutes in 3 days

C = calibration for the measured peak, (μg nuclide/g)/cpm

The detection limits for U, Th and K are given in Table 2.14.

Table 2.14 Rock U and Th determinations by intrinsic Ge. γ-ray spectroscopy calibrations and detection limits.

Nuclide	Energy KeV	Calibration μg/g U or Th	Background cpm	Detection limit* μg/g U or Th	
^{238}U series nuclides					
^{234}Th	63	0.0834	0.11	1.1	0.3
^{235}U+^{226}Ra	186	0.3527	0.25	0.3	0.1
^{214}Bi	611	0.7590	0.22	0.1	0.03
^{232}Th series calibration					
^{228}Ac	129	0.0427	-	2.2	0.6
^{228}Ac	209	0.0535	-	1.7	0.4
^{228}Ac	912	0.0945	0.13	0.9	0.2
^{228}Ac	≈970	0.0736	0.03	1.3	0.3

Detection limits are calculated for a significance level of 5% for a 3-day count. Number of counts are determined by peak areas.

2.4 Summary of development of experimental methods

Adsorption on MnO_2 whether on precipitated MnO_2 or MnO_2-loaded acrylic fibres enabled the selective preconcentration of radium from groundwaters. This allowed the measurement of the $^{228}Ra/^{226}Ra$ activity ratio from groundwaters with up to seawater ionic strength.

Adsorption on powdered MnO_2 is limited to the most manageable size of water carrier, 60 litres. No constraints were necessary for MnO_2-loaded fibres.

Unfortunately the recovery of MnO_2-loaded fibres in this study was not quantitative for the flow rates employed. Quantitative recovery could be obtained through dropwise addition of water to the fibres but this is not feasible for field application. Separate samples were taken for ^{226}Ra determination to yield ^{228}Ra activities when combined with $^{228}Ra/^{226}Ra$ ratios from the MnO_2 preconcentration.

Measurement of the aquifer rock (Th/U) activity ratio by high resolution Intrinsic Germanium γ-ray spectroscopy was investigated. Although results were obtained with good precision there was a systematic difference between these results and those obtained by NaI γ-ray spectroscopy.

CHAPTER THREE: RESULTS

Introduction

In this study, the hydrochemistry of Ra and its daughter isotopes was investigated for a variety of geological settings and groundwater geochemistry. In the following presentation of results, each aquifer system is described separately.

The geological setting and groundwater chemistry of each aquifer system is described to set the geochemical context of the results. The sampling procedure for ^{226}Ra and $^{228}Ra/^{226}Ra$ activity ratios is described and the results are tabulated. The relationship between the results and the aquifer groundwater chemistry and aquifer rock lithologies are discussed. The short-lived nuclides ($^{212}Pb/^{212}Bi$, $^{214}Pb/^{214}Bi$) discussed in this study were all measured in samples taken from the King's Spring thermal waters, Bath. Full details of the sampling and analytical procedures for these nuclides are given in the section dealing with results from the Bath-Bristol Sedimentary Basin.

3.1 Stripa granite groundwaters

3.1.1 Introduction

The long term storage of high level radioactive wastes is likely to be in geological formations such as salt domes, argillacious sediments and crystalline rocks. The distribution of naturally occurring U and Th series radionuclides in groundwaters associated with potential repository sites must be investigated for two reasons:
(i) Radionuclide wastes contain significant quantities of naturally occurring radionuclides so monitoring of a deposit will provide information on the environmental impact of leakage of these nuclides into groundwaters from the repository.
(ii) The chemical similarities between natural and artificial nuclides means that studies of the mobility of natural nuclides can provide information upon the fate of chemically similar artificial radionuclides accidentaly leaked into groundwaters.

In Sweden, the International Stripa Project has been established to investigate the hydrology and hydrochemistry of groundwaters within Stripa granite, a possible disposal site for highly active nuclear waste. The project is centred around a disused iron ore mine located at Stripa, 250 Km west-northwest of Stockholm (Fig. 3.1). The investigated area is a small intrusive body of granite of Precambrian age in a belt of older supercrustal metamorphic rock.

Figure 3.1.
Location of the Stripa Ore Mine

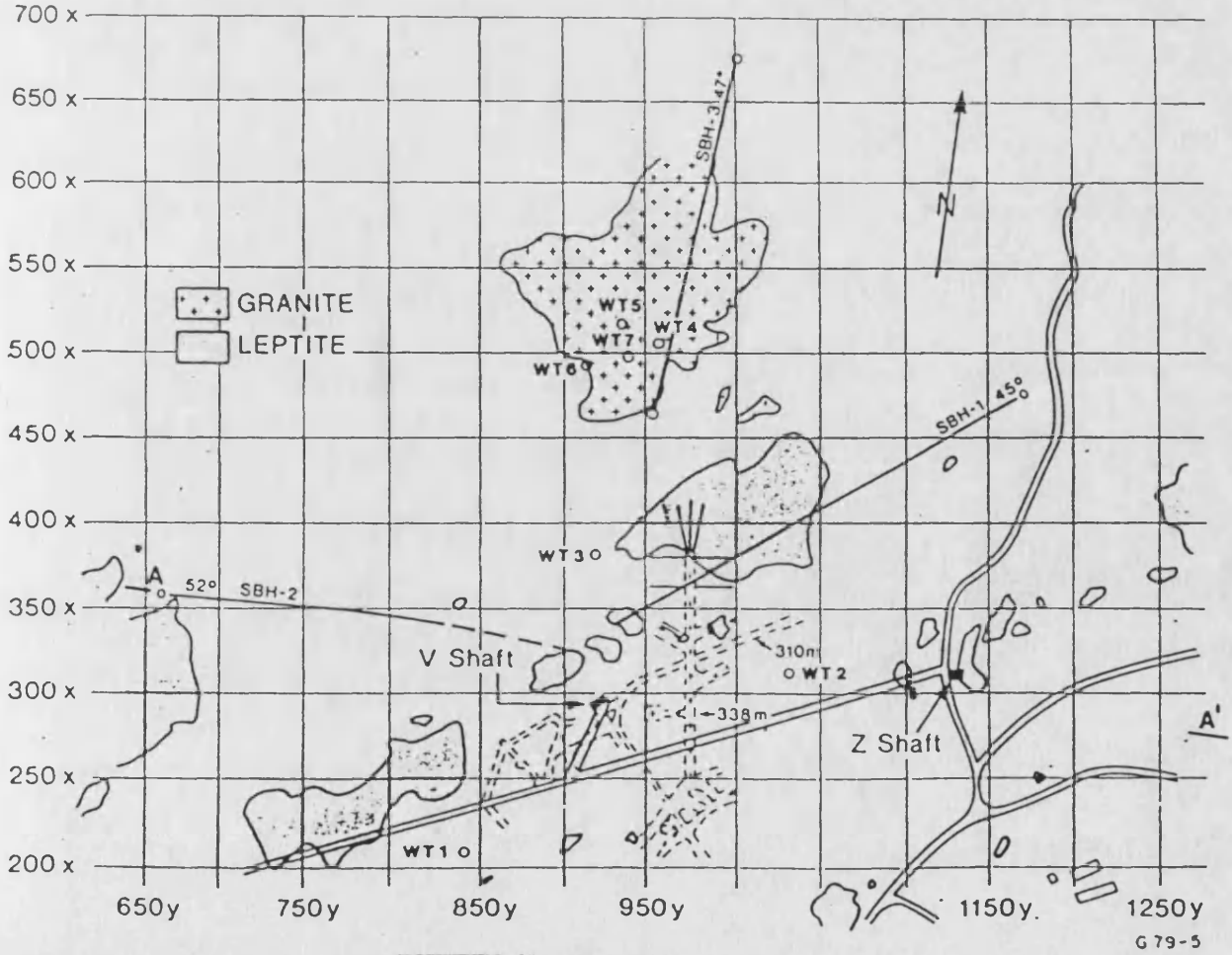

Fig.3.2. General geology and hydrology borehole locations. Squares are 50m on a side.

The groundwater flow system within the granite has been extended by the drilling of boreholes at selected sites within the mine (Fig. 3.2). These boreholes have been drilled at the 360 m mine level. Two are subhorizontal (E1 and N1) and one is vertical (V1), extending to a depth of 860 m below ground. Another borehole, V2, is an extension of a previous borehole, Ch V1, and extends to a depth of 1230 m below ground.

The groundwater chemistry has been extensively investigated by Nordstrom et al, (1985) and references therein. The groundwater changes significantly with depth. Surface and shallow waters have low chlorinity and are predominantly calcium bicarbonate waters, with pH varying between 6.5 and 8, with depth. This is a consequence of calcite undersaturation in the groundwaters which results in the dissolution of calcite.

If chlorine is used as a conservative tracer then calcium decreases in concentration after reaching a maximum in shallow waters (Fig. 3.3). This is a consequence of the onset of calcite saturation and indicates precipitation of calcite.

At high chlorine contents corresponding to depths of 360 m or more (borehole N1) calcium again increases with increasing chlorinity despite calcite saturation, whereas bicarbonate continues to decrease. This can be explained as the result of increasing calcium input from either

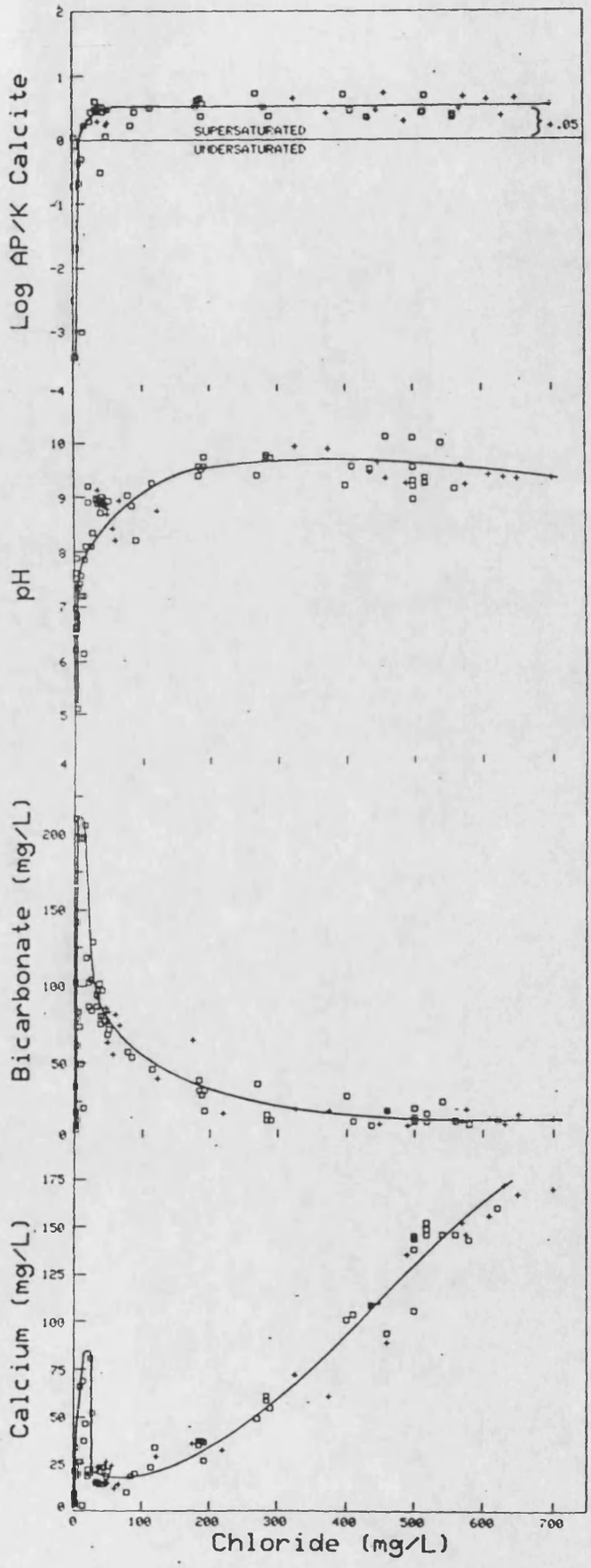

FIGURE 3.3. Ca, HCO_3, pH, and calcite saturation index plotted against Cl concentrations.

feldspar weathering and/or mixing with a saline source, such as fluid inclusions.

3.1.2 Analytical methods and results.

Sampling for $^{228}Ra/^{226}Ra$ activity ratios was performed during March 1985. Between 1700 and 9550 litres of water was passed through bottles containing MnO_2 impregnated fibres at flow rates up to 1.4 litres per minute. Separate samples were obtained for ^{226}Ra analysis and the radium recovery on the fibres based upon the difference between the ^{226}Ra picked up on the fibres to that of the separate samples varied between 7 and 61% (Table 2.2).* Radium results are reported in Table 3.1.

Groundwater chemical analysis results were obtained from Nordstrom et al. (1985). From these results the WATEFQ computer code was used to calculate the saturation indices of minerals (Table 3.2). Radium speciation was calculated using the anion activities calculated from the WATEQF program (Table 3.3).

*Field work was performed by J N Andrews, University of Bath.

Table 3.1 Dissolved radium contents in Stripa groundwaters

Borehole	Collection date	Depth below ground (m)	^{226}Ra* pCi/l	±	$^{228}Ra/^{226}Ra$	±	^{228}Ra pCi/l	±
M3	20.02.85	0- 14	3.57	0.05	0.17	0.02	0.51	0.07
			3.41	0.07			0.58	0.07
			(4.5)					
E1	20.02.85	3- 300	4.01	0.08	0.17	0.02	0.68	0.08
			3.51	0.04			0.60	0.07
V1	19.02.85	460- 862	115.9	0.4	0.16	0.02	18.5	2.3
			132.1	1.3			21.1	2.6
			(138)					
V2/1	21.02.85	969-1232	49.2	0.3	0.16	0.02	7.9	1.0
			58.3	0.5			9.3	1.0
			(80.6)					
V2/2	18.02.85	960- 968	35.4	0.3	0.20	0.02	7.08	0.71
			36.4	0.3			7.28	0.73
			(87)					
V2/3	19.02.85	400- 908	47.7	0.3	0.21	0.02	10.0	1.0
			44.9	0.3			9.4	0.9
			(81)					
V2/4	20.02.85	812- 820	80.5	0.3	0.13	0.01	10.5	0.8
			85.6	1.0			11.5	0.9
			(131)					
V2/5	19.02.85	799- 807	15.3	0.1	0.15	0.02	2.30	0.3
			14.1	0.2			2.12	0.3
			(18.4)					

*Figures in brackets represent the average ^{226}Ra content measured over several months between February 1985 and April 1986.

Table 3.2 Mineral saturation indices for Stripa groundwaters

Site	Depth interval (m)	^{226}Ra pCi/l	Anhydrite	Gypsum	Aragonite	Calcite	Barite	Celestite	Ionic strength (molar)
N1	3-300	2.5	-4.6	-4.86	0.07	0.31	-2.25	-5.64	0.003
E1	3-300	6.0	-3.01	-2.65	0.55	0.79	-0.93	-3.99	0.003
M3	0- 14	1.5	-3.48	-3.13	0.0001	0.25	-	-4.4	0.003
V1	103-505	138.	-1.51	-1.20	0.008	0.26	-0.38	-2.36	0.022
V2	412-417	45.	-1.76	-1.38	-0.15	0.09	-0.38	-2.66	0.018
V2	490-494	32.	-1.92	-1.54	-0.04	0.20	-0.48	-2.74	0.017
V2/1	562-822	80.6	-1.96	-1.57	0.49	0.74	-0.82	-3.0	0.02
V2/2	500-561	87.	-1.89	-1.52	0.88	1.13	-0.88	-2.78	0.017
V2/3	424-499	81.	-1.78	-1.40	0.03	0.28	-0.95	-2.68	0.018
V2/4	382-423	131.	-1.73	-1.34	0.12	0.36	-0.41	-2.71	0.02
V2/5		18.4	-	-	-0.09	0.16	-	-	0.007

Table 3.3 Radium speciation in Stripa groundwaters

Site	Species distribution (% of total Ra)					
	Ra^{2+}	$RaOH^{+}$	$RaCl^{+}$	$RaHCO_3^{+}$	$RaCO_3^{o}$	$RaSO_4^{o}$
M3	93.3	$6x10^{-4}$	0.06	4.4	0.67	1.6
E1	90.6	$1x10^{-3}$	0.03	4.7	1.5	3.1
N1	96.	$5x10^{-4}$	0.07	3.4	0.43	0.06
V1	86.9	0.001	0.6	1.88	0.06	12.2
V2/1	92.0	0.0026	0.62	0.17	0.15	7.0
V2/2	87.9	0.003	0.56	0.059	0.065	11.4
V2/3	85.59	0.003	0.68	0.08	0.09	13.5
V2/4	88.4	0.0012	0.75	0.09	0.04	10.7
V2/5	97.9	0.0019	0.29	0.42	0.26	1.1

3.1.3 Discussion of results for the Stripa groundwaters

3.1.3.1 $^{228}Ra/^{226}Ra$ activity ratios

The activity ratio varies between 0.13 and 0.21 with a mean of 0.17 and a standard deviation of 0.02. There is no systematic variation with depth or groundwater chemistry implying that the variation is due to localised variations in the uranium and thorium content of the granite.

However, the radium ratio is consistently below the average $^{238}Th/^{238}U$ rock ratio of 0.38. This confirms previous suggestions from high ^{222}Rn groundwater contents and measurement of dissolved thorium nuclides (Nordstrom et al., 1985) that uranium may be more accessible for leaching or recoil production into groundwaters than thorium. A more comprehensive treatment of this subject is given in the 'Discussion' section of this study.

3.1.3.2 Radium activity variation with groundwater chemistry

The highest activity of ^{226}Ra occurs in the V1 borehole with high activities also observed for the V2/4 sample. The lowest activities are those observed for M3 and E1 boreholes. It is noticeable that the radium activities do not increase with depth.

The relationship between ^{226}Ra and Ca^{2+}, Na^{+}, Cl^{-} and K^{+} are graphically dipicted in Fig. 3.4. These show that radium is linearly correlated to Ca^{2+} and K^{+} and non-linearly to Na^{+} and Cl^{-}. The relationship to the latter two species exactly mirrors the relationship between them and Ca^{2+}. Indeed, the relationship

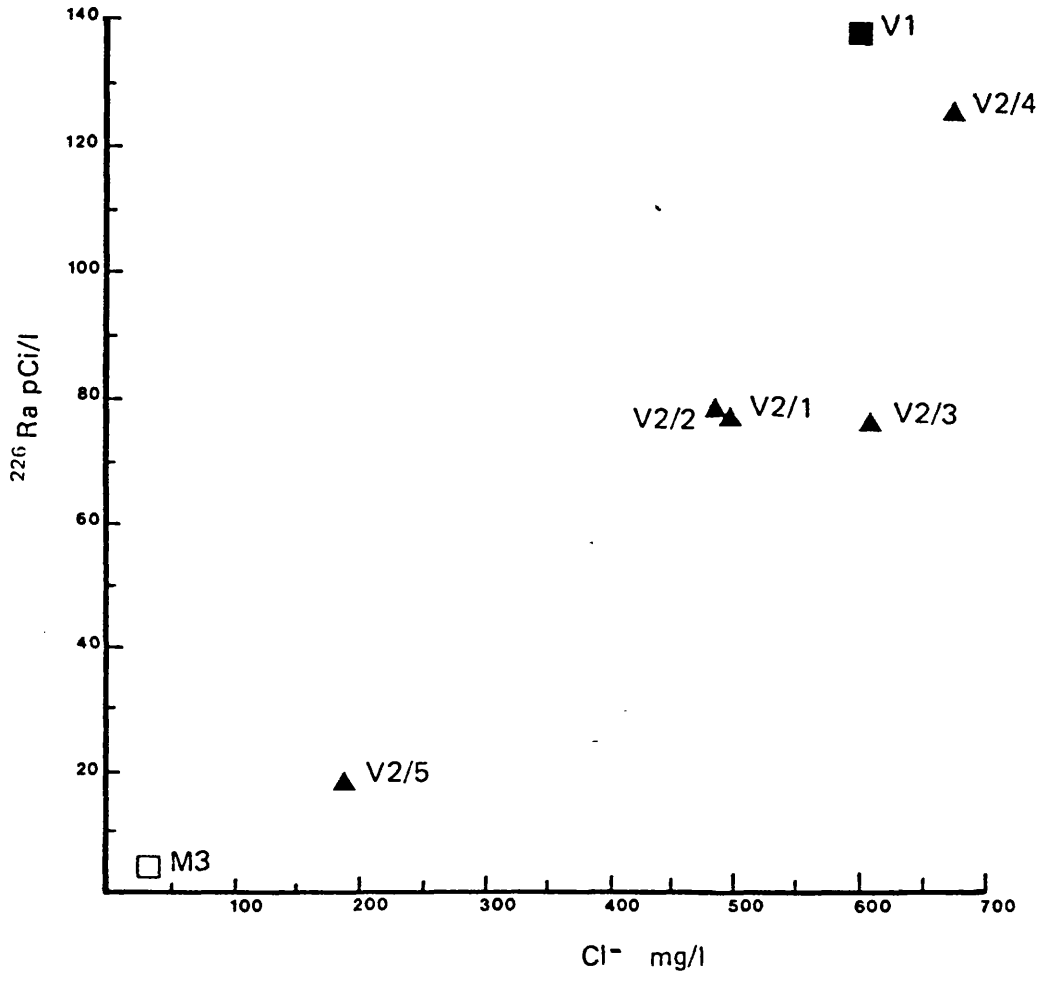

Fig 3.4 (a) ^{226}Ra against Cl^- for Stripa Groundwaters

Fig 3.4 B) ^{226}Ra against Na^+ Variation in Stripa Groundwaters

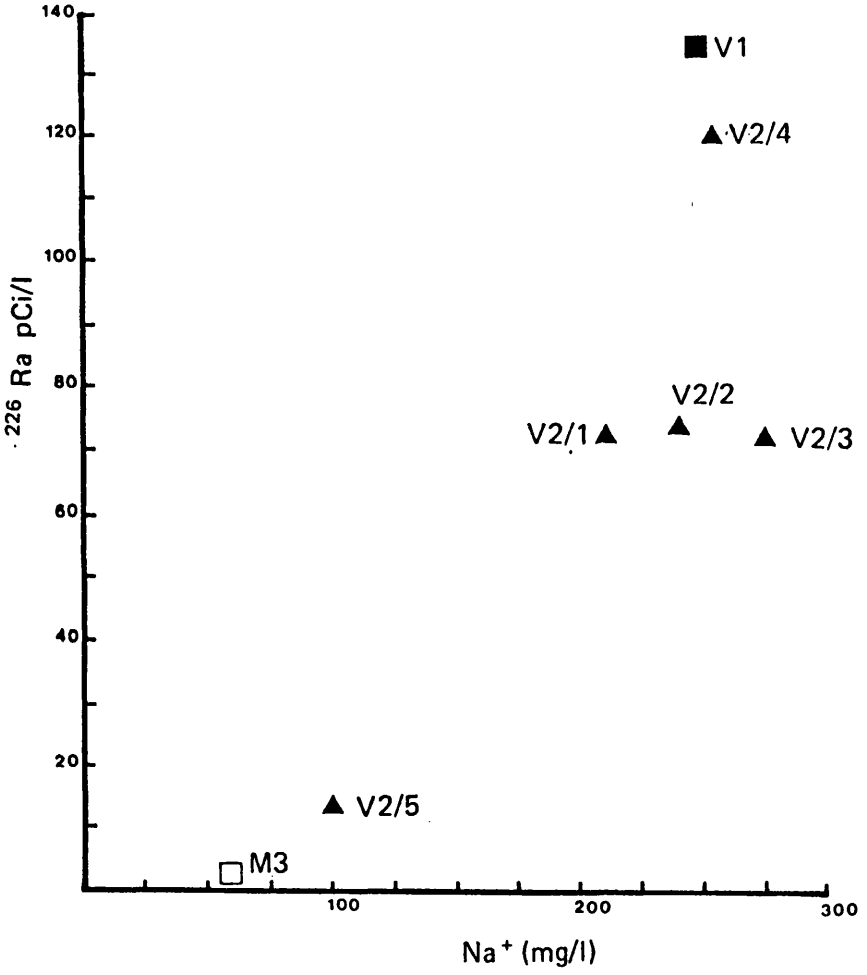

C) ^{226}Ra against K^+ Variation in Stripa Groundwaters

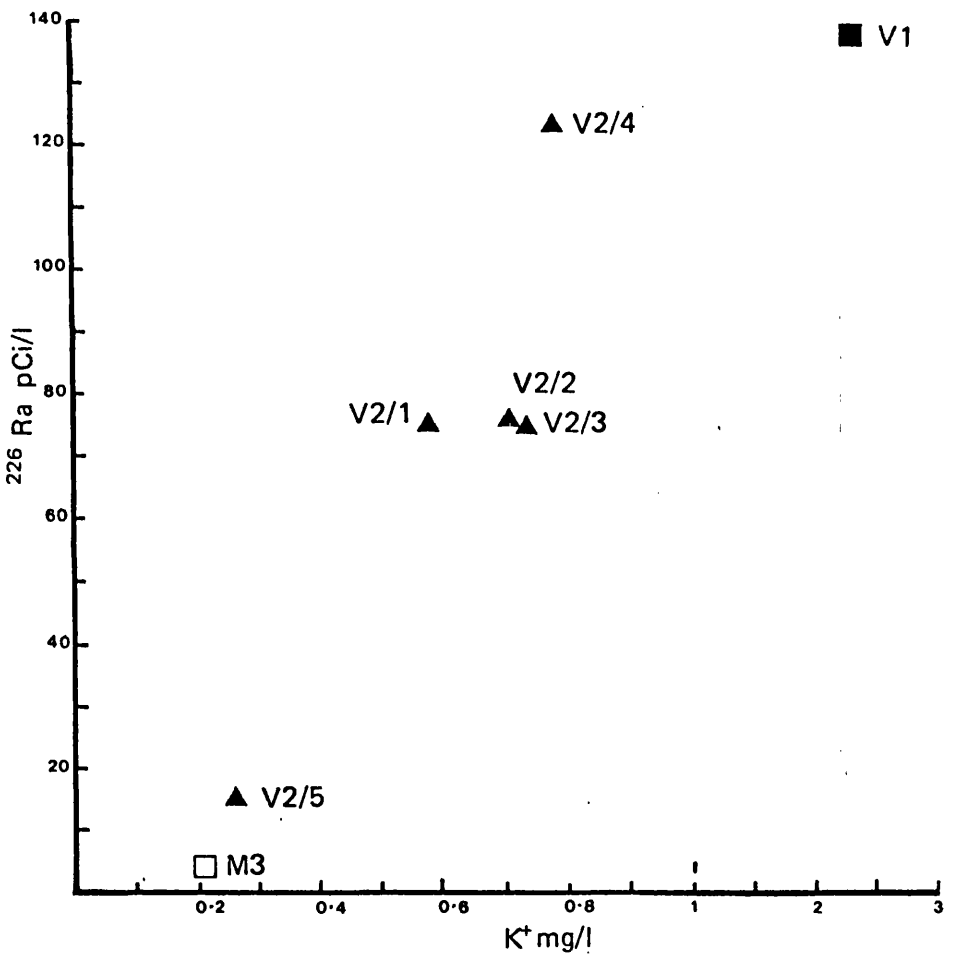

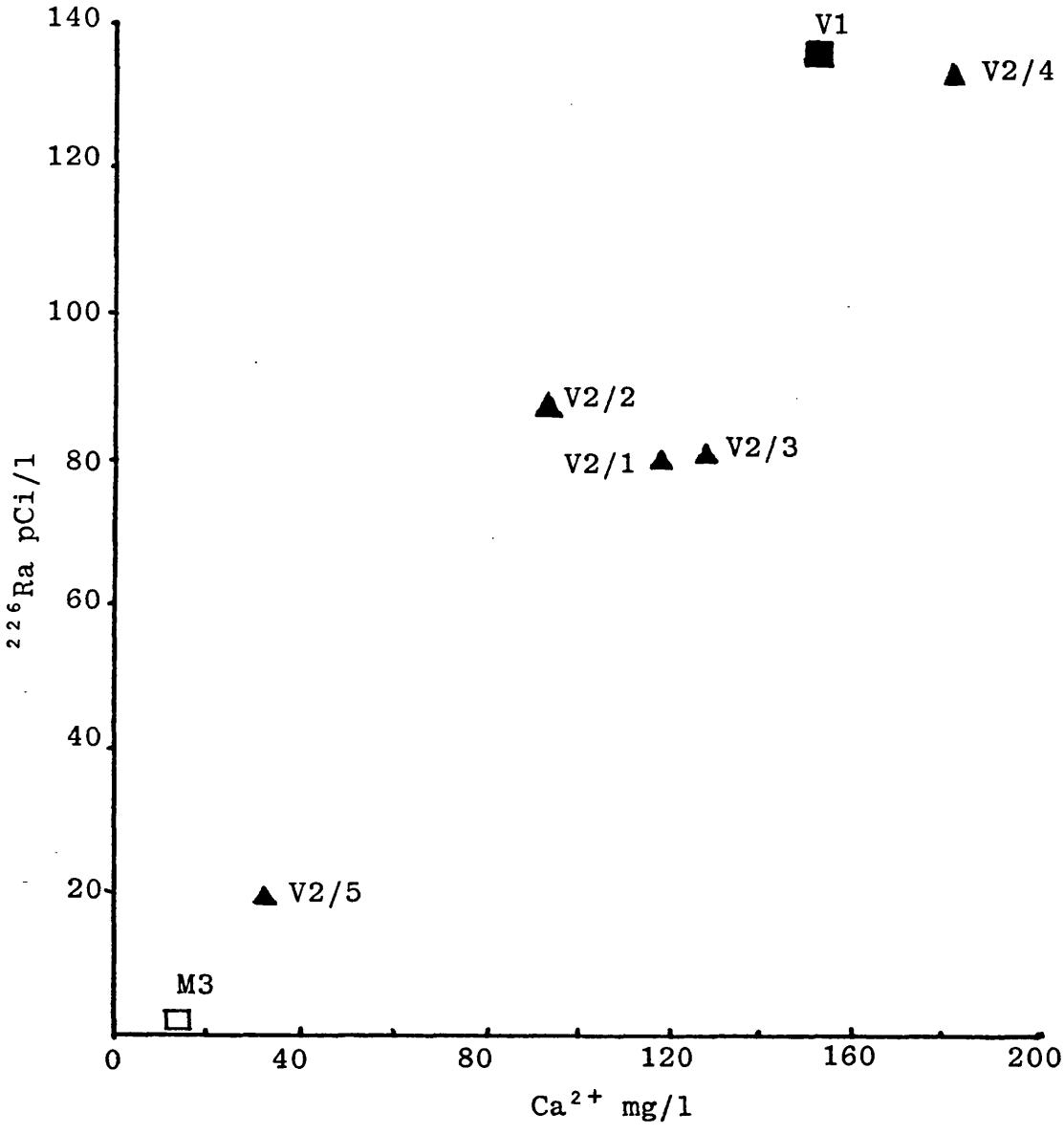

Figure 3.4 D) ^{226}Ra against Ca^{2+} for Stripa groundwaters

between Ca^{2+} and Cl^- has been taken as an indication of Ca^{2+} removal by calcite precipitation. The linear relationship between calcium and radium suggests that the chemical processes controlling Ca^{2+} concentration in these waters also control radium concentrations. There are two possibilities:-

i) Cation exchanges of Ca^{2+} with Ra^{2+}

ii) Co-precipitation of radium with calcium containing minerals and/or cation exchange with these minerals.

The former hypothesis is possible because although the granitic rock forming materials are poor adsorption or ion exchange materials, chlorite and sericite (muscovite) clay minerals are found as fracture coatings (Flexser, 1978). The ability of muscovite to "adsorb" radium has been investigated by Ames et al (1983). They showed that it has poor adsorption properties. However, biotite mica is a better adsorption material for radium and it is readily available in the granite. However there appears to be no data on competitive exchange between Ra^{2+} and Ca^{2+} so it is not at present possible to model the reaction.

The second possibility, of co-precipitation with calcium bearing minerals can only occur in waters saturated with respect to those minerals. Table 3.2 shows that calcite and aragonite are at or close to saturation. The relationship between calcite and aragonite saturation and ^{226}Ra activity is shown in Fig. 3.5. There is a maxima

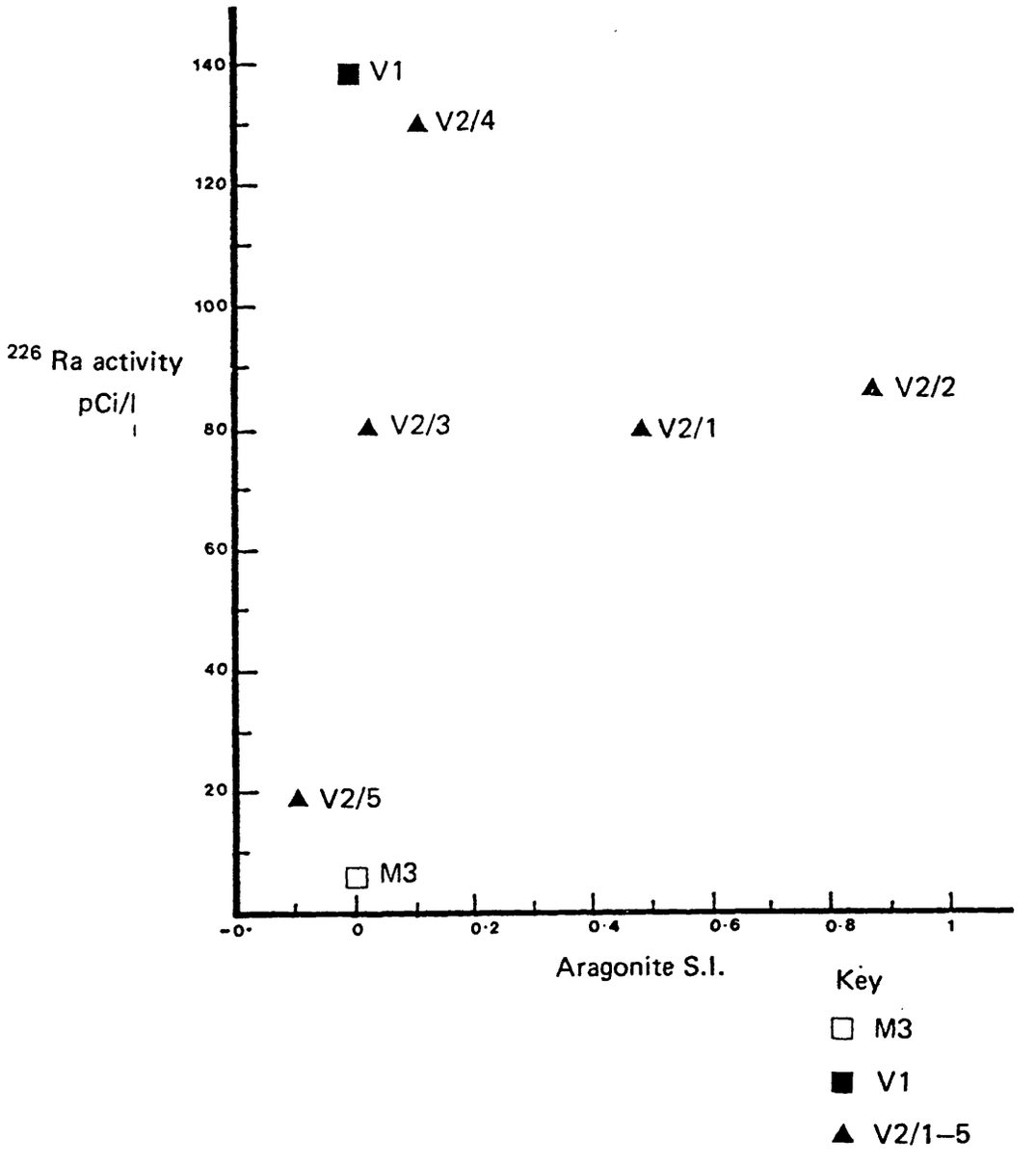

Fig 3.5 a) ^{226}Ra Variation with Aragonite Saturation Indices. in Stripa Groundwaters

Fig 3.5 B) ^{226} Ra variation with Calcite Saturation Indices

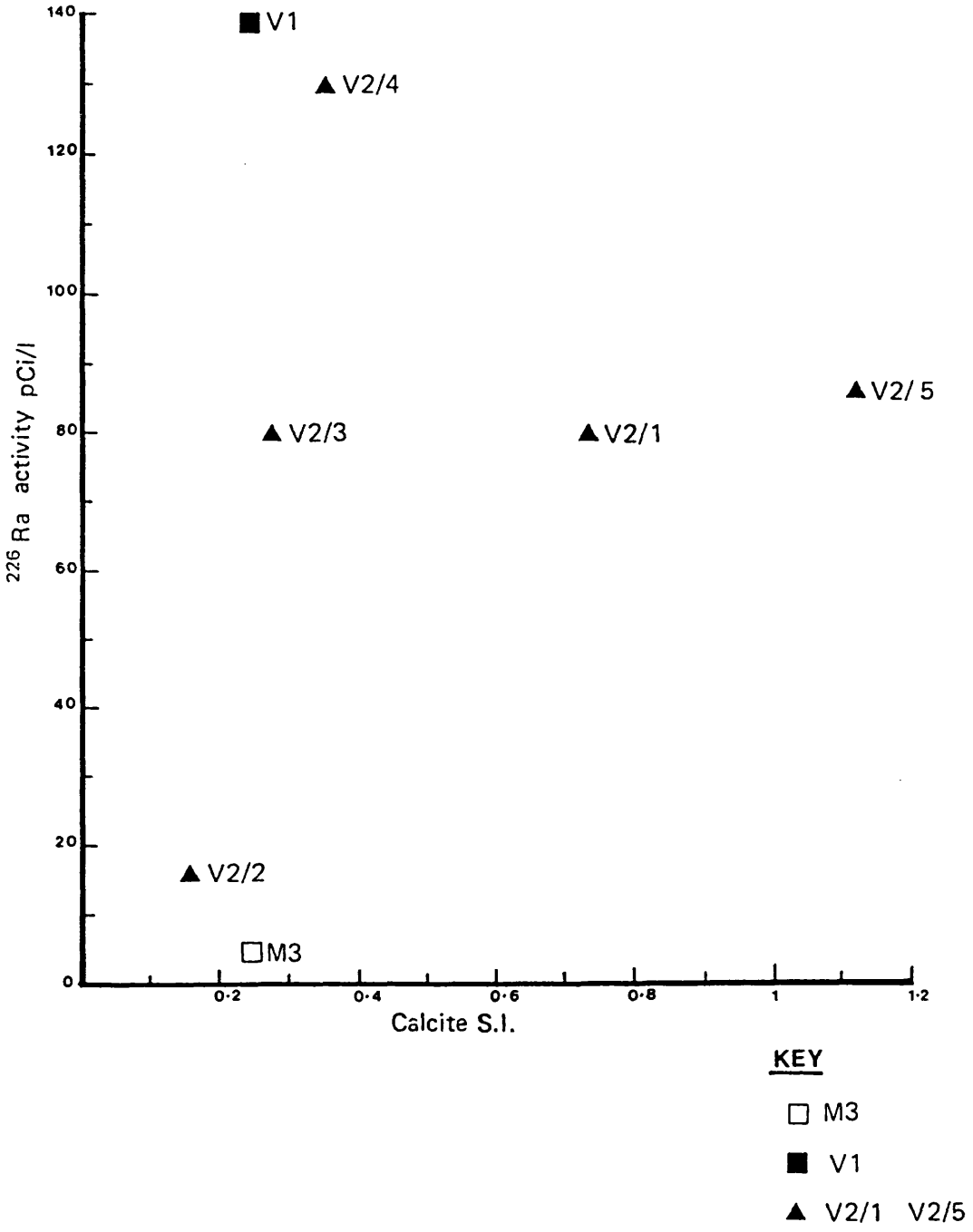

at 0.3 units of calcite saturation, but the radium activity is fairly constant at higher saturation. It was expected that at high saturation where calcite is most likely to precipitate, the ^{226}Ra content would decrease. However, comparison with calcium plotted against calcite saturation (Fig. 3.6) shows a similar relationship. The additional calcium at high saturation is possibly due to production by feldspar weathering.

If an exchange reaction between precipitated calcite and Ra^{2+} occurs as hypothesised by Langmuir and Melchoir (1985):-

$$Ra^{2+} + CaCO_3 \rightleftharpoons RaCO_3 + Ca^{2+}$$

with
$$K_{ex} = \frac{[\overline{RaCO_3}]\ (Ca^{2+})}{[\overline{CaCO_3}]\ (\overline{Ra^{2+}})} \qquad (3.1)$$

where ( ) = aqueous activities, moles/litre
[ ] = solid phase mole fractions
K_{ex} = equilibrium constant

Then with increased Ca^{2+} due to feldspar weathering, and constant solid phase molefractions in the above equation, the exchange equilibrium reaction will mean that the amount of Ra^{2+} will increase. This could account for the observed high radium activities at calcite supersaturation.

Given the chemical similarity of barium and radium it is possible to use barium as an indicator of radium leaching and solubility control. Barium concentrations

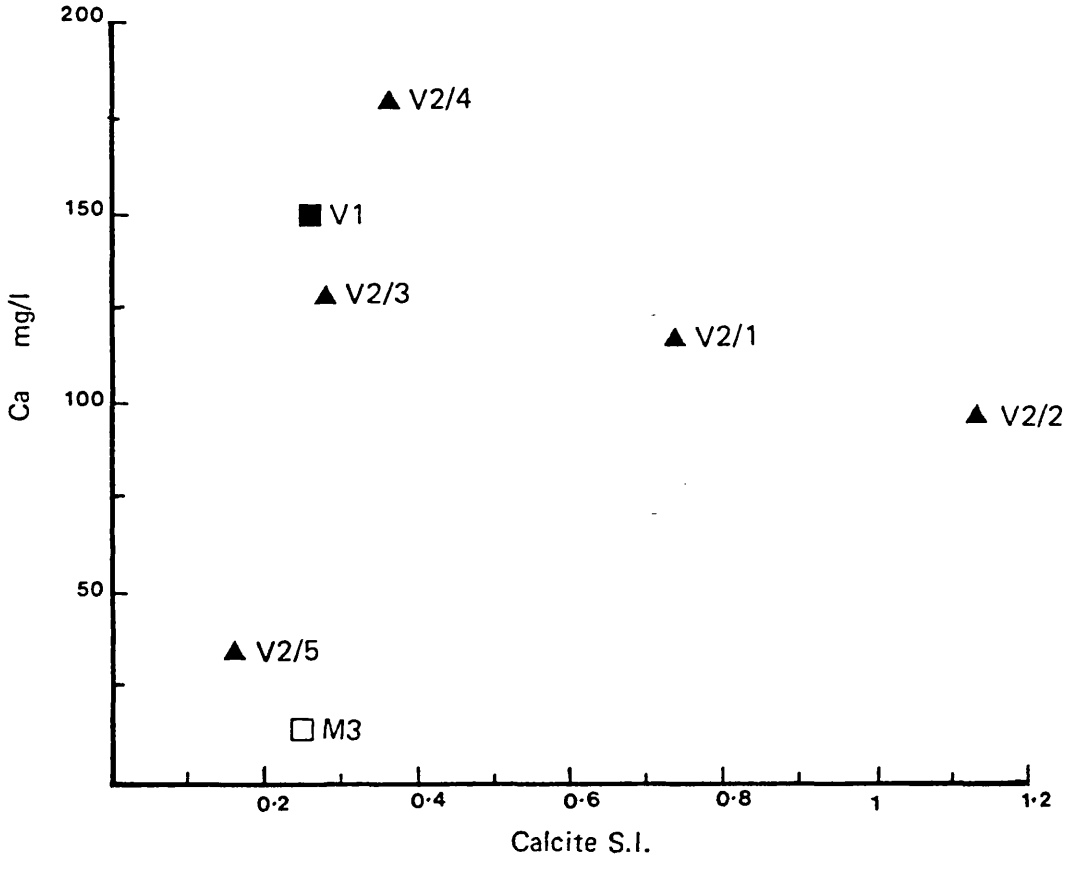

Fig 3.6 Ca $^{2+}$ variation with Calcite Saturation in Stripa Groundwaters

have been measured in these groundwaters between 1978 and 1984.

There is no clear relationship between Ba and ^{226}Ra indicating that radium nuclides are not controlled by the same processes as barium. Further evidence of this is obtained from the water/rock ratios of ^{226}Ra, ^{228}Ra, Ba and Ca (Table 3.4) defined by:

$$R_i = W_i/S_i \qquad (3.2)$$

where R_i = water/rock ratio for element, i

W_i = water content of i (mg/l or pCi/l)

S_i = rock content of i (mg/kg or pCi/kg)

Despite the fact that radium solubility should be lower than both Ca and Ba (and subsequently its water/rock ratio lower) the water rock ratios are in the order:

$$Ca >> {}^{226}Ra > {}^{228}Ra >> Ba$$

Dymond et al (1983) showed that the water/rock ratio for ^{226}Ra and barium were very similar which was interpreted as due to leaching of both radium and barium from the rock matrix, in their case, basalt. The difference between the ratios in this study could be due to two possible reasons:

(i) ^{226}Ra is produced by α-recoil into solution, not leaching.

(ii) ^{226}Ra and ^{228}Ra may be produced in minerals more accessible to leaching than barium, which is likely to come from the major rock forming minerals.

Both of these possibilities are likely to occur.

Table 3.4 ^{226}Ra, ^{228}Ra, Ca and Ba water/rock ratios* in Stripa minewaters

Site	Ca^{2+} mg/l	Ba^{2+} mg/l**	Water/rock ratio ^{226}Ra	^{228}Ra	$Ba \times 10^{-5}$	Ca
M3	14	0.004	0.0003	0.0001	0.73	0.0019
E1	-	0.012	0.003	0.001	2.18	-
V1	150	0.024	0.0095	0.0033	4.36	0.0208
V2/1	118	0.019	0.0056	0.0014	3.43	0.0164
V2/2	93	0.009	0.0060	0.0012	1.64	0.0129
V2/3	128	0.007	0.0056	0.0016	1.27	0.0178
V2/4	178	0.028	0.0090	0.0018	5.09	0.0247
V2/5	34	-			-	

* The rock concentrations were expressed either in mg/Kg or pCi/Kg. The values used were:

Ba = 550 ppm = 550 mg/kg

Ca = 0.72% = 7200 mg/kg

^{226}Ra = 32.4 dpm U/g = 14600 pCi/kg

^{228}Ra = 13.2 dmp Th/g = 5950 pCi/kg

All values for rock concentrations were obtained from Nordstrom et al (1985).

Recoil production of radium can be modelled by equation (1.34) using [U] = 14.6 pCi/g, L = 3×10^{-6} cm, ρ = 2.6, the surface area/unit volume of water, S, may be calculated thus:

$$S = \frac{A}{0.028}$$ where A = ^{226}Ra activity in solution (pCi/l)

Using the average radium activities from Table 3.1, enabled S to be calculated for these waters (Table 3.5) assuming a unit surface area of 1 m^2 average fracture openings of the flow system have also been calculated. The maximum value of 4930 cm^2/cm^3 for S is within the expected value of 10^4 cm^2/cm^3 for fracture flow systems in which significant flow is in microfractures. The minimum fracture opening of 4 μm is obtained for the highest radium activities in solution. The above calculation assumes that the removal process for radium is by decay in solution, and that radium resident times are all greater than 10,000 years so that equilibrium is established between the aqueous and solid phases.

If the residence times are not greater than 10,000 years then the values of S and fracture opening are maximum values. The largest radium residence times are probably in those waters with the highest radium activities. The 4 μm fracture openings are therefore the most probable fracture size. These calculations certainly show that in these waters ^{226}Ra may be generated by α-recoil ejection into solution within micro fractures.

Table 3.5—Surface area/water volume and fracture width values

Site	S* cm^2/cm^3	Fracture width (μm)
M3	160	124
E1	214	93
V1	4930	4
V2/1	288	69
V2/2	3107	6
V2/3	2890	7
V2/4	4680	4
V2/5	657	30

* Calculated using radium activities from Table 3.1

3.1.3.3 Radium speciation

The most important aqueous radium species in these waters are $Ra^{2+}(aq)$ and $RaSO_4^{o}(aq)$ (Table 3.3). The relationship between ^{226}Ra activity and radium speciation is illustrated in Fig. 3.7. There is a pronounced increase (from ∿0% to 15%) in $RaSO_4^{o}(aq)$ with increasing ^{226}Ra activity. This is paralleled by a decrease in $Ra^{2+}(aq)$. It is therefore possible that $RaSO_4^{o}(aq)$ increases the solubility of radium in solution. However, the behaviour of this species in solution is unknown, so it is not possible to predict for instance, the ability of the species to be adsorbed or take part in co-precipitation reactions with sulphate bearing minerals.

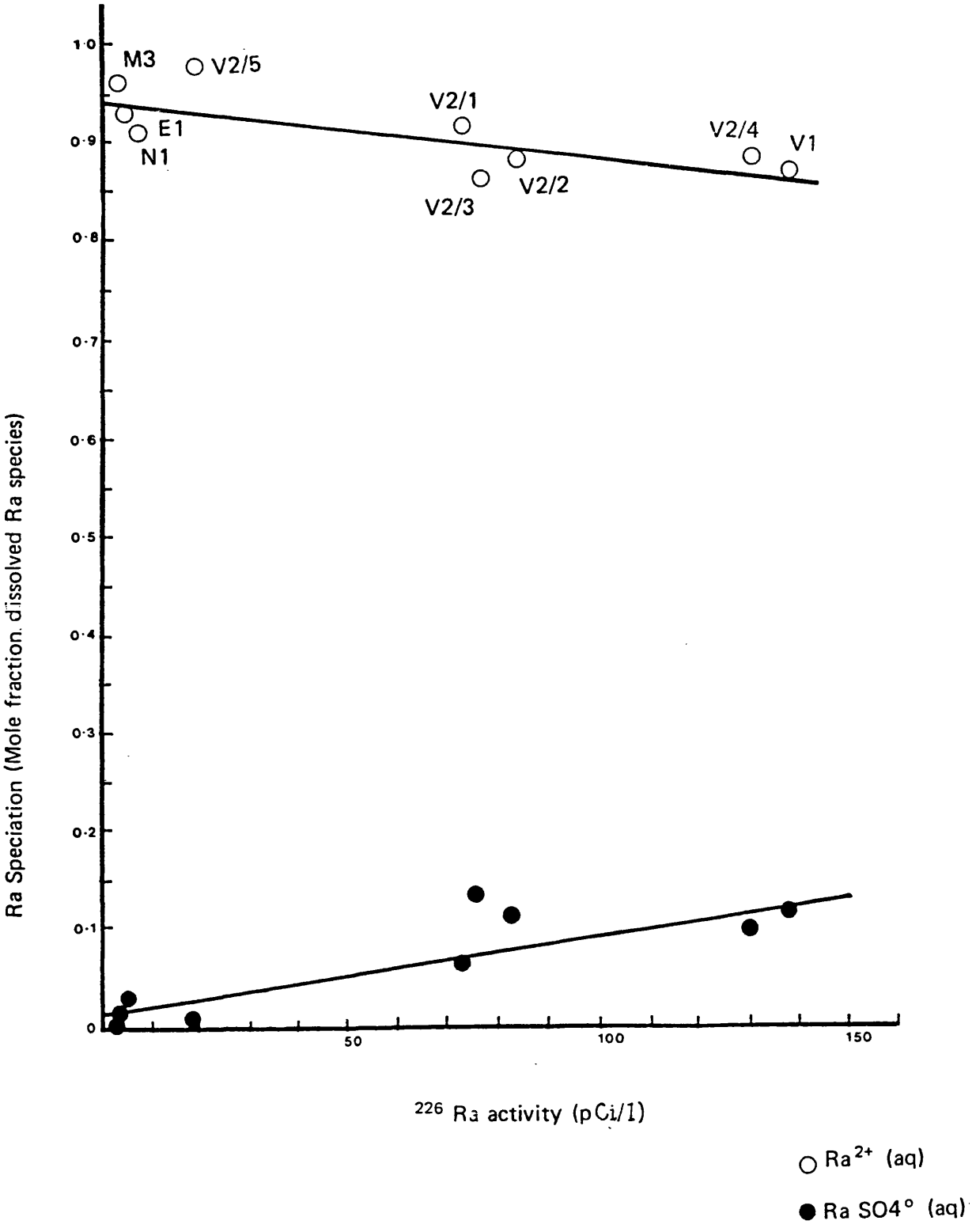

Fig 3.7 Dissolved Radium Speciation in Stripa Groundwaters

3.2 Groundwaters from the Molasse Basin (Austria)

3.2.1 Introduction

The Molasse Basin of Austria is of major importance as a source of potable water, and also contains oil and natural gas bearing horizons. A hydrological, radiochemical and dissolved gas study is being undertaken to establish water flow patterns and determine groundwater ages. The study presents an ideal opportunity to study the dissolved radionuclide distribution and to determine the effect of such factors as aquifer rock lithology, groundwater salinity and composition and water temperature.

3.2.2 Geological setting

The geological and hydrological setting has been described by Andrews et al (1985), and the following is a brief resume of their description.

The location and geology of the Molasse Basin is illustrated by Fig. 3.8. The basement rocks for the basin are the crystalline rocks of the Bohemian Massif which rises from the Northern border of the basin. Jurassic and Cretaceous sediments overlay the basement rock, and the Malm which consists of Jurassic dolomites and limestones forms the most important deep aquifers and also contains oil deposits.

The basin had three distinct sedimentation phases. The first was due to erosion of the Bohemian Massif, and comprises of the Upper Eocene and Lower Rupelian sediments. The Rupelian shales appear to be the source rock

for Upper Eocene, Upper Jurassic and Cenomanian oil deposits.

The majority of basin sediments arose as a result of erosion of the Alps to the south of the basin. This period formed late Rupelian to Ottangian sediments, including the high porosity and permeability Puchkirchen formations which are composed of intercalations of pelagic clay and coarse sediments.

The third basin sedimentation resulted in the formation of the Upper Freshwater Molasse formations containing coarse sediment with unconfined shallow lying groundwaters. The stratigraphy of the basin is given in Fig. 3.9.

3.2.3 Hydrochemistry

The chemical analysis of groundwaters has been performed by Inst. f Geothermie u Hydrogeol. (Graz) for the wells from whic radionuclide samples were obtained. This analytical data, together with Eh, pH, temperature and dissolved oxygen contents for these wells were fed into the WATEQF computer code to enable the calculation of the groundwater speciation and mineral saturation. The state of mineral saturation for minerals of interest are given in Table 3.6.

The waters investigated in this study came from the deeper lying formation waters in the basin, the Hall, Upper and Lower Puchkirchen, Cenoman and Upper Eocene formations. Some of the waters have salinities approaching those of seawater, indeed, the groundwater chemistry is thought to

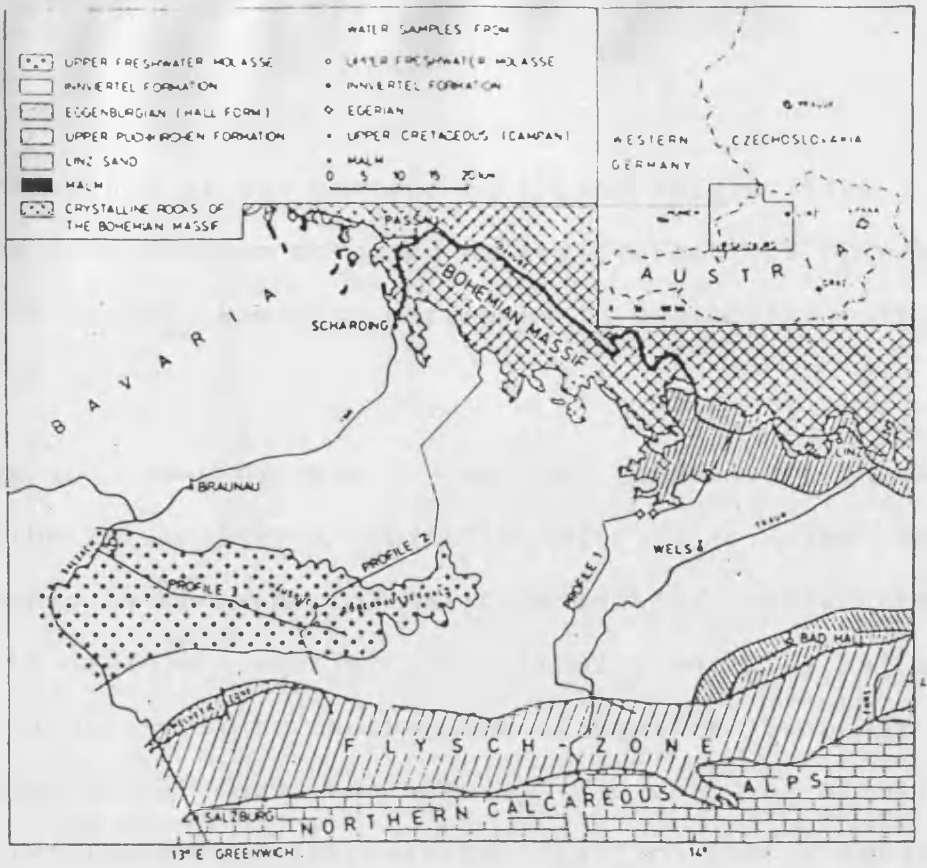

Fig. 3.8 Location & geology of the Molasse Basin

	EPOCH	STAGE	LITHOLOGY	FORMATION	AQUIFERS	OIL GAS	THICKNESS IN METRES
QU	HOLOCENE PLEISTOCENE			MORAINES and TERRACES			0 - 300
MOLASSE SEDIMENTS / TERTIARY / NEOGENE	PLIOCENE	UPPER PLIOCENE					0 - 300
	MIOCENE	PANNONIAN - KARPATIAN		COAL - BEARING FRESH WATER BEDS			
		OTTNANGIAN		INNVIERTEL FORM			0 - 700
		EGGENBURGIAN		HALL FORM			0 - 800
PALAEOGENE	OLIGOCENE	EGERIAN		UPPER PUCHKIRCHEN FORM			0 - 1050
				LOWER			0 - 1000
		RUPELIAN		SMALE STAGE BANDED MARL LIGHT MARLY LIMEST			0 - 550
		LATDORFIAN		FISH-BEARING SHALE			0 - 40
	EOCENE	UPPER EOCENE		SANDSTONE STAGE LITHIC SERIES			0 - 120
BASIN FLOOR SEDIMENTS / MESOZOIC / CRETACEOUS	UPPER CRETACEOUS	CAMPANIAN - TURONIAN					0 - 1000
		CENOMANIAN					
JURASSIC	MALM			CARBONATE-GROUP			0 - 500
				BASAL SANDSTONE			
	DOGGER						
PAL	PERMOTRIAS						0 - 230
CARB	UPPER CARB WESTFAL						0 - 40
CRYSTALLINE BASEMENT							

GRAVEL, CONGLOMERATE
SAND, SANDSTONE
MARL, SHALE
CLAY, CLAY STONE
COAL
LIMESTONE
DOLOMITE
OOLITHIC LIMESTONE
OIL DEPOSIT
GAS DEPOSIT
OIL AND GAS DEPOSIT
AQUIFER AND RELATIVE IMPORTANCE

Fig. 3.9 Stratigraphy of the Molasse zone.

be determined by the mixture of saline interstitial waters with younger meteoric waters (formations waters are, of course, seawater entrapped in sediments at the time of deposition).

The relationship between Cl^- and Na^+ (Fig. 3.10) shows that the waters obey a typical dilution line. The relationship is the same for all four aquifers represented despite different aquifer rock lithologies. The Na^+ and Cl^- contents must be independent of aquifer lithology, as expected for formation waters. However, the dilution line is offset from the seawater dilution line towards excess sodium (Riley and Skirrow, 1975). This is likely to be a consequence of cation exchange processes within the aquifer which remove Ca and Mg from solution and release sodium. This process could easily take place given that clay minerals commonly occur in shales and sandstones.

Calcium has a chemistry similar to radium so a brief investigation of calcium behaviour in these waters could be useful in understanding chemical controls on Ra solubility. If chlorine is conserved in these waters then it serves a useful purpose as an indicator of the behaviour of other ions in solution. A plot of calcium against chloride ion content (Fig. 3.11). The Puchkirchen and Hall formations appear to be correlated, but the U. Eocene shows no clear relationship between calcium and chlorine. Clearly, calcium is controlled by chemical interactive processes, such as cation exchange with clay minerals, precipitation and dissolution of calcium

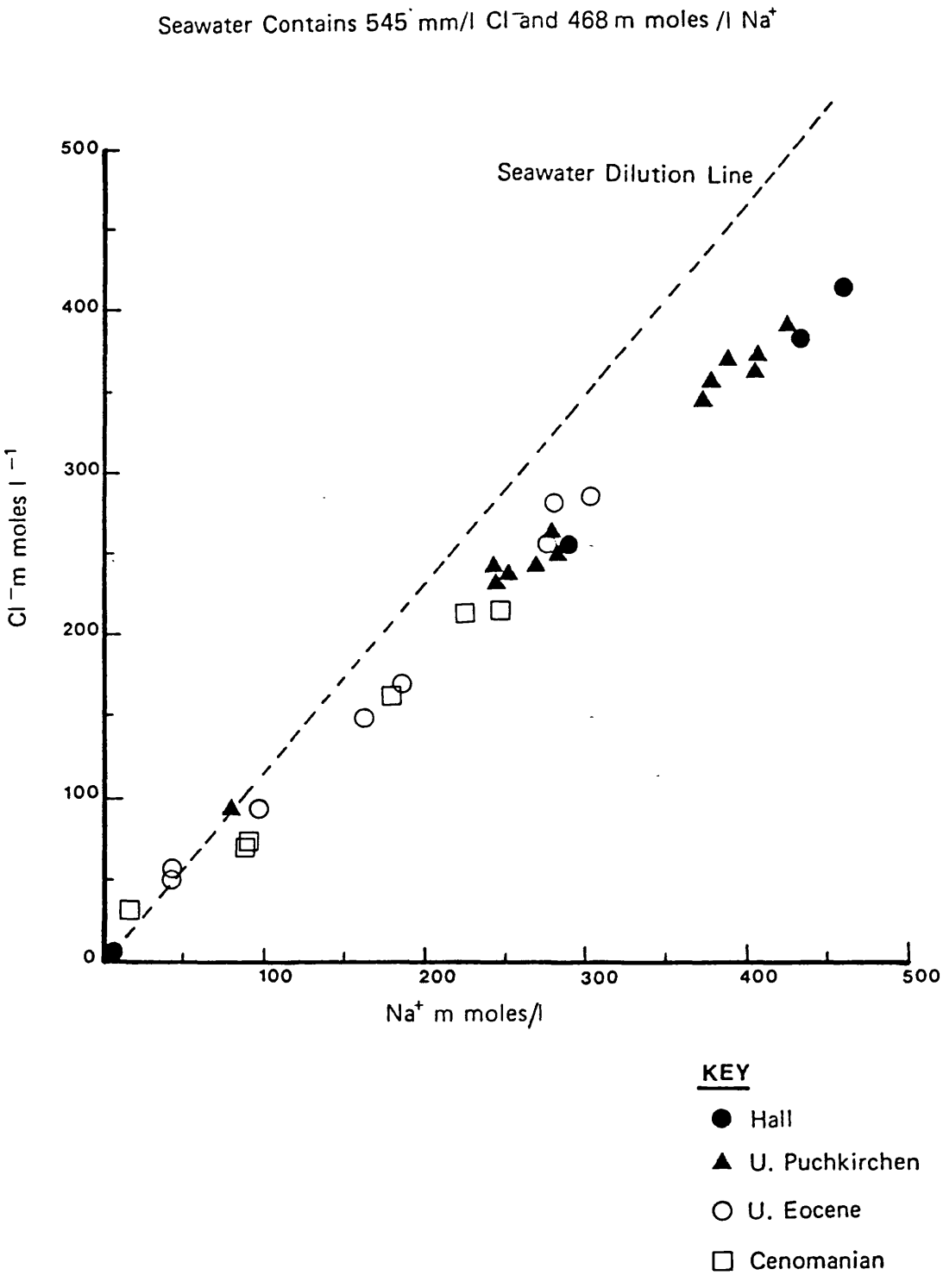

Fig 3.10 Variation of Na^+ with Cl^- in Molasse Basin Groundwaters

Fig 3.11 Ca^{2+} against Cl^- for the Molasse Basin Formation Waters

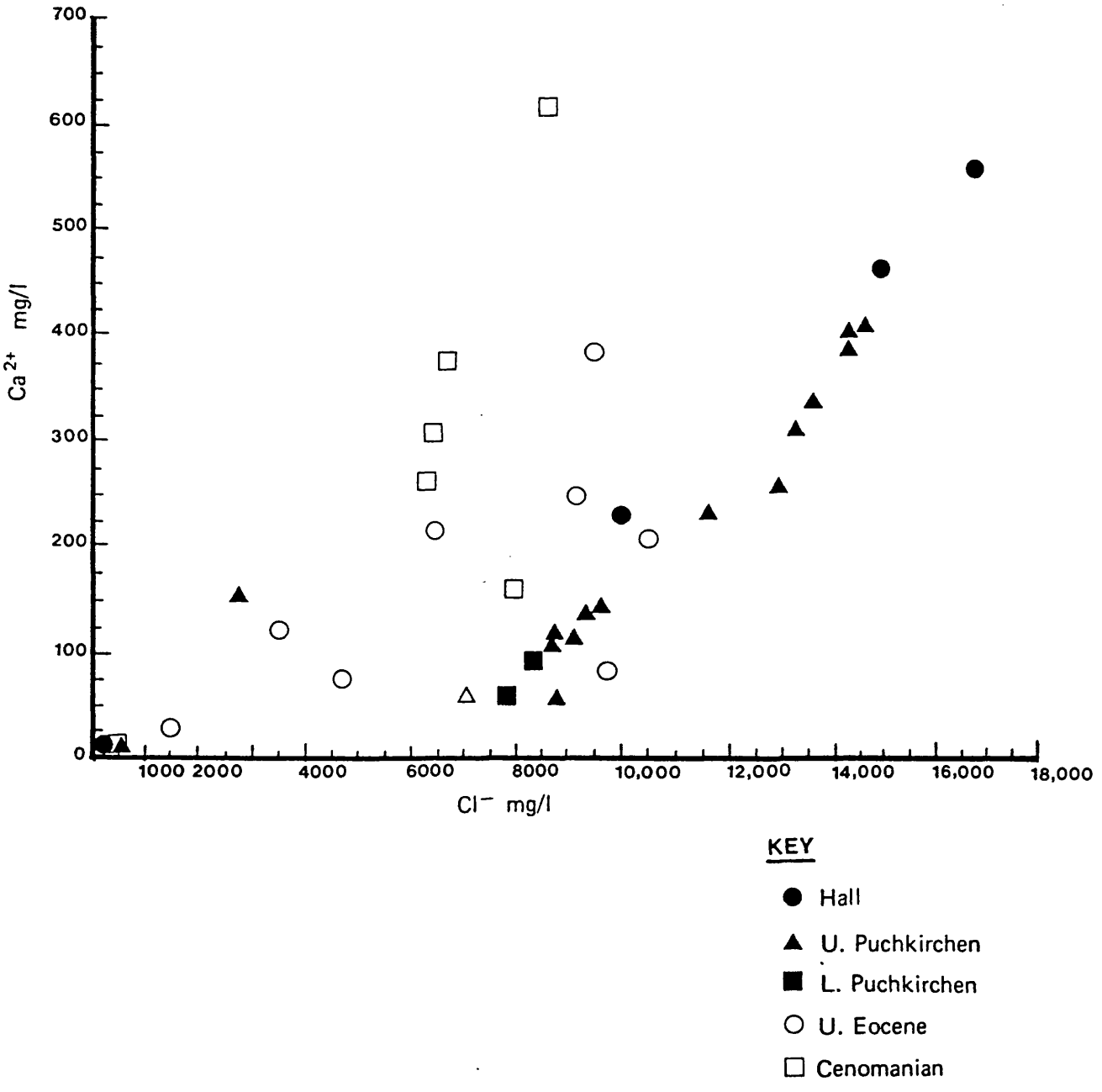

minerals (S.K. Frape, P. Fritz and R. McNutt, 1984).

The relationship between calcium and bicarbonate (Fig. 3.12) shows a trend towards decreasing calcium content with increasing bicarbonate. This trend is indicative of calcium removal by calcite precipitation. It is noticeable that the Upper Eocene data is highly scattered and by itself does not show a clear trend. This is perhaps due to the difficulty in obtaining accurate pH, Eh and bicarbonate concentrations from boreholes with water under high pressure, in many cases the sample containing an oil-water emulsion.

The relationship between Mg^{2+} and HCO_3^- is very similar to that of calcium and bicarbonate (Fig. 3.13). Again decreasing dissolved magnesium with increasing bicarbonate indicates removal of magnesium by precipitation of its carbonate magnesite, $MgCO_3$. However an alternative, given the possibility of magnesite and calcite solubility control, is the formation of the mixed carbonate dolomite $CaMg(CO_3)_2$.

The potential for precipitation of minerals is of course given by the calculated saturation indices (SI) of the minterals. Table 3.6 shows that although the minerals gypsum and anhydrite are highly undersaturated, the carbonate minerals, calcite, aragonite and dolomite are at, or close to saturation. Dolomite has a higher saturation index than the other two phases and magnesite

Fig 3.12 Ca^{2+} against HCO_3^- for Molasse Basin Groundwater

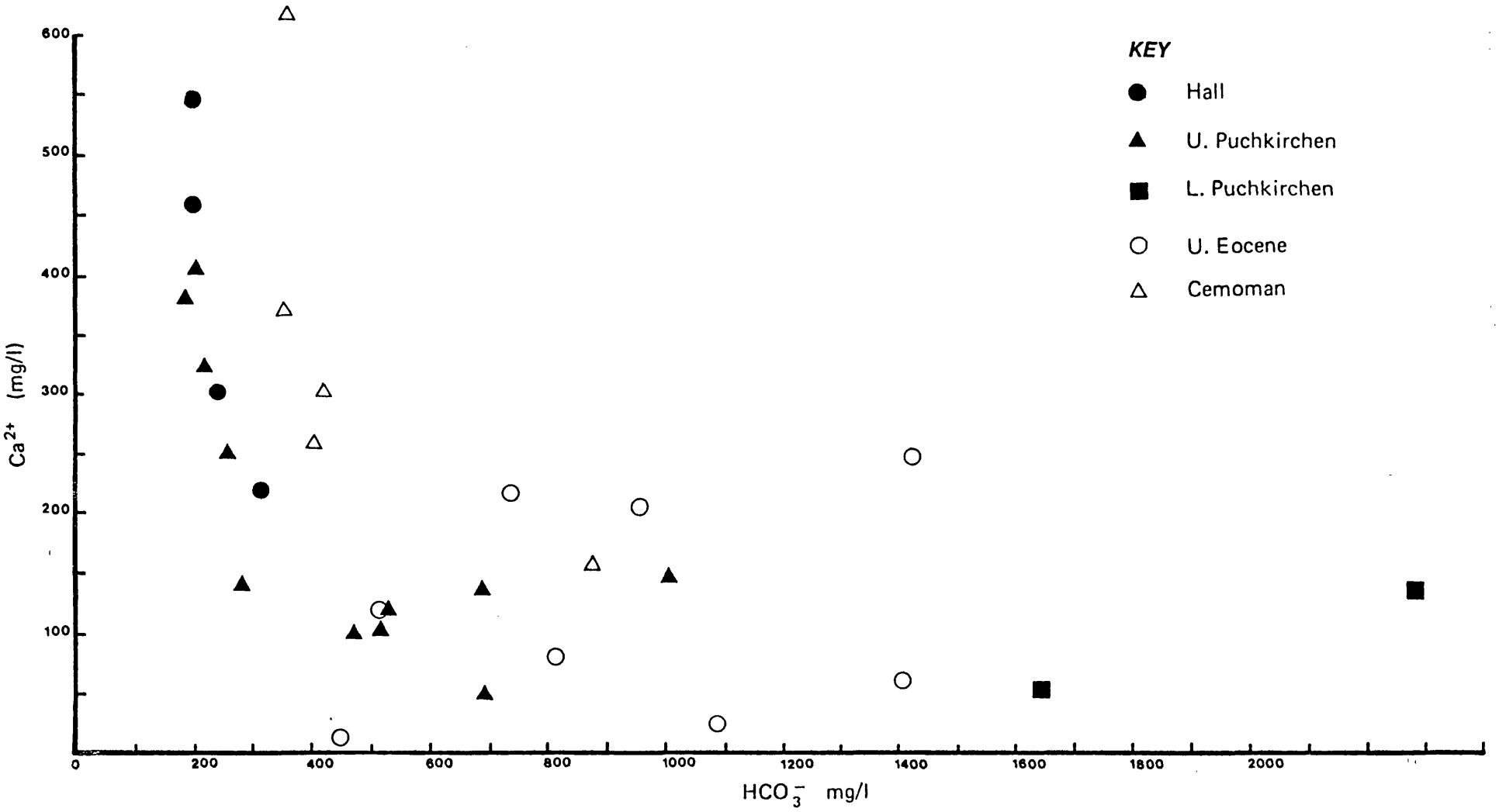

Fig 3.13 Magnesium Variation with Bicarbonate Concentration in Molasse Basin Groundwaters

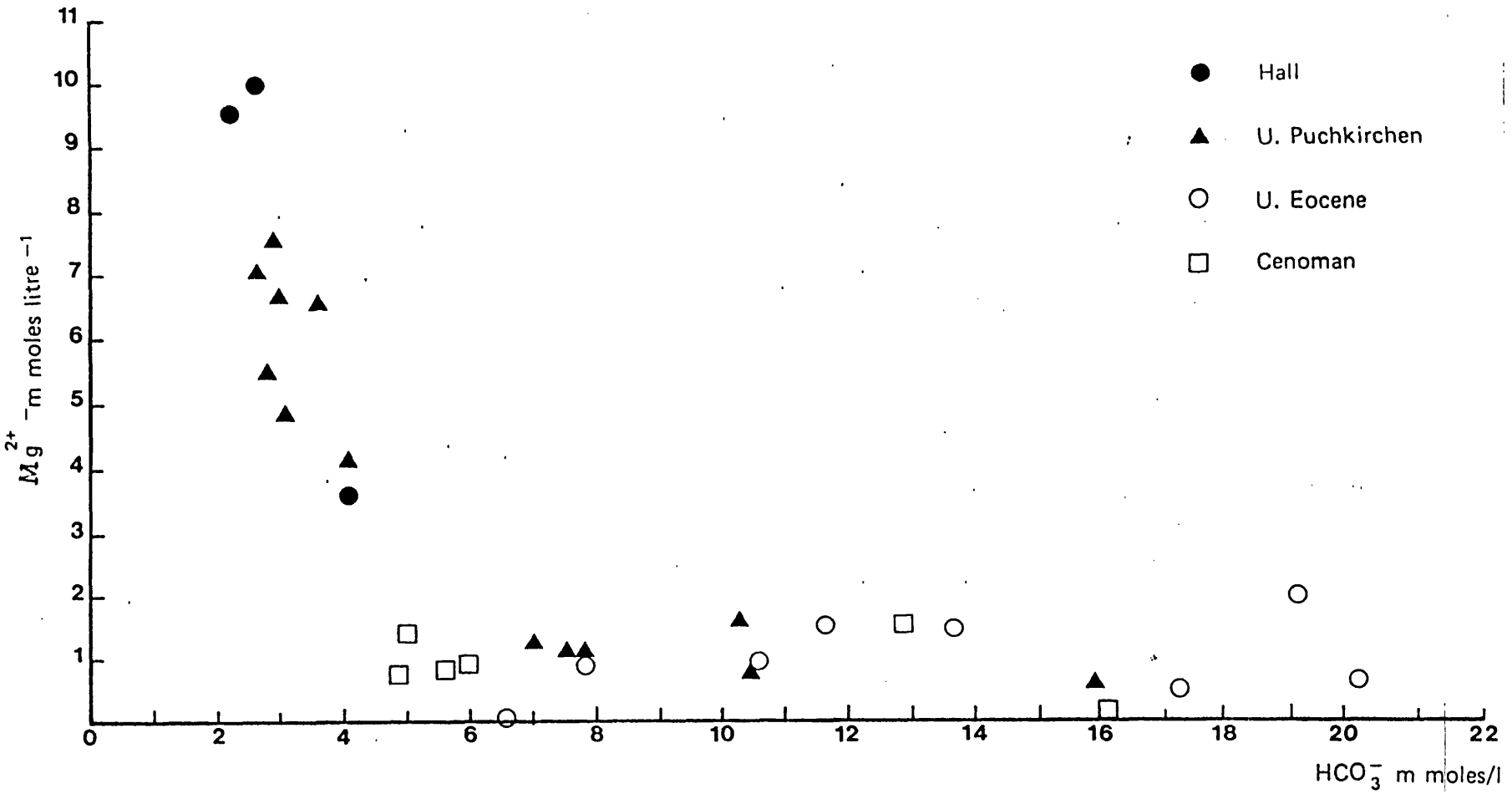

Table 3.6 Saturation indices of Molasse Basin groundwaters

Site	Well type	Formation	Dolomite	Calcite $CaCO_3$	Aragonite $CaCO_3$	Brucite $Mg(OH)_2$	Magnesite $MgCO_3$	Gypsum $CaSO_4$	Anhydrite $CaSO_4$	Ionic Strength
Munderfing	G	H	1.67	0.83	0.57	-3.5	0.57	-3.73	-3.79	0.29
Steinerkirchen 1	G	H	0.6 1.4	0.32 0.67	0.07 0.44	-5.2 -3.7	-0.04 0.45	-3.81	-3.88	0.49
Puchkirchen Ost 1	G	H	-3.7 -3.	-1.3 -1.	-1.6 -1.3	-7.8 -6.7	-2.7 -2.3	-2.86	-2.92	0.003
Schwanenstadt 4	W	H	2.3	0.73 1.11	0.48 0.85	-4.5 -2.6	0.34 0.94	-	-	0.46
Gundersdorf H1	W	UP	1.16	0.54	0.28	-3.9	0.34	-	-	0.46
Maierdorf H1	W	UP	0.93	0.43	0.17	-3.9	0.24	-	-	0.43
Desselbrunn 2	G	UP	0.24	0.23	-0.02	-6.2	-0.32	-2.1	-2.4	0.30
Atzbach 1	G	UP	-0.5	-0.18	-0.43	-6.5	-0.63	-2.4	-2.6	0.28
Friedburg 2	G	UP	0.41	0.28	0.02	-5.2	-0.16	-2.1	-2.3	0.26
Puchkirchen 20	O	UP	0.41	0.52	0.28	-6.7	-0.46	-0.8	-1.2	0.14
Bad Hall Tassilo Q	W	UP	-3.6	-0.01	-0.26	-5.7	-0.25	-	-	0.28
Bad Hall Para Q	W	UP	1.45	0.68	0.43	-4.3	0.68	-3.8	-4.13	0.39
Puchkirchen 27	G	UP	0.56	-0.07 0.38	-0.31 0.12	-6.8 -4.9	-0.8 -0.1	-1.9	-2.	0.26
Schwanenstadt 17	G	UP	0.41	-0.18 0.27	-0.42 0	-6.9 -5.	-0.8 -0.13	-2.	-2.	0.27
Puchkirchen 24	G	UP	-0.19	-0.03 0.44	-0.28 0.17	-6.3 -4.4	-0.51 0.19	-3.44	-3.79	0.33
Eberstalzell H1	W	UP	1.1	0.1 0.54	-0.15 0.27	-5.9 -4.	-3.9 0.27	-	-	0.45
Eberstalzell H2	W	UP	1.3	0.21 0.64	-0.03 0.38	-5.7 -3.8	-0.29 0.37	-	-	0.41

Table 3.6 continued

Site	Well type	Formation	Dolomite	Calcite $CaCO_3$	Aragonite $CaCO_3$	Brucite $Mg(OH)_2$	Magnesite $MgCO_3$	Gypsum $CaSO_4$	Anhydrite $CaSO_4$	Ionic strength
Eberstalzell H5	W	UP	1.5	0.3 0.74	0.06 0.47	-5.5 -3.6	-0.2 0.45	-	-	0.39
Hocheck 2	G	LP	1. 1.6	0.58 0.87	0.33 0.57	-5.7 -4.5	-0.11 0.52	-2.69 -2.7	-2.8	0.23
Pfaffenstadt 3	G	LP	0.2 0.8	0.2 0.46	-0.05 0.19	-6.9 -5.8	-0.61 0.08	-	-	0.28
Eggerding 1	O	R	0.3 -0.1	0.21 0.35	-0.02 0.08	-5.2 -4.6	-0.25 0.06	-4.1	-4.4	0.04
Engenfeld 1	O	UE	-0.43	-0.03	-0.29	-5.4	-0.68	-3.6	-3.7	0.053
Steinhaus 1	O	UE	+1.5	0.81	0.55	-4.5	0.44	-2.	-2.	0.16
Kemating 5	O	UE	2.4	1.3	1.06	-4.2	0.79	-1.9	-1.9	0.29
Maria Schmolln	O	UE	-0.37	0.017	-0.23	-7.03	-0.7	-2.9	-3.3	0.068
Kemating N1A	O	UE	-	-	-	-	-	-	-	-
Kohleck 2	O	UE	2. 2.6	1.2 1.4	0.95 1.18	-4.7 -3.5	0.48 0.87	-2.	-2.3	p.32
Kohleck 6	O	UE	1.47 2.1	0.77 1.	0.52 0.74	-4.8 -3.6	0.38 0.78	-3.5	-3.7	0.29
Voitsdorf 11	O	UE	2.4	1.09 1.33	0.83 1.07	-4.9 -3.7	-0.12 0.26	-1.8	-1.9	0.21
Voitsdorf 10	O	UE	1.33	0.9 1.15	0.64 0.89	-4.9 -3.7	0.1 0.51	-1.98	-2.23	0.11
Oberaustell 6	O	C	1.09	0.9 1.15	0.64 0.89	-4.9 -3.7	0.1 0.51	-0.98	-0.99	0.11
Trattnach 4	O	C	-0.5	-0.1	-0.37	-5.6	-0.66	-3.07	-3.1	0.03
Hogersteig 1	O	C		-	-	-	-	-	-	-

Table 3.6 continued

Site	Well type	Formation	Dolomite	Calcite $CaCO_3$	Aragonite $CaCO_3$	Brucite $Mg(OH)_2$	Magnesite $MgCO_3$	Gypsum $CaSO_4$	Anhydrite $CaSO_4$	Ionic strength
Trattnach 11	O	C	-0.04 0.6	0.22 0.46	-0.03 0.21	-5.9	-0.58	-2.3	-2.5	0.04
Voitsdorf 15	O	C	1.3 1.9	1.1 1.33	0.83 1.06	-4.9 -3.7	-0.12 0.26	-1.4	-1.6	0.21
Voitsdorf 30	O	C	1.4 2.	1.09 1.34	0.84 1.07	-4.9 -3.7	-0.003 0.4	-1.5	-1.7	0.21
Voitsdorf 2	O	C	1.6 2.2	1.27 1.5	1. 1.24	-4.8 -3.6	0 0.41	-0.7	-0.9	0.28
Voitsdorf 13	O	C	1.9	1.11	0.85	-4.8	0.45	-1.6	-1.8	0.24

Note: Well Type: O = Oil; G = Gas; W = Water
Formation: H = Hall; UP = Upper Puchkirchen; LP = Lower Puchkirchen; UE = Upper Eocene; C = Cenoman

Where 2 values are given, no temperature was available for the sample. The 2 values therefore represent the state of saturation for 20°C and 40°C respectively.

which shows that from a thermodynamic point of view calcium and magnesium are controlled by dolomite solubility in these waters although dolomite precipitation is kinetically very slow and calcite precipitation may be dominant.

3.2.4 Analytical methods and results

Samples for ^{226}Ra were taken in 5-litre aliquots which were then acidified with hydrochloric acid. These were transferred to glass containers and stored until the initial unsupported ^{222}Rn decayed away and the supported ^{222}Rn grew to secular radioactive equilibrium with its parent ^{226}Ra. Problems were encountered with the oil well samples due to the formation of oil/water emulsions. These were stored until sufficient water had separated for analysis. Another problem encountered was the formation of a white precipitate in the stored containers. This may be due to the formation of a barium sulphate precipitate which forms slowly in solution due to the supersaturation of barite which can occur due to loss of water temperature and pressure on sample collection (M. Youngman, pers. comm.). This has been observed in other measurements of ^{226}Ra in formation waters (Kraemer and Reid, 1984) and had led in that instance to a decrease in measured ^{226}Ra activities due to the efficient scavenging effect of barite for radium. Therefore some of the measured ^{226}Ra activities could be lower limits on radium activities.

Measurement of $^{228}Ra/^{226}Ra$ activities was performed by mixing manganese dioxide powder with 25-litre samples and

allowing the powder to settle. The powder was separated by decanting and brought back to the laboratory in small containers after which they were isolated, dried and weighed. After measuring the $^{228}Ra/^{226}Ra$ activity ratio by γ-spectrometry, the bulk activities were corrected for the weight loss of MnO_2 during isolation. Unfortunately, many of the oil well samples contained too much oil to allow large volume water samples to be taken. Also, the oil formed an emulsion in aqeuous solution, and it proved impossible to separate MnO_2 from this emulsion. For this reason only a limited number of radium activity ratio measurements could be made.

The ^{226}Ra activities, $^{228}Ra/^{226}Ra$ activity ratios and ^{228}Ra activities measured in these waters are given in Table 3.7. Field work in the Molasse Basin was performed by J N Andrews, University of Bath.

Table 3.7 Radium nuclide activities in Molasse Basin groundwaters

Well name	Well type	Formation	^{226}Ra pCi/l		$^{228}Ra/^{226}Ra$		^{228}Ra pCi/l	
Munderfing	G	H	14.45	0.05	ND		ND	
Steinerkirchen 1	G	H	28.5	0.7	0.5	0.04	14.25	1.19
Puchkirchen Ost 1	G	H	0.33	0.01	BD		ND	
Schwanenstadt 4	W	H	31.3	1.3	ND		ND	
Gundersdorf H1	W	UP	33.3	1.0	ND		ND	
Maierdorf H1	W	UP	51.8	1.6	ND		ND	
Desselbrunn 2	G	UP	16.3	0.7	ND		ND	
Atzbach 5	G	UP	0.7	0.01	ND		ND	
Atzbach 1	G	UP	7.3	0.4	ND		ND	
Friedburg 2	G	UP	13.2	0.7	ND		ND	
Puchkirchen 20	O	UP	79.	4.0	ND		ND	
Bad Hall Tassilo	W	UP	14.35	0.45	ND		ND	
Bad Hall Para	W	UP	24.7	2.5	ND		ND	
Puchkirchen 27	G	UP	12.6	0.1	0.8	0.04	10.1	0.51
Schwanenstadt P7	G	UP	10.	0.8	0.4	0.02	4.	0.2
Puchkirchen 24	G	UP	22.9	0.8	0.6	0.07	13.74	1.67
Eberstalzell H1	W	UP	67.75	5.25	0.6	0.08	40.65	6.1
Eberstalzell H2	W	UP	46.0	0.1	1.0	0.06	46.0	2.7
Eberstalzell H5	W	UP	50.3	0.3	0.6	0.06	30.18	3.02
Holheck 2	G	LP	7.0	0.7	0.3	0.06	2.1	0.47
Pfaffstadt 3	G	LP	15.5	1.2	0.7	0.04	10.85	1.04
Eggerding 2	O	R	1.8	0.7	ND		ND	
Engenfeld 1	O	UE	13.75	0.05	ND		ND	
Steinhaus 1	O	UE	9.7	1.0	ND		ND	
Kemating 5	O	UE	76.7	1.6	ND		ND	
Maria Schmolln	O	UE	5.8	0.04	ND		ND	
Kemating N1A	O	UE	52.6	0.3	ND		ND	
Kohleck 2	O	UE	47.8	8.7	ND		ND	
Kohleck 6	O	UE	33.3	1.4	ND		ND	
Voitsdorf 10	O	UE	92.6	0.4	ND		ND	
Oberaustall 6	O	C	3.6	0.2	ND		ND	
Trattnack 4	O	C	0.7	0.1	ND		ND	

Table 3.7 continued

Well name	Well type	Formation	^{226}Ra pCi/l	$^{228}Ra/^{226}Ra$	^{228}Ra pCi/l
Horgersteil 1	O	C	ND	ND	ND
Trattnack 11	O	C	1.15 0.15	ND	ND
Voitsdorf 15	O	C	79.05 0.95	ND	ND
Voitsdorf 30	O	C	41.0 2.0	ND	ND
Voitsdorf 2	O	C	53.95 1.95	ND	ND
Voitsdorf 13	O	C	22.65 1.25	ND	ND

Note: Well Type: O = Oil; G = Gas; W = Water
Formation: H = Hall; UP = Upper Puchkirchen; LP = Lower Puchkirchen; UE = Upper Eocene; C = Cenoman
ND = Not Determined; BD = Below Detection

3.2.5 Discussion of Results

3.2.5.1 $^{228}Ra/^{226}Ra$ Activity Ratios

From Table 3.7 there appears to be no correlation between the activity of the two radium isotopes and aquifer lithology or the type of oil well. The latter is assumed to be true because radium does not form soluble organic complexes with crude oil so that it was assumed that oil-water mixtures would not enhance radium activities. The lack of correlation of the individual nuclide activities with aquifer lithology is a consequence of the dependance of radium production both upon the rock radionuclide content and its rock surface area/water volume ratio.

The effect of varying rock surface/water volume within aquifers will mask the inter-rock radionuclide variations. However the activity ratio of $^{228}Ra/^{226}Ra$ should be dependant mainly upon the aquifer Th/U activity ratio as both nuclides should undergo the same specific surface area variations which will therefore cancel out in the ratio; but will vary independantly upon the parent radionuclide distribution in the aquifer rock.

Figure 3.14 shows a linear relationship between ^{228}Ra and ^{226}Ra indicating a constant Th/U ratio. The average $^{228}Ra/^{226}Ra$ value is 0.61 +/- 0.2 compared to a range of 1 - 2.4 for the aquifer rock (Andrews et al., 1984). This suggests an enhancement of ^{226}Ra relative to ^{228}Ra. The cause is not due to the enhanced solubility of ^{238}U compared to ^{232}Th as the uranium activities in these waters are many orders of magnitude below that required

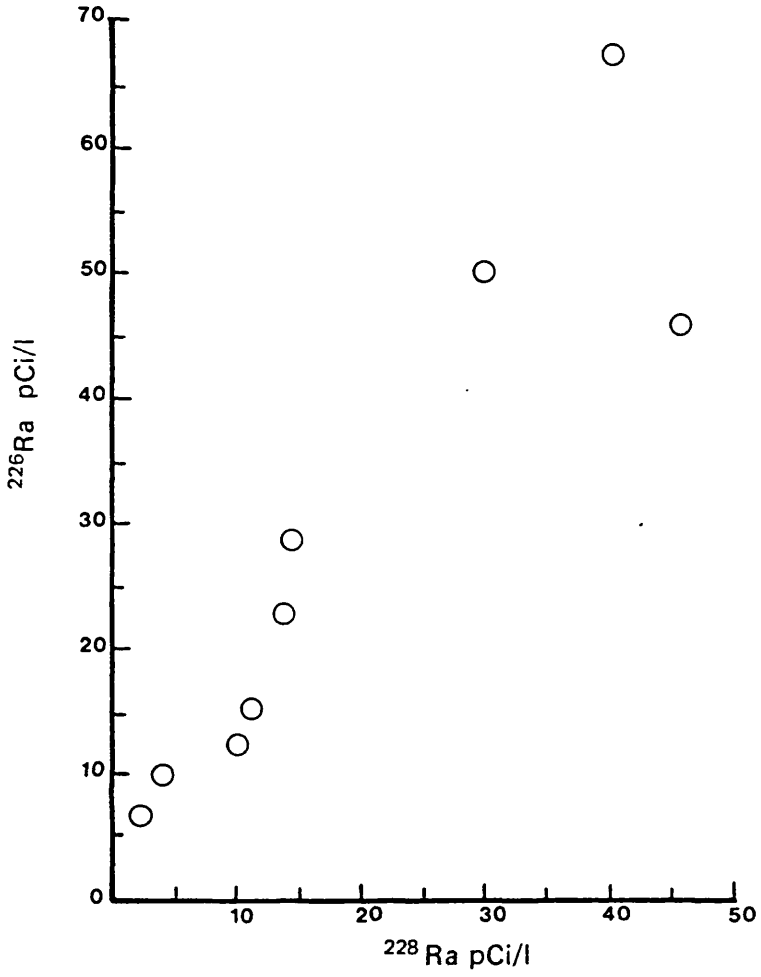

Fig 3.14 ^{228}Ra against ^{226}Ra for Molasse Basin samples

to support ^{226}Ra (ranging between 0.001 and 0.17µg/kg water, Andrews et al., 1984). Instead it is likely to be a consequence of either uranium being more accessible to leaching than thorium within the aquifer rocks; or recoil effects due to the greater number of decays occurring in the uranium series until ^{226}Ra is reached compared to the direct disintegration of ^{232}Th to ^{228}Ra. These alternatives will be discussed at greater length in the 'discussions' section of this study.

Due to the relative consistancy of the $^{228}Ra/^{226}Ra$ ratio it can be assumed that in solution the radium nuclides are subject to the same removal processes. It is the removal processes which will determine the magnitude of the radium activities. Therefore due to the larger data set of ^{226}Ra measurements, this nuclide will be used to illustrate the various possible removal processes. The same arguments should apply to ^{228}Ra.

3.2.5.2 Radium Nuclide Variations with Groundwater Chemistry

Several studies have shown correlations between radium activities and dissolved chloride concentration or salinity (Bloch & Key, 1981; Kraemer & Ried, 1984) and high radium activities in oil field brines (Amhurst & Kuroda, 1955). For instance, the highest ^{226}Ra measured by Kraemer and Ried was 1600 pCi/l for a salinity of 200 g/l.

In this study the highest measured ^{226}Ra activity was 80 pCi/l for both Puchkirchen 20 and Voitsdorf 15. Salinities were not measured for these samples, but the ionic strength (IS), calculated as:

$$IS = \tfrac{1}{2}\Sigma C_i q_i$$

where C_i = concentration of species i

q_i = charge of species i

was determined for each sample by WATEQF calculations (Table 3.6). Like salinity, this measurement provides a measure of the dissolved salt contents of waters. The relationship between ionic strength and the ^{226}Ra activity is shown in Fig. 3.15. There is a striking relationship for the Upper Puchkirchen, Hall and Lower Puchkirchen samples, less so, but still apparent for the U. Eocene and Cenomanian samples.

A number of hypotheses have been put forward to explain this relationship:

1. Radium forms a chloride complex which retains radium in solution and therefore facilitates the leaching of radium from the aquifer rock.
2. The cations associated with chlorine, such as Na^+, Ca^{2+} and Mg^{2+}, competitively exchange with Ra^{2+} for cation adsorption sites in clay minerals. Therefore the greater the concentration of Ca^{2+}, Na^+ or Mg^{2+}, the fewer sites will be occupied by Ra^{2+} and radium will be kept in solution.

Fig 3.15 ^{226}Ra Variation with Ionic Strength in Groundwaters from the Molasse Basin

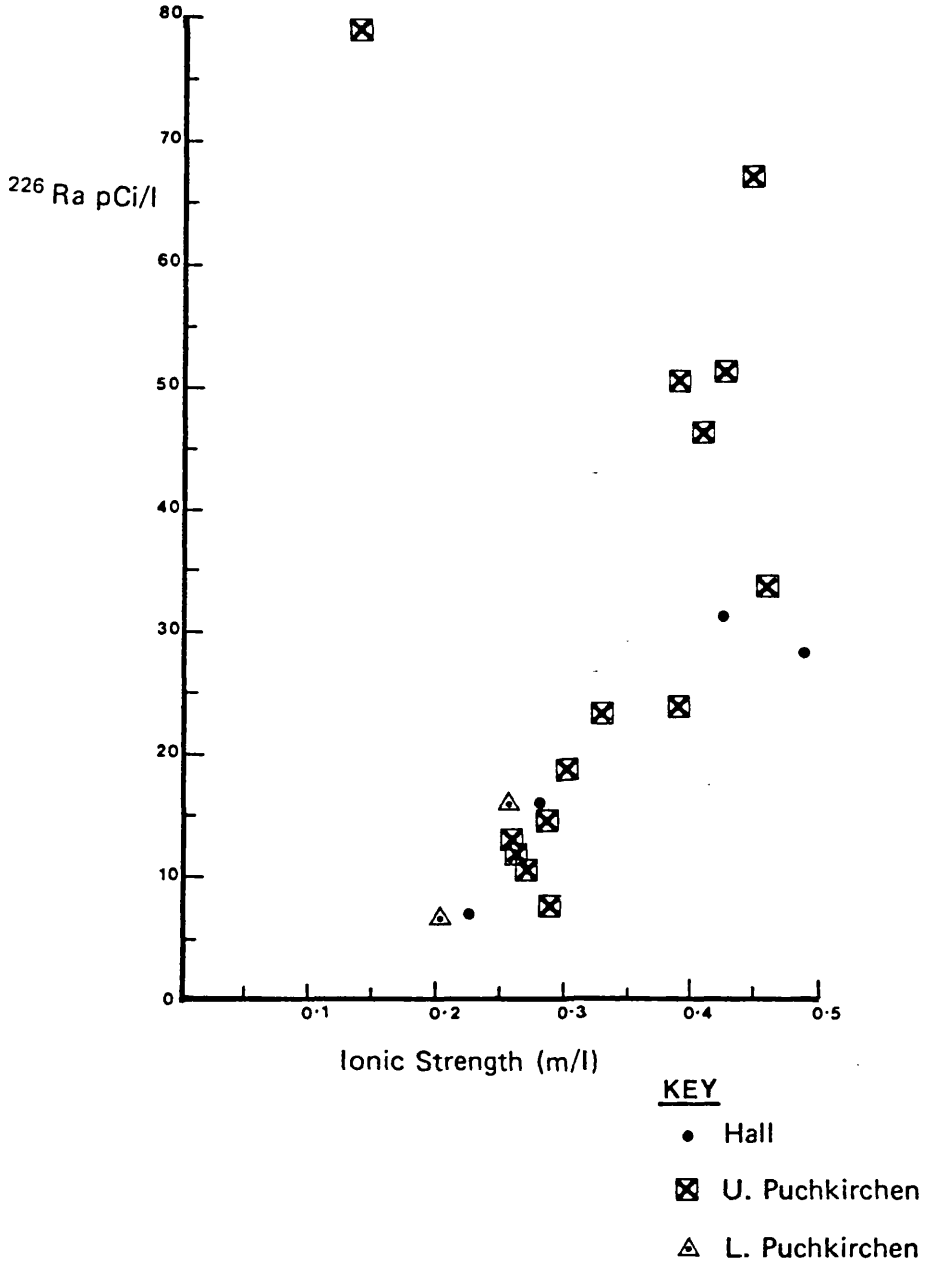

Fig 3.15 ^{226} Ra Variation with Ionic Strength in Groundwaters from the Molasse Basin

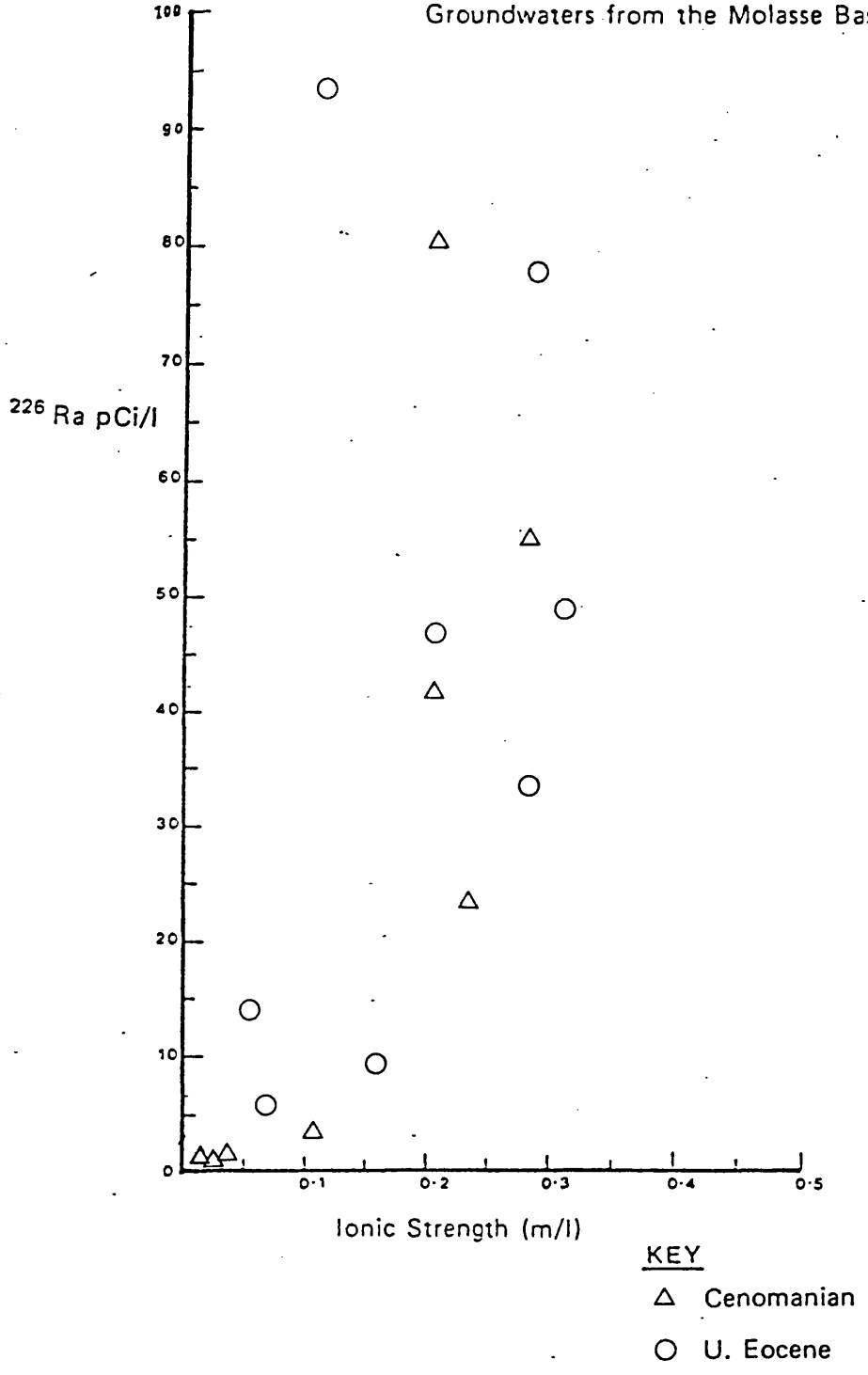

3. Precipitation of calcite, dolomite, gypsum, barite and other minerals will remove radium by co-precipitation or equilibrium exchange processes.

The first hypothesis may easily be tested using the association constants of radium complexes supplied by Langmuir and Melchior (1985). The speciation of radium in these waters so calculated shows that the predominant species is $Ra^{2+}(aq)$ (Table 3.8), although up to 20% of $RaHCO_3^+$ and $RaSO_4^0$ are also estimated. It is noticeable that the species $RaCl^+$ has a very small contribution. However there is a relationship between the concentration of $RaCl^+$ and ionic strength for the Upper and Lower Puchkirchen and Hall formations which suggests either an underestimation of the value for the $RaCl^+$ association constant or that the radium-ionic strength relationship is independant of the radium choride complex which would be the more reasonable explanation.

The second hypothesis may easily be tested by plotting graphs of Ra^{2+} versus Ca^{2+} (Fig. 3.16). Such a plot for the Upper Puchkirchen, Hall and Upper Eocene formations shows linear relationships for each of the formations, but the slope is different for each formation. From a cation-exchange point of view the different slopes may be explained if different clay mineral assemblages exist in each of the formations. Then the competitive ion exchange constant for Ra^{2+} adsorption in the presence of Ca^{2+} will have different values depending

Table 3.8 Radium speciation in the Molasse Basin

Sample Name	% Distribution coefficient Ra^{2+}	$RaCl^{+}$	$RaHCO_3^{+}$	$RaSO_4^{0}$
Hall Formation				
Munderfing 1	91	5	4	
Stienerkirchen 1	81-89	19-7	4	
Puchkirchen Ost 1	92-87		6-11	1
Schwanenstadt 4	92-90	6	2-3	
Upper Puchkirchen				
Gundersdorf H1	89	6	4	1
Maiersdorf H1	89	6	4	1
Desselbraun 2	86	4.5	8	1.5
Atzback 1	84-78	4-3	9-16	3-2
Friedburg 2	84	4	9	3
Puchkirchen 20	68	12	10	21
Bad Hall Tassilo	92	5	3	
Bad Hall Para	92	6	2	
Puchkirchen 27	85-80	4	8-13	2-3
Schwanenstadt 17	85-80	4	8-12	2-4
Eberstalzell H1	91-89	6	3-4	
Eberstalzell H2	91-89	6	3-5	
Eberstalzell H5	91-89	6	3-5	
Lower Puchkirchen				
Hocheck 2	73-63	3	23-32	1
Pfaffenstadt 3	68-58	3	28-39	1
Rupelian				
Eggerding 1	75-62		23-37	
Upper Eocene				
Engenfeld 1	82	13	16	
Steinhaus 1	58	2	36	4
Kemating 5	78-67	4	16-27	2
Maria Schmolln	82	11	16	
Kohleck 2	82-75	5	11-17	1-2
Voitsdorf 11	84-77	34-33	10-17	2
Voitsdorf 10	85-78	2	10-17	2-3
Cenoman				
Oberaustall 6	71	3	12	14
Trattnach 4	76	3	19	4
Trattnach 11	65-54		21-32	13-12
Voitsdorf 15	87-84	34	5-6	4-3
Voitsdorf 30	86-82	4	6-10	3
Voitsdorf 2	81-78	4	4-7	10-11

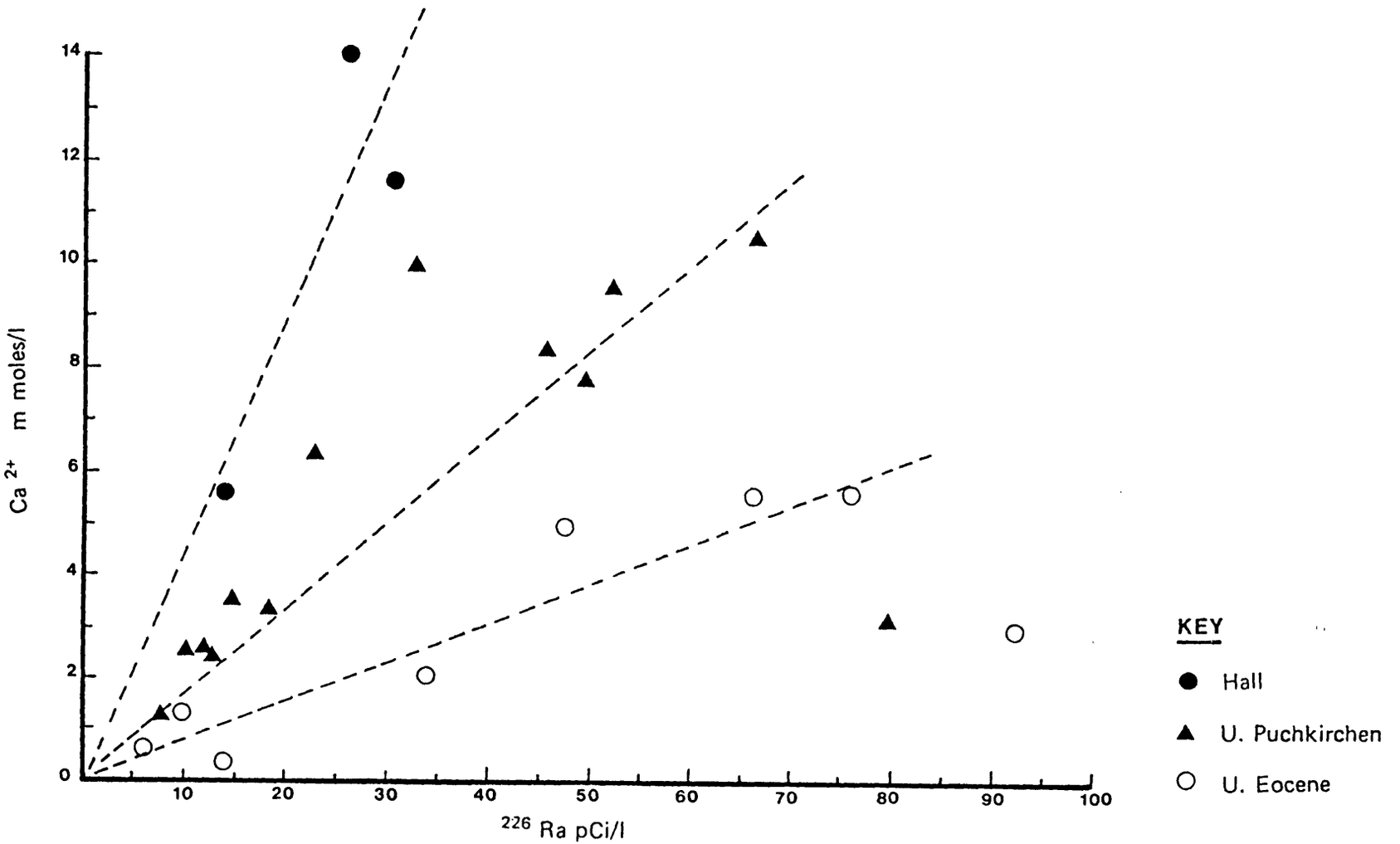

Fig 3.16 Ca $^{2+}$ variation with ^{226}Ra for Molasse Basin Groundwaters

upon the clay minerals present. The Puchkirchen formations are intercalations of coarse sediments with pelagic clays, and the Inviertel formations are known to contain clay minerals which implies that the cation exchange sites required for this hypothesis are available.

Control of radium solubility by co-precipitation or solid solution formation with secondary minerals may be investigated using the calculated saturation indices of the secondary minerals. The minerals with the greatest ability to encorporate radium into their lattices are those formed by the alkaline earth elements. Graphs of calcite, aragonite, dolomite saturation indices against radium activity are given in Fig. 3.17. If radium activities were controlled by solubility limits then the activities would rise to a maximum at the point of mineral saturation. For all of the graphs, the maximum radium activity occurs after the calculated point of mineral saturation (saturation index = 0). However thermodynamic calculations of mineral saturation are limited by kinetic considerations and the crystalline state of the precipitate may not be the same as the laboratory experiments performed to determine the thermodynamic parameters. Therefore it is quite feasible that the actual mineral solubility limits may be higher than those calculated.

To illustrate this point, the aragonite saturation indices are plotted against Ca^{2+} concentration (Fig. 3.18).

Fig 3.17 a) ^{226}Ra Variation with Aragonite Saturation Indices in Groundwaters from the Molasse Basin

(1)

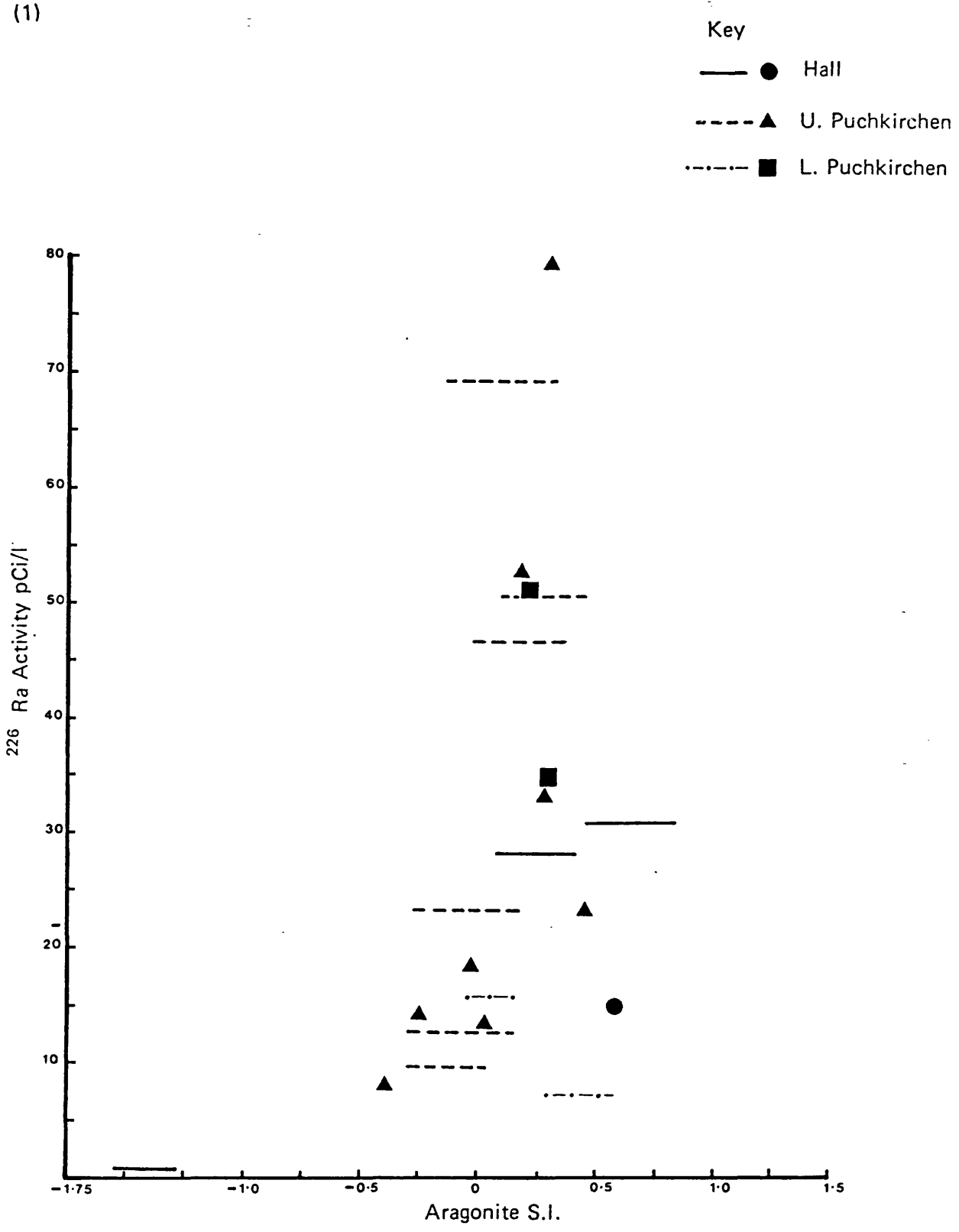

Fig3.17 a) ^{226}Ra Variation with Aragonite Saturation Indices in Groundwaters from the Molasse Basin

(2)

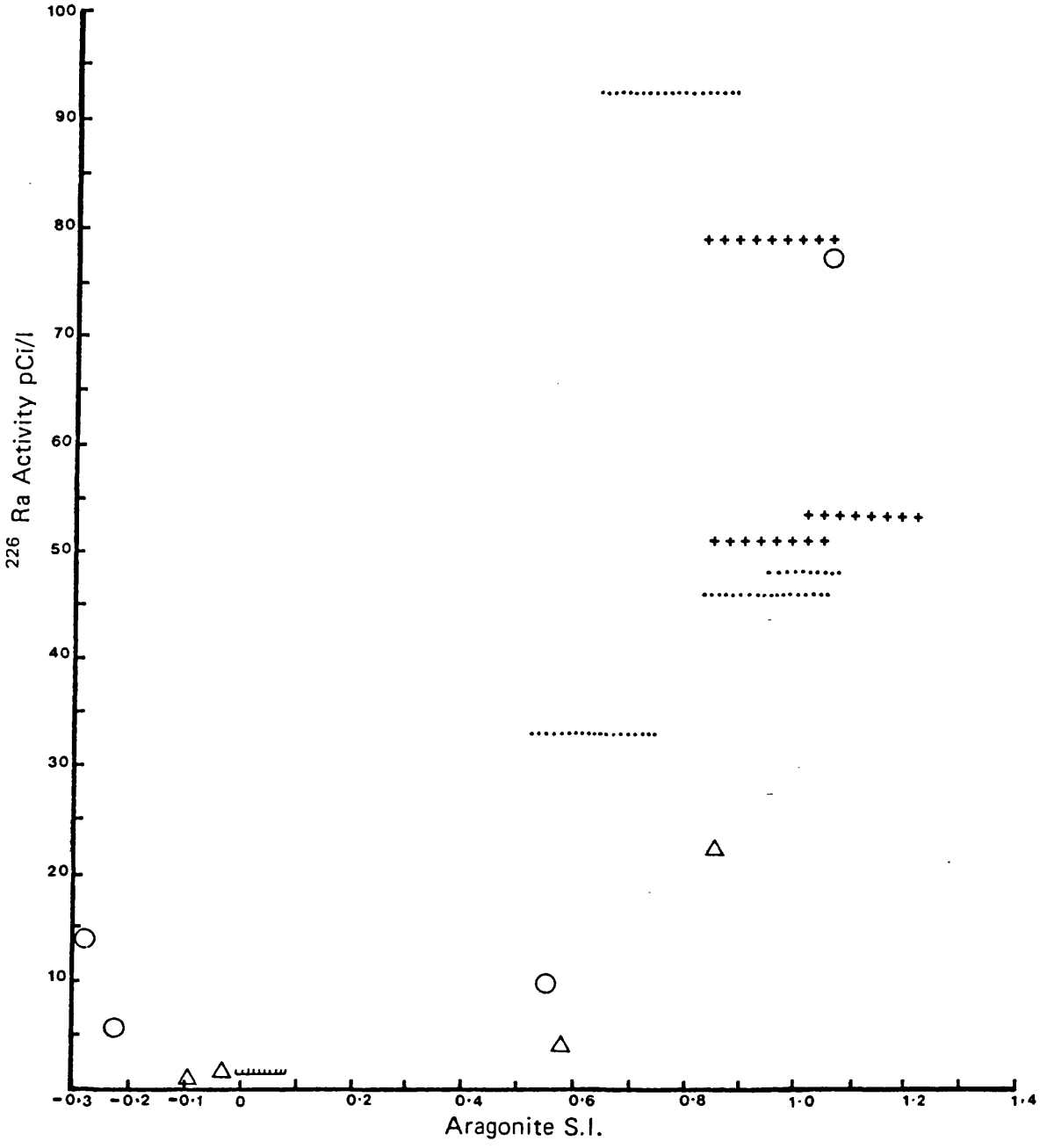

Fig 3.1.7 b) ^{226}Ra Variation with Dolomite Saturation Indices

(1)

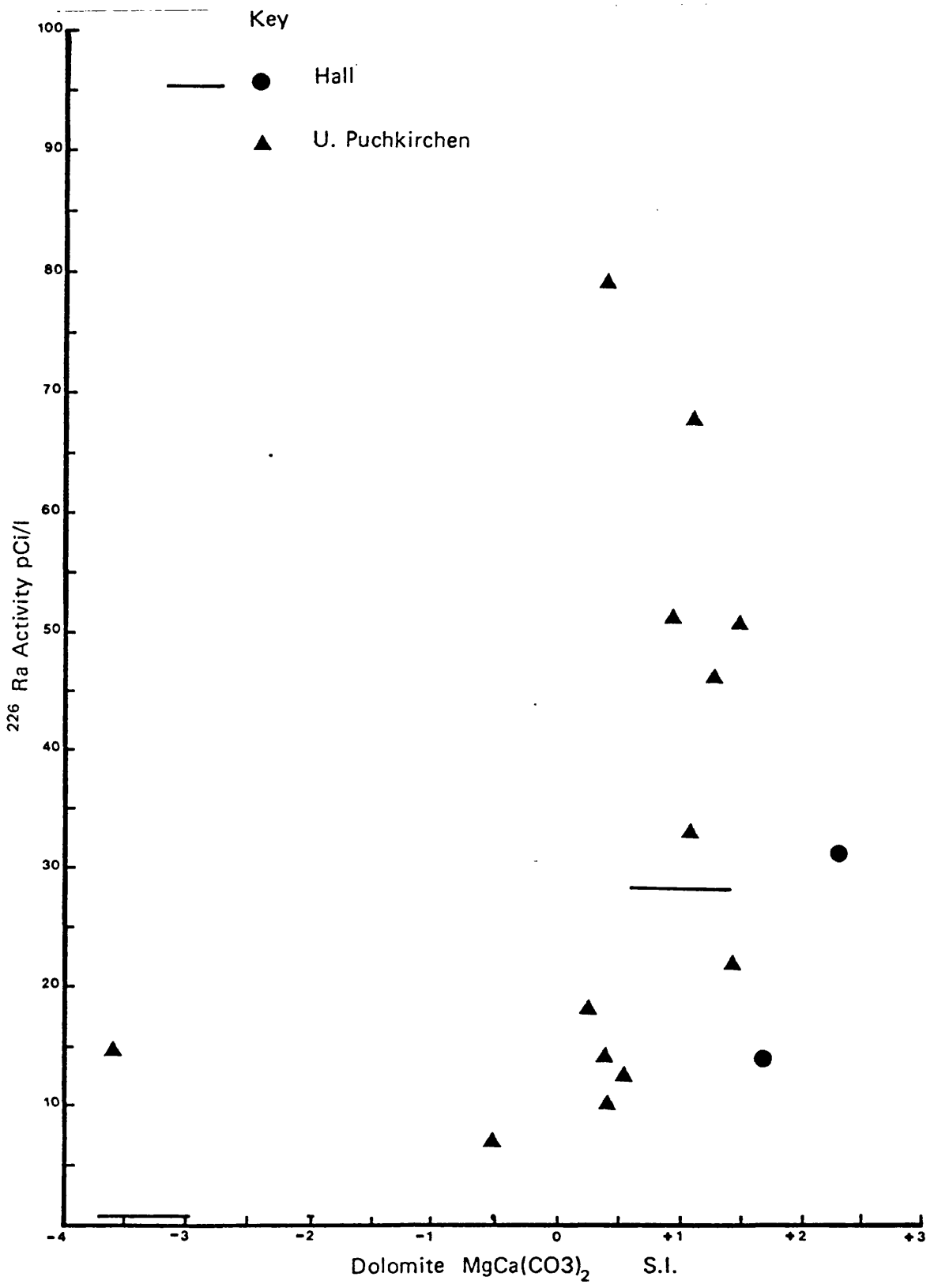

Fig 3.17 b) ^{226}Ra Variation with Dolomite Saturation Indices

(2)

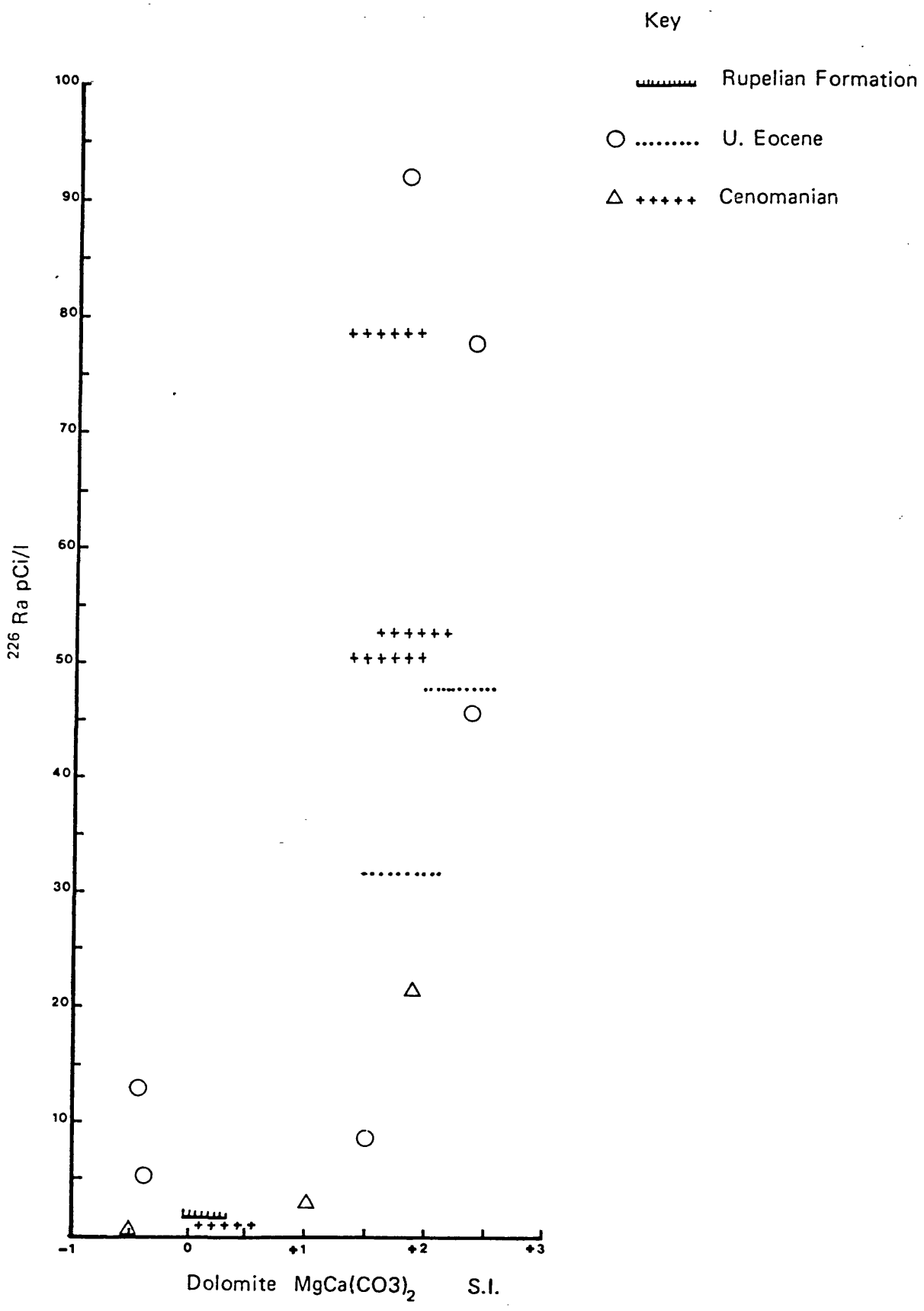

Fig 3.17 c) Calcite Saturation Indices of Molasse Basin Groundwaters

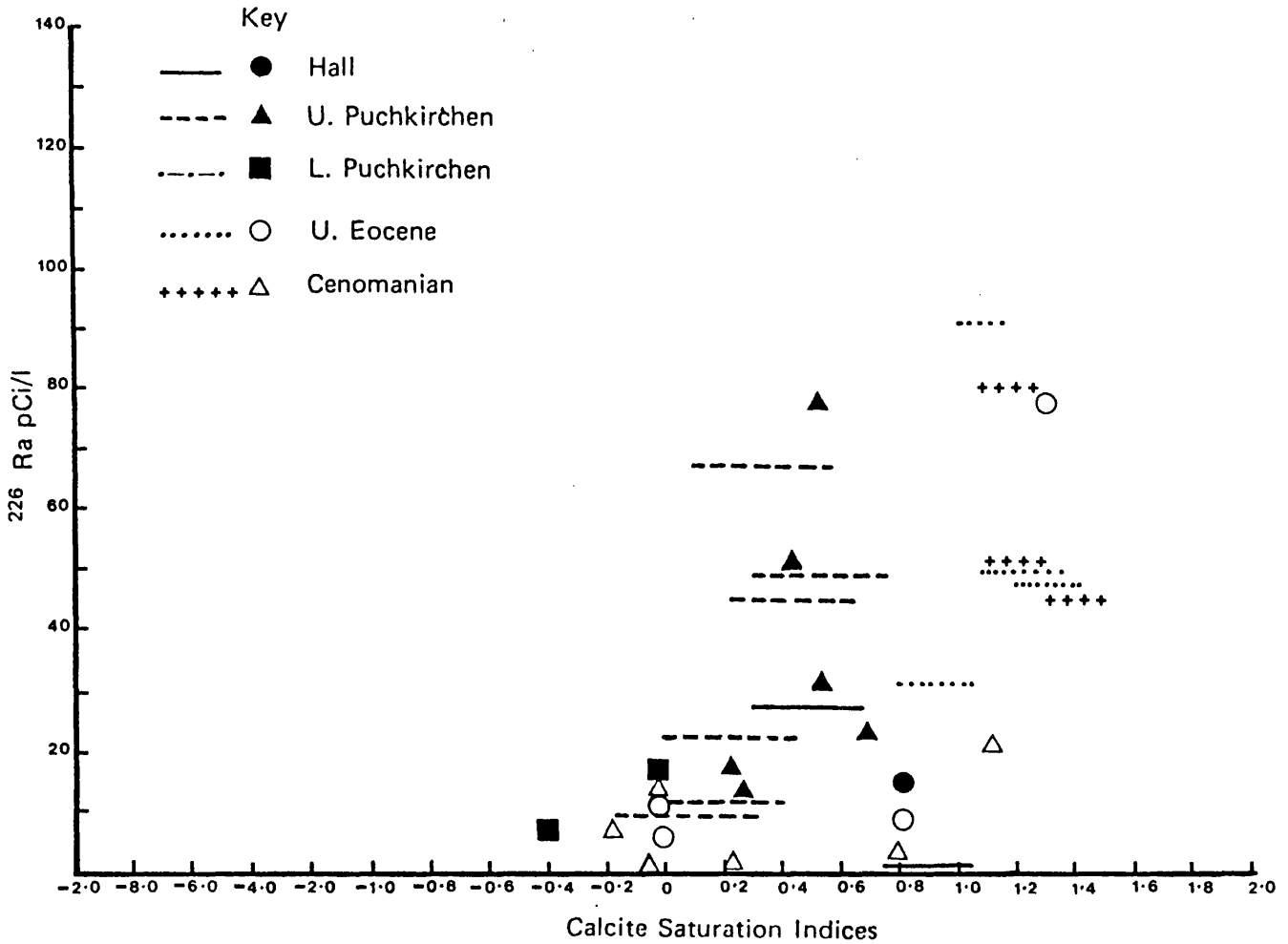

Fig 3.18 Ca $^{2+}$ against Aragonite Saturation Indices for Molasse Basin Groundwaters

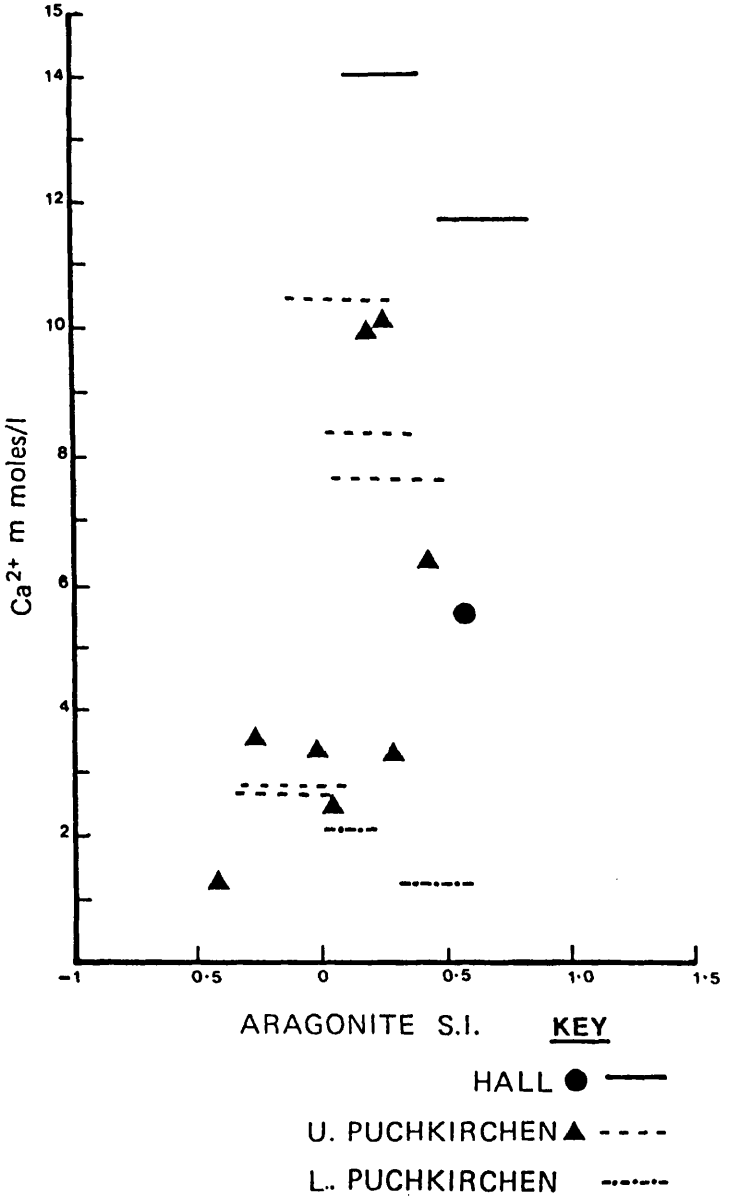

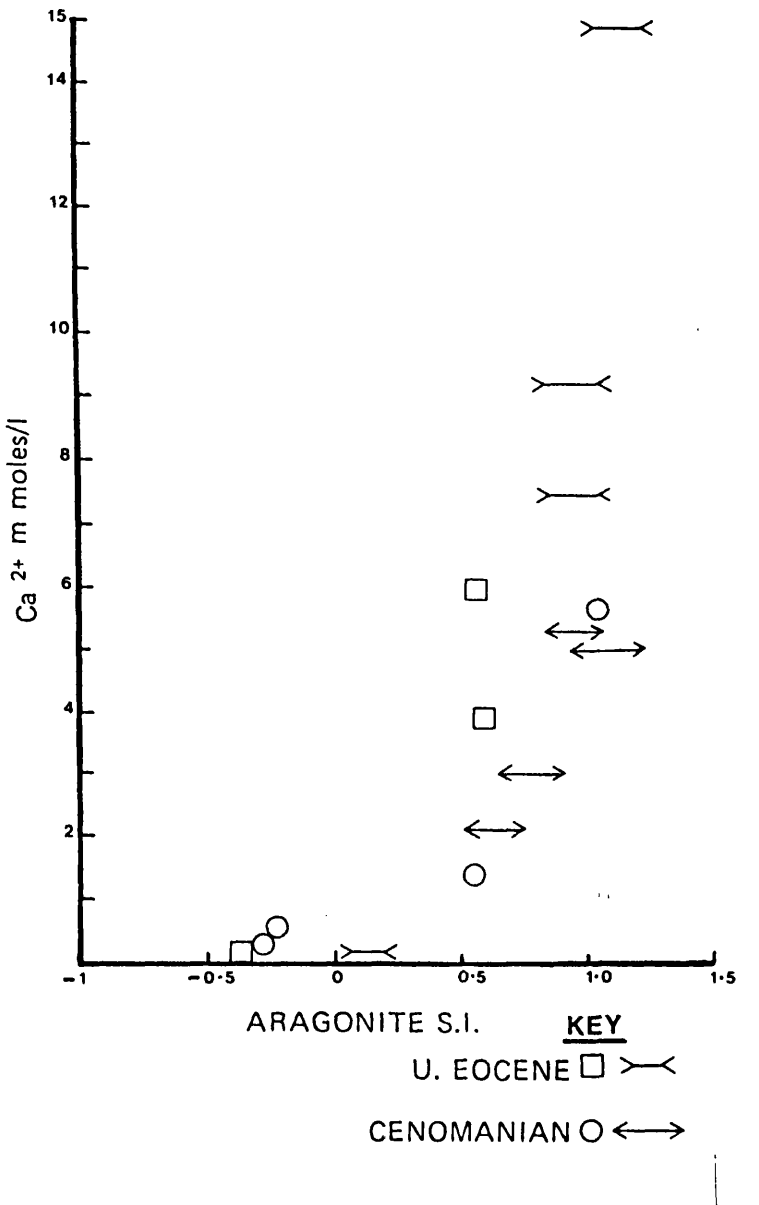

The patterns of the graphs are very close to those of aragonite S.I. against ^{226}Ra activity (Fig. 3.17). The same pattern is repeated if graphs were drawn for the other calcium containing secondary minerals against Ca^{2+}. Clearly if calcium is controlled by secondary mineral formation then radium solubility may be limited by co-precipitation with these minerals.

3.3 Pennant Sandstone groundwaters (The Forest of Dean)

3.3.1 Introduction

The Pennant series of sedimentary rocks located in the Forest of Dean is composed of two series of rocks. The supra Pennant series is composed of interlacing sandstones and shales. The main Pennant Sandstone is a separate sandstone bed underlain by dolomites and lower limestone shales. A detailed description of the geology, hydrology and groundwater chemistry has been given by P. Aldous (1986). A brief resume is given below of the groundwater chemistry and hydrology.

The Supra Pennant Sandstones form a series of minor aquifers with each aquifer separated by impermeable underlying shale. Of the three sites sampled, only the Independant Level site is from a sandstone bed confined over most of its surface. By contrast, the main Pennant sandstone comprises a single confined aquifer underlain by "seat earth" and dolomite beds. The groundwater chemical compositions are presented in Table 3.9 (they are quoted as the average result over 3 years of measurements between 1983 and 1985). The waters are dominated by Ca, Mg, HCO_3. Thermodynamic

Table 3.9 Chemical composition of Pennant Sandstone groundwater

Site	Aquifer	Groundwater Composition (mg/l) Cl^-	SO_4^{2-}	HCO_3	Ca^{2+}	Mg^{2+}	Saturation Indices* Calcite	Dolomite	Ionic Strength (m/l)
Kensley Lodge	S.P.	19.9	26	61	12	12.2	0 to -1.9	-1.5 to -4.9	0.0056
Lower Supra Spring	S.P.	-	-	-	-	-	-	-	-
Independant Level	S.P.	19.5	8.6	366	80	48.6	.02 to -0.8	-0.2 to -1.8	0.013
Miles Level	P	15.9	115	109	64	25	-.43 to -1.7	0.66 to -3.7	0.0085
Old Furnace Level	P	9.6	163	122	160	73	-0.8 to -1.2	-2.8 to -1.8	0.02
Tufts Level	P	17.8	35.5	275	64	34	-4 to -1.2	0.6 to -1.5	0.009
Pennant Spring	P	12.4	115	6.1	200	14.6			0.004
Norchard Drift	P	117	864	366	320	122	0.18 to -0.34	0.2 to -0.8	0.04

Note: S.P. = Supra Pennant Sandstone
P = Pennant Sandstone
* Ranges given for samples collected between 1983 and 1985

calculations show that the waters are close to saturation for calcite and dolomite, although the presence of dolomite underlying the sandstones suggests water equilibrium with these dolomites. Gypsum saturation is approached for the Supra Pennant Sandstone site, Norchard Drift. This may be a consequence of iron pyrites oxidation due to meteoric water incursion into the mine workings.

3.3.2 Results and discussion

Radium activity ratios were sampled by placing MnO_2 impregnated fibres at the entrance of adits or at spring risings. The fibres were retained for 2 weeks, then collected, washed with distilled water and analysed. Samples for absolute ^{226}Ra determinations were taken at the time of collection of the MnO_2 impregnated fibres, and analysed by ^{222}Rn emanation from 5 litres of acidified sample. Samples of Pennant Sandstone were also obtained from quarries and 200 g samples were analysed for U/Th by α-spectrometry. The radium results are given in Table 3.10 and the U/Th results in Table 3.11.

Due to the very low ^{226}Ra activities, which only reached a value of 0.35 pCi/litre, it was difficult to compare radium activities with groundwater chemistry. This is probably due to the poorer analytical precision of ^{226}Ra measurements at this low level of radium. However, the MnO_2 fibres picked up several hundred pCi of both ^{226}Ra and ^{228}Ra over a 2-week period so the

Table 3.10 Pennant Series Results (collected on 29.3.85)

Sample Name	^{226}Ra content[1] (pCi/l)	+/-	$^{228}Ra/^{226}Ra$ Activity ratio	+/-	^{228}Ra content[2] (pCi/l)	+/-
Supra Pennant samples						
Kensley Lodge	0.35	0.01	1.62	0.01	0.57	0.02
Lower Supra Spring	0.30	0.01	1.13	0.02	0.34	0.01
Independant Level	0.18	0.01	1.00	0.01	0.18	0.01
Pennant Series samples						
Miles Level	0.17	0.01	1.04	0.02	0.18	0.01
Old Furnace Level	5.15	0.01	1.48	0.02	0.22	0.01
Tufts Level	0.18	0.01	1.01	0.02	0.18	0.01
Pennant Spring	0.30	0.01	1.46	0.03	0.44	0.02
Norchard Drift	0.24	0.01	1.29	0.01	0.31	0.01

Note: All errors are one standard deviation from the mean, calculated from counting statistics.

[1]Determined by ^{222}Rn outgassing.

[2]Determined as activity ratio x ^{226}Ra content.

Table 3.11 Uranium and thorium contents of Pennant Series aquifer rock samples*

Sample	Uranium content ug/g	±	Thorium content ug/g	±	$^{232}Th/^{238}U$ activity ratio
Pennant Sandstone (1)**	1.08	0.17	7.04	0.63	2.19
Pennant Sandstone (2)*	1.19	0.03	7.06	0.14	2.14
Norchard Drift Ochre	7.82	0.1	-		-
Independant Level Ochre	4.0	0.1	-		-

* Samples supplied by P. Aldous (University of Bristol)
** Analysed by NaI(Tl) gamma-ray spectrometry

$^{228}Ra/^{226}Ra$ measurements were made with reasonable precision.

Nevertheless, the variation of ^{226}Ra with HCO_3^- concentration does show a tentative decrease in ^{226}Ra with increasing bicarbonate concentration (Fig. 3.19) which would be consistent with radium control by equilibria with carbonate minerals. It could also be due to competitive cation exchange between Ra^{2+} and Ca^{2+} for clay mineral exchange sites. The ^{226}Ra activity will then reflect Ca^{2+} behaviour, which would itself decrease with increased HCO_3^- content due to carbonate equilibria.

Speciation calculations show that there is a high degree of sulphate and bicarbonate complex formation (Table 3.12), with the majority of radium complexed to sulphate at the Norchard Drift site. Despite this complexation, the radium activities are low. A number of possibilities could account for this discrepancy:

(i) The waters are dominated by dolomite saturation and therefore radium may take part in carbonate water-mineral exchange processes which could decrease its activity in solution.

(ii) Low chlorinity in these waters suggests a low rate of rock leaching which could limit the supply rate of radium into solution.

The first possibility is clearly feasible due to dolomite saturation for most of these waters. However it is difficult to prove unless dolomite samples known

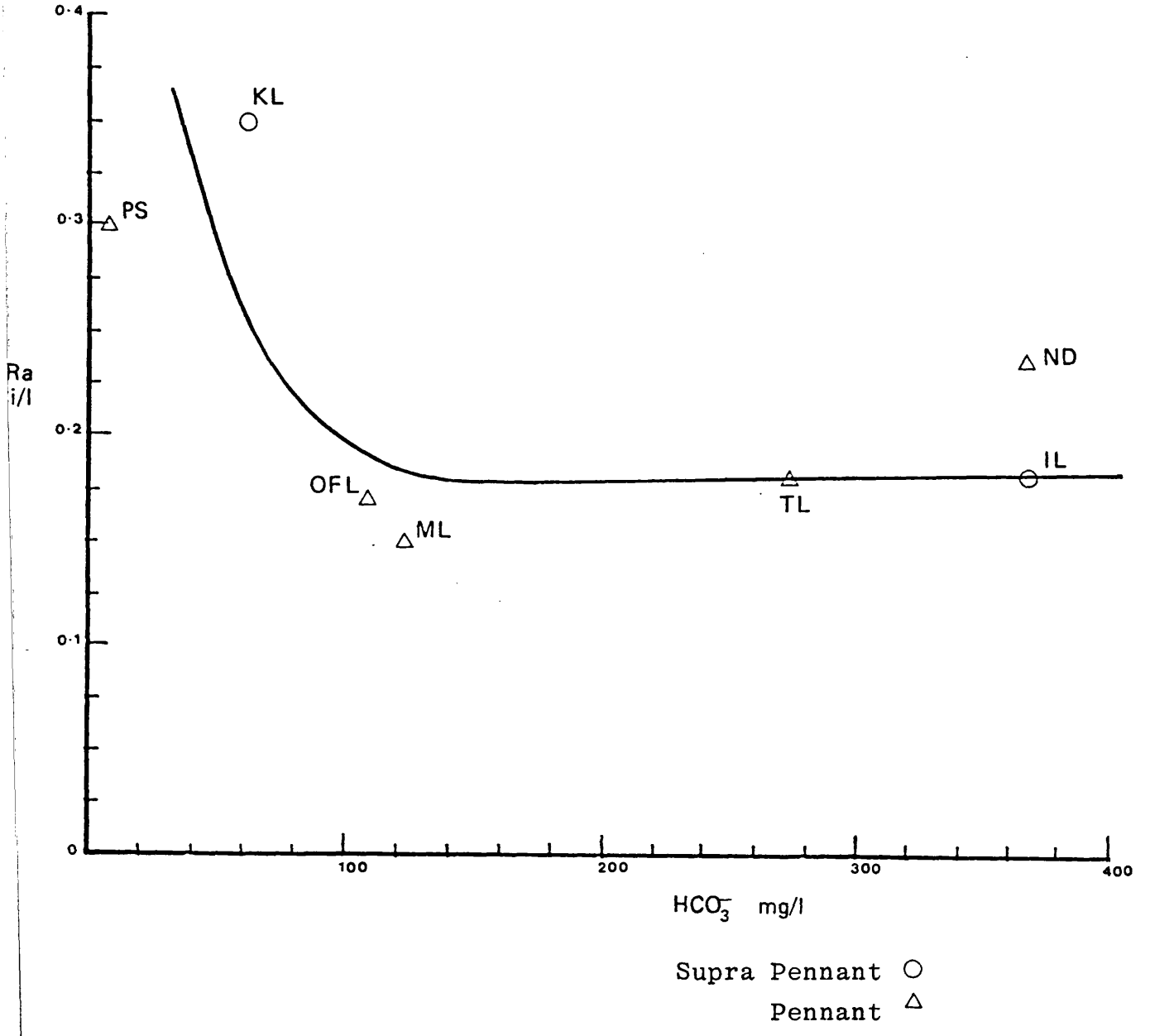

Fig 3.19 Variation of ^{226}Ra Activity with HCO_3^- content for Pennant Series Groundwaters.

Table 3.12 Speciation of Radium in Penant Series groundwaters

Site	Species in solution (%) Ra^{2+}	$RaHCO_3^-$	$RaSO_4^0$
Kensley Lodge	87.0	3.2	9.7
Independant Level	65.4	13.2	21.4
Miles Level	65.2	4.2	30.6
Old Furnace Level	61.2	3.8	35.0
Tufts Level	76.7	12.3	11.0
Pennant Spring	76.6	0.2	23.2
Norchard Drift	34.4	5.7	59.8

to come from dolomite in intimate association with aquifer water, are found to contain surface coatings of radium.

The second possibility is feasible because the supra Pennant aquifers respond rapidly to rainfall and will therefore have short water residence times. If leaching supply of radium is low, then radium must be supplied by recoil. However, a long residence time is required for recoil to become a significant contributor to radium activity and this may not be the case.

3.4 Continental Intercalaire and Complex Terminal groundwaters, North Africa

3.4.1 Introduction

The Complex Terminal and Continental Intercalaire sedimentary rock sequences are located in the Algerian and Tunisian regions of North Africa. Groundwaters from both of these lithologies were sampled between 1984 and 1985. The resulting ^{226}Ra, ^{228}Ra and $^{226}Ra/^{228}Ra$ activities are presented in Table 3.13.

The geology of the region and its hydrology and groundwater chemistry have been described by Elliot (1987). Extensive groundwater monitoring has shown that the waters in the Algerian Continental Intercalaire are classified as "mixed sulphate-chloride" with $SO_4^{2-} > Cl^- > HCO_3^-$ and $Na^+ > Ca^{2+} > Mg^{2+}$. The salinity of the waters increased towards the discharge zone. However, the SO_4^{2-}/Cl^- ratio decreases from recharge

Table 3.13 Radium ratios and activities from the Continental Intercalaire and Complex Terminal aquifers of North Africa*

Site	$^{228}Ra/^{226}Ra$ Activity ratio	+/-	^{226}Ra activity (pCi/l)	+/-	^{228}Ra activity (pCi/l)	+/-	Formation
A) Algeria							
Berriane 2	0.65	0.1	0.43	0.03	0.28	0.05	CT
Ghardaia	0.80	0.12	0.66	0.06	0.53	0.09	CT
Metliti	0.74	0.22	0.49	0.02	0.36	0.11	CI
Zelfana 4	0.65	0.08	0.06	0.13	0.56	0.11	CI
Ouargla 2	1.04	0.12	1.46	0.12	1.52	0.20	CI
Rhoude el Baguel (2)	1.35	0.18	2.21	0.02	2.98	0.39	CI
Gassi Touil	0.79	0.10	2.65	0.01	2.09	0.26	CI
Hassi Messaoud	0.65	0.03	2.13	0.20	1.38	0.14	CI
El Hadjira	0.67	0.05	2.54	0.21	1.70	0.18	CI
Djamma 2	0.42	0.08	2.50	0.15	1.05	0.20	CI
Djamma S14	1.01	0.13	1.07	0.03	1.08	0.14	CT
Tolga	1.32	0.14	2.75	0.17	3.63	0.45	CT
B) Tunisia							
Chott Fedjej 8	0.95	0.11	15.35	0.27	16.1	0.4	CI
Chott Fedjej F2	1.23	0.14	10.09	0.23	14.0	0.51	CI
Seftimi 3	0.99	0.13	2.95	0.10	3.3	0.2	CT
Taouargha	0.17	0.07	0.61	0.10	0.11	0.09	CT
Menchia	0.85	0.11	2.84	0.14	3.3	0.3	CI
Ksar Ghilane	0.62	0.07	4.57	0.15	4.2	0.2	CI
Oum El Farethe	1.31	0.17	1.92	0.13	2.9	0.3	CI
Bou Abdellah	1.03	0.12	4.05	0.10	2.9	0.1	CI
Mahassen	0.66	0.06	6.91	0.19	4.8	0.2	CT/CI
9013	0.59	0.14	0.64	0.14	0.5	0.2	CI

Note: CI = Continental Intercalaire

CT = Complex Terminal

* Field work performed by J N Andrews and T Elliot, University of Bath.

to discharge, with SO_4^{2-} at its greatest in the recharge zone where the aquifer is unconfined. Calcium is correlated to sulphate which indicates calcium supply by gypsum dissolution while magnesium decreases with increasing dolomite saturation, indicating magnesium removed by dolomite precipitation. Both calcite and dolomite are at or close to saturation for the majority of waters whereas gypsum and anydrite are undersaturated.

Groundwater chemical analysis for some of the Continental Intercalaire samples are given in Table 3.14.

3.4.2 Results and Discussion

Activities of ^{226}Ra and ^{228}Ra both reach a maximum for the Chott Fedjej sampling site with ^{226}Ra activities up to 15 pCi/litre. However the majority of groundwaters range up to a maximum of 4.5 pCi/litre for ^{226}Rn, and we can regard the Chott Fedjej samples as exceptional. There appears to be no difference in the distribution of ^{226}Ra and ^{228}Ra activities (Fig. 3.20). Radium activity rates reach a maximum of 1.35 for the Rhoude el Baguel site but the majority of Tunisian and Algerian samples have activity ratios less than 1. The mean ratio is 0.84 with a standard deviation of 0.3 (Fig. 3.20). The high standard deviation indicates that there is a great deal of scatter in the ratios. Nevertheless, in comparison with Th/U activity ratios in possible aquifer matrix material (Table 3.15), the

Table 3.14 Groundwater chemistry of some Continental Intercalaire groundwaters

Site	Ca^{2+}	Na^{+}	Cl^{-}	HCO_3^{-}	SO_4^{2-}	Saturation Indices	
	(meq/l)					Calcite	Dolomite
Djamma	6.7	9	12	3	12.8	0.36	1.44
El Hadjira	11.5	8.5	9.9	2.4	13	0.17	0.05
Ouargla	5.3	9.5	11.7	2.7	10.7	0.58	0.52
Zelfani	-	-	-	-	10	-	-
Metlili	6.8	8.6	11.5	1.9	10.2	0.22	0.12
Hassi Messaoud	9.8	11.4	11.5	2.73	12.5	0.49	0.93
Gassi Touli	15.5	33.9	38	2.4	22.2	0.34	0.83
El Baguel	21.7	20.4	30.4	1.9	27	0.39	0.43

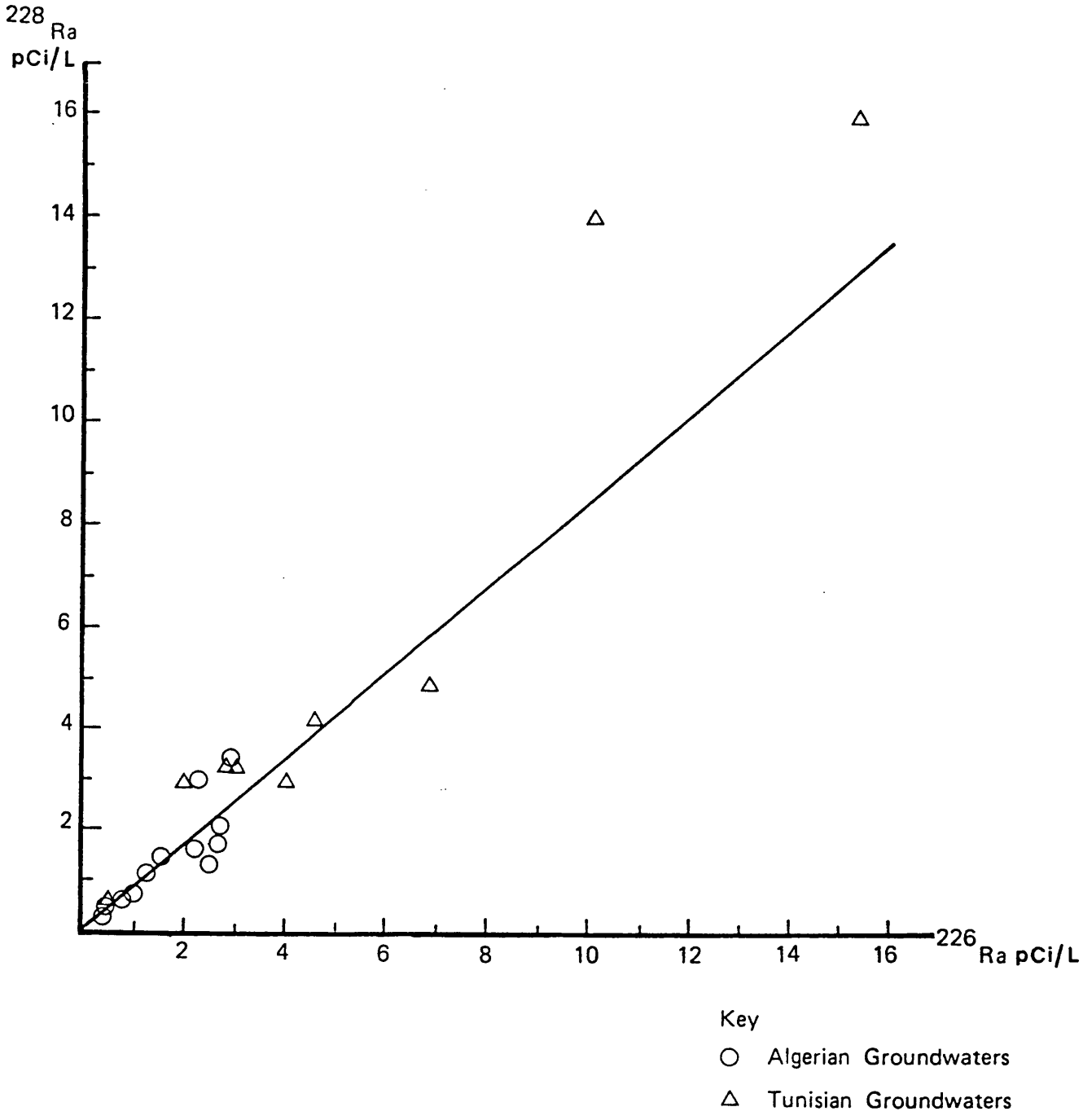

Fig. 3.20 Relationship Between ^{226}Ra and ^{228}Ra for Algerian and Tunisian Groundwaters

Table 3.15 Uranium and thorium contents of sedimentary rocks from the Complex Terminal and Continental Intercalaire aquifers*

Site	Aquifer	Lithology	Depth (m)	Th (ppm)	U (ppm)	Th/U Activity Ratio
Chott Fedjej	CI	Coarse sand + 25% shale	753-759	6.22	0.84	2.48
		Coarse sand + quartz	813-823	5.25	0.79	2.23
		Poorly cemented sandstone	811-861	5.18	1.00	1.74
		Sandstone + shale		9.53	1.31	2.44
Negga 6	CT	Limestone and marl		3.75	2.44	0.52
		Argillaceous marl		8.72	2.46	1.19
		Clays		7.37	1.23	2.00

Note: * = Samples analysed by a NaI gamma-ray spectrometer.

ratics are almost a factor of 2 lower than the expected ratios from Continental Intercalaire rock. The groundwater radium ratios are similar to the Complex Terminal Th/U ratios in the limestone and Argillaceous marls, but there are too few groundwater samples from the Complex Terminal to justify any conclusions.

However, for the Continental Intercalaire samples, while the variable $^{228}Ra/^{226}Ra$ ratios may indicate a variable uranium and thorium distribution in the various aquifer lithologies, there is a systematic difference between the radium ratios and Th/U ratios in the aquifer rock. Clearly some water rock interactive process is occurring which discriminates between ^{228}Ra and ^{226}Ra.

Radium speciation was calculated from the groundwater chemical data in Table 3.14. The majority of radium is in the form $RaSO_4^0(aq)$, in greater percentage than any other aquifer samples in this study (Table 3.16). Despite this the activities of both radium nuclides are not as great as the Molasse Basin groundwater samples. Bicarbonate complexes for instance, do not form more than 3% of the radium species in solution, and chloride complexes are negligible.

There is poor correlation between radium and other major ions in solution, although both Ca^{2+} and SO_4^{2-} show increasing concentration with increasing ^{226}Ra activity (Fig. 3.21). However calcium and sulphate are expected to be correlated because of gypsum dissolution. Radium

Table 3.16 Radium speciation in Algerian groundwaters

Site	Species distribution (%)			
	Ra^{2+}	$RaHCO_3^+$	$RaSO_4^0$	$RaCl^+$
Djamma	21.0	3.1	75.7	0.2
El Hadjira	20.9	2.4	76.5	0.2
Ouargla	24.2	3.2	72.5	0.1
Zelfana	26.2	-	73.8	-
Metlili	25.2	2.3	72.3	0.2
Hassi Messaoud	21.5	2.9	75.4	0.2
Gassi Touil	13.5	1.6	84.5	0.4
El Baguel	11.5	1.1	87.2	0.2

Fig 3.21 Variation of ^{226}Ra with Groundwater Chemistry for Algerian Groundwaters

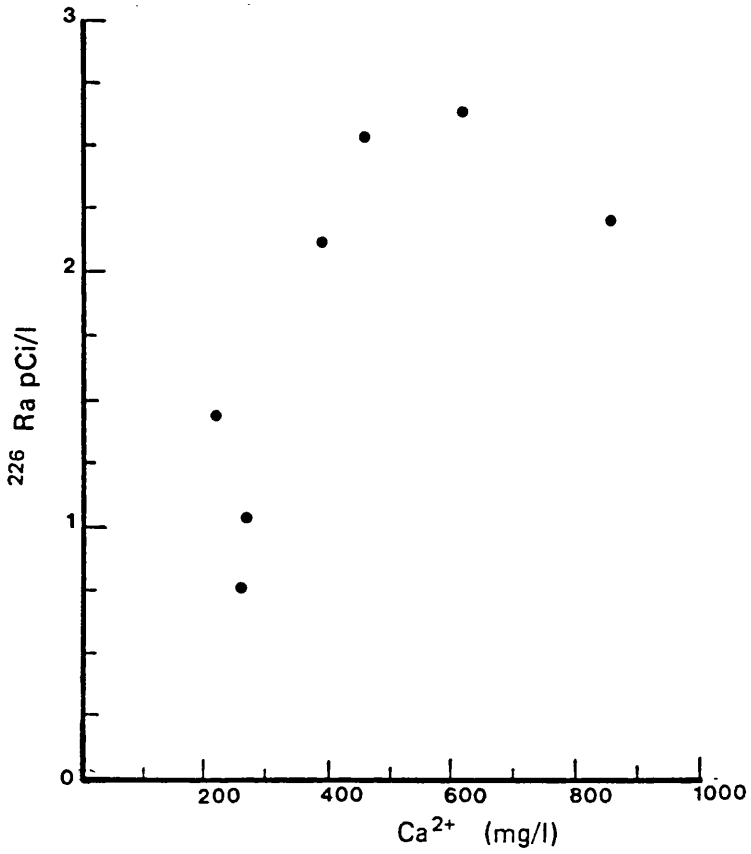

a) ^{226} Ra versus Ca^{2+}

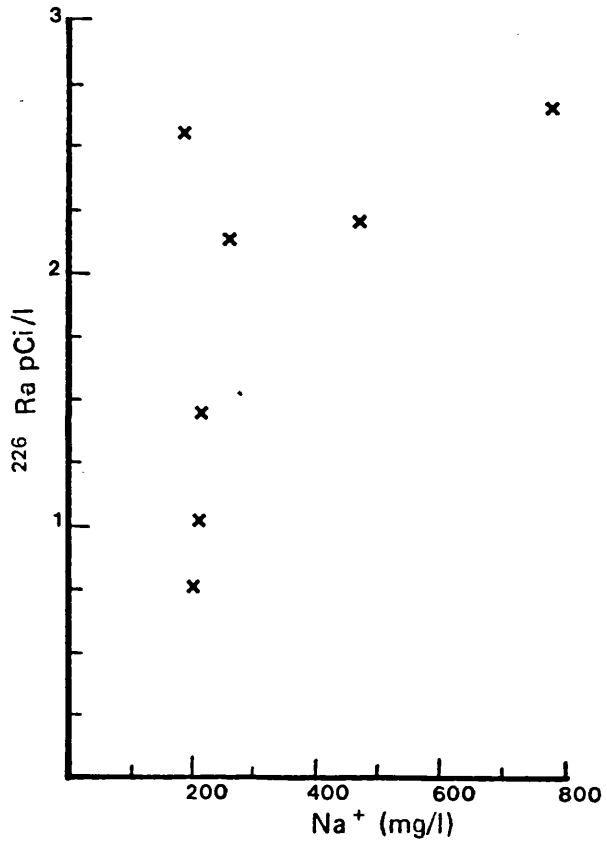

b) ^{226} Ra versus Na^{+}

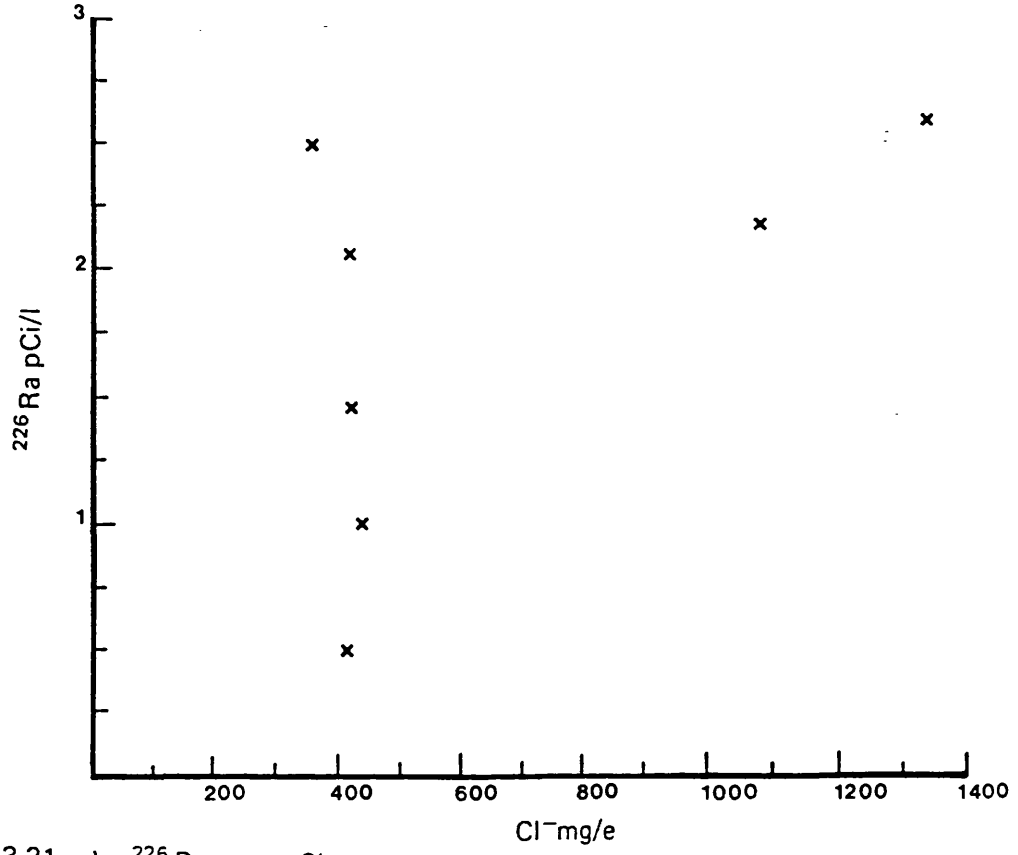

Fig 3.21 c) ^{226}Ra versus Cl^-

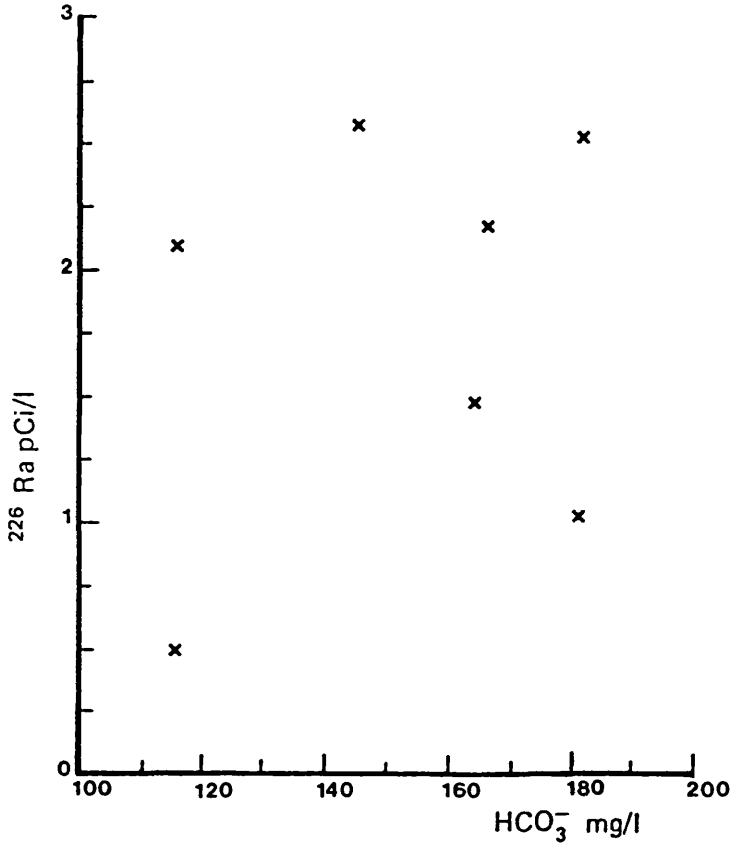

d) ^{226} Ra versus HCO_3^-

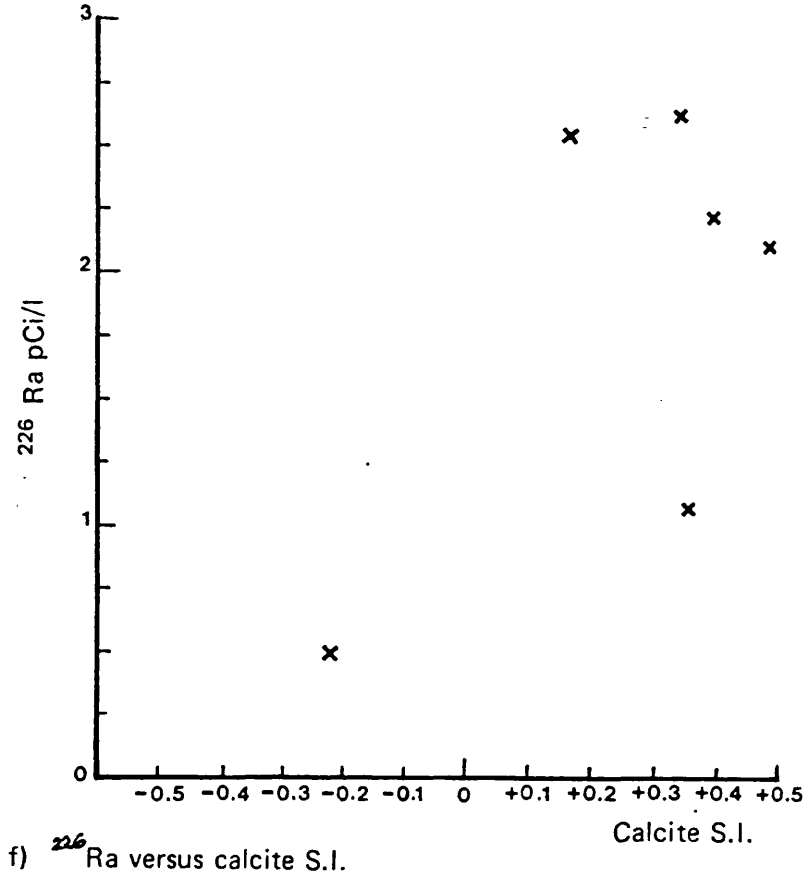

f) ^{226}Ra versus calcite S.I.

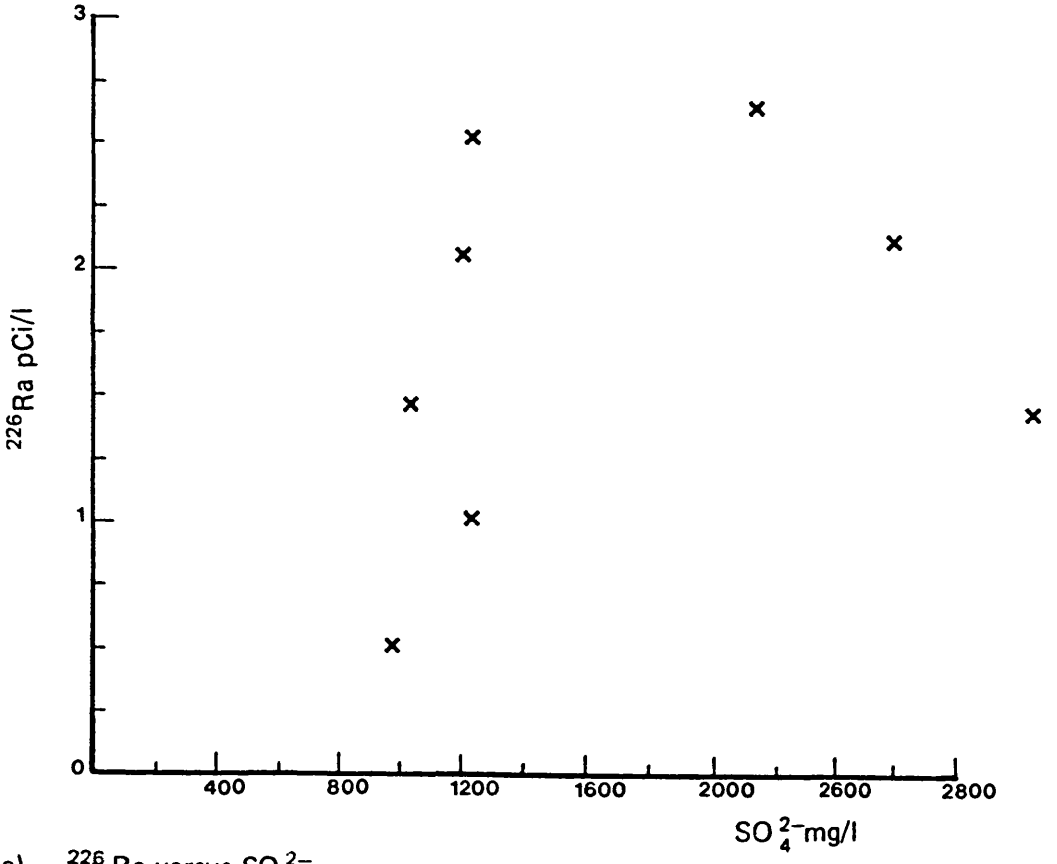

e) ^{226} Ra versus SO_4^{2-}

will not be supplied by gypsum dissolution unless a substantial amount of uranium and thorium is incorporated into the gypsum matrix, which is unlikely.

Instead the correlation is due to two possibilities:
(i) Ca^{2+} prevents adsorption of Ra^{2+} by cation exchange, so the greater the calcium content the greater the radium content.
(ii) Formation of $RaSO_4^0(aq)$ results in increasing radium activities with increasing sulphate concentration.

The first possibility is the more likely as the radium activities in the Gassi Touil and Rhoude el Baguel sites are not substantially greater than those of other sites despite sulphate concentrations in these waters being a factor of 2 greater than those in the other sites.

3.5 Groundwaters from the Bath-Bristol Sedimentary Basin and associated geological horizons

3.5.1 Introduction

Geothermal waters are known to have unusually high dissolved radionuclide contents as a result of water-rock interaction processes. Geothermal waters in areas which are not subject to heating by plate tectonic processes are heated by the geothermal gradient resulting from decay of ^{238}U, ^{232}Th and ^{40}K in rocks.

Significant discharges of thermal water arise at several places in the Bath-Bristol sedimentary basin through carboniferous limestone at Hotwells, Bath and

lower lias shale at Bath (Fig. 3.22). The flow rates for the two springs are 0.2 litres per second and 14 litres per second respectively (Andrews, et al., 1982).

The geothermal evolution of the thermal springs at Bath have been extensively investigated by Andrews et al. (1982). The waters in the Kings Spring are composed predominantly of Ca^{2+} and SO_4^{2-}. The waters are saturated with respect to calcite, dolomite, gypsum fluorite and barite, as calculated by the WATEQF program. The water-rock equilibration temperature is between 64^0C and 96^0C depending upon the choice of quartz or chalcedony as the polymorph for the SiO_2 geothermometer. Assuming an average geothermal gradient of 20^0C/km this gives a maximum water circulation depth of between 2700 and 4300 m. From the geology of the area this suggests either carboniferous limestone or Old Red Sandstone as the storage aquifer for the waters.

The ^{13}C and ^{14}C isotopes suggest that considerable exchange between rock carbonate and water carbonate has occured after initial congruent solution of carbonate. Evidence from the ^{13}C, ^{14}C and ^{4}He content of the water suggests that the waters are older than 10,000 years but dating is uncertain due to mixing between old thermal waters and local groundwaters. Oxygen and hydrogen isotope compositions suggest that the waters are of meteoric origin. Piezometric studies indicate that the only locality able to generate the piezometric

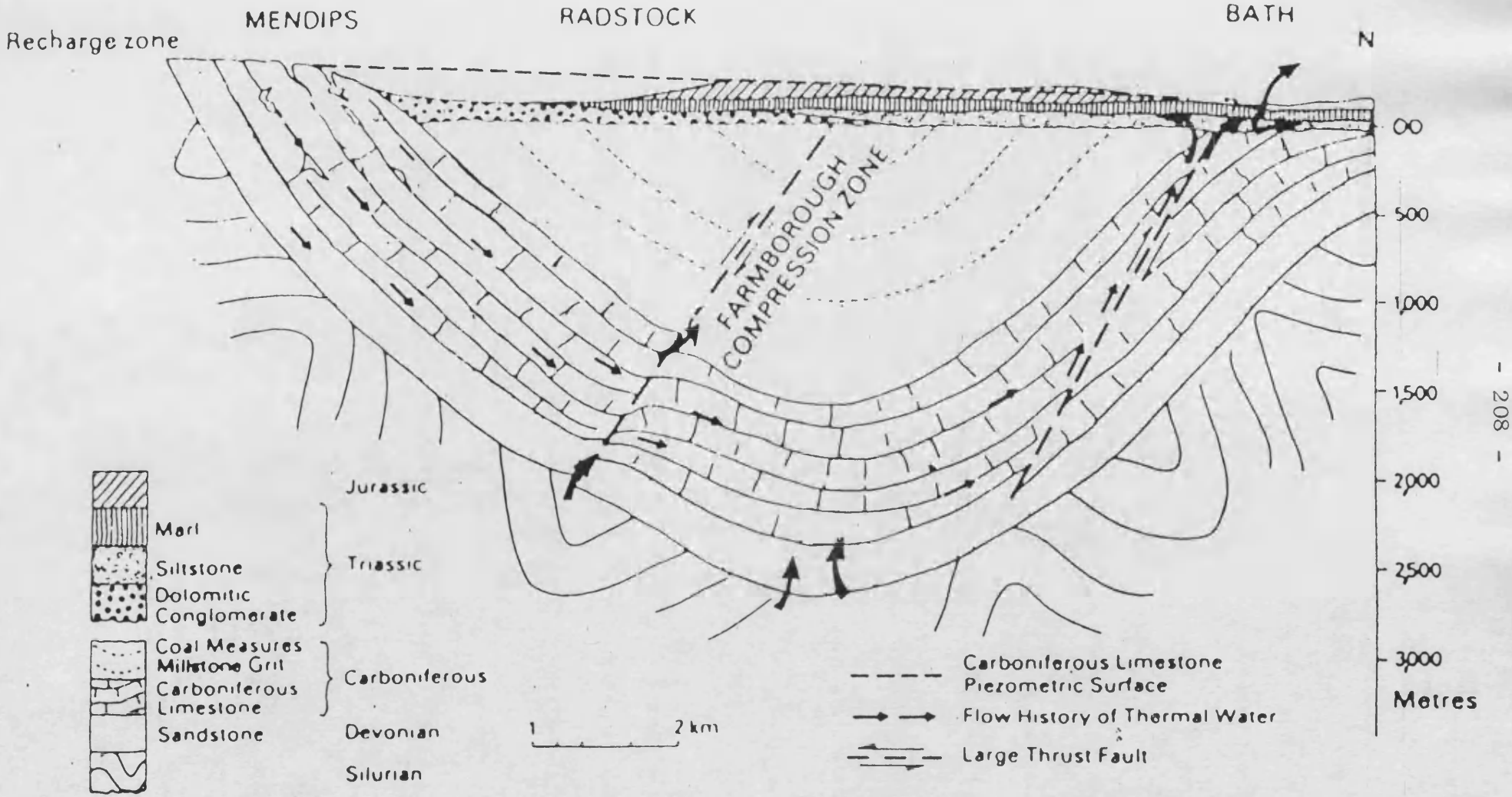

Fig. 3.22 Location of Kings Spring geothermal waters

level of the King's Springs is the Mendip Hills. Seasonal variations in dissolved oxygen and Eh also suggests that there is some mixing between geothermal and local groundwaters.

In this study the dissolved radium contents of local springs around the Bath area and from the Carboniferous Limestones and Old Red Sandstones in the Mendips were measured, together with the measurement of radium and lead nuclides in the King's Springs, Bath.

3.5.2 Sampling Procedure

3.5.2.1 Carboniferous Limestone and Old Red Sandstone Risings, Mendip Hills

Manganese dioxide impregnated acrylic fibres were placed at or as close as possible to the source of springs arising from Carboniferous Limestone or Old Red Sandstone in the Mendip Hills. After a period of 2 weeks the fibres were collected and brought back to the laboratory for processing. The sample taken from Biddlecombe Hospital spring was obtained from the pipe used to pump water from the spring to the Hospital water storage tank, approximately 200 m away. The absolute ^{226}Ra activity in solution may be depressed by adsorption on the pipe. However the $^{228}Ra/^{226}Ra$ ratio should not be affected. The results are reported in Table 3.17.

It was found that considerable quantities of sediment had accumulated in the fibres. This was removed by washing the fibres with distilled water until no further sediment loss was observed.

3.5.2.2 Midford Sand, Inferior and Greater Oolite Groundwaters, near Bath

Dissolved radium activities of springs originating from the locality surrounding the thermal springs at Bath are reported in Table 3.18. Quantitative ^{226}Ra was determined by 5-litre water samples and the $^{228}Ra/^{226}Ra$ activity ratio from fibres suspended in flowing water close to the spring source. Samples of Greater Oolite limestone were obtained from Bath Stone Quarries for Th/U analysis.

3.5.2.3 King's Spring Geothermal Waters, Bath

The $^{228}Ra/^{226}Ra$ activity ratio and ^{226}Ra activity of the King's Spring borehole were measured over several months, both by adsorption on MnO_2 and on MnO_2-loaded acrylic fibres. The activity of ^{224}Ra was also measured by placing MnO_2 impregnated fibres in flowing borehole water for several hours. The fibres were processed immediately. Counting of barium sulphate sources was performed at 8-12 hour intervals for 1 hour periods to follow the decay of ^{212}Pb picked up on the fibres and the ingrowth of ^{212}Pb by decay of ^{224}Ra picked up on the fibres. The chemical efficiency of the pick up of lead by co-precipitation with barium sulphate is uncertain, so this method could not be used to estimate the original activity of ^{212}Pb with certainty.

The ingrowth and decay of ^{212}Pb on the fibres can be expressed by the following relationship:

Table 3.17 Groundwater radium ratios and radiums

Sample	Aquifer formation	$^{228}Ra/^{226}Ra$ activity ratio	+/-	^{226}Ra activity pCi/l	+/-	^{228}Ra analysis pCi/l	+/-
Cheddar Rising	Carboniferous Limestone	0.89	0.04	0.12	0.05	0.11	0.05
Rickford Rising	"	0.92	0.03	0.32	0.01	0.29	0.1
Lanford Rising	"	0.88	0.01	0.26	0.01	0.23	0.1
Biddlecombe Hospital Spring	Old Red Sandstone	1.01	0.01	0.30	0.01	0.3	0.1

Table 3.18 Groundwater radium results from local superficial aquifers, Bath

Sample	Aquifer formation	$^{228}Ra/^{226}Ra$ activity ratio		^{226}Ra activity pCi/l		^{228}Ra activity pCi/l	
Midford 1	Midford Sand	1.31	0.03	0.76	0.1	0.99	0.13
Midford 2	Midford Sand	1.25	0.03	0.76	0.1	0.95	0.12
Chaterhouse Springs	Inferior Oolite	1.14	0.05	0.20	0.01	0.23	0.01
Tucking Mills	Midford Sand	1.65	0.07	0.11	0.04	0.18	0.07
'Bath Stone' Quarry	Greater Oolite	1.53	0.06	0.097	0.01	0.15	0.02

$$A_{Pb,t} = \left(\frac{\lambda 212}{\lambda 212-\lambda 224}\right) A^{o}_{Ra} \left(e^{-\lambda 224 t} - e^{-\lambda 212 t}\right) + A^{o}_{Pb} e^{-\lambda 212 t} \qquad (3.3)$$

where

A_{Pb},t = activity of ^{212}Pb on the $BaSO_4$ source

A^{o}_{Ra} = initial activity of ^{224}Ra at the time of $BaSO_4$ precipitation

A^{o}_{Pb} = initial activity of ^{212}Pb at the time of $BaSO_4$ precipitation

$\lambda 212$ = decay constant of ^{212}Pb

$\lambda 224$ = decay constant of ^{224}Ra

Both $A^{o}Pb$ and $A^{o}Ra$ are unknown. However, A_{Pb},t can be measured at several different times to yield at least 2 equations with 2 unknowns which may be solved for $A^{o}Pb$ and $A^{o}Ra$. The value of $A^{o}Ra$ must be corrected for decay between the time of collection and barium sulphate co-precipitation. The correction can be calculated by the equation (1.32) with:

t = time between sample collection and $BaSO_4$ precip.

A_{Ra} = ^{224}Ra activity at time of sample collection

λ = decay constant of ^{224}Ra

The time of sample collection in this case was taken as the midpoint of the time the fibres were immersed in flowing spring water.

Samples for ^{212}Pb, ^{214}Pb and ^{210}Pb were measured by adding lead nitrate and ferric chloride carriers and precipitating $Fe(OH)_3$ which co-precipitated lead. After processing the sample, the weight of $PbSO_4$ recovered was used to calculate the chemical recovery of lead.

Measurement of ^{214}Pb began generally 40 minutes after sample collection (approximately 2 half-lives of ^{214}Pb). The calculated ^{214}Pb activity of each measurement was plotted against $e^{-\lambda 214 t}$ where t = time from sample collection, $\lambda 214$ = decay constant of ^{214}Pb. The activity at the time of sample collection is simply the slope of the graph. The fact that the points plot smoothly on the graph illustrates the purity of the lead extraction. (Fig. 3.23).

For ^{212}Pb this approach did not give consistent results due to the very low activity of ^{212}Pb in the water. The quoted result is simply the average value of $A^{O}Pb$ calculated for each measurement. There was no increase with time of ^{212}Pb activity due to the decay of ^{224}Ra. Therefore ^{224}Ra was not co-precipitated with $Fe(OH)_4$ and did not contribute to the measured ^{212}Pb activity.

Activities of ^{210}Pb were very low in the King's Spring borehole water, and were not detected in samples taken for ^{212}Pb and ^{214}Pb. A 100 litre sample was taken which was outgassed for about 40 minutes to remove ^{222}Rn which may decay to produce ^{210}Pb. Lead and iron carriers were added and the sample processed normally.

Results for ^{226}Ra, ^{228}Ra, ^{224}Ra, ^{214}Pb, ^{210}Pb and ^{212}Pb from the King's Spring, Bath are presented in Table 3.19.

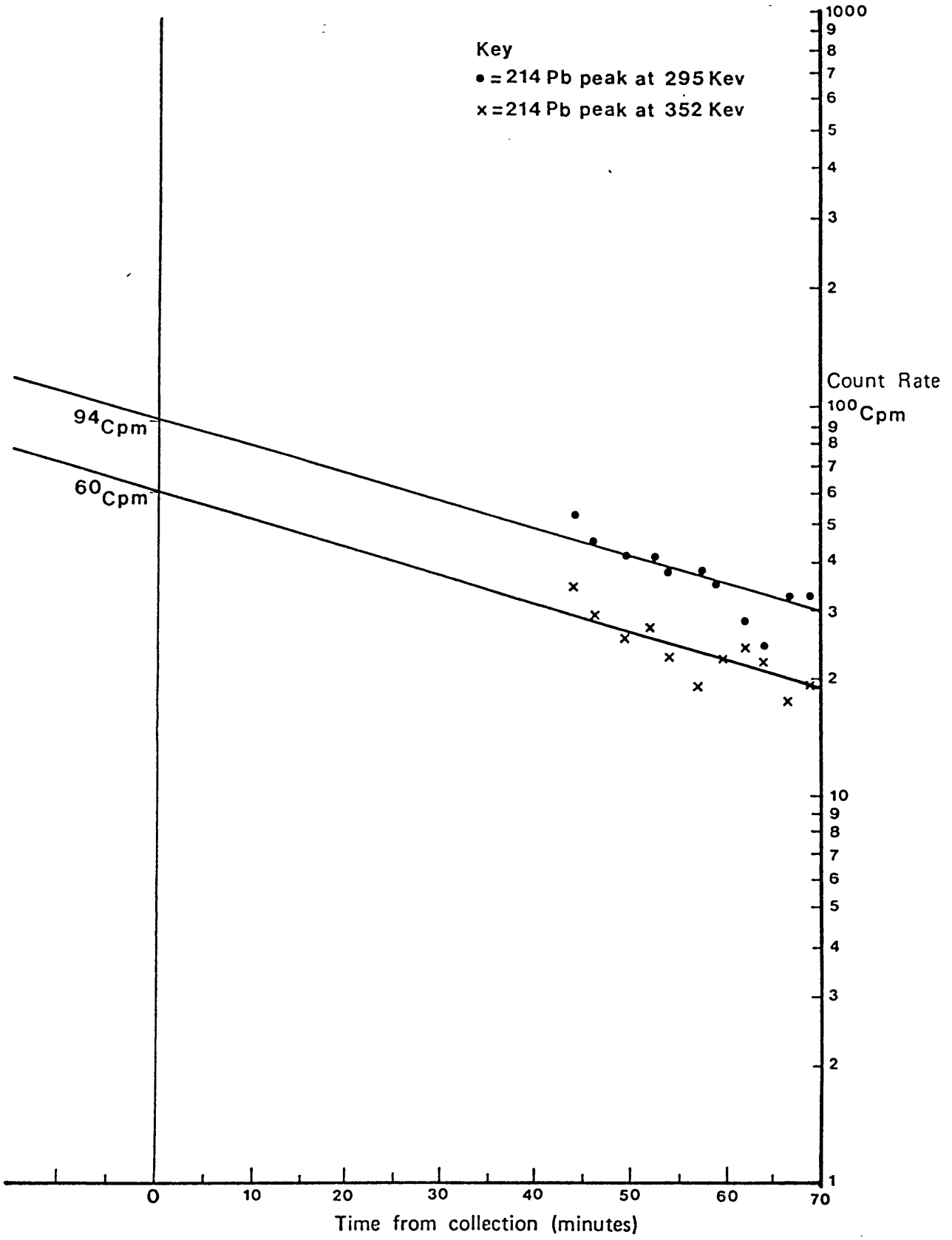

Fig 3.23 Measurement of Pb peak decay on a Planchett containing Pb^{2+} carrier isolated from 5L Kings Spring Water

Table 3.19 Dissolved radium and lead radionuclide contents of Kings Spring, Bath

(i) Activities

	^{226}Ra		^{228}Ra[1]		^{224}Ra (pCi/l)		^{214}Pb	^{212}Pb		^{210}Pb	^{228}Th	
		+/-		+/-		+/-			+/-			+/-
12		1.8	0.94		2.02	0.08	1963	2.04	0.12	<0.01	0.0093[4]	
13		1.2	0.92		1.98	0.05	2100	1.81	0.08	<0.01	0.0042	0.001
14		0.9	1.12		1.60	0.09	2680			<0.01		
9.2			0.797				2768					
12.2			0.72									
11.4		0.9	0.89	0.09								

(ii) Activity Ratios

$^{228}Ra/^{226}Ra$		$^{224}Ra/^{228}Ra$[2]		$^{214}Pb/^{222}Rn$[3]		$^{228}Th/^{228}Ra$	
	+/-		+/-		+/-		+/-
0.071	0.006	2.03	0.35	1.02	0.06	0.0099	0.0009
0.069	0.004			0.90	0.08		
0.078	0.005						
0.086	0.005						
0.079	0.005						
0.079	0.005						
0.084	0.006						

[1] ^{228}Ra measurements from $^{228}Ra/^{226}Ra$ and ^{226}Ra measurements taken at the same time of sampling.

[2] ^{224}Ra and ^{228}Ra were not sampled simultaneously. The quoted value is from the average of each separate analysis.

[3] Ratios only quoted when both ^{222}Rn and ^{214}Pb were sampled on the same day.

[4] Value supplied from thorium nuclide analysis performed by D. Ford (pers. Comm.).

3.5.3 Discussion of results

3.5.3.1 Mendip groundwaters

Activities of ^{226}Ra for the Carboniferous Limestone lithology risings were in the range 0.12 - 0.26 pCi per litre and 0.11 - 0.29 pCi per litre for ^{228}Ra. The activity ratio ($^{228}Ra/^{226}Ra$) was constant within experimental error at 0.9. This compares with the average value of 1.35 +/- 0.6 obtained for the Th/U activity ratio in Carboniferous Limestone rock samples obtained from an exploratory borehole drilled close to the King's Spring borehole in Bath (M. Youngman, pers. comm.). Although the values are different the average water radium ratio is still within 1σ of the mean rock activity ratio so it is difficult to make a meaningful comparison between the two values.

Assuming a constant supply rate of ^{226}Ra and ^{228}Ra into solution from the rock matrix, and a constant removal rate (e.g. decay in solution), equation (1.32) shows that ^{226}Ra will reach its maximum value in 8000 years. However the risings are fed by surface streams which sink underground, and also by water percolating through soil and migrating through fracture planes. The time taken for 'swallet' water to reach major risings has been determined using water tracers such as fluorescent dyes, averaging 5 hours per km of water course for swallet to spring distances of 0.7 - 3 km. (Andrews and Wood, 1972). Swallet water contributions to the risings therefore respond rapidly to rainfall. Percolation waters also respond to rainfall, but more

slowly, occurring within 24 hours. Although percolation water accounts for the constant 'base line' flow of rising water which is independent of weather conditions, it is extremely unlikely that the residence time of water is in the region of 8000 years. It is therefore unlikely that constant supply and radioactive decay account for the radium activities in solution and the closeness of the dissolved $^{228}Ra/^{226}Ra$ activity ratio to rock Th/U ratios. Instead, a faster rate of removal by adsorption will limit radium concentrations in solution.

Adsorption can occur either on manganese/ferric oxyhydroxides or by cation exchange on clay minerals. The former minerals are likely to be the most important adsorbers in the highly oxygenated waters of the swallet and rising waters. The content of manganese oxides in carbonate rich sediments may reach >0.5% (Wedepohl, 1978). Given the high selectivity of radium adsorption on manganese 'hydroxides' this may control radium mobility. Unfortunately, no measurements of dissolved Mn^{2+} were made for these waters, but given the highly oxygenated state of the waters it is certain that manganese hydroxides remain precipitated and capable of adsorbing radium nuclides.

3.5.3.2 Local Inferior and Greater Oolite and Midford sand

Water issuing from the Midford sands aquifer has a higher dissolved ^{228}Ra and ^{226}Ra content than the

Mendip Carboniferous Limestone and Old Red Sandstone groundwaters, and superficial local springs issuing from Greater and Inferior Oolite rock formations. The activity of ^{238}U in the aquifer rock has been estimated as 0.46 pCi ^{238}U/g rock. This is in fact lower than the uranium content of Carboniferous Limestone, so higher ^{226}Ra activities in Midford Sand groundwaters cannot arise due to enhanced concentration of natural uranium in the aquifer rock. The residence time of water in the Midford Sands is estimated to be in the order of several months, longer than other shallow local aquifers. It is therefore possible that radium accumulates with time in Midford Sand waters due to recoil production from rock surfaces and/or leaching of the aquifer rock. Given the 1600 year half-life of ^{226}Ra it is unlikely that significant amounts of ^{226}Ra will enter solution by α-recoil, although this is the mechanism whereby ^{222}Rn activities of up to 600 pCi/l accumulates in these waters (Andrews and Wood, 1972).

3.5.3.3 Kings' Springs, Bath

a) ^{226}Ra

The Kings Spring thermal waters have a far greater dissolved ^{222}Rn and ^{226}Ra content than any of the shallow local springs and also springs originating in the possible recharge area for the thermal waters. This is similar to the observations in many geothermal waters (e.g. Zukin et al., 1987). A common feature of

geothermal waters is the high activity of the lower members of the uranium decay series while ^{238}U activities in solution are low. A similar pattern is exhibited in the Kings Spring waters where $^{226}Rn \approx$ 10 pCi/l, $^{222}Rn \approx 2000$ pCi/l and $^{238}U \approx 0.02$ pCi/l. The $^{234}U/^{238}U$ activity ratio ≈ 3, compared to 2.8 for instance in a Triassic sandstone geothermal borehole at Marchwood near Southampton (Andrews, 1983).

The difference between ^{226}Ra and uranium contents obviously exists because of their different geochemical characteristics. As a possible mechanism of radium removal is co-precipitation of alkaline earth sulphates, the state of saturation of the groundwaters with respect to gypsum anhydrite and baryte was calculated with the WATEQF computer program. This showed that the water was saturated with respect to these minerals and therefore co-precipitation could limit radium solubilities.

The source of the ^{226}Ra in solution is uncertain. As already illustrated, the $^{228}Ra/^{226}Ra$ activity ratio of groundwaters (in what could be thermal water aquifer rocks) in the Mendip Hills, and those of the local surfacial waters reflect the Th/U activity ratio of their host aquifer rock. However, the $^{228}Ra/^{226}Ra$ ratio of the thermal waters is between 0.09 and 0.07, which is far lower than the activity ratio of Carboniferous Limestone and Old Red Sandstone rocks in the

Mendip Hills, and also rock cores from boreholes drilled into Carboniferous Limestone near the Kings Spring.

High $^{234}U/^{238}U$ activity ratios in solution have been observed in many geothermal waters (e.g. Cowart and Osmond, 1976), and have been interpreted as a consequence of uranium precipitation in reducing conditions at high temperatures. Deposition of uranium on fracture or pore surfaces provides a concentrated source of ^{226}Ra available for leaching or recoil into solution. Coupled with a suppression of adsorption at high water temperatures (Dymond, et al., 1983) and lack of manganese oxy-hydroxide minerals for adsorption under reducing conditions, this mechanism may explain the high ^{226}Ra activities observed.

If the assumption is made that the ^{226}Ra activity is close to its maximum recoil production rate, i.e. that ^{226}Ra has reached equilibrium with the aquifer rock, then estimates may be made of the extent of water-rock contact in the flow system. Equilibrium between solution and rock for ^{226}Ra is reached in 8000 years. The residence time of Kings Spring water has been estimated between 10,000 years by ^{14}C dating, and 250,000 years by ^{4}He dating; however, the general view is that the water is > 10,000 years old, also confirmed by piezometric studies (Andrews et al., 1982). If radium is retained in solution then the radium residence time must be of a similar magnitude to the groundwater age.

The maximum ^{226}Ra activity of 12 pCi/l may represent the maximum thermal water composition with little mixing with shallow groundwater during ascent.

From equation (1.34):

$$[U]\ S\rho = \frac{4\ A_{226}}{L \times 1000}$$

with A_{226} = 12 pCi/l, L = 5 x 10^{-6} cm, ρ = 2 g/cm^3 and [U] = 0.58 pCi/g from Andrews and Wood (1972), 1000 converts pCi/l to pCi/cm^3. These values give:

$$S = 8280\ cm^2/cm^3$$

This is high compared to 'normal' ranges of S between 1 and 20 cm^2/cm^3 (Andrews, 1983) but S may be high because of flow through "tight" fractures within the Carboniferous Limestone. This treatment does not take into account uranium deposition on the fracture surfaces which is indicated by high $^{234}U/^{238}U$ activity ratios (Andrews et al., 1982). This possibility is discussed in Chapter 4.

Radium Speciation

The data of Langmuir and Riese (1986) can be utilised to determine the distribution of radium complexes within the thermal waters. Assuming a maximum temperature of 80°C at depth (from the SiO_2 geothermometer, Andrews et al., 1982) a temperature correction can be made utilising the Van't Hoff isotherm:

$$\ln \frac{k_2}{k_1} = \frac{\Delta H^o}{R} \left(\frac{1}{T_1} - \frac{1}{T_2} \right) \qquad (3.4)$$

where:

T_1 = the reference (standard state) temperature of 25°C

T_2 = water temperature

ΔH^o = enthalpy of reaction K cal/mole

k_2 = final association constant

k_1 = initial association constant

The temperature corrected constants and the radium speciation in solution given the Kings Spring chemical composition is given in Table 3.20. The temperature corrections are quite small due to the small enthalpy of formations, however the results clearly show that the majority of radium solution is complexed as $RaSO_4^0$ (aq). It is a reasonable assumption that this species is not adsorbed onto aquifer rock minerals as adsorption tends to be a cation displacement process.

The dominance of $RaSO_4^0$(aq) in solution implies that radium will be retained in solution and the primary removal mechanism will be decay in solution rather than adsorption.

b) ^{228}Ra

Although ^{228}Ra is higher than many of the local superficial aquifer groundwaters (with the notable exception of the Midford sands springs) it is far lower in activity than the ^{226}Ra activity of the thermal waters. The large difference between dissolved $^{228}Ra/^{226}Ra$ activities and those of the aquifer rock suggest that ^{228}Ra is not supplied to the thermal waters to the same

Table 3.20 Distribution of radium speciation in Kings Spring, Bath, water and temperature corrections to the association constants of the complexes

1. Assuming a maximum temperature of 80°C the complexes will have the following constants:

	ΔHo Kcal/mole	K_1	K_2
$RaCl^+$	0.5	0.79	0.8
$RaSO_4^0$	1.3	562.3	572.5
$RaHCO_3^+$	6.05	46.77	50.85

2. The following are the distribution coefficients for the 3 main radium species given the quoted groundwater anion concentrations:

Species	Anion concentration (m moles/l)	Distribution coefficient (%)
$RaCl^+$	0.808	0.808
$RaSO_4^0$	10.75	84.01
$RaHCO_3^+$	0.315	2.19
$Ra^{2+}(aq)$	-	13.7

extent as ^{226}Ra. It can be assumed that the waters are greater than 30 years old. Therefore the recoil supply rate must be at a maximum. Using equation (1.34), and assuming that all of the ^{228}Ra is supplied by recoil yields a value of S of $\approx$ 225 cm^2/cm^3 for a water activity of 0.9 pCi/l.

Again, this is very high and can only be explained by movement of water through "tight" fractures in the limestone. Nevertheless the result is far less than the surface area predicted for ^{226}Ra for recoil assuming no uranium deposition. These are 2 possibilities which could explain the difference:

(i) Uranium deposition within the geothermal system.

(ii) Selective leaching of ^{226}Ra.

The first possibility is investigated further in the "discussion" section of this study. Selective leaching appears unlikely as the $^{228}Ra/^{226}Ra$ activity ratios measured for Mendip Risings groundwaters were similar in value to the Carboniferous Limestone rock Th/U ratio. This suggests that leaching of radium nuclides is not selective for ^{226}Ra in this particular aquifer matrix.

c) The ^{228}Ra - ^{228}Th - ^{224}Ra in Kings Spring water

Three measurements of ^{224}Ra were made for the Kings Spring, Bath. The results consistently show a $^{224}Ra/^{228}Ra$ dissolved activity ratio of 2.

This clearly rules out the interpretation of Laul et al, 1985 which assumed that ^{228}Ra supplies ^{228}Th into

solution, this is adsorbed and ^{224}Ra is supplied into solution only as a result of desorption from adsorbed ^{228}Th. Such a mechanism would result in a maximum value of (^{224}Ra) max = (^{228}Ra) max. Clearly this is not the case in these waters, and for $^{224}Ra/^{228}Ra$ activity ratios measured in groundwaters by several other studies (e.g. Krishnaswami et al., 1982; Elsinger et al., 1982). A more practicable mechanism is illustrated in Fig. 3.24. If a purely recoil based model is considered, with irreversible adsorption of ^{228}Th, then only 0.5 of the adsorbed ^{228}Th will recoil ^{224}Ra directly into solution. Combining this with (^{228}Ra)recoil = (^{224}Ra)recoil yields

$$A^{224}Ra = 3/2\ A^{228}Ra \quad \text{hence} \quad {}^{224}Ra/^{228}Ra = 3/2$$

which is not the observed value. If instead all of the ^{224}Ra is desorbed from the adsorbed ^{228}Th then the ratio will reach its observed value of 2. The value of 2 for $^{224}Ra/^{228}Ra$ should only be reached in waters older than 30 years if radium nuclides are not adsorbed by aquifer minerals. Then the amount of ^{224}Ra released by desorption from surface adsorbed ^{228}Th will equal the activity of dissolved ^{228}Ra, since because ^{228}Th is produced by a beta decay and thorium should be difficult to leach under groundwater conditions, ^{228}Ra decay in solution is the only supply of ^{228}Th to the groundwater. Making the observation that ^{224}Ra and ^{228}Ra are chemically equivalent and therefore equally leachable, and since they are in the same decay series and therefore

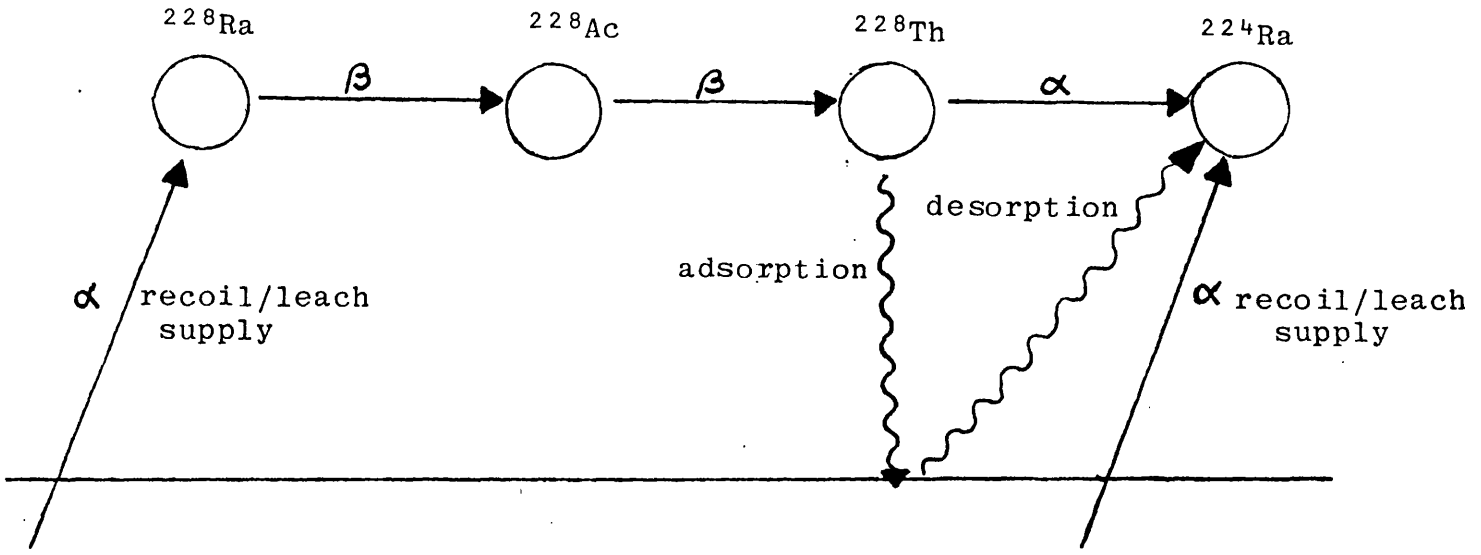

Fig. 3.24 Schematic representation of ^{232}Th series radioelement supply and removal mechanisms up to ^{224}Ra

should be distributed in similar lattice sites in minerals, then the supply rate of both nuclides from rocks into groundwaters by recoil and/or leaching should be equivalent. Therefore:

^{224}Ra supply into solution = desorption from adsorbed ^{228}Th + recoil/solution from the bulk rock

= 2 x ^{228}Ra

Although the results show that radium nuclides are soluble in these waters, the ^{228}Ra - ^{224}Ra results cannot yield further information. However, the ^{228}Th activities in solution may be used to estimate the thorium residence time. From mass balance constraints (assuming that the waters are older than 10 years), a steady state will be established.

$$P_{^{228}Th} = \lambda C + KC$$

where (λC) = dissolved activity of ^{228}Th

K = adsorption constant

C = ^{228}Th concentration, atoms/l

P = production rate of ^{228}Th

The production rate of ^{228}Th must be solely decay of dissolved ^{228}Ra from the considerations mentioned above. Hence:

$$\tau = \frac{1}{\lambda}\left(\frac{A}{P - A}\right) \qquad (3.5)$$

where:

λ = decay constant of ^{228}Th = 6.90×10^{-7}

τ = residence time (1/K) of ^{228}Th

A = dissolved ^{228}Th activity

substituting:

$P = A_{^{228}Ra} = 0.9$ pCi/l

$A = A_{^{228}Th} = 0.0093$ pCi/l

then τ = 15132 minutes $\approx$ 10.5 +/- 1 day

This is considerably longer than the residence times of thorium calculated in other groundwaters. For example, values of τ between 0.2 and 3 minutes were found for Connecticut groundwaters (Krishnaswami et al., 1982), and 23 - 176 minutes in groundwaters from Gujarat, India (Hussain and Krishnaswami, 1982).

Another estimate of ^{228}Th was made by adsorbing thorium on MnO_2 impregnated fibres by passing 127 litres Kings Spring water through 100 g of prepared fibre at a rate of 350 mls water/minute. The fibre was then leached with hot 6M HCl and the leachate diluted to 25 litres. Then a thorium tracer was added and thorium pre-concentrated and counted by alpha spectrometry. The ^{228}Th activity must only be a lower limit on the dissolved thorium content of the water as the thorium extraction efficiency of the fibres was not known. However, using the activity of ^{228}Th so obtained (0.0042 pCi/l) determines a ^{228}Th residence time of 6144 minutes which is only a factor of 2 from the first estimate made above.

Only one other measurement of both ^{228}Ra and ^{228}Th measured from samples taken at the same time has been performed. This was for a groundwater from the Carnmenellis Granite, Cornwall. The dissolved radionuclide contents of the sample are presented in Table 3.21.

Using equation (3.5) the ^{228}Th residence time is calculated as τ = 9.7 days. This is very close to the value obtained for the Kings Spring waters, despite the different aquifer lithologies which will have different ion-exchange properties.

Table 3.21 Dissolved radionuclide content of Wheal Jane Mine groundwaters from the Carnmenellis Granite, Cornwall

Radionuclide Content (pCi/l)*							
^{226}Ra		^{228}Ra		^{232}Th	^{228}Th		
	+/-		+/-			+/-	
101.5	0.6	53.8	2.1	0.018	0.516	0.002	

* samples collected on 26.10.84

Activity Ratios					
$^{228}Ra/^{226}Ra$		$^{228}Th/^{232}Th$		$^{228}Th/^{228}Ra$	
	+/-		+/-		+/-
0.53	0.02	28.3	0.1	0.0096	0.0004

d) ^{214}Pb

The activities of ^{214}Pb in the Kings Spring water were measured several times and show some considerable variation with a range of 1963 - 2768 pCi/l. Although at first this was thought to be poor experimental precision due to the rapid decay of ^{214}Pb between sample collection

and analysis, measurement of ^{222}Rn collected at the same time as ^{214}Pb for one of the samples showed that the ^{214}Pb activities follow the variation in ^{222}Rn activities. Such similarity between ^{214}Pb and ^{222}Rn activities is at odds with $^{214}Pb/^{222}Rn$ measurements of 0.15 - 0.30 in Gujarat groundwaters (Hussain and Krishnaswami 1982). However these results duplicated the results obtained in a previous study of the Kings Spring water (Andrews et al., 1982).

Equilibrium between ^{222}Rn and ^{214}Pb strongly implies that ^{214}Pb is not adsorbed on aquifer minerals. Implicit in this statement is the observation that ^{218}Po (intermediate between ^{222}Rn and ^{214}Pb) must either also be conserved or that its rate of removal must be slower than the amount of time taken to establish secular radioactive equilibrium between ^{222}Rn dissolved in the water and its ^{218}Po daughter. This equilibrium is established within 15 minutes. Also assumed is that supply of ^{218}Po by alpha-recoil from the rock surface into groundwaters, and recoil supply of ^{214}Pb also by alpha-decay, is negligible. This is reasonable because even if the recoil supply of ^{218}Po and ^{214}Pb equalled the activity of ^{226}Ra in solution, assuming radium is conserved, then the combined addition to the ^{214}Pb activity in solution would be 2 x 12 = 24 pCi/l. This is only $\sim$ 1% of the observed ^{214}Pb activity and is less than experimental error on ^{214}Pb measurement.

In this estimation the ^{222}Rn activity is not taken as a measurement of the alpha-recoil rate of ^{218}Po and ^{214}Pb into solution because of the dominant role of radon diffusion through the rock into solution as opposed to alpha-recoil directly from the rock surface into solution.

e) ^{210}Pb

Attempts were made to measure ^{210}Pb activities several times from different sample volumes culminating in a sample volume of 100 litres. No ^{210}Pb could be detected, so based upon the 100 litre sample a limit of detection of 0.1 pCi/l is quoted in Table 3.20. The result cannot be due to a failure to preconcentrate ^{210}Pb because ^{214}Pb was measured from these waters using exactly the same technique.

If the ^{210}Pb activity is assumed to be 0.1 pCi/l then an upper limit can be obtained for the ^{210}Pb residence time. Using equation (3.5) with λ = decay constant of ^{210}Pb, and a minimum and maximum value of ^{222}Rn = 2000 and 3000 pCi/l gives a maximum ^{210}Pb residence time in the range 560 - 840 minutes.

However if ^{214}Pb is conserved then this constrains the lower limit of ^{214}Pb residence times. To achieve equilibrium with ^{222}Rn, the ^{214}Pb residence time must be greater than 5 x $t_{\frac{1}{2}}$ ^{214}Pb = 5 x 26.8 = 134 minutes. The lead residence time from these 2 nuclides is therefore between 134 and 840 minutes.

f) ^{212}Pb

Although only 2 measurements were made of ^{212}Pb activity the range of values (1.81 - 2 pCi/l) is similar to the range of values obtained for ^{224}Ra (1.6 - 2 pCi/l), which indicates that equilibrium has been established between ^{224}Ra - ^{220}Pb - ^{212}Pb. This was unexpected as the equivalent trio of nuclides in the uranium series, ^{226}Ra - ^{222}Rn - ^{214}Pb had activities in the order $^{226}Ra << {}^{222}Rn \simeq {}^{214}Pb$.

The fact that equilibrium exists between the three nuclides has important consequences. It can be infered that:

1. ^{224}Ra must be conserved in these waters.
2. The supply rate of ^{220}Rn must be similar to or the same as that of ^{224}Ra and ^{212}Pb and not greater as expected from ^{226}Ra - ^{222}Rn measurements.
3. For ^{212}Pb to be at equilibrium the nuclide must be either conserved or the lead removal rate must be greater than 5 x $t_{\frac{1}{2}}$ of ^{212}Pb or 3180 minutes.

However, 3) contradicts the earlier calculation of lead residence times in the order of 130 - 840 minutes. It is possible that either the ^{210}Pb or the ^{212}Pb measurements are incorrect. In view of the fact that ^{210}Pb is quoted only as a detection limit implies that detection limit is set too low. If equation (3.5) is

used for ^{210}Pb with P between the ranges of 2000 and 3000 pCi, and the lead residence time set at 3180 minutes as derived above, then A ≈ 0.35 - 0.5 pCi/l for ^{210}Pb. This is above the quoted detection limit, but if a previously published detection limit for ^{210}Pb in these waters quoted as 1 pCi/l is taken into account (Andrews et al., 1983), then a detection limit of 0.5 pCi/l for ^{210}Pb seems a reasonable figure.

The implication is that the residence time of radioactive lead nuclides in these thermal waters is > 3200 minutes or 2.2 days so that both ^{214}Pb and ^{212}Pb are conserved whereas ^{210}Pb is almost completely adsorbed.

CHAPTER FOUR: GENERAL DISCUSSION

4.1 Introduction

The preceeding section showed that the radium nuclide content of groundwaters is related to groundwater chemistry, as well as to the activity of parent nuclides in the aquifer rock and the physical characteristics of the water/rock contact.

Models predicting radium transport in groundwaters have concentrated upon recoil production (Krishnaswami et al., 1982; Davidson and Dickson, 1986). The alternative dissolution or "leaching" supply is poorly understood. Opinion is divided upon its timescale, being regarded as either a slow diagenetic process (e.g. Bloch and Key, 1985; Kraemer and Reid, 1984) or as a fast leaching process (Dickson, 1985). A constant ratio between ^{226}Ra and salinity has been regarded as an indicator of leaching processes (Kraemer and Reid, 1984). However this correlation could also occur as a result of radium adsorption or equilibration with aquifer secondary minerals as will be shown later.

In the following discussion radium supply will be estimated by recoil production due to the insufficient knowledge of leaching processes. The correlation of radium nuclide activities with calcium as well as the observation of decreased $^{228}Ra/^{226}Ra$ activity ratios with increasing ^{226}Ra activity will be discussed.

4.2 Radium recoil supply and groundwater residence times

As indicated by equation (1.34) recoil supply is commonly modelled on the basis of a constant recoil rate into solution, followed by decay in solution. The $^{228}Ra/^{226}Ra$ must also vary with time. The expression for this change is:

$$^{228}Ra/^{226}Ra = \frac{\frac{1}{4}L_8 S_8 \rho_8 [Th] (1-e^{-\lambda_8 t})}{\frac{1}{4}L_6 S_6 \rho_6 [U] (1-e^{-\lambda_6 t})} \qquad (4.1)$$

where L_6, L_8, S_6, S_8, ρ_6, ρ_8 are the physical parameters for U,Th If the assumption is made that the aquifer uranium and thorium distribution is homogeneous, and that the physical parameters are the same for both nuclides, then:

$$^{228}Ra/^{226}Ra = \frac{[Th] (1-e^{-\lambda_8 t})}{[U] (1-e^{-\lambda_6 t})} \qquad (4.2)$$

The variation of this activity ratio with time is illustrated by Fig.4.1. Clearly, very high activity ratios may be generated by waters with very low residence times. Such ratios have not been observed during this study. However, a value of 25 for $^{224}Ra/^{228}Ra$ has been observed (Davidson and Dickson, 1986) which may be the result of recoil production in waters of low residence time.

Adsorption of radium from solution onto aquifer surfaces greatly increases the rate at which radium equilibrium is reached. The adsorption process may be modelled as irreversible first order (assumed by Krishnaswami et al., 1982). The rate of change of radium with time is given by:

Fig. 4.1 **Radium Activity Ratio Variation with Time**

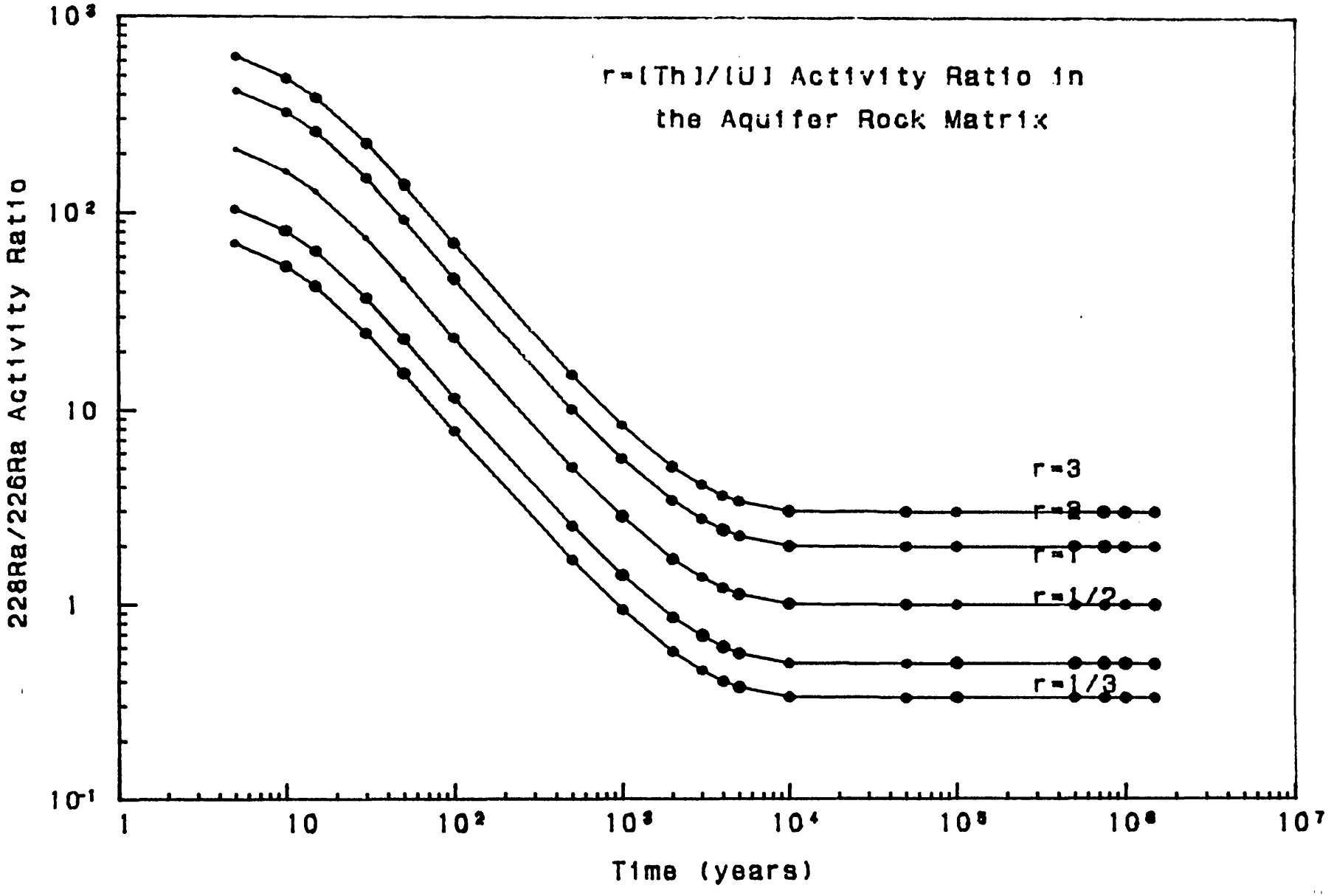

$$\frac{d(Ra)}{dt} = C - \lambda(Ra) - k(Ra) \qquad (4.3)$$

where k = 1st order removal rate, years $^{-1}$

(Ra) = Radium nuclide concentration, atoms ℓ^{-1}

C = Recoil production rate, atoms $yr^{-1}\ell^{-1}$

with N=0 at t=0, the solution of this equation is:

$$\lambda(Ra) = \frac{\lambda C}{(\lambda+k)} (1-e^{-(k+\lambda)t})$$

with rapid adsorption $k \gg \lambda$ hence

$$A = \lambda(Ra) = \frac{\lambda C}{k} (1-e^{-(\lambda+k)t}) \qquad (4.4)$$

Comparison with equation (1.32) shows that a smaller amount of radium will remain in solution than the case when no adsorption occurs. The difficulty in estimating the recoil rate C, makes the determination of k very difficult.

Nevertheless, estimates of the recoil supply rate may be made using equation (1.34). For instance a uranium content of 1 pCi/g rock, with $L = 5\times10^{-6}$, $\rho = 2.5$ g/cm^3, determines a recoil rate of

$$C = \frac{0.0125}{4} S = 0.003125\ S$$

The value of S for fracture flow systems may easily be determined as illustrated in Figure 4.2, all that is required is an estimate of the fracture openings. The value of S for various fracture sizes are listed in Table 4.1. Also calculated are the recoil rates for

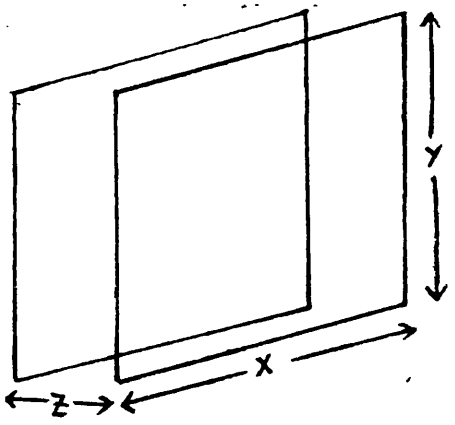

Fracture flow can be envisaged as flow between 2 parallel plates of dimension xy.

Total surface area = 2xy
Volume between the plates
$v = xyz$

Surface area/volume =

$$S = \frac{2xy}{xyz} = \frac{2}{z}$$

Fig. 4.2 Calculation of surface area/volume ratio for fracture flow.

Table 4.1 Surface area/volume ratios and recoil rates for various fracture openings

Fracture width µm	S cm^2/cm^3	Supply rate atoms/ℓ/min
1	20,000	65
5	4,000	13
10	2,000	6.5
50	400	1.3
100	200	0.65

these surface areas given the paramters above.

Without estimates of fracture diameters the only means of determining recoil production rate is to assume that the activity of ^{222}Rn in solution represents the production rate for waters with residence time greater than 21 days. Despite the dangers inherent in making this assumption (Rama and Moore, 1984) the ^{222}Rn activity of Stripa minewaters was used as an estimate of recoil production rate of ^{226}Ra. The radium residence time is then given by equation (3.5), with

τ_R = radium residence time (minutes)

τ_λ = mean life of $^{226}Ra = 1/\lambda_{226}$

R = activity of ^{226}Ra/activity of ^{222}Rn

Calculated residence times for Stripa minewaters are presented in Table 4.2

Table 4.2 Residence times of ^{226}Ra in Stripa minewaters

Borehole	^{226}Ra pCi/ℓ	^{222}Rn* pCi/ℓ	Residence time (d)
M3	4.5	1.06	3.6
E1	4.0	0.042	80.
V1	138.	0.264	441.
V2/1	80.6	0.201	338.
V2/2	87.	0.573	128.
V2/3	81.	0.627	109.
V2/4	131.	0.421	262.
V2/5	18.4	0.531	29.

* ^{222}Rn activities are from samples taken between 18.2.85 and 21.2.85 except for V2/4 borehole, when the sample was taken on 10.4.86.

As the calculated residence times will be underestimated because the ^{222}Rn activity is an over-estimate of recoil supply rate, the residence times may be the lower limit on radium residence times, perhaps by an order of magnitude (Rama and Moore, 1984). Nevertheless, the residence times range from 3 days in M3 borehole, to 441 days in V1 borehole which is one of the deepest boreholes. These values are far higher than values obtained in surface streams and shallow groundwaters from a variety of aquifer lithologies in Connecticut (Krishnaswami et al., 1982).

4.3 Variation of radium contents of groundwaters with water chemistry

4.3.1 Introduction

The model presented above cannot explain the relationship between radium activities and calcium concentrations in groundwaters, as demonstrated by the Molasse Basin, Stripa granite and Algerian Continental Intercalaire aquifers. Many studies have indicated correlation between ^{226}Ra and groundwater salinity but in this study it is noticeable that the correlation is distinctly more noticeable for ^{226}Ra and calcium than ^{226}Ra against ionic strength which should be a measure of salinity (c.f. Molasse Basin results). There are two possible explanations for this behaviour:

(i) Calcium may be a chemical homologue of radium during aquifer rock matrix weathering; the correlation shows that both are released by rock leaching.

(ii) Calcium and radium undergo competitive cation exchange processes with clay or other ion exchange mineral constituents of the aquifer rock matrix. High calcium concentrations will prevent adsorption of radium and lead to high radium activities.

The former hypothesis is unlikely as in many of these waters sampled, WATEQF calculations show calcium to be controlled by equilibrium with secondary minerals such as calcite, gypsum and dolomite. Calcium content is under these circumstances not controlled by its production rate from aquifer weathering processes, but by the solubility of secondary minerals, which should vary with solution ionic strength. Also, the calcium may come not from aquifer rock weathering of major minerals, but from dissolution of other minerals such as dolomite and gypsum (for Pennant Sandstone and Algerian aquifers respectively). It is unlikely that radium will be supplied from these minerals due to their low uranium content.

4.3.2 Radium control by competitive cation exchange onto adsorption sites

The second hypothesis is tenable because clay minerals are a common secondary mineral in crystalline bedrock as a consequence of chemical weathering, or a minor constituent of sedimentary rocks, especially sandstones and shales. Tanner (1964) suggested that the cations associated with high ionic strength brines competed with radium for ion exchange sites. Langmuir and Melchior (1985)

have also quoted Ra-Ca cation exchange as a process affecting radium nuclide activities.

Equilibrium cation exchange can be modelled with the following relationship:

$$Ra^{2+}(aq) + CaX(s) \rightleftharpoons RaX(s) + Ca^{2+}(aq)$$

where $Ra^{2+}(aq)$, $Ca^{2+}(aq)$ are aqueous concentrations of radium and calcium respectively. RaX and CaX are the concentration of ion exchange material with radium and calcium adsorbed, respectively.
The rate of change of radium with respect to the exchange process is

$$\frac{d(Ra^{2+})}{dt} = k_1 (Ra^{2+}) [CaX] - k_2 (Ca^{2+}) [RaX] \qquad (4.5)$$

where k_1 = forward rate constant and k_2 = reverse reaction constant,
at equilibrium when a steady state applies,

$$K_E = \frac{k_1}{k_2} = \frac{(Ca^{2+}) [RaX]}{(Ra^{2+}) [CaX]} \qquad (4.6)$$

where K_E = equilibrium constant.

The concentration of adsorbed radium and calcium are difficult to determine , however as both are solid phases, for simplicity the activity (concentration) in the solid phase can be taken as 1.

$$\text{then} \quad K = \frac{k_1}{k_2} = \frac{(Ca^{2+})}{(Ra^{2+})} \qquad (4.7)$$

However this assumption is of doubtful validity and equation (1.47) should be used to describe equilibrium exchange.

4.3.3 Radium control by equilibration with secondary minerals

Although the relationship between calcium and radium can be modelled as competitive cation exchange with clay minerals, it may also be the result of precipitation with secondary minerals such as calcite and barite. The process may be modelled by the exchange reaction:

$$Ra^{2+}(aq) + MX(s) \rightleftharpoons M^{2+}(aq) + RaX(s)$$

where M = metal cation in the host mineral; X = anion in the host mineral.

Radium should be most easily substituted into the lattices of minerals containing calcium and barium due to the chemical similarity of Ra^{2+} to Ba^{2+} and Ca^{2+}. The equilibrium constant describing this process is given by:

$$K = D\, N_{RaX} \qquad (4.8)$$

where D is the ratio M^{2+} / Ra^{2+} as described in Section 1.6.2.3.

It has been shown that the minerals calcite and gypsum are saturated in many of the groundwaters in this study, which is a prerequisite for the exchange process. The value of the equilibrium constant, K, together with the calculated value of D was used to calculate N_{RaX} for the Molasse Basin groundwater samples (Table 4.3). Unfortunately it is not possible to test the validity of the exchange reaction as N_{RaX} can only be determined if fracture solids in intimate contact with aquifer water can be analysed.

Table 4.3 Calculated ^{226}Ra activities in calcite and aragonite precipitated by Molasse Basin groundwaters

Site	Formation*	Secondary Mineral: Calcite		Secondary Mineral: Aragonite	
		N_{RaCO_3} (molefraction) $x10^{-11}$	Activity** pCi/g $CaCO_3$	N_{RaCO_3} (molefraction) $x10^{-11}$	Activity** pCi/g $CaCO_3$
Munderfing	H	0.88	1.99	1.	2.26
Steinerkirchen 1	H	0.66	1.5	0.78	1.8
Puchkirchen Ost 1	H	0.98	2.2	-	-
Schwanenstadt 4	H	1.0	2.26	1.1	2.5
Gundersdorf H1	UP	1.7	3.8	1.2	2.7
Maierdorf H1	UP	1.7	3.8	2.	4.5
Desselbraun 2	UP	1.6	3.6	1.9	4.3
Friedburg 2	UP	1.6	3.6	1.9	4.3
Purchkirchen 20	UP	6.	13.6	7.	15.8
B.H. Para	UP	1.3	2.9	1.5	3.4
Purchkirchen 27	UP	1.3	2.9	1.5	3.4
Schwanenstadt 17	UP	1.2	2.7	1.5	3.4
Eberstalsell H1	UP	2.0	4.5	2.	4.5
Eberstalsell H2	UP	1.7	3.8	2.	4.5
Eberstalsell H5	UP	2.0	4.5	2.5	5.7
Hocheck 2	LP	1.3	2.9	1.5	3.4
Pfaffenstadt 3	LP	1.5	3.4	1.7	3.8
Steinhaus 1	UE	1.4	3.2	1.7	3.8
Kemating 5	UE	3.9	8.8	4.5	10.2
Maria Schmollen	UE	2.6	5.9	3.	6.8
Kohleck 2	UE	2.9	6.6	3.5	7.9
Kohleck 6	UE	-	-	-	-
Voitsdorf 11	UE	2.5	5.7	2.9	6.6
Voitsdorf 10	UE	8.9	20.1	10.	26.6

Cont'd./....

Table 4.3 continued...

Site	Formation*	Secondary Mineral: Calcite N_{RaCO_3} (molefraction) $x10^{-11}$	Calcite Activity** pCi/g $CaCO_3$	Aragonite N_{RaCO_3} (molefraction) $x10^{-11}$	Aragonite Activity** pCi/g $CaCO_3$
Ouberstall 6	C	1.5	3.4	0.18	0.41
Trattnach 11	C	1.4	3.2	1.7	3.8
Voitsdorf 15	C	2.7	6.1	3.	6.8
Voitsdorf 30	C	2.	4.5	2.6	5.9
Voitsdorf 2	C	2.	4.5	2.5	5.7
Voitsdorf 13	C	-	-	-	-

* Formations labelled according to Table

** Activity calculated with the formula: $pCi/g\ CaCO_3 = \frac{N_{RaCO_3}}{MW_{CaCO_3}} .226.10^{12}$

The theoretical basis of equation (4.8) is subject to doubt. As presented, the equation is based upon the formation of a solid solution of RaX-MX. For equilibration to be established between solid and aqueous phases there must be diffusion from the solid to the aqueous phase. This is problematic in view of the slow rate of ionic diffusion through a crystal lattice. If both radium nuclides are at or close to equilibrium as indicated by the value of the $^{228}Ra/^{226}Ra$ activity ratio then continuous re-equilibration must take place at a very fast rate. Otherwise, given the half-life of ^{228}Ra (5.8 years) then ^{228}Ra at least will decay in the solid phase, so disrupting the chemical equilibrium.

A more appropriate reaction for incorporation of radium in secondary minerals may be precipitation of a mixed mineral-radium solid, utilising "stoichiometric saturation" (Thorstenson and Plummer, 1977). The concept of stoichiometric saturation implies that the solid phase reacts with the fluid as if the solid has a fixed composition. For example, the co-precipitation of radium with calcite may be modelled by:

$$X\ Ra^{2+}(aq) + (1-X)Ca^{2+}(aq) + CO_3^{2-}(aq) \rightleftharpoons Ra_XCa_{(1-X)}CO_3\ (s)$$

where X = mole fraction of $RaCO_3$ in the solid phase.
The equilibrium constant may then be expressed as:

$$\log K = X\log(Ra^{2+}) + (1-X)\log(Ca^{2+}) + \log(CO_3^{2-}) \quad (4.9)$$

where K = equilibrium constant,

Whereas K is an equilibrium constant but not a thermodynamic equilibrium constant such as K_s in equation (4.6). The advantage of stoichiometric saturation as opposed to thermodynamic equilibrium is that the solid is treated as a compound with a fixed composition. Hence the solid does not need to be modelled as a solid solution, and its activity is 1. Stoichiometric saturation only occurs with freshly precipitated solids. With increasing age, the solid undergoes slow dissolution followed by recrystallisation, re-establishing the conditions required for thermodynamic equilibrium. However for the present purposes this equilibration process is assumed to be slow with respect to decay of radium radionuclides which are contained within the solid phase.

The application of stoichiometric saturation has been illustrated for bromide partition between halite and brines in many waters (Stoessell and Carpenter, 1986). The study utilised many experimental results for both stoichiometric saturation and thermodynamic equilibrium and enabled the position of final thermodynamic equilibium to be calculated from initial measurements of stoichiometric saturation. Unfortunately there is no data of any kind for thermodynamic equilibrium between radium and secondary minerals, let alone stiochiometric saturation. Such studies would at least enable the relative importance of co-precipitation in controlling radium activities to be established.

4.4 Effect of speciation on radium activities

Speciation studies have shown that the dominant radium species in solution are Ra^{2+}, $RaHCO^{2+}$ and $RaSO_4^0(aq)$. That these are predominant was expected simply by observing the trends in complex formation within group 2 (alkaline earth) metals. Calcium for instance, exists predominantly as sulphate, bicarbonate complexes and as the hydrated ion in solution.

Despite a high degree of complex formation in Pennant Sandstone and Algerian Continental Intercalaire groundwaters (up to 60% and over 70% sulphate complex formation respectively) the activities of radium nuclides in solution were low. This contrasts with high ^{226}Ra activities coupled with 84% $RaSO_4^0(aq)$ complex formation for Kings Spring geothermal water.

Numerous authors have indicated that complex formation should hinder removal processes such as adsorption or co-precipitation and thereby maintain high radium activities in solution (eg. Benes, 1983; Bloch and Key, 1981). Although increasing sulphate complex formations was observed with increasing ^{226}Ra content for Stripa groundwaters this could simply be a result of the increase in sulphate content with increasing ionic strength. There appears to be no relationship between complex formation and groundwater activity for Molasse Basin groundwaters.

These observations suggest that either complex formation has a minimal effect on the amount of radium retained in solution, or that the thermodynamic data utilised for

complex formation calculation is a poor approximation to the actual thermodynamic description. The latter is tenable because the formation constants were estimated using an extrapolation of the log k (formation constant) values of other group II elements rather than experimentally determined values. Also the extrapolations were based upon the trend from only 3 points in many instances.

Clearly experimental work is required to produce accurate values for radium complex formation constants. Once these values have been accurately obtained it is possible to combine adsorption and complex formation to give a complete description of the chemical behaviour of radium. Such an approach has been adopted successfully for lead in groundwaters (Hem, 1976). Taking the same approach:

$$\Sigma Ra = Ra \text{ adsorbed} + Ra \text{ (solution)} \qquad (4.10)$$

For the adsorbed state, assuming a single adsorbant, the cation exchange capacity (CEC) of the adsorbant is given by:

$$CEC = 2\{Ra\}ad + 2\{Ca\}ads + \{Na\}ads + \text{all other adsorbed cations}$$

where { } represent moles of cation on exchange site, per litre water (4.11)

But, the adsorbants are subject to competitive cation exchange adsorption, for instance, consider Ca^{2+} - Ra^{2+}:

$$k_E = \frac{\{Ra\}(Ca^{2+})}{\{Ca\}(Ra^{2+})} \qquad (4.12)$$

where k_E = competitive cation exchange constant for Ra^{2+} - Ca^{2+} pair

( ) = concentrations of ions in solution (moles/ℓ)

Combining the equations to solve for {Ra}:

$$\{Ra\} = \frac{(CEC - \Sigma \text{ sorbed ions})}{2\left(1 + \dfrac{(Ca^{2+})}{k_E\ (Ra^{2+})}\right)} \qquad (4.13)$$

The value of (Ra^{2+}) must be obtained from equation (1.39) which takes into account formation of radium complexes. This approach has been suggested by Harloff and Lanau (1984), although they neglected complex formation and assumed values for CEC's and cation exchange constants. It is relatively easy to incorporate a production term and a decay term into the approach outlined above, although the lack of any values for competitive cation exchange constants with radium make this a model unworkable for the near future.

4.5 Enhancement of ^{226}Ra relative to ^{228}Ra

Examination of the $^{228}Ra/^{226}Ra$ activity ratios occuring when high dissolved radium activities are observed shows that the ratios tend to be low; i.e. high ^{226}Ra activities are measured relative to ^{228}Ra. This was observed for Kings Spring, Bath geothermal waters and Stripa crystalline rock groundwaters. Low radium activity ratios are also observed for Molasse Basin groundwaters.

Previous studies (King et al., 1982 and Asikainen, 1981) have also shown that increasing ^{226}Ra activities are paralleled by decreasing $^{228}Ra/^{226}Ra$ activity ratios.

As with this study, both previous studies covered a wide range of aquifer lithologies. The study by Asikainen (1981) covered granitic, amphibolite, gneiss and schist aquifer lithologies, whilst that by King et al (1982), covered granitic, carbonate and sandstone aquifer lithologies. Clearly the decrease of the $^{228}Ra/^{226}Ra$ activity ratio is independent of aquifer lithology.

There are three possible causes for this anomalous behaviour:

(1) Uranium is not homogenously distributed within the rock matrix and may be concentrated at or close to the water rock interface, possibly due to formation of secondary uranium minerals.

(2) Deposition of uranium may have occurred as the water chemistry changes from oxidising to reducing. Enhanced recoil production of radium may then occur-

(3) Recoil damage of the mineral lattice may be more extensive for ^{226}Ra than ^{228}Ra due to the three alpha decays upon reaching ^{226}Ra from its parent ^{238}U, as opposed to only one alpha decay from ^{232}Th to ^{228}Ra. Subsequent leaching or recoil of ^{226}Ra will then be enhanced over ^{228}Ra.

4.5.1 Heterogeneous uranium and thorium distribution in aquifer rocks

The first explanation is possible for Stripa groundwaters. Uranium in the granite is concentrated as uraninite within open microfractures in feldspars (Nelson et al, 1979). It is readily accessible to aqueous leaching.

Whereas the distribution of thorium has not been ascertained, it is unlikely to be redistributed onto fracture surfaces in the same way as for uranium. Therefore ^{226}Ra may be readily leached from uraninite or subject to enhanced alpha recoil production, whereas ^{228}Ra may come from a more homogeneous thorium distribution with a lesser weathering or recoil rate of supply.

For example, consider the Stripa granite average uranium content of 44.6 µg/g U and 50.5 µg/g Th. Assuming recoil production and using equation (1.34) with $\rho = 2.6$, $L = 5 \times 10^{-6}$ cm, $[Th] = 5.6$ pCi/g and $[U] = 14.7$ pCi/g, then the activities in solution are given by:

$$A_{226} = 0.25 \times 5 \times 10^{-6} \times 2.6 \times 14.7 \times 1000 \times S$$

$$= 0.0478\ S \text{ pCi/}\ell \text{ of } ^{226}Ra$$

with $A_{226} = 50$ pCi/litre

$S = 1046\ cm^2/cm^3$

similarly for ^{228}Ra, $[Th] = 5.6$ pCi/g. For the same value of S, $A_{22} = 19$ pCi/ℓ

But, the ratio $^{228}Ra/^{226}Ra = 19/50 = 0.38$, which although in accordance with the aquifer rock Th / U ratio, is not in accordance with the groundwater value of $^{228}Ra/^{226}Ra \simeq 0.2$. If the cause is uranium enrichment on fracture surfaces, then this can only mean a change in the value of [U]. For a constant [Th], the value of [U] required to generate the observed discrepancy is:

$$\frac{0.38}{0.2} \times 14.7 = 27.9 \text{ pCi/gram or } 84.5 \mu g \text{ U/g rock.}$$

This is almost twice the bulk rock uranium content. To generate the required ^{226}Ra enhancement, the uranium con-

tent of fracture surfaces needs to be enhanced by only a factor of 2 over the bulk rock activity.

4.5.2 Deposition of uranium on rock surfaces

Deposition of uranium from groundwaters upon entering reducing conditions should result in a layer of high uranium activity at the water-rock interface. Recoil ejection of ^{226}Ra from this layer should result in high ^{226}Ra activities in solution and low $^{228}Ra/^{226}Ra$ activity ratios.

The Stripa groundwaters show evidence for uranium deposition due to very high $^{234}U/^{238}U$ activity ratios which coincide with high ^{222}Rn activities ($^{234}U/^{238}U$ = 11 and $^{222}Rn = 10^6$ pCi/ℓ for the M3 borehole samples where uranium deposition is thought to be most active (Nordstrom et al, 1985)). However ^{226}Ra activities do not correlate with either ^{222}Rn activities or the $^{234}U/^{238}U$ activity ratios. Also, the $^{228}Ra/^{226}Ra$ activity ratios do not correlate with ^{226}Ra activities. As enhanced recoil becomes increasingly important for ^{226}Ra the $^{228}Ra/^{226}Ra$ activity should decrease as ^{228}Ra will remain constant. Given the above discussion it is not possible to distinguish whether recoil enhancement from precipitated uranium or concentration of uranium secondary minerals on fracture surfaces is responsible for decreased $^{228}Ra/^{226}Ra$ ratios.

The Kings Spring borehole, Bath, provides a more convincing case for recoil enhancement. The average Th/U

activity ratio for carboniferous limestone rock from a borehole drilled close to the King's Spring borehole was 1.35 +/- 0.6 (1σ) for 15 samples at different depth intervals (M. Youngman, pers. comm.). This compares with $^{228}Ra/^{226}Ra$ = 0.08 for the King's Spring waters. Also, the ^{222}Rn activity of ≈ 2350 pCi/ℓ is far higher than for other groundwaters in the locality (Andrews and Wood, 1972). The low ^{238}U content of 0.038 μg/g and the $^{234}U/^{238}U$ average of 3.24 +/- 0.26 between 15/6/84 and 4/2/86 (D. Ford, pers. comm.) indicate that uranium deposition is occurring within the geothermal groundwater circulation system. With S = 225 cm^2/cm^3 from ^{228}Ra measurements (assuming that ^{228}Ra is generated by α-recoil from the rock surface):-

$$12 \text{ pCi}/\ell = 0.25 \times 5 \times 10^{-6} \times 2 \times 1000 \times 225 \times [U]$$

from which $[U]$ = 21.3 pCi/g rock

= 64.5 μg U/g rock

Although this is low compared to the uranium content of a layer of pure UO_2 deposited upon the rock surface, the calculation assumes that recoils occur from a layer one recoil length thick. Any precipitated uranium may form a layer very much thinner than this but with a higher specific activity, and still produce the observed ^{226}Ra activity.

4.5.3 Redistribution of uranium series nuclides due to successive recoils

The 3 alpha decays preceding ^{226}Ra decay mean that ^{226}Ra may be in a more damaged crystalline mineral lattice than

^{228}Ra which ~~is~~ preceeded by only 1 alpha decay, resulting in enhanced $^{228}Ra/^{226}Ra$ ratios. It may also result in redistribution of the uranium series radioelements resulting in enhanced recoil production of ^{226}Ra relative to ^{228}Ra.

The second case may be modelled if it is assumed that:
(i) A recoil rate of surplus U, is constant throughout the uranium series nuclides.

(ii) Leaching or rock dissolution processes are negligible in importance compared to recoil supply.

(iii) Thorium nuclides are essentially immobile in natural waters.

(iv) Decay in solution is the only mechanism removing radium from solution.

Given these assumptions it is possible to derive the rate of change of ^{226}Ra with time. This is outlined in Appendix 4, resulting in the expression:

$$A_{226} = \frac{\mu f}{2.22}\left[(1-1.02e^{-\lambda_3 t}) + (1-e^{-\lambda_4 t}) + \frac{(1-e^{-\lambda_6 t})}{f}\right] \quad (4.14)$$

where subcripts 4, 3, 6 refer to ^{234}U, ^{230}Th and ^{226}Ra respectively, μ = recoil supply rate of U series nuclides into solution, atoms/min/litre; f = fraction of ^{226}Ra released from a thin layer of adsorbed ^{230}Th, and 2.22 = n° dpm/pCi.

The final value of ^{226}Ra very much depends upon the fraction of adsorbed ^{230}Th which releases radium into solution. For total release (f=1) and a total residence time greater than 1.25 m years, $A_{226} = 3\mu/222$. Comparison with equation (1.34) shows that $\mu = \frac{1}{4}LS\rho[U]$, in other words this model allows for three times as much ^{226}Ra to reach solution than a single recoil mechanism. For residence times up to 10,000 years the contribution from adsorbed ^{230}Th is negligible and the build up in activity is described by equation (1.34). The $^{228}Ra/^{226}Ra$ activity ratio will now reach a constant value in 1.25 m years. For f = 1

$$^{228}Ra/^{226}Ra = \frac{\mu_8}{3\mu_6} = \frac{1}{3}\frac{[Th]}{[U]} \qquad (4.15)$$

where μ_8 = supply rate of ^{228}Ra

μ_6 = supply rate of ^{226}Ra

The ingrowth of ^{226}Ra in solution and the change in the $^{228}Ra/^{226}Ra$ with time are illustrated in Fig. 4.3.

A recoil based model requires a very long residence time to build up the activity of ^{226}Ra and removal of radium nuclides by adsorption is not taken into account. Following the approach of Krishnaswami et al (1982), the removal process may be modelled as a first order adsorption. The derivation of the combined recoil and adsorption model outlined in Appendix 4, yields the equation

$$A_{226} = \frac{\lambda_6 \mu f}{2.22k}\left[(1-e^{-\lambda_4 t}) + (1-e^{-\lambda_3 t}) + \frac{(1-e^{-kt})}{f}\right] \qquad (4.16)$$

where k = removal rate for radium (yrs^{-1}).

The maximum activity of both radium nuclides will depend upon the radium residence time in the groundwater, given by $\zeta = 1/k$.

High ^{226}Ra activities and low $^{228}Ra/^{226}Ra$ activities will only be observed from this mechanism when groundwaters have very long residence times. The only groundwaters with the required residence times are those of the Molasse Basin groundwaters (as these are formation waters). A previous study concerning the Upper Molasse Basin aquifers (Andrews et al., 1985) has calculated groundwater residence times utlising $^{3}He/^{4}He$ ratios. The deepest aquifers within Miocene aged sediments were sampled from the Innviertel Formation. If the "Group 3" waters, the most evolved Innviertel waters, are close to the Hall and Upper Puchkirchen formation in groundwater evolution and residence times, then an order of magnitude estimate of the groundwater age is 70,000 years. There was also measurement of 2 waters from Oligocene aged sediments. These may be representative of the Lower Puchkirchen and Cenomanian groundwaters in this study. The groundwater ages were calculated between 210,000 to 772,000 years old.

The deepest and most evolved waters measured by Andrews et al, 1985, were those of the Jurassic Malm. The

Fig 4.3 :Enhanced Recoil 228Ra/226Ra -> Time

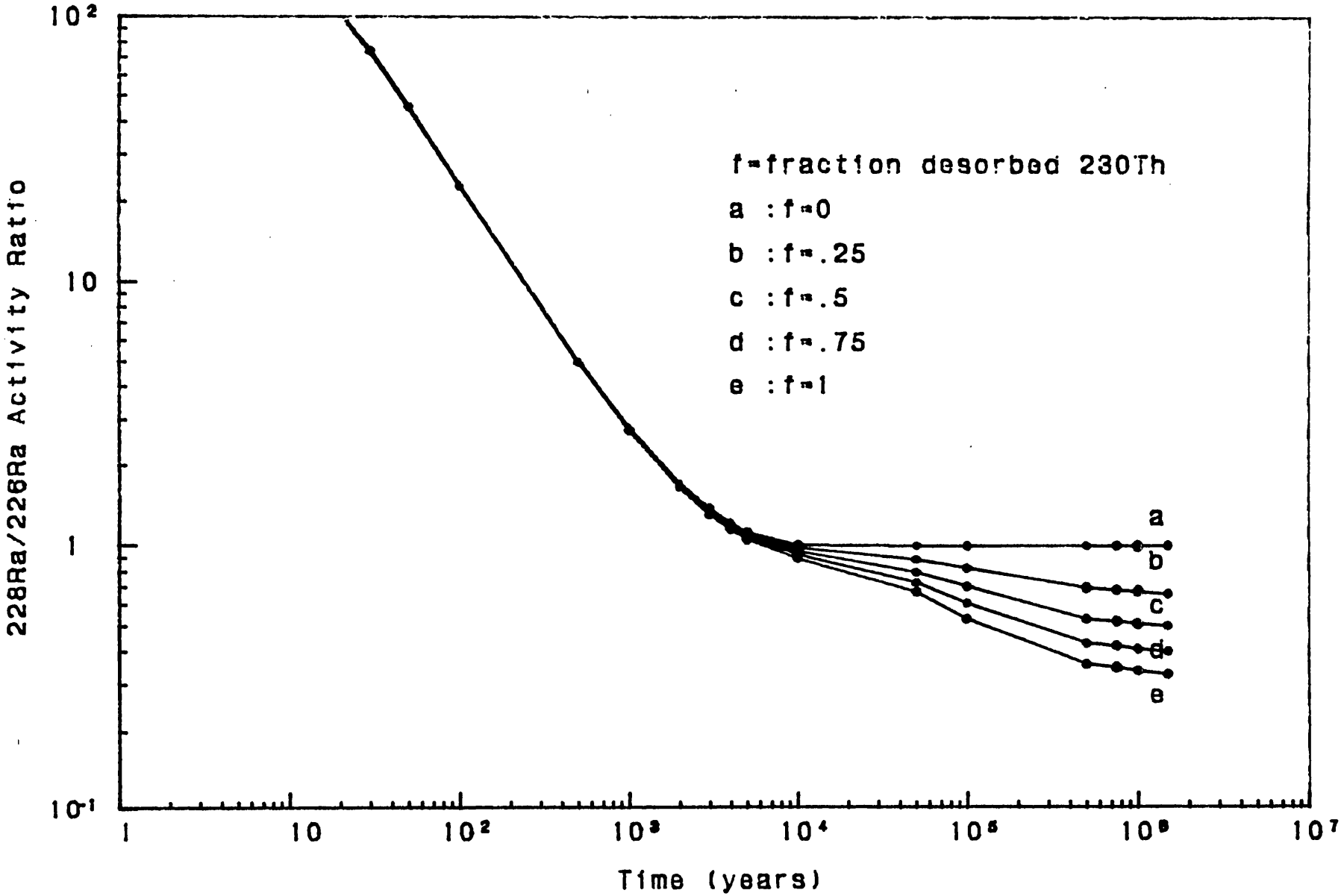

groundwater residence times for the two samples covered the ranges 540 - 650 ka and 1.5 - 1.8 Ma respectively, although ^{3}He diffusion from underlying crystalline rocks may account for the highest age. These ages may be representative of interstitial or formation waters with little mixing of younger meteoric water.

Estimates of groundwater age from the study of Andrews et al (1985), may be very conservative estimates of ages for waters in this study. The ^{226}Ra activities reached only a maximum of 2 pCi/ℓ (for the Malm samples) compared with up to 80 pCi/ℓ for this study. The groundwaters in this study must have far greater residence times if radium content increases with increasing time.

Taking the above values as estimates for the lower limit of water residence time at least allows empirical calculations to be made. Table 4.4 shows calculated $^{228}Ra/^{226}Ra$ values for groundwater residence times discussed above. For groundwater residence times >200,000 years, the range is $\frac{1}{2}[Th]/[U] < {}^{228}Ra/{}^{226}Ra < 1/3[Th]/[U]$, making the assumption that all of the adsorbed ^{230}Th releases ^{226}Ra into solution upon decay. Observed values for $^{228}Ra/^{226}Ra$ are in the range 0.3 - 1. However, the value of $[Th]/[U]$ itself varies considerably, between 1 - 2.4 for Inviertel outcrop samples (Andrews et al., 1985). Taking this range to be representative of other Molasse Basin sediments, the range of $^{228}Ra/^{226}Ra$ by calculation is 0.3 - 0.8. This is close to the observed values and implies that this mechanism can result in the decrease of $^{228}Ra/^{226}Ra$ ratios with increasing ^{226}Ra.

Table 4.4 Variation of $^{228}Ra/^{226}Ra$ activity ratios calculated using equation (A4.13) for selected residence times

Time (years)	$^{228}Ra/^{226}Ra$ (units of [Th]/[U])	
	F* = 1	F = 0.5
10,000	1.11	1.06
70,000	1.65	1.33
200,000	2.26	1.63
600,000	2.81	1.91
700,000	2.86	1.93
800,000	2.90	1.95
1,500,000	3.	2.

*F = fraction of adsorbed ^{230}Th releasing ^{226}Ra into solution upon decay.

CHAPTER FIVE: CONCLUSIONS

The results of this study have shown that the mobility and isotope geochemistry of radium in groundwaters is affected by a number of geochemical parameters. This chapter summarises how each of these parameters were shown to influence the radium mobility in the aquifer systems studied. Also outlined are the conclusions from the estimation of Ra, Th and Pb residence times from disequilibrium studies.

5.1 The $^{228}Ra/^{226}Ra$ Activity Ratio in Groundwaters in Relation to the Th/U Activity Ratio in the Aquifer Rock

The importance of the distribution of U and Th in the rock matrix upon Ra solubility was investigated by means of the $^{228}Ra/^{226}Ra$ activity ratio in groundwaters. The $^{228}Ra/^{226}Ra$ activity ratio in the Pennant Sandstone aquifer was similar to the Th/U activity ratio in the aquifer rock. This suggests that the groundwaters have had similar access to, and interaction with, minerals containing U and Th.

Groundwaters from the Complex Terminal and Continental Intercalaire sandstone aquifers in Algeria and Tunisia however, had $^{228}Ra/^{226}Ra$ activity ratios lower than the Th/U activity ratio in the aquifer rock. The $^{228}Ra/^{226}Ra$ activity ratios were also lower than the Th/U activity ratio for groundwaters from the Molasse Basin, Upper Austria. Both of these aquifers have very long groundwater residence times which could result in the progressive build up of ^{230}Th onto aquifer rock surfaces, resulting

in enhanced recoil supply of ^{226}Ra into solution relative to ^{228}Ra. However enhanced Ra activities in solution may also be geochemically controlled by high solution ionic strengths as will be discussed later.

The $^{228}Ra/^{226}Ra$ activity ratio in groundwaters from the Carboniferous Limestone locations in the Mendip Hills were shown to be similar to the Th/U activity ratio in the limestone. However the $^{228}Ra/^{226}Ra$ activity ratio in the thermal waters of the Kings's Spring, Bath, was shown to be greatly reduced despite originating from the same aquifer lithology. This resulted from the precipitation of dissolved uranium onto aquifer rock surfaces within the geothermal system, resulting in enhanced release of ^{226}Ra into the thermal waters.

Groundwaters from the Stripa Granite also had a much lower $^{228}Ra/^{226}Ra$ activity ratio than the Th/U activity ratio in the aquifer rock. In this case the difference was due to the location of U in microfractures which are readily accessible to groundwater, resulting in enhanced ^{226}Ra recoil/leach supply into solution. Furthermore, Th is contained within the bulk rock matrix and is much less accessible to groundwaters, resulting in lower ^{228}Ra activities in solution. For a groundwater from the Rosemanowes Granite (South West England), the $^{228}Ra/^{226}Ra$ activity ratio was similar in this case to the aquifer rock Th/U activity ratio, indicating that Th and U were similarly distributed within the aquifer rock matrix.

In general, the $^{228}Ra/^{226}Ra$ activity ratio in groundwaters did not always reflect the bulk rock Th/U activity ratio, but reflected the accessibility of U and Th to groundwater interaction. In particular, the $^{228}Ra/^{226}Ra$ activity ratio responded to the redistribution of U and its daughters by geochemical processes such as the precipitation of U in thermal waters. Thorium is not redistributed in this manner due to its low solubility in groundwaters.

5.2 The Effect of Groundwater Residence Time on Radium Activities in Solution

Because of their respective half lives of 1600 yrs and 5.75 years, the dissolved activities of the radium isotopes ^{226}Ra and ^{228}Ra due to recoil processes must reach equilibrium within 8000 years and 30 years respectively. However, groundwater residence times greater than these can indirectly affect radium activities in solution because the geochemical nature of the groundwater will continue to evolve with time.

Groundwaters from the Bath/Bristol sedimentary basin (Carboniferous Limestone, Jurassic Limestones and Shales) and the Pennant Sandstone aquifers were examples of groundwaters with residence times in the range of a few days to a few months. Consequently, the Ra isotopes cannot have reached their maximum activities in solution by recoil or geochemical processes. This was reflected by the very low ^{226}Ra activities in these waters.

High ^{226}Ra activities were found in groundwaters from the Stripa Granite, which are known to have long residence times. Some of the groundwaters may have reached their maximum recoil supplied activity in solution, and the observed relationship between Ra activity and Ca^{2+} concentration may relate to geochemical controls limiting the Ra solubility.

Molasse Basin groundwaters were formation waters of great age. Therefore Ra isotopes must be at their equilibrium activities. Because of this, the observed relationship between ^{226}Ra and ionic strength must be caused by the increasing groundwater salinity with age, consequently increasing Ra solubility.

5.3 Groundwater Chemical Controls on Radium Solubility

The relationship between groundwater chemistry and the solubility of radium was investigated. The distribution of the Ra species Ra^{2+}, $RaSO_4^0$, $RaCl^+$, $RaHCO_3^+$ were calculated for each groundwater.

Speciation calculations for Pennant Sandstone groundwaters indicated that the dominant Ra species in solution was Ra^{2+} with lesser formation of $RaSO_4^0$. Solution activities of ^{226}Ra related to bicarbonate concentrations. Together with groundwater saturation indices (SI) which indicated precipitation of calcite or dolomite, this suggested that Ra was controlled by Co-precipitation with either calcite or dolomite.

Groundwaters from the Algerian/Tunisian sedimentary basin were shown to contain predominantly the $RaSO_4^0$ ion pair, with minor quantities of the Ra^{2+} species. A weak correlation was observed between ^{226}Ra activities and Ca^{2+} in solution. Together with the evidence that Ca was controlled by saturation with respect to calcite and dolomite, this showed that Ra was controlled by co-precipitation with calcite or dolomite.

Speciation calculations for Ra in the Molasse Basin groundwaters showed that Ra was primarily in the form of Ra^{2+}, with minor quantities of $RaHCO_3^+$ and $RaCl^+$. There was a strong correlation with dissolved Ca^{2+}. Calcium concentrations in solution were shown to be controlled by equilibration with the Ca secondary minerals calcite, dolomite and aragonite. This shows that the solubility of Ra was primarily controlled by co-precipitation with secondary carbonate minerals. However, the value of the $^{226}Ra/Ca^{2+}$ ratio varied with aquifer lithology. This can only be explained if a contributory influence on Ra solubility was competitive cation exchange between Ra^{2+} and Ca^2, and the change in ratios corresponded to changes in the cation exchange characteristics of the different aquifer lithologies.

The ^{226}Ra activities in Stripa Granite groundwaters again correlated with dissolved Ca^{2+} concentrations. No relationship was observed between ^{226}Ra and Ba^{2+} despite

the chemical similarity of Ra and Ba. This discrepancy was resolved by the WATEQF speciation program which showed that Ca^{2+} in solution was controlled by the solubility of calcite or aragonite, while Ba secondary minerals were soluble in these waters. Radium solubilities were again controlled by co-precipitation with calcite or aragonite.

These investigations showed that Ra solubilities were controlled by the solubility of carbonate secondary minerals or by cation exchange sorption. The predominant Ra species in solution were Ra^{2+} and $RaSO_4^0$. However, the type of species in solution did not affect the solubility of Ra.

5.4 The Residence Times of Lead Isotopes, ^{224}Ra and ^{228}Th

Investigation of the ^{228}Ra-^{228}Th-^{224}Ra-^{212}Pb and ^{222}Rn-^{214}Pb-^{210}Pb groups made it possible to estimate the residence times of some Ra, Th and Pb isotopes in the King's Spring waters, Bath.

From the ^{228}Ra-^{228}Th-^{224}Ra triad, the ^{224}Ra residence time was found to be >5.2 days. Similarly, the ^{228}Th residence time was found to be 10.5 days. A residence time of 9.7 days was calculated for ^{228}Th in groundwater from the Rosemanowes Granite (wouthwest England), despite the different aquifer lithologies and groundwater chemistry.

The triad ^{222}Rn-^{214}Pb-^{210}Pb established that the lower limit to the ^{214}Pb residence time was 134 minutes. From the ^{224}Ra-^{212}Pb pair it was established that the ^{212}Pb

residence time was 3180 minutes. The activity of ^{210}Pb was so low in these waters that it could not be measured. It was shown that if the ^{210}Pb residence time was similar to that of ^{212}Pb then the activity of ^{210}Pb that would result in solution from decay of its parent ^{222}Rn would be close to the analytical detection limit for ^{210}Pb.

The lead isotope residence times were much greater than those measured in other studies from low temperature, oxidising groundwaters. Clearly the lead isotope residence times depend upon the groundwater chemistry.

5.5 Scope for Further Work

This study highlights a number of unresolved issues which should be investigated in future work in this field. These issues are detailed below:

a) This study showed that the availability of Ra isotopes depended upon the accessibility of groundwaters to U and Th within the aquifer rock. Future work should characterise the mineralogical distribution of U and Th in aquifer rocks as well as the bulk rock concentrations and relate these to the supply rates of natural decay series daughters to groundwaters.

b) Laboratory experiments are required to characterise both the competitive cation exchange between Ra and Ca on mineral sorption sites, and co-precipitation of Ra with Ca secondary minerals. This will facilitate both the identification of these processes in groundwater and subsequent modelling of radium migration.

c) Experimental work is also required to obtain the thermodynamic properties of radium complexes in groundwater. This would allow greater confidence to be placed on speciation calculations, which had to be performed using thermodynamic data extrapolated from the Group II elements.

d) This study showed that Pb isotope residence times are not uniformly low in groundwaters as previously supposed. Further investigations should determine the influence of varied groundwater chemistries upon Pb-isotopes.

APPENDIX 1 RADIOMETRIC COUNTING APPARATUS

This appendix contains descriptions of the nuclear counting equipment used for the measurements detailed in this study. The following instrumentation is described:

A1.1 The NaI γ-Ray Spectrometer

A1.2 The High Purity Intrinsic Ge γ-Ray Spectrometer

A1.3 Low Background Geiger-Muller Counter for β-particle Counting of ^{210}Pb

A1.4 Alpha-particle Scintillation Counting

A1.1 The NaI (Tl) Gamma Spectrometer

a) Principles of Gamma Spectrometry by NaI(Tl) Crystal Scintillation Counting

The high atomic weight of I makes it ideal for stopping γ-rays. Gamma rays interact with NaI resulting in the emission of photons in the range 3300-5000 Å. The light pulse is detected in the photomultiplier tube which converts the photon energy into an electrical pulse. This signal is amplified, then converted into a digital form by an analogue to digital converter (ADC) and the signal processed by a multi-channel analyser.

b) Specifications

The γ-ray spectrometer consisted of a 6" diameter x 4" NaI(Tl) crystal and a 5" diameter photomultiplier operated with a Canberra 814 amplifier. The signal was processed by a Nuclear Data 575 ADC, and analysed by a

micro-MCA multi-channel analyser and interpreted using Nuclear Data "Analyser spectroscopy applications" program software on an Opus P.C. The operating conditions were:

(i) Ortec EHT supply P M tube voltage: 1200V

(ii) Canberra 814 PAD (Pre-amplifier, Amplifier, Discriminator).

Coarse gain	32V
Fine gain	7V
Discriminator	0.16V
Polarity	+ve
Preamplifier	in

(iii) Nuclear Data ADC

Coincidences	off
Aquire	on
Conversion gain	4K full scale
ULD	maximum
LLD	adjusted to eliminate electronic noise
Zero	adjusted to zero energy at Channel 0.

c) Detector Calibration

The calibration was performed using Cs-137 and Cs-60 sources. A typical calibration produced the following characteristics:

Energy range : 0-2.96 MeV over 4K channels

Slope : 0.7401 keV/channel

Energy in channel 0: -2.404 keV

A1.2 The High Purity Intrinsic Ge Gamma Spectrometer

a) Principles of Gamma Spectrometry using an Intrinsic Ge Gamma Spectrometer.

The size of the difference between the valency energy bands and the conducting energy bands in Ge crystals is such that few electrons will be promoted from the valency to the conductance bands at room temperature under normal conditions. This classifies Ge as a semiconductor.

The interactions of γ-rays with Ge crystals results in the promotion of valence electrons into the conductance band, resulting in a conducting electron and a 'hole' in the valency band. An applied electrical field allows the mirgration of electrons and holes to p (positive) and n (negative) junctions. The electrical signal detected may be amplified and then processed in a multi-channel analyser in the same way as the signal generated in a NaI γ-ray detector. Although the Ge crystal must be maintained at $-196^{o}C$ (cooled by liquid N_2) to minimise thermal excitation of electrons into the conductance bands, the small energy difference between valence and conduction bands gives good energy resolution to the Ge crystal γ-ray detector.

The greater atomic weight of I means that more interactions will take place between I and γ-rays than Ge, giving NaI crystal γ-ray detectors a better detection efficiency than Intrinsic Ge γ-ray detectors. However as described above, the Intrinsic Ge γ-ray detector will have better γ-ray resolution.

b) Detector Specifications.

The Intrinsic Ge γ-spectrometer comprises a 57mm x 36mm length high purity single crystal, mounted in a Canberra type 7500 vertical dipstick cryostat (Figure A1.1). The high purity Ge crystal has a co-axial hole in which a p-type Ge contact has been formed, and a surface n-type Ge contact (Figure A1.2). The crystal is mounted with its closed end facing the cryostat window. The detector specifications are as follows:

Ge crystal	: 57mm x 36mm
Active Area Facing Window	: 25cm^2
Depletion Voltage	: 3000V
Bias	: +3500V

Efficiency relative to a 3" by 3" NaI detector : 20% (^{60}Co source)

Detector settings were:

E.H.T. (Canberra 3015) : +3500V

Amplifier gain (Canberra 3100/02) : Coarse 10V

N.D. micro-MCA (16K channels) approx 1.33 keV/channel.

c) Detector Calibration.

Full details of the calibration of the detector are outlined in Chapter 2.

A1.3 The Low Background Geiger-Müller Counting

Principles of Low Background Geiger-Müller Counting.

A Geiger-Müller (GM) counter may be described as a gas conization detector. An electrically conducting cylinder encloses an inert gas and acts as an outer electrode (Figure A1.3). A thin wire is located in the centre of

the cylinder but is electrically insulated from the cylinder surface. This wire acts as an inner electrode. A thin window at one end of the tube allows ionizing radiations into the tube. The interaction of radiation with the gas in the tube results in the formation of charged particles which are swept onto the electrodes by an electrical field applied between the electrodes.

The intense electrical field that is applied for Geiger Müller counting means that electrons moving towards the positive electrodes will collide with gas molecules with sufficient energy to induce more ions to form. This multiplication effect causes the eventual "pulse" of charge reaching the electrodes to be easily detected.

Unfortunately the multiplication effect in GM tubes cannot differentiate between different types of radiation interacting with the detector gas. Highly penetrating background radiation (such as cosmic rays) can produce spurious pulses not associated with the source being counted. For this reason, the type of detector used for β-particle counting was one with a low background and an anti-coincidence guard counter. The guard counter surrounded the primary detector. Cosmic rays will penetrate and interact with both detectors. Therefore the output from both detectors were processed so that pulses from the primary detector were only accepted when not accompanied by a co-incident pulse in the outer detector. The detector used in this study is illustrated by Figure A1.4.

A1.4 Alpha Particle Scintillation Counting Applied to the Measurement of ^{222}Rn

The scintillator used for the alpha counting of ^{222}Rn was zinc sulphide activated with silver, ZnS(Ag). This scintillator was available as a crystalline powder which was coated onto the inside of 100 cm^3 scintillation flasks. After transferring ^{222}Rn from the adsorbent into scintillation flasks, the flasks were stored for a minimum of three hours to enable radioactive equilibrium between ^{222}Rn and its decay series daughters down to ^{214}Po to be reached (activities of ingrowing α-emitting daughters beyond ^{214}Po will be negligible due to their long half lives).

The ^{222}Rn loaded flasks were placed on a 3" diameter photomultiplier (EMI type 9758K/B) for α-counting using about 1 cm^3 of silicone oil as a coupling fluid. The duration of counting depended upon the activity of the sample and the counting statistics required. Generally 10000 counts were accumulated to limit the 95% probable error to +/- 2% error on the sample.

The method was calibrated by outgassing ^{222}Rn from 250 ml 0.1 M HCl solutions containing 1000 pCi of ^{226}Ra. These solutions had been stored for a minimum of 21 days to allow radioactive equilibrium to be reached between ^{226}Ra and ^{222}Rn.

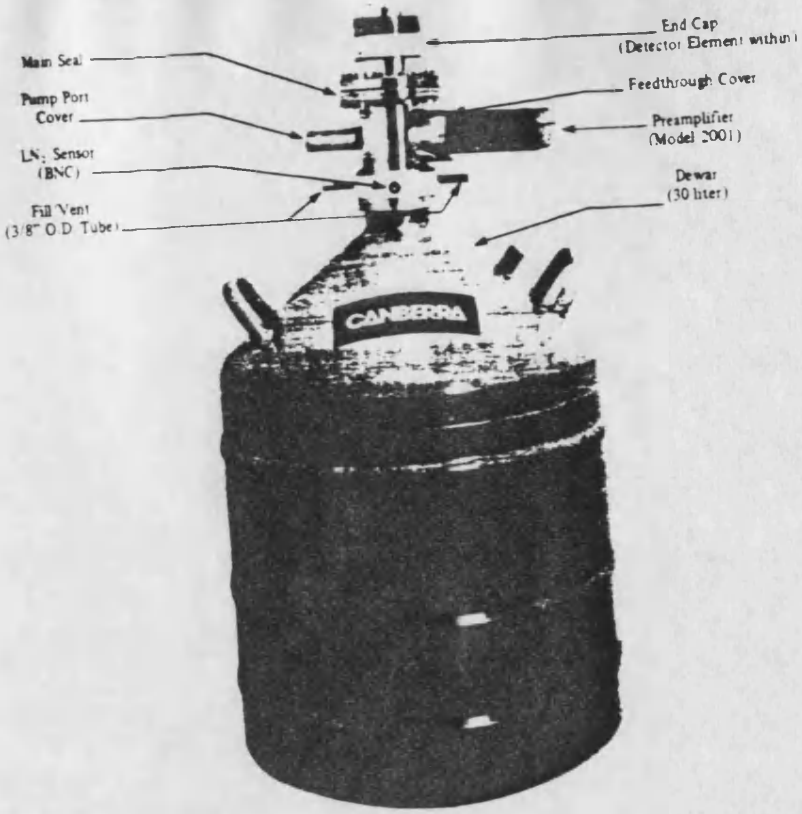

Figure A1.1 The intrinsic Ge detector showing preamplifier and cryostat.

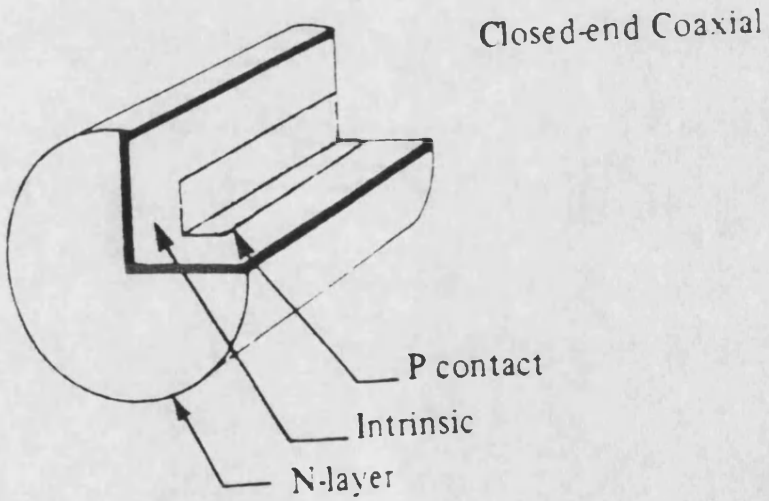

Figure A1.2 The p- and n- type semiconductor contact in the intrinsic Ge detector.

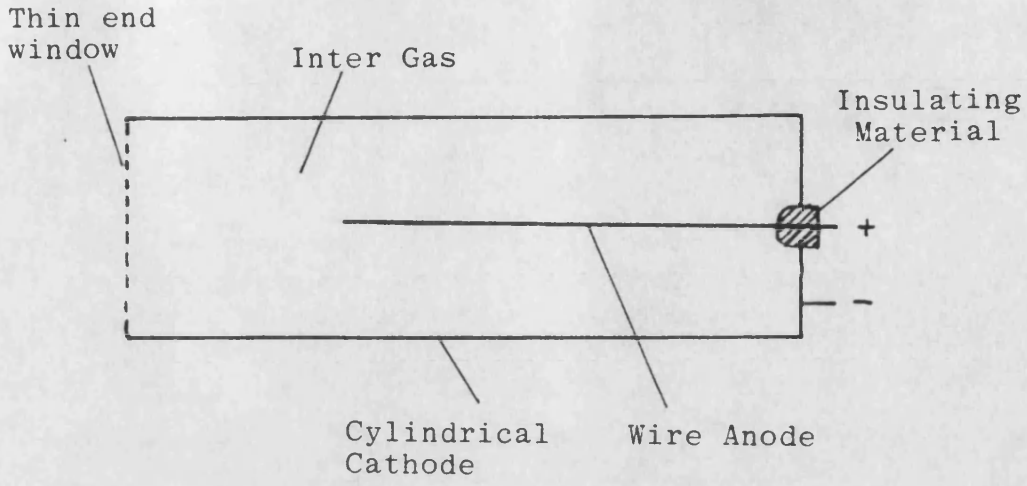

Figure A1.3 Schematic diagram of a G.M. Tube

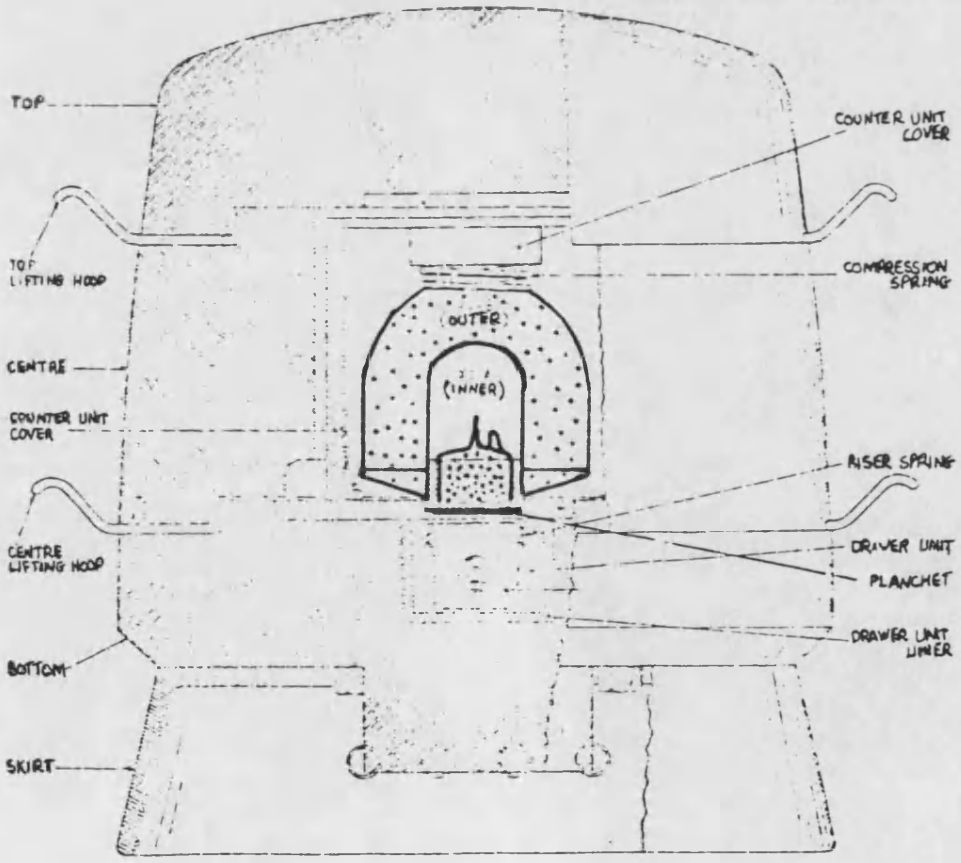

Figure A1.4 Low background counter type MX157 showing guard counter and lead castle detail.

APPENDIX 2. PROPAGATION OF ERRORS

Letting a value z consist of the variables x and y, then:

$$z = f(x,y)$$

Experimental values of z are obtained from the known function f. Knowing the errors in x and y, the error in z may be determined from the formula:

$$\sigma_z^2 = \sigma_x^2 \left(\frac{\delta f}{\delta x}\right)^2 + \sigma_y^2 \left(\frac{\delta f}{\delta y}\right)^2 \qquad \text{(A2.1)}$$

where σ_z, σ_x and σ_y are the standard deviations in the values of z, x and y respectively.

This equation may be extended for any function containing any number of variables. The simplest cases for addition, subtraction, division and multiplication of x and y are considered below.

1. Addition of errors

let $z = y + x$

then $\left(\frac{\delta f}{\delta x}\right)^2 = 1 \quad \left(\frac{\delta f}{\delta y}\right)^2 = 1$

and $\sigma_z^2 = \sigma_x^2 + \sigma_y^2$ (A2.2)

2. Subtraction of errors

let $z = y + x$

then $\left(\frac{\delta f}{\delta x}\right)^2 = 1 \quad \left(\frac{\delta f}{\delta y}\right)^2 = 1$

hence again $\sigma_z^2 = \sigma_x^2 + \sigma_y^2$

3. Division of errors

$$\text{let } z = \frac{x}{y}$$

$$\text{then } \left(\frac{\delta f}{\delta x}\right)^2 = \frac{1}{y^2} \qquad \left(\frac{\delta f}{\delta y}\right)^2 = \frac{1}{x^2}$$

$$\sigma_z^2 = \frac{\sigma x^2}{y^2} + \frac{\sigma y^2}{x^2}$$

$$\div z^2 \quad \frac{\sigma z^2}{z^2} = \frac{\sigma x^2}{x^2} + \frac{\sigma y^2}{y^2}$$

$$\left(\frac{\sigma z}{z}\right)^2 = \left(\frac{\sigma x}{x}\right)^2 + \left(\frac{\sigma y}{y}\right)^2 \qquad \text{(A2.3)}$$

4. Multiplication of errors

$$\text{let } z = xy$$

$$\text{then } \left(\frac{\delta f}{\delta x}\right)^2 = y^2 \qquad \left(\frac{\delta f}{\delta y}\right)^2 = x^2$$

$$\text{hence } \sigma_z = \sigma_x^2 y^2 + \sigma_y^2 x^2$$

$$z^2 \quad \frac{\sigma_z}{z^2} = \frac{\sigma_{x^2}}{x^2} + \frac{\sigma_{y^2}}{y^2}$$

$$\text{hence } \left(\frac{\sigma_z}{z}\right)^2 = \left(\frac{\sigma_x}{x}\right)^2 + \left(\frac{\sigma_y}{y}\right)^2 \qquad \text{(A2.4)}$$

Therefore addition and subtraction of numbers requires the addition or sum squared errors of components, whereas multiplication and division require the sum squared fractional errors.

APPENDIX 3. ANALYTICAL METHOD FOR THE DETERMINATION OF ^{238}U AND ^{232}Th IN ROCK SAMPLES BY ALPHA SPECTROMETRY.

This appendix describes briefly the procedure employed for the α-spectrometric analysis of rock samples. The description is based upon a laboratory manual outlining the analysis method (J.N. Andrews, 1979).

1. In a teflon container add a weighed quantity of ^{236}U/^{239}Th tracer solution to 1.000 g of rock sample. The weight of added tracer should be of similar ^{236}U and ^{239}Th activity to the estimated uranium and thorium contents of the rock sample.

2. Add 20 mls conc. HCl, 20 mls conc. HNO_3 and 120 mls 40% HF. Warm until the sample has dissolved, generally overnight.

3. Evaporate to dryness.

4. Add 10 mls conc. HCl and again evaporate to dryness.

5. Dissolve in the minimum of 6M HCl and dilute to 5 litres with distilled water.

6. Add 300 mg Fe^{3+} as $FeCl_3$ solution, thoroughly mix the solution and precipitate $Fe(OH)_3$ by the addition of conc. NH_4OH dropwise to ≈pH 9.

7. Separate the precipitate by syphoning and decanting.

8. Dissolve the precipitate in 6M HCl and evaporate the resulting solution to dryness.

9. Redissolve the residues in 30 mls 6M HCl and extract Fe^{3+} with an equal volume of MIBK. Discard any organic layer, add a fresh volume of MIBK and repeat. Separate the aqueous phase.

10. Evaporate the aqueous phase to dryness and redissolve in the minimum of 10M HCl.

11. Separate and purify uranium and thorium in the solution by ion-exchange using a column of Dowex 50-X8; 100-200 mesh anion exchange resin.

12. Evaporate the separated U and Th containing solutions to dryness and dissolve in 1M $(NH_4)_2SO_4$ electrolyte solution at pH 2.4.

13. Transfer the solution to electrolysis cells and deposit the Th and U on stainless steel planchetts.

14. Count the sources with a lithium drifted surface barrier alpha spectrometer until counting statistics of $\sim$1% are obtained, or over a maximum 3 day count.

15. Determine the ^{232}Th and ^{238}U contents utilising ^{239}Th and ^{236}U as tracers respectively after correcting for background count rates.

APPENDIX 4. RECOIL PRODUCTION OF ^{226}Ra INTO SOLUTION AFTER RECOIL PRODUCTION OF ITS PRECEEDING PARENT RADIONUCLIDES

In this model the alpha decay of a parent nuclide at the water/rock interface produces a recoil supply of its daughter into solution. The recoil supply rate should depend upon equation (1.34) but for the present purposes it is just assumed to be constant (μ). The supply rate is assumed to be constant for all nuclides in the same decay chain although Krishnaswami, et al. (1982) have derived equations describing the depletion of radionuclides within a recoil length of the rock surface.

The first α-decay produced nuclide in the ^{238}U series is ^{234}U (table 1.1). The rate equation describing its production is:

$$\frac{dN_{234}}{dt} = \mu - (\lambda N)_{234} \qquad (A4.1)$$

where $(\lambda N)_{234}$ = Activity of ^{234}U.

This assumes that recoil supply of ^{234}U predominates, as observed in reducing groundwater conditions (Osmond & Cowart 1976). The solution to this equation is:

$$(\lambda N)_{234} = \mu(1-e^{-\lambda_4 t}) \qquad (A4.2)$$

where λ_4 = decay constant of ^{234}U.

The rate of change of the α-decaying daughter, ^{230}Th, is given by:

$$\frac{dN_{30}}{dt} = (\lambda N)_{234} + \mu - (\lambda N)_{30} \qquad (A4.3)$$

where $(\lambda N)_{30}$ = activity of ^{230}Th

= decay of ^{234}U in solution + "recoil" - decay of ^{230}Th in solution

Substituting (A4.2) yields:

$$\frac{dN_{30}}{dt} = (1-e^{-\lambda_4 t}) + \mu - (\lambda N)_{30}$$

$$\therefore \quad \frac{dN_{30}}{dt} + (\lambda N)_{30} = \mu (1-e^{-\lambda_4 t}) + \mu$$

$$\times e^{+\lambda_{30} t} \quad \frac{dN_{30}}{dt} e^{+\lambda_{30} t} + (\lambda N)_{30} e^{-\lambda_{30} t} = \mu(2-e^{-\lambda_4 t})e^{\lambda_{30} t}$$

Integrating both sides:

$$\lambda N_{30} e^{\lambda_{30} t} = \mu \left[\frac{2}{\lambda_{230}} e^{\lambda_{30} t} - \frac{e^{(\lambda_{30}-\lambda_4)t}}{\lambda_{30}-\lambda_4} \right] + C \qquad (A4.4)$$

at t=0, N=0 hence

$$C = \mu \left[\frac{1}{\lambda_{230}-\lambda_{234}} - \frac{2}{\lambda_{230}} \right] \qquad (A4.5)$$

Substituting into equation (A4.4) gives

$$Ne^{\lambda_{30} t} = \mu \left[\frac{2(e^{\lambda_{30} t} - 1)}{\lambda_{30}} + \frac{1 - e^{(\lambda_{30}-\lambda_4)t}}{\lambda_{30}-\lambda_4} \right] \qquad (A4.6)$$

Multiplying by $e^{-\lambda_{30} t}$

$$N_{30} = \mu \left[\frac{2(1 - e^{-\lambda_{30} t})}{\lambda_{30}} + \frac{(e^{-\lambda_{30} t} - e^{-\lambda_4 t})}{(\lambda_{30}-\lambda_4)} \right]$$

But $\lambda_{30} >> \lambda_4$ hence:

$$(\lambda N)_{30} = \mu \left[2(1 - e^{-\lambda_{30}t}) + e^{-\lambda_{30}t} - e^{-\lambda_4 t}\right]$$

$$(\lambda N)_{30} = \mu \left[(1 - e^{-\lambda_{30}t}) + (1 - e^{-\lambda_4 t})\right] \qquad (A4.7)$$

The third recoil is $^{230}Th \rightarrow {}^{226}Ra$. However ^{230}Th is rapidly adsorbed onto aquifer surfaces (Hussain and Krishnaswami, 1980). The above equation therefore represents the growth in activity of adsorbed ^{230}Th/litre of water. The rate of change of ^{226}Ra is given by:

$$\frac{dN_6}{dt} = \begin{array}{l}\text{Release of } {}^{226}Ra \\ \text{from decay of} \\ \text{adsorbed } {}^{230}Th\end{array} + \begin{array}{l}\text{Recoil of} \\ {}^{226}Ra \text{ from} \\ \text{the bulk} \\ \text{rock}\end{array} - \begin{array}{l}\text{decay in} \\ \text{solution}\end{array}$$

$$= \mu f \left[(1-e^{-\lambda_{30}t}) + (1-e^{-\lambda_4 t}) + \mu - (\lambda_6 N_6)\right] \qquad (A4.8)$$

$$\therefore \quad \frac{dN_6}{dt} + \lambda_6 N_6 = \mu f \left[(1-e^{-\lambda_{30}t}) + (1-e^{-\lambda_4 t})\right] + \mu$$

$$\int \frac{dN_6}{dt} e^{\lambda_6 t} + \lambda_6 N_6 e^{\lambda_6 t} = \int \mu f \left[(1-e^{-\lambda_{30}t}) + \ldots \right.$$
$$\left. \ldots (1-e^{-\lambda_4 t})\right] e^{\lambda_6 t} + e^{\lambda_6 t}$$

integrating both sides:

$$Ne^{\lambda_6 t} = \mu f \left[\frac{2}{\lambda_6} e^{\lambda_6 t} + \frac{e^{\lambda_6 t}}{f\lambda_6} - \frac{e^{(\lambda_6-\lambda_{30})t}}{(\lambda_6-\lambda_{30})} - \ldots \right.$$
$$\left. \ldots \frac{e^{(\lambda_6-\lambda_4)t}}{(\lambda_6-\lambda_4)}\right] + C \qquad (A4.9)$$

at t=0, N=0

$$\therefore \quad C = \mu f \left[\frac{1}{(\lambda_6-\lambda_{30})} - \frac{2}{\lambda_6} - \frac{1}{f\lambda_6} + \frac{1}{(\lambda_6-\lambda_4)}\right] \qquad (A4.10)$$

Substituting into (A4.9) and multiplying by $\lambda_6 e^{-\lambda_6 t}$:

$$A_{226} = \lambda_6 N_6 = \mu f \left[2(1-e^{-\lambda_6 t}) + \frac{(1-e^{-\lambda_4 t})}{f} + \frac{\lambda_6}{\lambda_6-\lambda_{30}} \ldots \right.$$
$$\left. \ldots (e^{-\lambda_6 t} - e^{\lambda_{30} t}) \right] \qquad (A4.11)$$

but, $\lambda_6/(\lambda_6-\lambda_{30}) = 1.021$.

$$A_{226} = \mu f \left[(1-1.021e^{-\lambda_3 t}) + (1-e^{-\lambda_4 t}) + \ldots \right.$$
$$\left. \ldots (1-e^{-\lambda_6 t})/f \right] \qquad (A4.12)$$

where λ_4 = decay constant of ^{234}U

λ_{30} = decay constant of ^{230}Th

λ_6 = decay constant of ^{226}Ra

f = fraction of adsorbed ^{230}Th releasing ^{226}Ra to the aquifer water after decay.

The $^{228}Ra/^{226}Ra$ activity ratio (assuming both nuclides are produced by recoil) is then given by the equation:

$$^{228}Ra/^{226}Ra = \ldots$$
$$\ldots \frac{[Th]\,(1-e^{-\lambda_8 t})}{[U]\left[(1-e^{-\lambda_6 t}) + f(1-e^{-\lambda_3 t}) + f(1-e^{-\lambda_4 t})\right]} \qquad (A4.13)$$

Recoil with ^{226}Ra adsorption

If recoil for ^{230}Th and ^{234}U is modelled as before, but ^{226}Ra is adsorbed by a first order adsorption process then the rate of change of ^{226}Ra is given by:

$$\frac{dN_6}{dt} = \mu f \left[(1-e^{-\lambda_4 t}) + (1-e^{-\lambda_3 t})\right] + \ldots$$
$$\ldots \mu - \lambda_6 N_6 - kN_6 \qquad (A4.14)$$

$$\therefore \quad \frac{dN_6}{dt} e^{(k+\lambda_6)t} + (k+\lambda_6)Ne^{(k+\lambda_6)t} = Ne^{(k+\lambda_6)t}$$

$$= \mu f \left(\int 2e^{(k+\lambda_6)t} - \int e^{(k+\lambda_6-\lambda_4)t} - \int e^{(k+\lambda_6-\lambda_3)t} \right.$$

$$\left. + \int \frac{e^{(k+\lambda_6)t}}{f} \right)$$

following the same process as before, the solution to this equation is:

$$A_6 = \lambda_6 \mu f \left[\frac{2(1-e^{-(k+\lambda_6)t}}{k} - \left(\frac{e^{-\lambda_4 t} - e^{-(k+\lambda_6)t}}{k+\lambda_6-\lambda_4} \right) - \ldots \right.$$

$$\left. \ldots \left(\frac{e^{-\lambda_3 t} - e^{-(k+\lambda_6)t}}{k+\lambda_6-\lambda_3} \right) + \frac{1-e^{-(k+\lambda_6)t}}{(\lambda_6+k)f} \right] \qquad (A4.15)$$

But, $k >> \lambda_6, \lambda_3, \lambda_4$ in the majority of groundwaters, hence:

$$A_6 = \frac{\lambda_6 \mu f}{k} \left[(1-e^{-\lambda_4 t}) + (1-e^{-\lambda_3 t}) + \left(\frac{1-e^{-kt}}{f} \right) \right] \qquad (A4.16)$$

The $^{228}Ra/^{226}Ra$ activity ratio in this case is given by:

$$^{228}Ra/^{226}Ra = \ldots$$

$$\ldots \frac{k \left[Th\right] (1-e^{-kt})}{\lambda_6 \left[U\right] \left(f(1-e^{-\lambda_4 t}) + f(11e^{-\lambda_3 t}) + (1-e^{-kt}) \right)} \qquad (A4.17)$$

REFERENCES

Adler, H.H., 'Concepts of uranium-ore formation in reducing environments in sandstones and other sediments'. in Proceedings, Symposium on the Formation of Uranium Ore Deposits, Athens, 1974 (IAEA, Vienna) 141-168.

Ames, L.L., McGarrah, J.E. and Walker, B.A. (1983) 'Sorption of Uranium and Radium by Biotite Muscovite and Phlogopite.' Clay and Clay Minerals, 31, 343-351.

Ames, L.L., McGarrah, J.E. and Walker, B.A. (1983) Sorption of Trace Constituents from Aqueous solutions into Secondary Minerals, II Radium. Clay and Clay Minerals, 31, 335-342.

Aldous, P. Personal communication, University of Bristol (1985).

Andrews, J.N. and Wood, D.F. (1972) Mechanism of radon release in rock matrices and entry into groundwaters. Trans. Inst. Min. Metall. Soc. B81, 197-209.

Andrews, J.N. and Kay, R.L.F. (1978) The Evolution of Enhanced $^{234}U/^{238}U$ activity ratios for dissolved uranium and groundwater dating. 4th Int. Conference on Geochemistry, Cosmochemistry and Isotope Geology. Denver, USA. USGS Open File Report 78-701, p.11

Andrews, J.N. (1979) Unpublished manual for determining the uranium and thorium content of groundwaters by alpha spectrometry. University of Bath.

Andrews, J.N., Burgess, W.G., Edmunds, W.M., Kay, R.L.F. and Lee. D.J. (1982) The Thermal Springs of Bath. Nature, 298, p. 339.

Andrews, J.N., Giles, I.S., Kay, R.L.F., Lee, D.J., Osmond, J.K., Cowart, J.B., Fritz, P., Barker, J.F. and Gale, J. (1982) Radioelements, radiogenic helium and age relationships for groundwaters from the granites at Stripa, Sweden. Geochim. Cosmochim. Acta., 46, 1533.

Andrews, J.N. and Kay R.F.L. (1982) $^{234}U/^{238}U$ activity ratio of dissolved uranium in groundwaters from a Jurassic Limestone aquifer in England. Earth Planet. Sci. Letts., 57, 139-151.

Andrews, J.N. (1983) Dissolved radioelements and inert gases in geothermal investigations. Geothermics, 12, 67-82.

Andrews, J.N. and Kay, R.F.L. (1983) The U contents and $^{234}U/^{238}U$ activity ratios of dissolved uranium in groundwaters from some Triassic sandstones in England. Isot. Geosci., 1, 101-117.

Andrews, J.N., Goldbrunner, J.E., Darling, W.G., Hooker, P.J., Youngman, M.J., Eichinger, L., Rauert, W. and Stichler, W. (1985) A radiochemical, hydrochemical and dissolved gas study of groundwaters in the Molasse basin of Upper Austria. Earth Planet. Sci. Letts., 73, 317-332.

Armburst, B.F. and Kuroda, P.K. (1955) On the isotopic composition of radium $^{224}Ra/^{226}Ra$ and $^{228}Ra/^{226}Ra$ in petroleum brines. Trans. A.G.U., 37, 216-220.

Asikainen, M. (1981) Radium content and the $^{226}Ra/^{228}Ra$ activity ratio in groundwaters from bedrock. Geochim. Cosmochim. Acta., 45, 1375-1381.

Bateman, H. (1910) The solution of a system of differential equations occurring in the theory of radioactive transmutations. Proc. Cambridge Phil. Soc., 16, 423.

Benes, P. (1982) Physico-chemical forms and migration in continental waters of radium from uranium mining and milling, in Proc. Symp. on the Environmental Migration of Long Lived Isotopes, I.A.E.A., Vienna, 2-23.

Bloch, S. and Key, R.M. (1981) Modes of formation of anomalously high radioactivity in oil field brines. Am. Assoc. Pet. Geol. Bull., 65, 154-159.

Busenberg, E., Plummer, L.N. and Parker, V.B. (1984) The solubility of strontianite ($SrCO_3$) in CO_2-H_2O solutions between 2 and 91°C. Geochim., Cosmochim. Acta., 48, 2021-2035.

Cherdyntsev, V.V. (1971) Uranium-234. Israel Program for Scientific Translations, Jerusalem. 62-68.

Chouk, A., Vuister, P., Piac, G., Berrada, M. and Csikai, J. (1978) Determination of U and Ra in rock samples by gamma-spectrometric methods. J. Radioanalytical Chem., 45, 445-451.

Cotton, F.A. and Wilkinson, G. (1972) Advanced Inorganic Chemistry. 3rd Edition, Wiley, New York.

Cowart, J.B. and Osmond, J.K. (1976) Dissolved uranium series nuclides in geothermal waters. Geol. Soc. Amer. Abstr. Prog., 8, 823.

Dall'Aglio, M., Graynami, R. and Locardi, E. (1974) Geochemical factors controlling the formation of secondary minerals of Uranium. in Formation of Uranium Ore Deposits, I.A.E.A., Vienna.

Davidson, M.R. and Dickson, B.L. (1986) A porous flow model for steady state transport of radium in groundwater. Water Res. Research, 22, 34-44.

Dearnally, G. and Northrop, D.C. (1966) Gamma spectrometry in semiconductors for Nuclear Radiation, E.F. & Spon Ltd., London.

Dickson, B.L. (1985) Radium isotopes in saline seepages, South Western Yelgarn, Western Australia. Geochim. Cosmochim Acta., 49, 361-368.

Dyck, W. (1978) The mobility and concentration of uranium and its decay products in temperate surficial environments, in Uranium Deposits, their Mineralogy and Origin., Vol.3, ed. M. Kimberly, Mineralog. Assoc. Canada. 57-100.

Dymond, J., Cobler, R., Gordon, L., Biscaye, P. and Mathieu, G. (1983) ^{226}Ra and ^{222}Rn contents of Galapagos Rift hydrothermal waters - the importance of low-temperature interactions with crustal rocks. Earth Planet. Sci. Letts., 64, 417-429.

Elliot, T., personal communication (1986).

Elsinger, R.J., King. P.T. and Moore, W.S. (1982) Radium-224 in natural waters measured by gamma-ray spectrometry. Anal. Chem. Acta., 144, 277-281.

Elsinger, R.J. and Moore, W.S. (1983) ^{224}Ra, ^{228}Ra and ^{226}Ra in Winyah Bay and Delaware Bay. Earth Planet. Sci. Letts., 64, 430-436.

Fleischer, R.L. (1983) Theory of alpha recoil effects on radon release and isotopic disequilibrium. Geochim. Cosmochim. Acta., 47, 779-784.

Fleischer, S. (1978) Description of thin sections from borehole N1 in the timescale room. Unpublished manuscript, University of California, Lawrence Berkeley Laboratories.

Frape, S.K., Fritz, P. and McNutt, R.H. (1984) Water-rock interaction and chemistry of groundwaters from the Canadian Shield. Geochim. Cosmochim. Acta., 48, 1617-1627.

Gale, G.E. and Rouleau, A. (1985) Hydrogeochemical characterisation of the ventilation drift area. Proc. Int. Symp. on In-situ Experiments in Granite Associated with the Disposal of Radioactive Waste. O.E.C.S. Nuclear Energy Agency.

Gadde, R.R. and Laitinen, H.A. (1973) Study of the sorption of lead by hydrous ferric Oxide. Environ. Lett., 5, 223-235.

Gray, M..J. and Malati, M.A. (1979) Adsorption from aqueous solution by Manganese dioxide: 1 Adsorption of the alkaline earth cations. J. Chem. Tech. Biotechnology, 29, 127-134.

Harloff, G.J. and Landau, M.M. (1984) Trace metal migration transport with ion exchange for multi-components and multi-substrates with application to radium transport. In. Situ. 8(4) 401-433.

Hasany, S.M. and Chaudhary, M.N. (1981) Adsorption studies of strontium on manganese dioxide from aqueous solutions. Int. J. Applied Radiat. Isotop. 32, 899-904.

Hem, J.D. (1976) Geochemical controls on lead concentrations in stream water and sediments. Geochim. Cosmochim. Acta., 40, 599-609.

Hem, J.D. (1981) Rate of manganese oxidation in aqueous systems. Geochim. Cosmochim. Acta., 45, 1369-1374.

Hiyuchi, H., Vesugi, M., Satoh, K. and Ohashi, N. (1984) Determination of radium in water by liquid scintillation counting after preconcentration with ion-exchange resin. Anal. Chem., 56, 761-763.

Hostetler, P.B. and Garrels, R.M. (1962) Transportation and precipitation of uranium and vanadium at low temperatures with special reference to sandstone type uranium deposits. Econ. Geol., 57, 137-167.

Hussain, N. and Krishnaswami, S. (1980) U-238 series disequilibrium in groundwaters; implications to the origins of excess U-234 and the fate of reactive pollutants. Geochim. Gosmochim. Acta., 44, 1287-1291.

Hussain, N. and Krishnaswami, S. (1982) The behaviour of short lived radiogenic lead isotopes (^{214}Pb and ^{212}Pb) in groundwaters and laboratory leaching experiments. Earth Planet. Sci. Letts., 58, 430-438.

Ivanovich, M. and Herman, R.S. (eds) (1982) Uranium series disequilibrium: Applications to environmental problems Oxford Press. 571 pp.

Kehinde, L.O., Oluwole, A.F., Oshin, I.O. and Flemming, R. (1983) Assay of Nigerian Uranium ores by passive gamma-ray spectrometry. Int. J. Appl. Radiat. Isot., 34, 936-938.

Kigoshi, K. (1971) Alpha recoil Th-234: Dissolution into water and the U-234/U-238 disequilibria in nature. Science, 173, 47-48.

Kim, K.H. and Burnett, W.C. (1983) Gamma-ray spectrometric determination of uranium series nuclides in marine phosphates. Anal. Chem., 55, 1796-1800.

King, P.T., Michel, J. and Moore, W.S. (1982) Groundwater chemistry of ^{228}Ra, ^{226}Ra and ^{222}Rn. Geochim. Cosmochim. Acta., 46, 1173-1182.

Kraemer, T.F. and Reid, D.F. (1984) The occurrence and behaviour of radium in saline formation water of the U.S. Gulf Coast Region. Isotop. Geosci., 2, 153-174.

Krauskopt (1969) Introduction to geochemistry. McGraw-Hill, New York.

Krishnaswami, S., Graustein, W.C. and Turekian, K.K. and Dowd, J.F. (1982) Radium, thorium and radioactive lead isotopes in groundwaters: application to the in-situ determination of adsorption-desportion rate constants and retardation factors. Water Resour. Res., 18, 1633-1675.

Krishnaswami, S, and Turekian, K. (1982) ^{238}U, ^{226}Ra and ^{210}Pb in some vent waters of the Galapogos spreading centre. Geophys. Res. Lett., 9, 827-830.

Langmuir, D. (1978) Uranium solution mineral equilibria at low temperatures with applications to sedimentary ore deposits. Geochim. Cosmochim. Acta., 42, 547-568.

Langmuir, D and Herman, J.S. (1980) The mobility of thorium in natural waters at low temperatures. Geochim. Cosmochim. Acta., 44, 1753-1766.

Langmuir, D. and Ozsvath, D. (1980) A general model for metal adsorption onto geological materials. Abstr. Am. Chem. Soc. Nat. Meet., Houston, COL 013.

Langmuir, D and Melchoir, D (1985) The geochemistry of Ca, Sr, Ba and Ra sulphates in some deep brines from the Paulo Dura Basin, Texas. Geochim. Cosmochim. Acta., 49, 2423-2432.

Langmuir, D. and Riese, A.C. (1985) The thermodynamic properties of radium. Geochim. Cosmochim. Acta., 49, 1593-1601.

Laul, J.C., Perkins, R. and Hubbard, N. (1983) Abstract, Spring Meeting, Am. Geophys. Union, 64, 227.

Lee, D. (1980) Inert gases and radioelements in groundwater studies. Ph.D. thesis, University of Bath.

Matthews, K.M. (1983) Pb extraction from natural waters. Anal. Lett., 16(A8), 633-642.

Michel, J., Moore, W.S. and King, P.T. (1981) Gamma-ray spectrometry for the determination of radium-228 and radium-226 in natural waters. Anal. Chem., 53, 1885-1889.

Moore, W.S. (1976) Sampling Ra-228 in the deep ocean. Deep Sea Research, 23, 647-651.

Moore, W.S. and Reid, D.F. (1973) Extraction of Radium from Natural Waters using Manganese Impregnated Acrylic Fibres. I. Geophys. Res., 78, 8880-8886.

Murray, J.W. (1975) The interaction of metal ions at the manganese dioxide-solution interface. Geochim. Cosmochim. Acta., 89, 505-520.

Nathwani, J.S. and Phillips, C.R. (1979) Adsorption of ^{226}Ra by soils in the presence of Ca^{2+} ions. Specific adsorption (II). Chemispheres. 5, 293-299.

Nelson, P., Paulsson, B., Rachiele, R. Andersonn, L., Schrauf, T., Hustrulid, W., Furan, D. and Magnusson, K.A. (1979) Preliminary report on the geophysical and mechanical borehole measurements at Stripa. Rep. LBL-8280 Lawrence Berkeley Lab., Univ. of Calif.

Nordstrom, D.K. and Andrews, J.N. (1985) Progress in the geochemical investigations of water-rock interaction at Stripa: in Proc. Symp. In situ Experiments in Granite Associated with the Disposal of Radioactive Waste. OECD Nuclear Energy Agency, 96-106.

Osmond, J.K. and Cowart, J.B. (1976) The theory and uses of natural uranium isotopic variations in hydrology. Atomic Energy Review, 14, 621-679.

Plant, J.A. (1983) Natural radioactivity in the environment: in Applied Environmental Geochemistry. ed. I. Thornton. Academic Press, London.

Plummer, L.N., Jones, B.F. and Truesdell, A.H. (1976) WATEQF - A Fortran IV version of WATEQ, a computer programme for calculating chemical equilibria of natural waters. USGS Water Resources Investigations, 76(13), 61 pp.

Paic, G., Reggoug, A., Paic, A. and Chouak, A. (1982) Absolute measurement of the Ra/U ratio in uranium ores using a hyper-pure germanium detector. Int. J. Appl. Radiat. Isot., 33, 1389-1392.

Rama, K. and Moore, W.S. (1984) Mechanism of transport of U-Th series radioisotopes from solids into groundwaters. Geochim. Cosmochim. Acta., 48, 395-399.

Rankama, K. and Sahama, T.G. (1950) Geochemistry. University of Chicago Press, London.

Reardon, E.J. and Langmuir, D. (1974) Activity coefficients of $MgCO_3^0$ and $CaSO_4^0$ ion pairs as a function of ionic strength. Geochim. Cosmochim. Acta., 40, 459-554.

Reid, D.F., Key, R.M. and Schink, D.R. (1979) Earth Planet. Sci. Lett., 43, 223-226.

Riley, J.P. and Skirrow, G. (1975) Chemical Oceanography, Vol.3 2nd edition. Academic Press, London.

Rogers, J.J.W. and Adams, J.A.S. (1969) 'Uranium': in Handbook of Geochemistry, ed. K.H. Wedepohl. Springer-Verlag, Berlin.

Rosholt, J.N., Shields, W.R. and Gamer, E.L. (1963) Isotopic fractionation in sandstone. Science, 139, 224-226.

Schotzig, U. and Debertin, K. (1983) Photon emission probabilities per decay of ^{226}Ra and ^{232}Th in equilibrium with their daughter products. Int. J. Appl. Radiat. Isot., 34, 533-538.

Sebasta F., Sedlacek, J., John, J. and Sandrik, R. (1981) Behaviour of radium and barium in a system including uranium mine waste waters and adjacent surface waters. Environ. Sci. Technol., 15(1), 71-75.

Sato, J., Hirose, T. and Sato, K. (1980) Application of Ge(Li) detectors to voluminous geochemical samples. Int. J. Appl. Radiat. Isot., 31, 130-132.

Senftle, F.E. and Keeval, N.B. (1947) Thorium-Uranium ratios in the genesis of lead ores. Trans. Am. Geophys. Union, 28, 372.

Shannon, R.D. (1976) Reviewed effective ionic radii and systematic studies of interatomic distances in halides and chalcogenides. Acta. Cryst. A., 32, 751-767.

Spalding, R.F., Druliner, A.D., Whiteside, L.S. and Struempler, A.W. (1984) Uranium geochemistry in groundwaters from Tertiary sediments. Geochim. Cosmochim. Acta., 48, 2679-2692.

Stoessell, R.K. and Carpenter, A.B. (1986) Stoichiometric saturation tests of $NaCl_{1-x}Br_x$ and $KCl_{1-x}Br_x$. Geochim. Cosmochim. Acta., 50, 1465-1474.

Stumm, W. and Morgan, J. (1970) Aquatic Chemistry. John Wiley and Sons, Inc., London.

Suarez, D.L. and Langmuir, D. (1976) Heavy metal relationships in a Pennsylvanian soil. Geochim. Cosmochim. Acta., 40, 589-598.

Tanner, A.B. (1964) Physical and chemical controls on distribution of radium-226 and radon-222 in groundwater near Great Salt Lake, Utah. Proc. Symp. on the Natural Radiation Environment. 253-276.

Thorstensen, D.C. and Plummer, L.N. (1977) Equilibrium criteria for two-component solids reacting with fixed composition in an aqueous phase - example magnesium calcites. Amer. J. Sci., 277, 1202-1223.

Tripathy, V.S. (1979) Comments on "Uranium solution-mineral equilibria at low temperatures with applications to sedimentary ore deposits". Geochim. Cosmochim. Acta., 43, 1369-1374.

Ulomov, V.I. and Mavashev, B.Z. (1967) Dokl. Akad. Nauk. Fiz. Zemli, 176, 319.

Wedepohl, K.H. (1978) (ed.) Handbook of Geochemistry, Vol II/3 Springer, Berlin.

Zereshki, A. (1981) Solution of Rn-222 by groundwaters. M.Sc. thesis, University of Bath.

Zukin, J.R., Hammond, D.E., Ku, T.L. and Elders, W.A. (1987) Uranium-Thorium series radionuclides in brines and reservoir rocks from two deep geothermal boreholes in the Salton Sea Geothermal field, Southeastern California. Geochim. Cosmochim. Acta., 51, 2719-2731.